Integration of dual-clutch transmissions in hybrid electric vehicle powertrains

Doctoral Dissertation
Doctoral Program in Mechanical Engineering (30th Cycle)

Integration of Dual-Clutch Transmissions in Hybrid Electric Vehicle Powertrains

By

Guido R. Guercioni

******

Supervisor(s):

Prof. Alessandro Vigliani, Supervisor

Doctoral Examination Committee:

Prof. Francesco Braghin, Referee, Politecnico di Milano.

Prof. Francesco Pellicano, Referee, Università degli Studi di Modena e Reggio Emilia.

Prof. Giorgio Rizzoni, The Ohio State University.

Prof. Mauro Velardocchia, Politecnico di Torino.

Prof. Elvio Bonisoli, Politecnico di Torino.

Politecnico di Torino

2018

Declaration

I hereby declare that, the contents and organization of this dissertation constitute my own original work and does not compromise in any way the rights of third parties, including those relating to the security of personal data.

Guido R. Guercioni

2018

* This dissertation is presented in partial fulfillment of the requirements for **Ph.D. degree** in the Graduate School of Politecnico di Torino (ScuDo).

Ai miei genitori

Acknowledgment

Scrivendo i ringraziamenti, mi sono reso conto che questa sezione della tesi non è, come pensavo all'inizio, fra le più semplici da completare. Il grande numero di persone che rendono la mia vita speciale e che, in un modo o nell'altro, hanno contribuito al raggiungimento di questo traguardo, mi ha certamente messo in difficoltà.

Inizio ringraziando i miei genitori, ai quali dedico questo lavoro. Ringrazio loro, ed anche mio fratello, per aver sempre creduto nelle mie capacità, sostenendomi in ogni circostanza. Solo grazie a questo supporto, sono riuscito ad inseguire la mia sete di conoscenza, che mi ha portato a raggiungere i più alti livelli dell'istruzione universitaria. Estendo i ringraziamenti al resto della mia famiglia per tutto l'affetto dimostrato nel corso degli anni.

Ringrazio il mio tutore, Prof. Alessandro Vigliani, per avermi dato la possibilità di inseguire i miei interessi scientifici, sostenendomi nei momenti di difficoltà che ci sono stati durante l'attività di dottorato. Inoltre, lo ringrazio, insieme al Prof. Galvagno, per avermi insegnato come affrontare il mondo della ricerca e come interfacciarsi con la realtà industriale. Grazie per avermi trasmesso la vostra passione per le tematiche su cui abbiamo lavorato insieme, per tutte le cose che mi avete insegnato e per la vostra sincera amicizia. Ringrazio anche il Prof. Velardocchia per avermi accolto nel suo gruppo di ricerca e per aver creduto nelle mie capacità fin dai tempi della tesi di laurea. Un ringraziamento speciale va fatto al Ing. Giovanni Bracco per il suo supporto quando l'onere computazionale della programmazione dinamica ha avuto la meglio sui PC a nostra disposizione.

Ringrazio il Dr. Giancarlo Osella e tutto il suo team di lavoro al CRF per la disponibilità mostrata nello svolgere attività di ricerca insieme e per il loro supporto durante il dottorato.

Un sentito ringraziamento agli attuali e vecchi membri del nostro gruppo di ricerca: Antonio, Pablo, Alberto, Mariangela, Hamid, Sara, Andrea, Mattia, Luca, Domenico e il Prof. Bonisoli. Con loro l'ambiente di lavoro al Politecnico di Torino è sempre stato piacevole.

Ringrazio tutti gli amici di Torino (Alfonso, Andrea, Elisa, Carlo, Federico, Katia, Federica e Piero) e i vari coinquilini (paganti e abusivi): Andrea, Fabrizio, Giovanni, Emanuele ed Alessandra. Grazie a tutti voi per aver reso Torino, una città a me una volta sconosciuta, un posto dove sentirmi a casa.

Agradezco a mis amigos de Caracas, con quien compartí muchos momentos felices: Maurizio, Pedro, Roberto, Douglas, Ulysses, Gregory, Jhasua, María Angélica y Francesca.

Finally, I would like to thank my colleagues and all the staff at the Center for Automotive Research of The Ohio State University. Specially, Dr. Rizzoni and Dr. Midlam-Mohler for supporting my research activity and giving me the opportunity of working with them. I would also like to thank my friend Tong with whom I learned many of the thigs regarding optimal control theory that allowed me to complete this dissertation. Last but not least, I thank all my friends from the OSU EcoCAR team: Simon, Greg, Dennis, Aditya, Wilson, Andrew, Brandon, Kristina, Stephanie and Phil. It was a privilege to have the opportunity of working with such a brilliant group of engineers and to be your friend.

Altresì un sincero pensiero va a tutti coloro che non sono riuscito a ringraziare ma che meriterebbero uno spazio all'interno di questa sezione.

Guido R. Guercioni

Abstract

This dissertation presents a study focused on exploring the integration of Dual-Clutch Transmissions (DCTs) in Hybrid Electric Vehicles (HEVs). Among the many aspects that could be investigated regarding the electrification of DCTs, research efforts are undertaken here to the development of control strategies for improving vehicle dynamic performance during gearshifts and the energy management of HEVs. In the first part of the dissertation, control algorithms for upshift and downshift maneuvers are developed for a Plug-in Hybrid Electric Vehicle (PHEV) architecture in which an electric machine is connected to the output of the transmission, thus obtaining torque filling capabilities during gearshifts. Promising results, in terms of the vehicle dynamic performance, are obtained for the two transmission systems analyzed: Hybrid Automated Manual Transmission (H-AMT) and Hybrid Dual-Clutch Transmission (H-DCT). On the other hand, the global optimal solution to the energy management problem for a PHEV equipped with a DCT is found by developing a detailed Dynamic Programing (DP) formulation. The main control objective is to reduce the fuel consumption during a driving mission. Based on the DP results, a novel real-time implementable Energy Management Strategy (EMS) is proposed. The performance of such controller, in terms of the overall fuel usage, is close to that of the optimal solution. Furthermore, the developed approach is shown to outperform a well-known causal strategy: Adaptive Equivalent Consumption Minimization Strategy (A-ECMS). One of the main aspects that differentiates the EMSs proposed here to those presented in previous works is the introduction of a model to estimate the energy consumption during gearshifts in DCTs. Thus, this dissertation illustrates how through the electrification of powertrains equipped with DCTs both the vehicle dynamic performance and the energy consumption can be improved.

Contents

List of Figures

List of Tables

List of Acronyms and Symbols

Acronyms

A-ECMS	Adaptive Equivalent Consumption Minimization Strategy
AMT	Automated Manual Transmission
APP	Accelerator Pedal Position
ARMA	Autoregressive Moving Average
BAS	Belt Alternator Starter
COG	Center Of Gravity
DC	Direct Current
DCT	Dual-Clutch Transmission
DCU	Dual-Clutch Unit
DOF	Degree Of Freedom
DP	Dynamic Programming
ECMS	Equivalent Consumption Minimization Strategy
ECU	Engine Control Unit
EEC	Emissions and Energy Consumption
EM	Electric Machine
EMS	Energy Management Strategy
EPA	Environmental Protection Agency
EV	Electric Vehicle

FUDS	Federal Urban Driving Schedule
H-AMT	Hybrid Automated Manual Transmission
H-DCT	Hybrid Dual-Clutch Transmission
HDS	Hybrid Dynamic System
HEV	Hybrid Electric Vehicle
ICE	Internal Combustion Engine
LHV	Lower Heating Value
MT	Manual Transmission
NEDC	New European Driving Cycle
OCV	Open Circuit Voltage
PHEV	Plug-in Hybrid Electric Vehicle
PI	Proportional-Integral controller
PMP	Pontryagin's Minimum Principle
PMR	Power-to-Mass Ratio
PTU	Power Transfer Unit
RMS	Root Mean Square
SMF	Single Mass Flywheel
SOC	State Of Charge
SOE	State Of Energy
TCU	Transmission Control Unit
TPBVP	Two-Point Boundary-Value Problem
TSF	Torque Split Factor

WLTC	World-wide harmonized Light duty Test Cycle
WLTP	World-wide harmonized Light-duty Test Procedure

Symbols

a	Vehicle longitudinal acceleration
A	Area
APP	APP
b	Distance from the vehicle COG to one of its axles
c	Generic coefficient
D	Distance
es	ICE start status
E	Energy
f	Generic function
fco	Fuel cut-off status
F	Force
g	Gravity acceleration
gn	Gear number
gs	Gearshift status
G	Inequality that the state variables must satisfy
$\mathbf{G}$	Set of inequalities that the state variables must satisfy
h	Height of the vehicle COG from the ground
H	Hamiltonian
I	Electric current

ICE	ICE
j	Generic index
J	Rotational inertia
$Jerk$	Jerk
k	Discrete step (when used for indexing)
k	Torsional stiffness
K	Generic gain
l	Vehicle axle base length
L	Instantaneous cost function
LHV	LHV
m	Number of state variables (when used for indexing)
m	Mass
M	Vehicle mass
n	Number of control variables (when used for indexing)
N	Final discrete step
P	Power
q	Number of defined final states
Q	Electric capacity
QD	Quick-disconnect clutch
R	Electrical resistance
s	Equivalence factor
SOC	SOC

SOE	SOE
t	Time
T	Torque
TSF	Torque split factor
u	Control variable
$\mathbf{u}$	Control vector
U	Set of admissible control variables
v	Vehicle longitudinal speed
V	Voltage
w	Penalty function
x	State variable
$\mathbf{x}$	State vector
X	Set of admissible state variables
y	Number of battery cells
z	Generic exponent
α	Road grade angle
$\Delta\omega$	Angular speed difference
ε	Charge-effectiveness factor
η	Efficiency
θ	Angular position
λ	Co-state variable
$\boldsymbol{\lambda}$	Co-state vector

μ	Friction coefficient
ρ	Density
σ	Cost of reaching/violating state boundaries
τ	Transmission ratio
T	Time length
ϕ	Terminal cost
ψ	Weighting factor for instantaneous cost function
Ψ	Performance index
ω	Angular speed

Subscripts and superscripts

0	Initial condition
1	First element
2	Second element
act	Actuation system element
aer	Aerodynamic resistance element
avg	Average value
b	Battery element
bea	Bearing element
br	Brakes element
BAS	BAS element
c	Clutch element
cd	Clutch disc element

cds	ICE cold start related element
$cell$	Battery cell element
chg	Battery charge element
cou	Coulombic element
CD	Clutch damper element
d	Discrete element
dis	Battery discharge element
dr	Driven element
$drag$	Drag losses element
Dr	Driving element
DCT	DCT element
DC/DC	DC/DC converter element
e	Electrical path element
ech	Electrochemical element
eng	Engaged element
eq	Equivalent element
err	Error element
es	ICE start related element
ex	Exit condition related element
EM	EM element
f	Final element (when used for indexing)
f	Fuel path element

fd	Final drive element
fil	Filtered element
g	Road grade element
gs	Gearshift related element
GB	Gearbox element
hs	Half-shaft element
hys	Hysteretic element
$idle$	Idle element
in	Inertial element
inp	Input element
inv	Inverter element
I	Integral element
ICE	ICE element
j	Generic index
k	Discrete step
lim	Limit related element
$loss$	Dissipative element
map	Map element
max	Maximum element
max/min	Peak-to-peak element
$mech$	Element of a certain mechanism
min	Minimum element

new	New element
ngs	No gearshift case element
nom	Nominal element
N	Final discrete step
o	Clutch transmissible torque element
out	Output element
OC	Open circuit element
p	Proportional element
pa	Element in parallel
pj	J^{th} phase
pre	Pre-selected element
$prev$	Previous element
ps	Primary shaft element
PTU	PTU element
QD	Quick-disconnect clutch element
$ratio$	Ratio among two variables
ref	Reference element
rel	Relative element
req	Required element
rr	Rolling resistance element
RMS	RMS element
s	Sampling related element

se	Element in series
$slip$	Slipping element
sp	Restoring element
ss	Secondary shaft element
syn	Synchronizer element
SMF	SMF element
th	Threshold
tot	Total value
u	Control element
v	Vehicle element
w	Wheel element
x	State
x	Longitudinal direction
z	Vertical direction
*	Optimal element

Chapter 1

1. Introduction

1.1 Motivation

The increasing demand seen in the last few years for improved vehicle dynamic performance and reduced fuel consumption has raised the interest in the automotive industry to explore new powertrain technologies.

The electrification of such systems provides energy efficiency benefits since it enables the possibility of performing regeneration during braking and engine downsizing [1]. Furthermore, the presence of an extra power generation device enables improvements in the overall vehicle performance [2]. However, these benefits can only be fully realized if the system is properly controlled.

In the field of transmission systems, Dual-Clutch Transmissions (DCTs) [3], [4] have been found to be good candidates to be integrated into Hybrid Electric Vehicle (HEV) powertrain architectures since they are able to combine efficiency levels similar to those seen for MTs [5] or AMTs (Automated Manual Transmissions) [6] and almost seamless gearshift operation with a high software tunability. This is done at the expense of an increased mechanical complexity when compared to the latter two transmission technologies.

Among the many aspects that could be explored regarding the electrification of DCTs, attention is focused on developing control strategies for improving vehicle dynamic performance during gearshift maneuvers and the energy management of HEVs.

The main reasons driving the research interest in the aforementioned topics will be discussed in the next paragraphs.

Integration of DCTs in HEV powertrains for vehicle dynamic performance improvement

The gearshift process must satisfy several and often conflicting requirements, *e.g.* short duration, smooth engagement and minimization of energy dissipation [7], [8].

Several previous studies have investigated gearshift quality for conventional DCTs [9]–[14] and MTs/AMTs [15]–[17] using a series of different metrics. Furthermore, research efforts have also been undertaken on exploring the integration of EMs into powertrains equipped with the mentioned transmission systems aiming at improving the vehicle dynamic performance [2], [18]–[20].

Among the different HEV architectures available, attention has been given in literature to the possibility of connecting an Electric Machine (EM) to the transmission output shaft, since this configuration enables full or partial compensation of the torque gap during gearshifts if the EM torque is properly controlled [20], [21]. In [2] an upshift control strategy is developed for a hybridized Manual Transmission (MT) in which the mentioned torque gap is successfully reduced thanks to the intervention of the EM. This controller could also be applied for hybrid powertrains equipped with AMTs. Moreover, improvements in terms of drive comfort can also be seen when the performance of the mentioned powertrain layout for the case of a H-DCT is compared to that of a conventional DCT [8].

Regarding the smoothness of the clutch re-engagement process, [22] analytically proves that the oscillations in the longitudinal vehicle acceleration generated at the clutch engagement, depend on the slip speed and acceleration at the clutch lock-up. Based on these considerations, a variety of control strategies have been proposed to reduce vibrations when the oncoming clutch is engaged using different techniques. For example, in [16] a solution based on cascaded and decoupled speed and torque control loops is proposed for a conventional AMT. Instead, in [20], an optimal controller for the clutch re-engagement phase performed with a H-AMT is discussed. The control algorithm is based on the augmentation of the reference trajectories, resulting into a homogeneous TPBVP (Two-Point Boundary-Value Problem). Moreover, a control strategy for a H-DCT is presented in [23]. The characteristics of a robust H_∞ controller are exploited to complete the speed synchronization of the Internal Combustion Engine (ICE) and the clutch driven plate.

As mentioned before, energy dissipation in the form of heat during clutch slip should be limited. This allows to reduce fuel consumption and increase component life. Several control algorithms with the objective of minimizing this form of energy dissipation during gearshift maneuvers can be found in literature for both conventional and hybrid powertrains [18], [20], [24], [25].

As it can be inferred from the previous remarks, the benefits of powertrain hybridization during gearshifts have been well established by previous works. In particular, H-DCTs are recognized as promising solutions to improve the vehicle dynamic performance. The fact that just a few publications regarding the control of such systems are available in literature presents an opportunity to undertake research efforts in that direction. Furthermore, the author is not aware of any study regarding a proper comparison of H-AMTs and H-DCTs performance, therefore, this topic is explored in the present dissertation.

Integration of DCTs into EMSs for HEV powertrains

The energy management in hybrid vehicles consists in deciding the amount of power delivered at each time instant by the onboard energy sources [1], [26]. An Energy Management Strategy (EMS), receives as inputs information coming from the vehicle (ICE speed, SOC, EM speed, etc.) together with the requests coming from the driver and process it, i.e. decides how to fulfil the power request at the wheels, to output a series of set-points to the powertrain actuators [27]. It is clear at this point that having a well-designed and properly tuned EMS is of fundamental importance to really take advantage of the capabilities that HEV powertrains have to offer.

In HEVs the control objectives are mostly integral in nature. Traditionally, EMSs are design with the goal of minimizing the total fuel consumption over a defined optimization horizon [28], [29]. However, other objectives could also be included as the reduction of pollutant emissions [30], [31] or the maximization of battery life [32], [33]. Furthermore, EMSs could be implemented to satisfy multiple and often conflicting requirements. For example, in [34] a control strategy is developed aiming at optimally tradeoff between fuel consumption and battery capacity loss while in [35], [36] the compromised is established between fuel consumption and vehicle drivability.

In order to fulfil the predefined control objectives, several EMSs can be found in literature designed using a series of different techniques. For example, rule-based approaches have been implemented in [27], [37], [38]. Numerical model based techniques can also be found in literature, e.g., Dynamic Programming (DP) [26],

[39], genetic algorithms [40] and stochastic dynamic programming [41]. On the other hand, in the realm of analytical model-based techniques, Pontryagin's Minimum Principle (PMP) [37] is one of the most widely used approaches. It has been proved that, under certain conditions, PMP gives a non-causal solution which is globally optimal [42], [43]. In addition, researchers have recently show interest in the use of convex optimization [44], [45], [46] since this approach can significantly reduce the computational time with respect to some numerical methods as DP. However, its use requires additional model approximations and discrete control variables, e.g., ICE state or the engaged gear number, cannot be included in a convex formulation [45]. In the field of real-time implementable model-based control methods, several research efforts have been dedicated to the Equivalent Consumption Minimization Strategy (ECMS) [27], [47]. This approach is implementable online since they are based on the minimization, at each time step, of a predefined cost function.

DP [48], [49], [50] is a numerical method to solve problems in which a sequence of interrelated decisions have to be taken [51]. A particular amount of attention has been given in literature to DP since is the only optimal control method capable of providing the optimal solution to problems of any complexity level within the accuracy limitations imposed by the discretization of problem variables [1]. Hence, it allows generating benchmark solutions for real-time implementable EMSs [31], [35], [52], [53]. Furthermore, despite not being real-time implementable, the results obtained with DP can be analyzed to extract rules that would allow to generate a control trajectory similar to that of the global optimal solution to the control problem at hand. However, for this method to work, an extensive calibration of the designed set of rules is needed to ensure proper results for a wide range of operating conditions [54]. Nevertheless, this approach has been successfully applied in literature for the energy management of HEVs [31], [55]–[57].

In production vehicles, EMSs must be causal since real-time implementation is required. This implies that the control actions are local in time. Moreover, other than deciding the power split among onboard energy sources, depending on the vehicle architecture, other decisions might need to be taken, e.g., the current engaged gear, ICE state, clutches states, etc. As mentioned above, approaches like the ECMS, based on the minimization of a predefined cost function, have received a lot of attention in literature due to their causal nature.

Even though ECMS was first introduced in [47] as a heuristic method derived from engineering intuition, it was later shown that under certain conditions it is equivalent to PMP [58], i.e., ECMS is able to provide the optimal solution to the energy management of HEVs. However, this depends on giving the proper value to the equivalence factor at each time instant. Considering that a real-time implementable strategy cannot retain the future driving conditions as known, an adaptation scheme for the equivalence factor should be in place to adjust the value of this parameter as driving conditions change. EMSs that perform this kind of adaptation online are referred to in literature as Adaptive Equivalent Consumption Minimization Strategy (A-ECMS) [29], [59], [60], [61].

A common issue found in EMSs that do not explicitly incorporate drivability metrics in their performance index, is that the requests sent to the powertrain actuators aiming at optimizing the onboard energy consumption may have negative effects on vehicle drivability [36]. In particular, two of the most relevant type of decisions that can potentially cause drivability issues in HEVs are [62], [63]: high frequency switching among powertrain operating points/modes, e.g., from ICE-only mode to EV-mode, and frequent gearshifts. Because of the way in which they are formulated, instantaneous minimization methods are especially inclined to provide control requests that would generate high frequency switching between operating points. The reason for this is that the cost related to several control candidates may be very similar, which makes it possible for small variations in the driving conditions to continuously favor the selection of substantially different operating points based on negligible improvements in the cost function of interest.

When fuel consumption is the main concern, requesting transient events such as gearshifts and ICE starts that would result in little to no improvement in this regard should be avoided since, in addition to the drivability issues discussed above, there is an energy loss associated to them.

Several research efforts have been dedicated to solve these issues using different approaches. In [64], [65] minimizing the overall number of ICE starts and gearshifts was included as one of the control objectives of a stochastic dynamic programming algorithm. Instead, in [27] to prevent frequent ICE starts/stops as a result of implementing ECMS, the cost function is incremented considering the fuel equivalent energy (electrical energy used to power the starter) that is required to accelerate the ICE from rest to idle speed. In addition to the energy needed to go through the ICE start process, the energy losses of ICE starts and gearshifts are considered in [66] for a powertrain equipped with an AMT. Properly accounting

for the energy needed to perform these operations allowed the developed DP formulation to minimize fuel consumption without providing a solution with frequent start/stops or the presence of gear hunting behavior.

To the best of the author's knowledge, there are not yet available EMSs in which physical considerations are used to model the energy consumption during gearshifts for DCTs. If the ICE start losses are also properly model, this would allow to develop control strategies in which these maneuvers are undertaken when it is more convenient in terms of the overall energy consumption with the extra benefit of having an EMS in which transient events are not frequently requested, thus improving also the vehicle drivability. A DP programming formulation that considers these losses would be more representative of the maximum capabilities of the HEV of interest. Hence, the analysis of the optimal solution could give insights on how to improve the currently available real-time implementable EMSs.

1.2 Contribution of the dissertation

As stated before, the primary objective of this dissertation is to investigate the integration of DCTs in HEV powertrains. The most relevant results obtained from the research efforts undertaken are briefly described in the following.

Development of gearshift control strategies for HEV powertrains equipped with AMTs or DCTs

Control algorithms for upshift and downshift maneuvers are developed for a Plug-in Hybrid Electric Vehicle (PHEV) architecture in which an EM is connected to the output of the transmission obtaining torque filling capabilities during gearshifts. Two different control logics are developed for the same vehicle depending on the type of transmission selected: AMT or DCT.

The strategies are very simple to implement and tune since they are based on the use of simple Proportional-Integral (PI) feedback controllers. Thus, transmission engineers without significant knowledge of advanced control theory will be able to use the developed tools.

The results obtained for both powertrains are promising in terms of vehicle dynamic performance. One fundamental implication of the previous remark is that the H-AMT studied has been proved capable of almost eliminating the torque gap during gearshifts while keeping the mechanical complexity of the system low with respect to its DCT counterpart. Since H-DCTs are already on the market, a comparison between these two transmission systems becomes of interest.

Implementation of DP for the energy management of HEV powertrains equipped with DCTs

A DP formulation is developed for the energy management of a PHEV equipped with a DCT. The main control objective is to minimize the overall fuel consumption during a driving mission. DCT gearshift losses and ICE start losses are considered in the DP algorithm. This allows to obtain an optimal solution to the control problem at hand in which these maneuvers are undertaken when it is more convenient in terms of the overall energy consumption. The importance of properly modeling the energy needed during these transient events is demonstrated by studying its effects on gear selection and ICE state variations. When the mentioned losses are considered, there is no gear hunting behavior or ICE state chattering in the solutions.

The results obtained can be used as a benchmark for other control strategies or to analyze the behavior of the optimal solution and derive causal EMSs from it.

Development and benchmarking of a real-time EMS for HEV powertrains equipped with DCTs

Learning from the behavior of the optimal solution, a real-time implementable EMS is developed in which gear selection in EV-mode is performed using a set of rules derived from the DP results while A-ECMS is employed to decide the powertrain operating mode and the current gear when power from the ICE is needed.

Simulation results show that, in terms of the total fuel consumption, the proposed approach does not only yield results that are close to the optimal solution but also outperforms those of the A-ECMS, a well-known EMS.

As for the DP formulation, one fundamental aspect that differentiates the causal control strategies developed here from those published in previous works, is the introduction of a model to estimate the energy consumption during gearshifts for powertrains equipped with a DCTs.

1.3 Organization of the dissertation

In order to properly illustrate how this dissertation is organized, the contents of each chapter will be briefly described in the following paragraphs.

Chapter 2: Powertrain Modeling

In this chapter, the modeling work undertaken in the dissertation is addressed in detail. The structure and capabilities of the PHEV powertrain architectures of

interest are also described. In order to assess gearshift quality and its impact on drivability, a nonlinear dynamic model of a series-parallel PHEV is developed. Two variants of this powertrain are studied, the main difference between them is in the type of transmission employed: AMT or DCT. On the other hand, a backward quasi-static model of a parallel PHEV is developed for energy management purposes. The model is designed to properly account for the energy needed to perform gearshift and ICE start operations.

Chapter 3: Gearshift Control Strategies for Hybrid Electric Vehicle Powertrains Equipped with Automated Manual Transmissions or Dual-Clutch Transmissions

In this chapter, gearshift control strategies for the two variants of the PHEV of interest are discussed: H-AMT and H-DCT. The objectives of each of the algorithm phases, the equations for computing the ICE, BAS, clutch(es) and EM torque requests are reported together with the conditions that determine the passage from one phase to the next. In addition, simulation results are presented and analyzed to illustrate the effectiveness of the control strategies. These results are also used to establish the benefits and limitations of the two transmission systems studied.

Chapter 4: The Energy Management Problem in Hybrid Electric Vehicles

In chapter 4, some of the most relevant EMSs for HEVs having as the main objective the task of reducing the overall fuel consumption during a driving mission are reviewed, setting the theoretical basis for understanding the work presented in chapters 5 and 6.

Chapter 5: Dynamic Programming Solution for the Energy Management Problem in Hybrid Electric Vehicle powertrains equipped with Dual-Clutch Transmissions

DP is used in chapter 5 to find the global optimal solution to the energy management of a parallel PHEV. The general problem formulation is given. Each state and control variable are defined and the reasons behind their introduction are explored. In addition, the way in which the modeling of the gearshift and ICE start losses are integrated into the DP formulation is described. The optimal solution obtained here is used in the next chapter for the development of real-time implementable EMSs.

Chapter 6: Real-time Energy Management Strategies for Hybrid Electric Vehicle Powertrains Equipped with Dual-Clutch Transmissions

A real-time implementable EMS is proposed in chapter 6 which combines a rule-based approach for the gear selection in EV-mode, designed from the DP results, with A-ECMS. Simulation results are presented to benchmark the mentioned causal strategy against the optimal solution and to compare its performance, in terms of

the total fuel consumption, with that of a well-known real-time implementable EMS: A-ECMS.

Chapter 7: Conclusions

The main conclusions drawn from the work presented in the previous chapters are reported here. In addition, insights are given regarding the topics in which future developments could be focused on.

Chapter 2

2. Powertrain Modeling

2.1 HEVs modeling for dynamic performance assessment

For the assessment of gearshift quality and its impact on drivability in powertrains systems with DCTs and AMTs, nonlinear dynamic models are required. The model used must be able to deal with the change in the number of kinematic Degree Of Freedom (DOF) due to variations in the clutch status (engaged/disengaged) or in the synchronizers position. Furthermore, the models should be able to properly account for the driveline components compliance and damping. In this way, the first torsional mode of the transmission is correctly estimated and an assessment of the vehicle drivability during gearshift maneuvers can be conducted [15]. Examples of nonlinear dynamic models can be found in [4], [20], [12], [16].

In this chapter, a detailed description of the model designed for dynamic performance assessment of HEVs is presented. The structure and capabilities of the powertrain of interest are also addressed. The mentioned model is used in chapter 3 for the development of gearshift control strategies.

2.1.1 Powertrain description

The vehicle of interest corresponds to the series-parallel PHEV architecture depicted in Figure 2-1. The powertrain consists of an ICE, a BAS, an EM, a battery pack and a mechanical transmission system. Two variants of this powertrain are studied, the main difference between them is in the type of transmission employed: AMT or DCT.

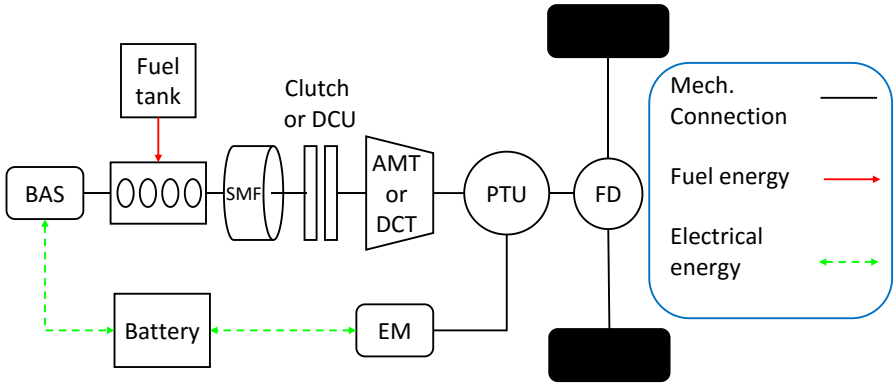

Figure 2-1. Powertrain layout.

PHEVs are characterized for being equipped with energy storage systems that are larger with respect to the ones found in regular HEVs. Given the superior dimensions of the battery pack, these components can be recharged by an external power source in addition to the energy that can be stored during vehicle operation when the EM works as a generator [38].

The proposed PHEV architecture enables the possibility of operating in several different modes. In order to obtain the highest possible tractive force at the wheels, BAS, ICE and EM can be used together to propel the vehicle, thus operating in parallel hybrid mode. Note that the ICE can produce additional power with respect to that required at the wheels, in this case, the EM or the BAS (Belt Alternator Starter) could use this extra energy to recharge the battery. On the other hand, the transmission systems considered allow to disconnect the ICE from the wheels. This enables the possibility of driving the vehicle in either series hybrid mode or EV-mode without having to drag the ICE inertia and compensate for its energy losses. In particular, the powertrain operates as a series hybrid when it uses the ICE to charge the battery through the BAS while the EM fulfils the power request at the wheels.

In the PHEV of interest, an EM is connected to the driveshaft through a mechanical coupler referred to as Power Transfer Unit (PTU). A single gear ratio is available to the electric motor. This configuration enables full or partial compensation of the torque gap during gearshifts if the EM torque is properly controlled [20], [21].

In addition to the EM connected to the transmission output, a BAS is employed to use electrical power to support the ICE in delivering the requested torque. Due to its fast response, the BAS helps on improving the control of ICE speed during gearshifts [67].

To filter torsional vibrations, a Single Mass Flywheel (SMF) is located between the ICE and the clutch (or dual-clutch unit for the DCT variant) input shaft. In addition, torsional dampers are incorporated to each clutch.

The main features of the HEV architecture described can be summarized as:

- Battery pack can be recharged by an external power source.
- Operation in ICE-only mode is possible.
- Operation in parallel hybrid mode is possible.
- Operation in series hybrid mode is possible.
- Operation in EV-mode can be undertaken with the possibility of decoupling the ICE from the wheels.
- BAS allows for better control of ICE speed during gearshifts.
- EM is connected to the output of the transmission obtaining torque filling capabilities during gearshifts.
- EM enables the possibility of performing regenerative braking.

The most relevant powertrain components specifications are shown in Table 2-1.

Table 2-1. Powertrain components specifications.

Component	**Data**
Vehicle mass	1920 kg
ICE	Diesel engine, 2.0 L, 104 kW
EM	112 kW (peak power)
BAS	32 kW (peak power)
DCT or AMT	6-speed transmission
Battery Pack	Li-ion, 18.9 kWh

2.1.2 Powertrain model overview

In this section, an overview of the HEV powertrain model developed for dynamic performance assessment is given. The main modelling assumptions and the simulator structure are described.

Both powertrain variants (with AMT or DCT) are modeled using the same assumptions.

2.1.2.1 Modeling considerations

As stated before, the models described in this section are designed to properly simulate the longitudinal vehicle dynamics with the objective of developing a tool that can be used both for control calibration and drivability assessment.

In order to achieve the mentioned goals, nonlinear dynamic models are developed based on the following considerations:

- Only vehicle longitudinal dynamics is considered.
- Zero grade is considered.
- Clutches are modeled using a LuGre dynamic friction model [68], [69].
- Clutch dampers stiffness and hysteresis characteristics are considered.
- Synchronizers torsional dynamics is modeled.
- Bearing losses are considered.

- Half-shafts stiffness and damping are considered.
- Wheels on the same axle are assumed to have the same speed.
- Pacejka'96 transient nonlinear tire model [70] is used.
- The efficiency of meshing gears is assumed to be 100 %.

The mentioned modeling considerations are addressed in more detail in section 2.1.3 where the models used for each powertrain component are described.

2.1.2.2 Model structure: AMT variant

A global layout of the model developed of the powertrain variant in which an AMT is employed can be seen in Figure 2-2.

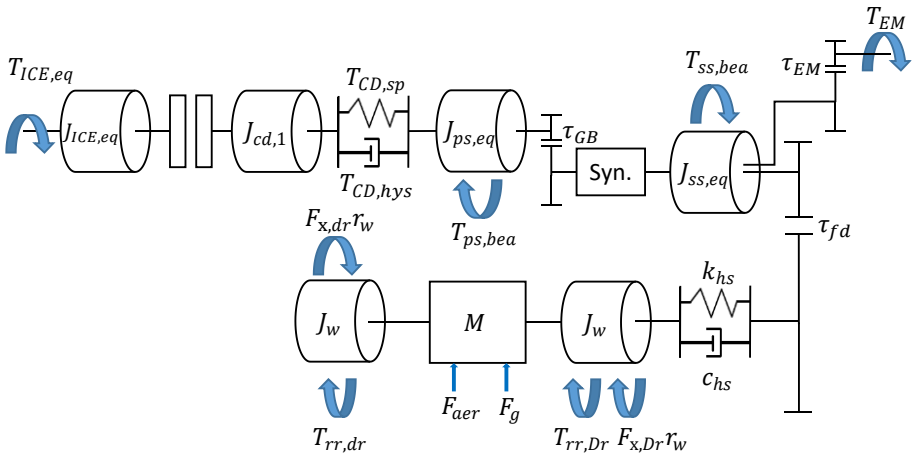

Figure 2-2. Powertrain model: AMT.

The sum of the torque coming from the ICE and the BAS $T_{ICE,eq}$ is applied to the first inertia of the system $J_{ICE,eq}$ while the EM torque T_{EM}, after being amplified by the transmission ratio of the mechanical coupler τ_{EM}, is applied to the inertia $J_{ss,eq}$.

The stiffness and hysteresis of the clutch damper interacts with the inertia $J_{cd,1}$, to which the torque passing through the clutch is applied, and with $J_{ps,eq}$. The motion of the latter is affected by the torque output of a sub-system introduced to model the torsional dynamics of the synchronizers. Note that the transmission shafts flexibility is neglected, thus only a transmission ratio τ_{GB} is interposed between $J_{ps,eq}$ and the synchronizer model. Moreover, the dissipation introduced by the

primary, secondary and differential shaft bearings, respectively $T_{ps,bea}$, $T_{ss,bea}$ and $T_{fd,bea}$ is also illustrated in Figure 2-2.

The tractive force generated by the powertrain actuators is transmitted through the half-shafts stiffness and damping characteristics to the inertia J_w. The rolling resistance $T_{rr,Dr}$ and the longitudinal forces exchanged at the driving wheel/road contact $F_{\mathrm{x},Dr}$ are also applied to this inertia. Another inertia block of the same entity is introduced to which the rolling resistance contribution $T_{rr,dr}$ and the force exchanged in the driven wheel/road contact $F_{\mathrm{x},dr}$ are applied. The link between these inertias, that represent the wheels, and the vehicle motion is established by the tire model. Furthermore, the grade and aerodynamic drag forces (F_g and F_{aer} respectively) are also considered when computing the vehicle longitudinal dynamics.

The complete mathematical formulation of the model depicted in Figure 2-2 is given in section 2.1.3.

A summary of the main model inputs and outputs is presented below.

Main inputs:

- Oncoming gear number.
- Offgoing gear number.
- Initial angular position and speed of each DOF.
- Control inputs:
  - APP
  - Torque request to ICE and BAS.
  - Torque request to EM.
  - Clutch transmissible torque request.
  - Synchronizer position request.

Main outputs:

- Angular position and speed of each DOF.

2.1.2.3 Model structure: DCT variant

A global layout of the model developed of the powertrain variant in which an DCT is employed can be seen in Figure 2-3. The complete mathematical formulation of this model is given in section 2.1.3.

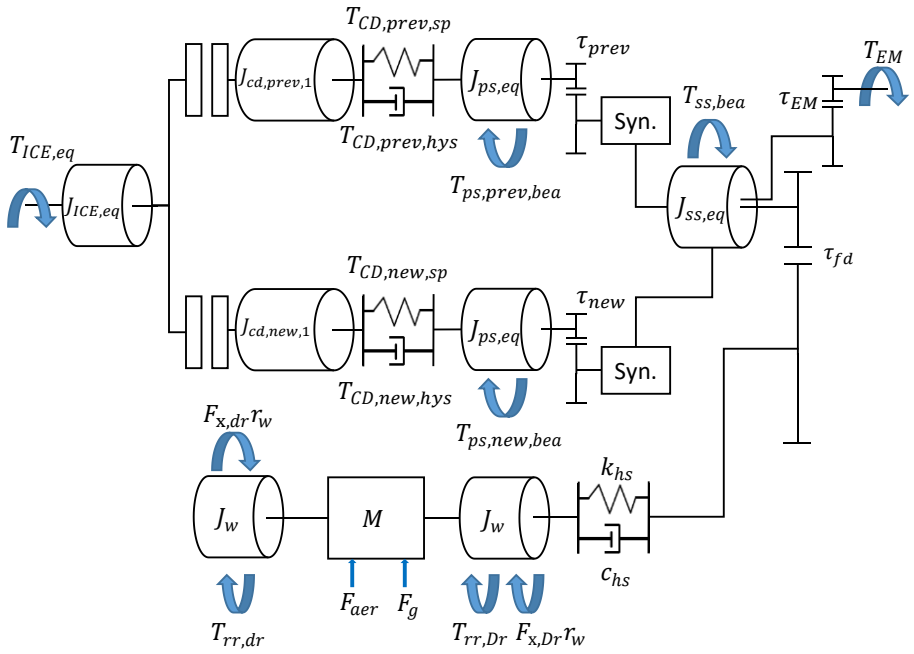

Figure 2-3. Powertrain model: DCT.

The model presented above has a similar structure with respect to the one developed for the AMT variant. The main difference between this model and the one illustrated in Figure 2-2 is in the fact that there is an additional transmission path to be considered.

A summary of the main model inputs and outputs is presented below.

Main inputs:

- Oncoming gear number.
- Offgoing gear number.
- Initial angular position and speed of each DOF.
- Control inputs:
  - APP
  - Torque request to ICE and BAS.
  - Torque request to EM.
  - Oncoming clutch transmissible torque request.
  - Offgoing clutch transmissible torque request.

Main outputs:

- Angular position and speed of each DOF.

2.1.3 Powertrain components

In this section, the modeling of the main powertrain components is described in detail.

Since the models here presented will be used to study gearshift maneuvers, the variables related to the transmission path in which the oncoming gear is located will be identified with the subscript new, instead, for the ones related to the transmission path in which the offgoing gear is mounted, the subscript $prev$ is employed.

2.1.3.1 ICE, BAS and clutch

The HEV of interest is equipped with a 2.0 L diesel engine with a maximum power output of 104 kW. Moreover, a BAS with a peak power of 32 kW is also employed.

The engine shaft dynamics is described by:

$$T_{ICE,eq}(t) - T_c(t) = J_{ICE,eq}\dot{\omega}_{ICE}(t) \tag{2-1}$$

$$J_{ICE,eq} = J_{ICE} + J_{SMF} + J_{c,mech} + J_{BAS}\tau_{BAS}^2 \tag{2-2}$$

where,

$T_{ICE,eq}(t)$ is the sum of the ICE and BAS torque.

$T_c(t)$ is the torque passing through the clutch(es).

$\dot{\omega}_{ICE}(t)$ is the angular acceleration of the crankshaft.

J_{ICE} is the ICE inertia.

J_{SMF} is the SMF inertia.

$J_{c,mech}$ is the clutch mechanism inertia.

J_{BAS} is the BAS inertia.

τ_{BAS} is the transmission ratio of the belt connecting the BAS to the crankshaft.

The torque transmitted through the clutch (or dual-clutch unit for the DCT variant) is computed using a LuGre dynamic friction model [68], [69].

The maximum and minimum torque of the ICE and the BAS are computed as a function of the crankshaft speed:

$$T_{ICE,max}(t) = f\left(\omega_{ICE}(t)\right) \tag{2-3}$$

$$T_{BAS,max}(t) = f\left(\omega_{ICE}(t)\right) \tag{2-4}$$

$$T_{BAS,min}(t) = f\left(\omega_{ICE}(t)\right) \tag{2-5}$$

2.1.3.2 Clutch damper

A torsional damper is incorporated in each of the clutches present in the driveline. These elements are modeled as a two-stage damper with piecewise linear stiffness and hysteresis.

The spring element generates a restoring torque based on a stiffness that is a function of the angular position difference between the DOF corresponding to the clutch disc (located before the damper) and the primary shaft $\theta_{cd,j}(t) - \theta_{ps,j}(t)$.

Therefore, for the offgoing gear transmission path:

$$T_{CD,prev,sp}(t) = k_{CD}(t)\left(\theta_{cd,prev}(t) - \theta_{ps,prev}(t)\right) \tag{2-6}$$

where,

$T_{CD,prev,sp}(t)$ is the restoring torque of the clutch damper.

$k_{CD}(t)$ is the clutch damper stiffness.

$\theta_{cd,prev}(t)$ is the angular position of the clutch disc.

$\theta_{ps,prev}(t)$ is the angular position of the primary shaft.

On the other hand, the energy dissipation introduced by the clutch damper is modeled using a Coulomb friction model (smoothed through a hyperbolic tangent

function) [68] based on the clutch damper hysteresis which is also a function of $\theta_{cd,j}(t) - \theta_{ps,j}(t)$:

$$T_{CD,prev,hys}(t) = T_{o,CD,hys}(t)\, tanh\left(3\frac{\omega_{cd,prev}(t) - \omega_{ps,prev}(t)}{\Delta\omega_{th,CD}}\right) \quad (2\text{-}7)$$

where,

$T_{CD,prev,hys}(t)$ is the dissipative torque of the clutch damper.

$T_{o,CD,hys}(t)$ is the clutch damper hysteresis.

$\omega_{cd,prev}(t)$ is the angular speed of the clutch disc.

$\omega_{ps,prev}(t)$ is the angular speed of the primary shaft.

$\Delta\omega_{th,CD}$ is a threshold to tune the shape of the smoothing function.

The total torque transmitted by the clutch damper is then:

$$T_{CD,prev}(t) = T_{CD,prev,sp}(t) + T_{CD,prev,hys}(t) \quad (2\text{-}8)$$

Finally, the dynamics of the clutch disc can be calculated as:

$$T_c(t) - T_{CD,prev}(t) = J_{cd,prev,1}\dot{\omega}_{cd,prev}(t) \quad (2\text{-}9)$$

where,

$J_{cd,prev,1}$ is the inertia of the clutch disc (part of its total inertia located before the damper).

$\dot{\omega}_{cd,prev}$ is the angular acceleration of the clutch disc.

The clutch damper torque and the clutch disc dynamics for the transmission path related to the oncoming gear, $T_{CD,new}(t)$ and $\dot{\omega}_{cd,new}(t)$, are computed in a similar manner. Note that for the AMT variant of this powertrain, the subscripts new and $prev$ are not needed for these variables since there is only one clutch damper and gearbox input shaft (see section 2.1.3.3).

2.1.3.3 AMT and EM

A synchronous EM with a peak power of 112 kW is connected through the PTU to the output of a 6-speed AMT.

A stick diagram of the AMT is visible in Figure 2-4. The transmission is composed of:

- A dry clutch.
- An input/primary shaft.
- Two output/secondary shafts (upper and lower) that are linked to the differential ring gear via pinion gears.
- Synchronizers mounted on the secondary shafts.

Note that the reverse gear is not represented in the figure.

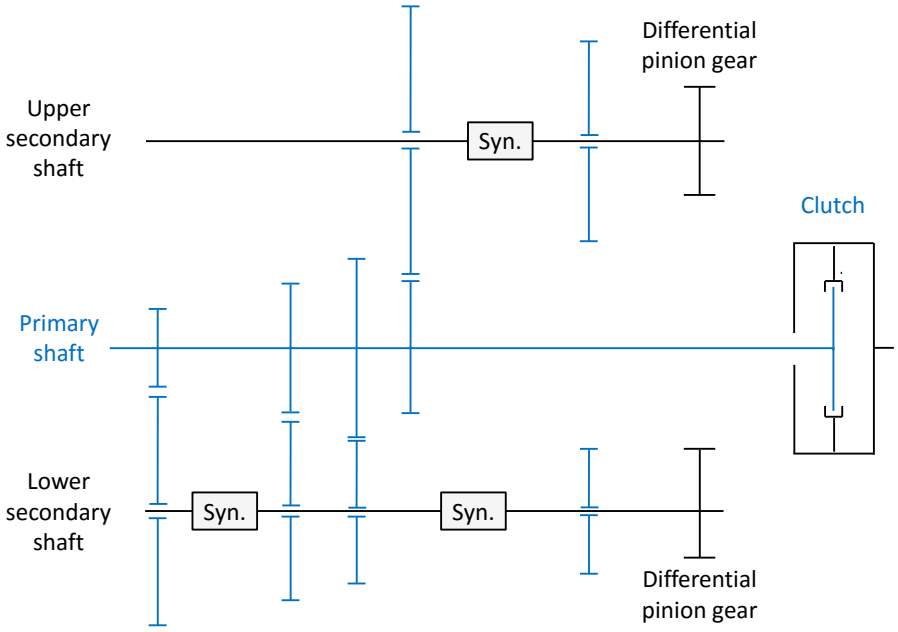

Figure 2-4. AMT schematic layout.

The primary shaft dynamics can be described as:

$$T_{CD}(t) - T_{ps,bea}(t) - \frac{T_{syn}(t)}{\tau_{GB}(t)} = J_{ps,eq}\dot{\omega}_{ps}(t) \qquad (2\text{-}10)$$

$$J_{ps,eq} = J_{ps} + J_{cd,2} \tag{2-11}$$

where,

$T_{ps,bea}(t)$ is the torque loss induced by the primary shaft bearings.

$T_{syn}(t)$ is the torque transmitted by the synchronizers.

$\tau_{GB}(t)$ is the transmission ratio according to the engaged gear.

J_{ps} is the inertia of the primary shaft.

$J_{cd,2}$ is the inertia of the clutch disc (portion located after the damper).

The bearings that support the transmission shafts introduce a torque loss (namely $T_{ps,bea}(t)$ for the primary shaft, $T_{ss,prev,bea}(t)$ and $T_{ss,new,bea}(t)$ for the secondary shafts and $T_{fd,bea}(t)$ for the differential) computed as the sum of two contributions: Coulomb friction (computed similarly to the friction losses of the clutch damper) and viscous damping.

To model the torsional dynamics of the synchronizers a switching model was developed: whenever a gear is engaged, the synchronizer is considered as a gear mesh; however, during the speed synchronization of the input and output shaft of the transmission, the synchronizer is modeled as a friction element.

The torque transmitted through the synchronizers when a gear is engaged is computed considering constant contact stiffness k_{syn} and damping c_{syn}:

$$\begin{aligned} T_{syn}(t) = \; & k_{syn}\left(\frac{\theta_{ps}(t)}{\tau_{GB}(t)} - \theta_{ss}(t)\right) \\ & + c_{syn}\left(\frac{\omega_{ps}(t)}{\tau_{GB}(t)} - \omega_{ss}(t)\right) \end{aligned} \tag{2-12}$$

where $\theta_{ss}(t)$ and $\omega_{ss}(t)$ are the angular position and speed of the secondary shaft. As mentioned before, the flexibility of transmission shafts is neglected. This implies that the motion of both secondary shafts is the same.

Instead, during the synchronization of the primary and secondary shaft, that occurs each time a new gear is to be engaged, the torque passing through the synchronizer is computed using a dynamic LuGre friction model.

Note that it is assumed for the AMT that only one synchronizer is transmitting torque at any given time.

The equation governing the secondary shaft motion is:

$$T_{syn}(t) + T_{EM}(t)\tau_{EM} - T_{ss,bea}(t) - \frac{T_{fd,bea}(t)}{\tau_{fd}} - 2\frac{T_{hs}(t)}{\tau_{fd}} = J_{ss,eq}\dot{\omega}_{ss}(t) \tag{2-13}$$

$$T_{ss,bea}(t) = T_{ss,prev,bea}(t) + T_{ss,new,bea}(t) \tag{2-14}$$

$$J_{ss,eq} = J_{ss,prev} + J_{ss,new} + J_{EM}\tau_{EM}^2 + J_{PTU} + \frac{J_{fd}}{\tau_{fd}^2} \tag{2-15}$$

where,

$T_{EM}(t)$ is the torque provided by the EM.

$T_{hs}(t)$ is the half-shaft torque.

τ_{EM} is the transmission ratio provided by the PTU.

τ_{fd} is the final ratio.

$J_{ss,j}$ is the inertia of the secondary shaft.

J_{EM} is the EM inertia.

J_{PTU} is the PTU inertia.

J_{fd} is the differential inertia.

Note that the maximum and minimum value that the EM torque can have are estimated as a function of angular speed:

$$T_{EM,max}(t) = f\left(\omega_{EM}(t)\right) \quad (2\text{-}16)$$

$$T_{EM,min}(t) = f\left(\omega_{EM}(t)\right) \quad (2\text{-}17)$$

2.1.3.4 DCT and EM

The same 112 kW synchronous EM used for the AMT variant is connected through the PTU to the output of a 6-speed DCT.

A stick diagram of the DCT is visible in Figure 2-5. This transmission system is composed of:

- A Dual-Clutch Unit (DCU) composed of dry clutches.
- Two concentric input/primary shafts (the inner one, carrying the odd driving gears, and the outer one the even driving gears).
- Two output/secondary shafts (upper and lower) that are linked to the differential ring gear via pinion gears.
- Synchronizers mounted on the secondary shafts.

Note that the reverse gear is not represented in the figure.

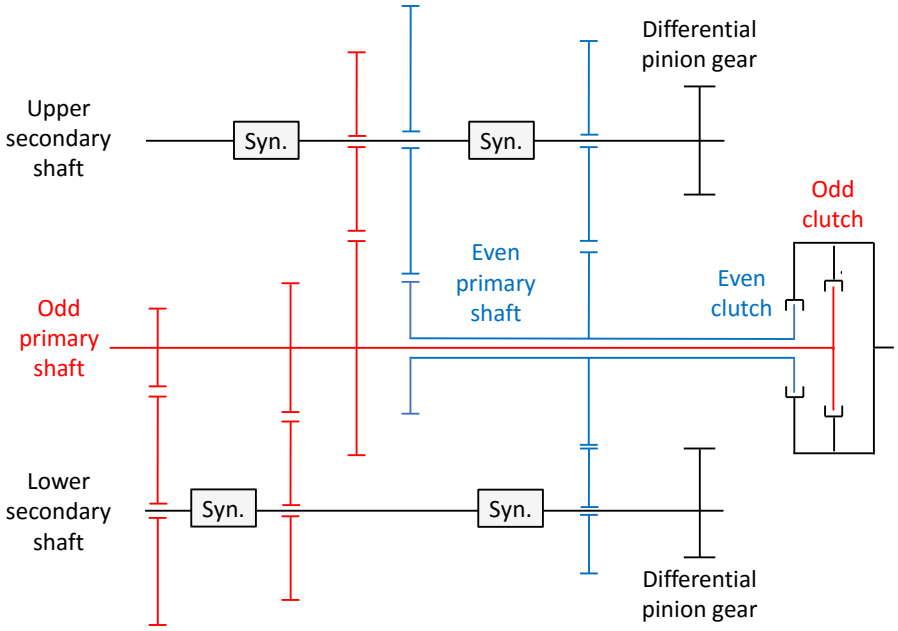

Figure 2-5. DCT schematic layout.

The similar layout seen in Figure 2-5 with respect to that of the AMT depicted in Figure 2-4 is due to the fact that the DCT studied here was designed starting from it. The fact that one transmission was derived from the other provides the opportunity of making a fairer comparison of both systems. Since several components are very similar, differences seen in the vehicle dynamic performance are more likely to be related to the functioning principle of each transmission technology.

The dynamics of the primary shafts can be described as:

$$T_{CD,prev}(t) - T_{ps,prev,bea}(t) - T_{ps,bea,rel}(t) - \frac{T_{syn,prev}(t)}{\tau_{prev}(t)} = J_{ps,prev,eq}\dot{\omega}_{ps,prev}(t) \quad (2\text{-}18)$$

$$J_{ps,prev,eq} = J_{ps,prev} + J_{cd,prev,2} \quad (2\text{-}19)$$

$$T_{CD,new}(t) - T_{ps,new,bea}(t) + T_{ps,bea,rel}(t) - \frac{T_{syn,new}(t)}{\tau_{new}(t)} = J_{ps,new,eq}\dot{\omega}_{ps,new}(t) \quad (2\text{-}20)$$

$$J_{ps,new,eq} = J_{ps,new} + J_{cd,new,2} \quad (2\text{-}21)$$

where,

$T_{ps,bea,rel}(t)$ is the torque loss introduced by the bearings located between the primary shafts.

$\tau_j(t)$ is the transmission ratio of the DCT.

$J_{cd,j,2}$ is the inertia of the clutch disc (part of its total inertia located after the damper).

The torque loss introduced by the DCT bearings is modeled as done for the AMT (see section 2.1.3.3).

Since the synchronizers of the current and oncoming gear are assumed to be engaged before the gearshift maneuvers performed with the DCT start, a friction model is not needed for these components as it was necessary for the AMT variant. Hence, the synchronizers are modeled as a gear mesh with constant stiffness and damping:

$$T_{syn,j}(t) = k_{syn}\left(\frac{\theta_{ps,j}(t)}{\tau_j(t)} - \theta_{ss}(t)\right) + c_{syn}\left(\frac{\omega_{ps,j}(t)}{\tau_j(t)} - \omega_{ss}(t)\right) \quad (2\text{-}22)$$

Note that, since the flexibility of transmission shafts is neglected, the motion of both secondary shafts is assumed to be the same.

Finally, the equation governing the secondary shaft motion is:

$$T_{syn,prev}(t) + T_{syn,new}(t) + T_{EM}(t)\tau_{EM} - T_{ss,bea}(t) - \frac{T_{fd,bea}(t)}{\tau_{fd}} - 2\frac{T_{hs}(t)}{\tau_{fd}} = J_{ss,eq}\dot{\omega}_{ss}(t) \quad (2\text{-}23)$$

$$J_{ss,eq} = J_{ss,prev} + J_{ss,new} + J_{EM}\tau_{EM}^2 + J_{PTU} + \frac{J_{fd}}{\tau_{fd}^2} \quad (2\text{-}24)$$

The EM torque limits are accounted for as explained in section 2.1.3.3.

2.1.3.5 Half-shafts

The half-shafts are modelled as linear stiffness and damping elements:

$$T_{hs}(t) = k_{hs}\left(\frac{\theta_{ss}(t)}{\tau_{fd}} - \theta_w(t)\right) + c_{hs}\left(\frac{\omega_{ss}(t)}{\tau_{fd}} - \omega_w(t)\right) \quad (2\text{-}25)$$

where,

k_{hs} is the half-shafts stiffness.

c_{hs} is the half-shafts damping coefficient.

$\theta_w(t)$ is the angular position of the driving wheels.

$\omega_w(t)$ is the angular speed of the driving wheels.

Note that for simplicity, the motion of the right and left wheel on the same axle is considered to be the same.

2.1.3.6 Wheels

The developed model has a DOF for each wheel. The Pacejka'96 transient nonlinear tire model [70] is used to compute the longitudinal forces exchanged at the wheel/road contact.

The dynamics of a single driving wheel is given by:

$$T_{hs}(t) - F_{x,Dr}(t)r_w - T_{rr,Dr}(t) = J_w\dot{\omega}_{w,Dr}(t) \tag{2-26}$$

Instead, for the driven wheels:

$$F_{x,dr}(t)r_w - T_{rr,dr}(t) = J_w\dot{\omega}_{w,dr}(t) \tag{2-27}$$

where,

$F_{x,Dr}$ and $F_{x,dr}$ are the outputs of the tire model.

$T_{rr,Dr}$ and $T_{rr,dr}$ are the rolling resistance torques.

$\dot{\omega}_{w,Dr}$ and $\dot{\omega}_{w,dr}$ are the angular acceleration of the wheels.

J_w is the inertia of a single wheel.

r_w is the tire radius.

The rolling resistance torque can be calculated as:

$$T_{rr,j}(t) = F_{z,j}(t)\left(c_{0,rr} + c_{1,rr}\frac{v^2(t)}{r_w^2}\right) \tag{2-28}$$

where,

$c_{0,rr}$ and $c_{1,rr}$ are the rolling resistance coefficients.

$v(t)$ is the vehicle longitudinal speed.

$F_{z,j}(t)$ is the vertical load acting on the tire.

Longitudinal load transfer for the estimation of the instantaneous tire vertical load is considered.

2.1.3.7 Vehicle road load

The vehicle possesses only one DOF, correspondent to the longitudinal motion.

The vehicle longitudinal dynamics is given by:

$$2F_{x,Dr}(t) - 2F_{x,dr}(t) - F_{aer}(t) - F_g(t) = Ma(t) \tag{2-29}$$

where,

M is the vehicle mass.

a is the vehicle longitudinal acceleration.

F_{aer} is the aerodynamic drag force.

F_g is the road grade force.

The aerodynamic drag force is computed as a quadratic function of the vehicle speed:

$$F_{aer}(t) = \frac{1}{2}\rho_{aer}A_v c_{aer} v^2(t) \tag{2-30}$$

where,

ρ_{aer} is the air density.

A_v is the vehicle frontal area.

c_{aer} is the aerodynamic drag coefficient.

The grade force is calculated as:

$$F_g(t) = Mg\ sin\big(\alpha(t)\big) \tag{2-31}$$

where $\alpha(t)$ is the road grade angle.

Since the road is assumed to be flat the gravitational force F_g is zero.

2.2 HEVs modeling for energy management

Model-based control strategies rely on a suitable mathematical model of the HEV powertrain of interest to provide a solution for the energy management problem. The level of complexity of the models employed is related to the predefined control objectives (see section 4.2.2 for more details). Moreover, plant simulators can also be used to assess the effectiveness of EMSs, making them an extremely valuable tool for the development of the mentioned control algorithms.

In this dissertation, since EMSs are studied aiming at minimizing the overall fuel consumption at the end of each driving schedule, the main modeling objective is to reproduce the most relevant energy flows in the HEV of interest. Hence, a low-order dynamic model of the powertrain, that considers the principal sources of energy dissipation present in the system is developed.

In this chapter, a detailed description of the model designed for the energy management of HEVs is presented. In particular, the estimation of the losses encountered in gearshifts and ICE start events is discussed. The structure and capabilities of the powertrain of interest are also addressed. The mentioned model is used in chapters 5 and 6 for both solving the energy management problem and testing the performance of the developed control algorithms.

2.2.1 Powertrain description

The vehicle of interest corresponds to the parallel PHEV architecture depicted in Figure 2-6. The powertrain consists of an ICE, an EM, a battery pack and a DCT.

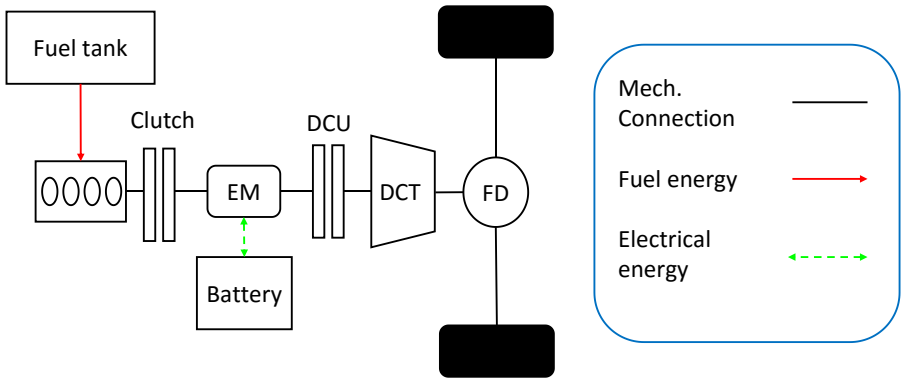

Figure 2-6. Powertrain layout.

As explained for the powertrain described in section 2.1, in addition to the energy stored during vehicle operation, PHEVs can be recharged by an external power source.

In the PHEV studied, the ICE and the EM are mounted on the same shaft that is connected to the transmission input through the DCU. Hence, it is possible to use them together to propel the vehicle. Note that the ICE could produce additional power with respect to the one required at the wheels in order for the EM to use this extra energy to recharge the battery. Moreover, a quick-disconnect dry clutch allows to separate the ICE from the wheels. This is particularly attractive when the powertrain operates in EV-mode since allows the EM to propel the vehicle without having to drag the ICE inertia and compensate for its energy losses.

Differently from the HEV architecture described in section 2.1, the configuration presented in Figure 2-6 does not provide torque-fill capabilities during gearshifts maneuvers since the EM is located before the DCU [8]. However, given the faster response time of EMs when compared to ICEs [67], this pre-transmission configuration allows for better speed control of the input side of the clutch during gearshifts [8].

The main features of the HEV architecture described can be summarized as:

- Battery pack can be recharged by an external power source.
- Operation in ICE-only mode is possible.
- Operation in parallel hybrid mode is possible.
- Operation in EV-mode can be undertaken with the possibility of decoupling the ICE from the wheels.
- EM enables the possibility of performing regenerative braking.
- EM allows for better speed control of the input side of the clutch during gearshift maneuvers.

The most relevant powertrain components specifications are shown in Table 2-2.

Table 2-2. Powertrain components specifications.

Component	**Data**
Vehicle mass	1520 kg
ICE	Gasoline engine, 1.4 L, 110 kW
EM	75 kW (peak power)
DCT	6-speed transmission
Battery Pack	Li-ion, 8.8 kWh

2.2.2 Powertrain model overview

In this section, an overview of the HEV powertrain model developed for energy management purposes is given. The main modelling assumptions and the simulator structure are described.

2.2.2.1 Modeling considerations

As stated at the beginning of section 2.2, the main modeling objective is to reproduce the most relevant energy flows in the vehicle. To accomplish this, quasi-static models [26] of the powertrain components are used in which the principal

sources of energy dissipation are considered. This last remark is important since oversimplified models may not be able to distinguish among operating points that yield to different levels of energy consumption [71].

A backward quasi-static approach [26] is adopted here for model development. The selection of such a modeling technique is explained in the next few lines.

In a backward-looking model, the computations are undertaken inverting the physical causality of the system, i.e., the model computes the required input to obtain a certain output [43]. For HEV modeling, this implies that the power required at the wheels is determined based on the velocity trace and grade profile of a predefined driving cycle. The described procedure can be very interesting for the development of EMSs since it allows the model to be used for:

- Assessment and comparison of different EMSs.
- Development of model-based EMSs (see section 4.2.2).

By using the mentioned type of simulators, no driver model is needed because the driving schedule is assumed to be followed exactly by the vehicle [1]. Quite obviously, this can be useful to assess and compare the performance of different EMSs in terms of the total energy consumption since simulation results are computed for a vehicle that follows the same trace every time.

On the other hand, considering that in most model-based control techniques it is required to estimate the total power needed at the wheels to test several possible different ways of fulfilling such request, embedded backward-looking models become necessary to perform those calculations [27], [72], [73].

Whenever a backward simulator is employed, it is required to solve an implicit differential equation. The solution of these equations may imply the need for an iterative procedure which could be computationally expensive. Hence, backward-looking simulators are usually built using simplified models [43]. Fortunately, quasi-static models have been shown in literature to be appropriate for the development of EMSs for HEVs [74]–[76]. According to the quasi-static approach, the driving cycle is divided into small time intervals and average values of speed, torque, and acceleration are considered. For the model at hand, a time step of 1 s is selected, thus neglecting the dynamics faster than 1 Hz [26], [77]. The internal dynamics of powertrain components, e.g., ICE, half-shafts, etc., is much faster than that of the main energy flows and therefore they are not considered by the model.

The following considerations were adopted for the development of a control-oriented model of the powertrain:

- Only vehicle longitudinal dynamics is considered.
- Zero grade is considered.
- Rigid shafts are assumed.
- Clutch is modeled as an ideal on/off component, thus neglecting the slipping phases except during ICE start events and gearshift maneuvers.
- Gearshift losses are considered.
- ICE start losses are considered.
- Constant gear efficiency is assumed.
- ICE and EM are modeled using efficiency maps.
- Battery is modeled using a zero-th order model [26].
- Constant inverter efficiency is considered.
- Constant power loss from the DC/DC converter is considered.
- Constant efficiency is assumed for the DC/DC converter.
- Regenerative torque is bounded by the vertical load acting on the wheels.
- Mechanical brakes are modeled as ideal torque sources.
- Powertrain components physical limitations are considered.
- Powertrain actuators response delay is neglected.
- Tires are modeled using a perfect rolling model.

The mentioned modeling considerations are addressed in more detail in the remaining sections of this chapter.

2.2.2.2 Model structure

A global layout of the model developed is visible in Figure 2-7.

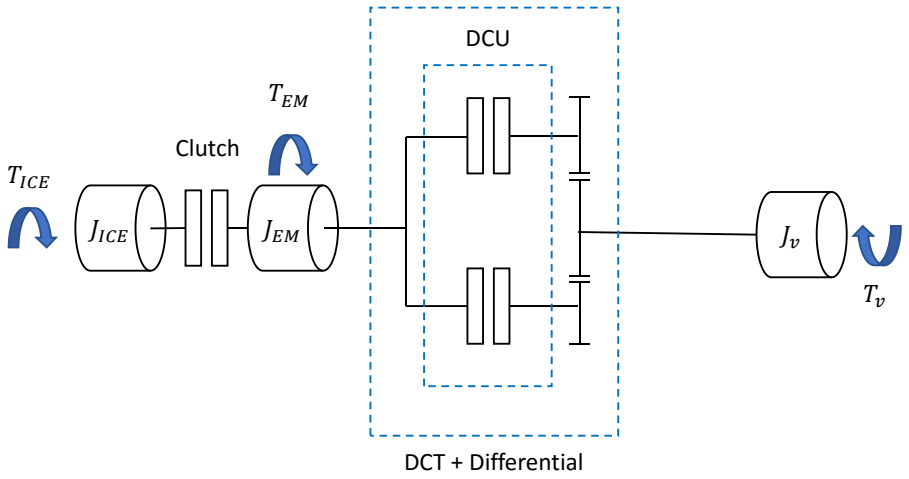

Figure 2-7. Powertrain model.

The ICE torque T_{ICE} is applied to the first inertia of the system J_{ICE} while the EM torque T_{EM} is applied to the inertia J_{EM}. When the powertrain is operating in parallel hybrid mode, the power from both power sources is transmitted, after torque multiplication according to the total transmission ratio of the engaged gear, to the vehicle equivalent inertia J_v through the DCT to satisfy the power request at the wheels represented in the figure as the torque T_v.

As mentioned in section 2.2.1, the quick-disconnect clutch allows to decouple the ICE from the rest of the driveline. It is considered as an ideal on/off element (engaged/disengaged) except during ICE start events (see section 2.2.5). The same applies to the DCU, only during gearshift events the clutches are regarded as something more than an element able to modify the number of kinematic DOFs of the system (see section 2.2.4).

A summary of the main model inputs and outputs is presented below.

Main inputs:

- Vehicle longitudinal speed.
- Vehicle longitudinal acceleration.
- Initial conditions for the state variables.
- Control inputs:
    - Torque split factor.

  - Gear command.
  - Quick-disconnect clutch command.

Main outputs:

- System states:
  - SOC.
  - Gear number.
  - Quick-disconnect clutch state.
  - ICE state.
  - EM torque counter state.
- Fuel consumption.

A description of the system states and control inputs is made in section 5.1.

2.2.3 Powertrain components

In this section, the modeling of the main powertrain components is described in detail. Further information about the models described here can be found in [26].

2.2.3.1 Vehicle road load

The vehicle model is designed to account for its longitudinal dynamics. The level of complexity of the formulation employed allows to properly estimate the power request at the wheels to follow a certain driving schedule.

If a vehicle is considered as a mass-point, the torque at the wheels T_v necessary to drive the system at a certain longitudinal speed v and acceleration a is:

$$T_v(t) = \Big(F_{rr}(t) + F_{aer}(t) + F_{in}(t) + F_g(t)\Big) r_w \qquad (2\text{-}32)$$

where $F_{in}(t)$ is the inertia force.

The aerodynamic resistance and road grade forces are computed as in section 2.1.3. On the other hand, the rolling resistance force is modeled as:

$$F_{rr}(t) = c_{rr} M g \cos\big(\alpha(t)\big) \qquad (2\text{-}33)$$

where c_{rr} is the rolling resistance coefficient.

Instead, the inertia force is:

$$F_{in}(t) = Ma(t) \tag{2-34}$$

In order to maximize the regenerative braking action, the torque request to the front axle, where the EM is able to act, will only be limited to avoid a demand higher than the torque at which the front wheels will lock-up. This torque is given by [78]:

$$T_{v,max}(t) = -\left(\frac{b_2}{l}Mg - \frac{h}{l}Ma(t)\right)\mu_w\, r_w \tag{2-35}$$

where,

l is the vehicle axle base length.

b_2 is the distance from the vehicle Center Of Gravity (COG) to the rear axle.

h is the height of the vehicle COG from the ground.

μ_w is the tire/road friction coefficient.

Therefore, the saturation of the torque request at the front axle can be seen in mathematical terms as:

$$T_v(t) = \begin{cases} T_{v,max}(t) & for\ T_v(t) > T_{v,max}(t) \\ T_v(t) & else \end{cases} \tag{2-36}$$

2.2.3.2 DCT and differential

As mentioned in section 2.2.1, the PHEV analyzed for the development of EMSs is equipped with a 6-speed DCT. The transmission has a layout which is very similar to the one presented in Figure 2-5 and therefore is not shown here.

For energy analysis, simple gear models that consider transmission ratios and constant efficiencies are employed [26]. Given that the speed ratio is established by kinematic constraints, a power loss necessarily means a reduction of the torque at the output shaft [1].

Based on the previous considerations, the following speed relations can be established:

$$\omega_{GB,out}(t) = \omega_w(t)\tau_{fd} = \frac{v(t)}{r_w}\tau_{fd} \tag{2-37}$$

$$\omega_{GB,inp}(t) = \omega_{GB,out}(t)\tau_{GB}(t) \tag{2-38}$$

where,

$\omega_{GB,out}(t)$ is the angular speed at the DCT output shaft in which the engaged gear is located.

$\omega_{GB,inp}(t)$ is the angular speed at the DCT input shaft in which the engaged gear is located.

Regarding the torque multiplication performed by DCT, it can be written for the input shaft in which the engaged gear is mounted:

$$T_{GB,inp}(t) = \frac{T_v(t)}{\tau_{GB}(t)\tau_{fd}}\eta_{GB}^{z(t)}\eta_{fd}^{z(t)} \tag{2-39}$$

$$z(t) = \begin{cases} -1 & for\ T_v(t) \geq 0 \\ 1 & else \end{cases} \tag{2-40}$$

where,

η_{GB} is the gearbox efficiency.

η_{fd} is the final drive efficiency.

2.2.3.3 EM

A synchronous EM with a peak power of 75 kW is modeled employing maps of torque and efficiency. The EM inertia is the only dynamic element considered.

According to the quasi-static approach adopted, the inertia torque is calculated at each time step based on an average value of vehicle acceleration as:

$$T_{EM,in}(t) = \dot{\omega}_{EM}(t)\, J_{EM} \tag{2-41}$$

where $\dot{\omega}_{EM}$ is the EM angular acceleration.

When a gearshift maneuver is not performed, the EM speed is assumed equal to the input speed of the DCT, which is directly linked to the wheel speed through Eq. (2-37) and Eq. (2-38), i.e.:

$$\omega_{EM}(t) = \omega_{GB,inp}(t) = \omega_w(t)\tau_{GB}(t)\tau_{fd} \tag{2-42}$$

On the other hand, the average EM speed during gearshift is estimated in a different manner, as discussed in section 2.2.4.

The efficiency of the EM is interpolated from the map presented in Figure 2-8 as a function of the EM speed ω_{EM} and torque request T_{EM}:

$$\eta_{EM}(t) = f\big(\omega_{EM}(t), T_{EM}(t)\big) \tag{2-43}$$

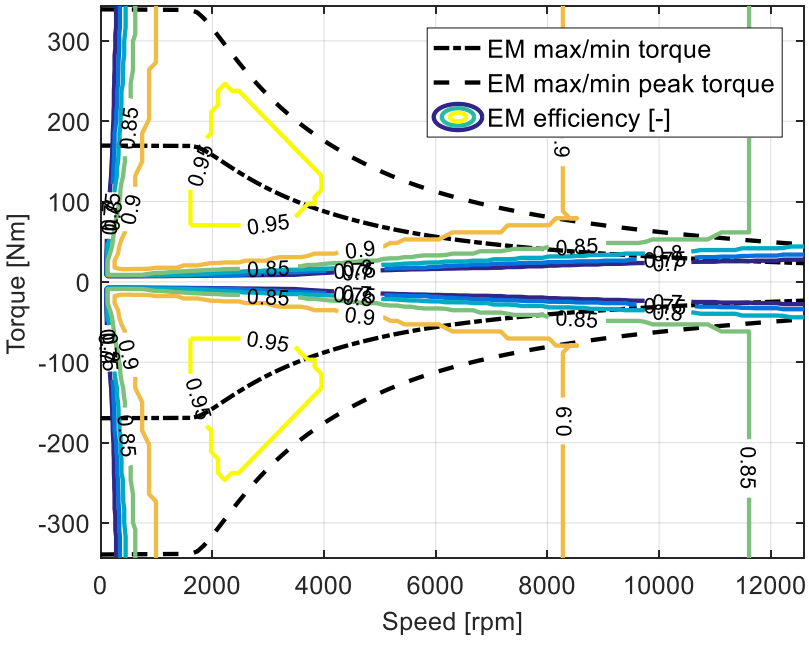

Figure 2-8. EM efficiency map.

Note that the torque request to the EM depends on how the total power request is divided among the different energy sources present onboard. This will be a subject of discussion in chapter 5.

Figure 2-8 also allows appreciating the physical limitations of the EM considered here:

- Maximum/Minimum peak torque (see Figure 2-8).
- Maximum/Minimum continuous torque (see Figure 2-8).
- Maximum/Minimum angular speed (± 12600 rpm).

In mathematical terms, the mentioned limits can be expressed as:

$$T_{EM,min}(t) \leq T_{EM}(t) \leq T_{EM,max}(t) \tag{2-44}$$

$$\omega_{EM,min} \leq \omega_{EM}(t) \leq \omega_{EM,max} \tag{2-45}$$

where,

$T_{EM,min}(t)$ is the minimum EM torque.

$T_{EM,max}(t)$ is the maximum EM torque.

$\omega_{EM,min}$ is the minimum EM angular speed.

$\omega_{EM,max}$ is the maximum EM angular speed.

Based on experimental testing results, a constraint for the use of the EM beyond its continuous torque limit is considered: if the continuous torque limit is breached for 7 consecutive seconds, 13 s must pass before the EM torque can go again above its continuous limit. This condition is set to ensure that the EM components operate on a desirable temperature range. Accordingly, either the peak or the continuous torque limit is enforced.

The maximum and minimum value to be considered for the EM torque request is estimated as a function of angular speed:

$$T_{EM,max}(t) = f\left(\omega_{EM}(t), \mathrm{T}_{EM,lim}(t)\right) \tag{2-46}$$

$$T_{EM,min}(t) = f\left(\omega_{EM}(t), \mathrm{T}_{EM,lim}(t)\right) \tag{2-47}$$

where $\mathrm{T}_{EM,lim}(t)$ is a counter used to select whether to enforce the peak or the continuous torque limit (see chapter 5).

Finally, the EM power can be computed as described in Eq. (2-48). Note that, for convenience, all the other sources of energy consumption in the electrical path are included in the expression. This implies that Eq. (2-48) can also be regarded as the power request at battery terminals $P_b(t)$.

$$P_{EM}(t) = P_b(t) = \begin{cases} T_{EM}(t)\,\omega_{EM}(t)\,\eta_{EM}(t)^{z(t)}{\eta_{inv}}^{z(t)} + P_{DC/DC} + P_{DCT,act,avg} + P_{DCT,act,gs} & for\ gs = 1 \\ T_{EM}(t)\,\omega_{EM}(t)\,\eta_{EM}(t)^{z(t)}{\eta_{inv}}^{z(t)} + P_{DC/DC} + P_{DCT,act,avg} & for\ gs = 0 \end{cases} \tag{2-48}$$

where,

gs is the gearshift status. It is equal to 1 when a gearshift is performed, otherwise, it is set to 0.

η_{inv} is the inverter efficiency.

$P_{DC/DC}$ is the power drawn of the DC/DC converter.

$P_{DCT,act,avg}$ is the average power drawn of the DCT actuation system.

$P_{DCT,act,gs}$ is the power consumed by the DCT actuation system each time a gearshift is performed.

In the former equation, $z(t)$ has the same meaning as in Eq.(2-40), the only difference is that it now depends on the sign of T_{EM} instead of T_v.

From an experimental assessment of the power consumption of the DCT actuation system, it was concluded that the electric power required during vehicle operation could be approximated by an average power drawn $P_{DCT,act,avg}$ and a component that is only considered when a gearshift is performed $P_{DCT,act,gs}$.

A high-pressure accumulator is a fundamental component of the DCT actuation system. The mentioned accumulator must be re-filled multiple times during vehicle operation by a motor-driven pump. The clutch fill events undertaken during

gearshift maneuvers, together with the leakage present in the actuation system, represent the main reason why it is necessary to re-fill the high-pressure accumulator. In order to account for the power required to perform such operations the term $P_{DCT,act,gs}$ is introduced.

On the other hand, according to data recorded during vehicle testing, the DC/DC converter energy losses can be considered by means of a constant power drawn. Furthermore, the efficiency of the inverter was also tuned using experimental data.

2.2.3.4 Battery

The model of a Li-ion battery pack with a capacity of 8.8 kWh (26.5 Ah) is studied in this section.

In general, the modeling of battery dynamics is not trivial since the main variables needed to characterize its behavior, e.g., state of charge, voltage, current, etc., are dynamically related to each other in a highly nonlinear fashion [1].

Since the main objective of the EMSs developed in chapters 5 and 6 is the minimization of the total fuel consumption over a drive mission, the battery model must be able to properly estimate the variation of the energy stored during vehicle operation [42], [71].

The state of charge (SOC) is defined as the amount of electrical charge stored in the battery relative to the total charge capacity:

$$SOC(t) = \frac{Q(t)}{Q_{nom}} \tag{2-49}$$

where,

Q_{nom} is the nominal charge capacity.

$Q(t)$ is the amount of charge stored.

The SOC dynamics is given by:

$$\dot{SOC}(t) = \frac{\dot{Q}(t)}{Q_{nom}} = -\frac{I(t)}{Q_{nom}} \tag{2-50}$$

where $I(t)$ is the battery current.

Since the current is considered positive during discharge, the minus sign in the former equation accounts for the expected reduction in SOC.

Battery models based on equivalent circuits are preferred for control applications [79]. This models the battery current and voltage to the power at battery terminals seen by the other powertrain components. For HEVs energy management, when fuel consumption reduction is the only objective, a control-oriented zero-th order equivalent circuit model [26] has been widely used in literature [42], [60], [80]. Figure 2-9 shows a depiction of the mentioned model.

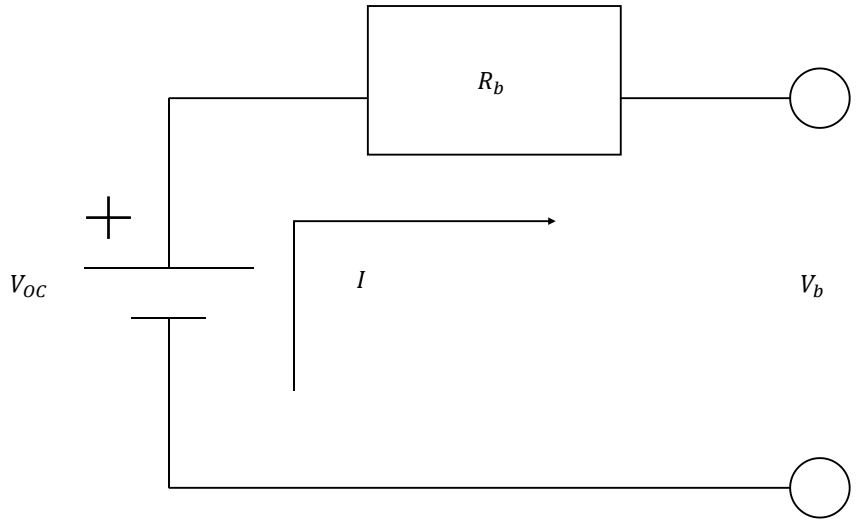

Figure 2-9. Zero-th order equivalent circuit model of the battery.

Applying Kirchhoff's voltage law to the circuit shown in Figure 2-9, the battery voltage can be written as:

$$V_b(t) = V_{OC}\big(SOC(t)\big) - R_b\big(SOC(t)\big)I(t) \tag{2-51}$$

where,

$V_{OC}\big(SOC(t)\big)$ is the battery Open Circuit Voltage (OCV).

$R_b\big(SOC(t)\big)$ is the battery internal resistance.

Hence, the power at battery terminals is:

$$\begin{aligned} P_b(t) &= V_b(t)I(t) \\ &= V_{OC}\big(SOC(t)\big)I(t) \\ &\quad - R_b\big(SOC(t)\big)I^2(t) \end{aligned} \tag{2-52}$$

or

$$P_b(t) = V_b(t)I(t) = -\frac{V_b^2(t) - V_{OC}\big(SOC(t)\big)V_b(t)}{R_b\big(SOC(t)\big)} \tag{2-53}$$

If the current is written as a function of battery power:

$$\begin{aligned} &I(t) \\ &= \eta_{cou}\frac{V_{OC}\big(SOC(t)\big) - \sqrt{V_{OC}^2\big(SOC(t)\big) - 4P_b(t)R_b\big(SOC(t)\big)}}{2R_b\big(SOC(t)\big)} \end{aligned} \tag{2-54}$$

where the coulombic efficiency η_{cou} is a constant only considered during charging.

The physical limits of the battery must be included in the model in order for it to be used for control purposes.

Eq. (2-53) allows appreciating that the battery power is zero for $V_b(t) = 0$ and $V_b(t) = V_{OC}\big(SOC(t)\big)$. For voltage values within that range, the power is positive and thus its curve has a maximum [26]. Setting to zero the derivate of the battery power with respect to the voltage yields a condition for the maximum discharge power which can be expressed according to:

$$P_{b,max}\big(SOC(t)\big) = \frac{V_{OC}^2\big(SOC(t)\big)}{4R_b\big(SOC(t)\big)} \tag{2-55}$$

On the other hand, negative power values would increase (in absolute terms) indefinitely with the battery voltage [26]. Hence, battery power is limited imposing a maximum value for the voltage which can be seen in terms of a minimum charge current:

$$I_{min}\big(SOC(t)\big) = \frac{V_{OC}\big(SOC(t)\big) - V_{b,max}}{R_b\big(SOC(t)\big)} \tag{2-56}$$

with the maximum battery voltage,

$$V_{b,max} = V_{cell,max}\, y_{se} \tag{2-57}$$

where,

y_{se} is the number of battery cells in series.

$V_{cell,max}$ is the maximum battery cell voltage (4.8 V).

Therefore, the minimum battery power can be expressed as:

$$\begin{aligned} &P_{b,min}\big(SOC(t)\big) \\ &= \Big(V_{OC}\big(SOC(t)\big) \\ &- R_b\big(SOC(t)\big) I_{min}\big(SOC(t)\big)\Big)\, I_{min}\big(SOC(t)\big) \end{aligned} \tag{2-58}$$

As it can be appreciated in the former set of equations, both the OCV and the battery internal resistance are modeled as a function of the SOC [43], [60].

The internal resistance of the battery pack can be calculated as:

$$R_b\big(SOC(t)\big) = \begin{cases} \dfrac{R_{cell,dis}\big(SOC(t)\big)\, y_{se}}{y_{pa}} & for\ P_b \geq 0 \\ \dfrac{R_{cell,chg}\big(SOC(t)\big)\, y_{se}}{y_{pa}} & else \end{cases} \tag{2-59}$$

where,

$R_{cell,dis}\big(SOC(t)\big)$ is the internal resistance of battery cells during discharge.

$R_{cell,chg}(SOC(t))$ is the internal resistance of battery cells during charge.

y_{pa} is the number of battery cells in parallel.

Regarding the OCV, for the entire battery pack can be written that:

$$V_{OC}(SOC(t)) = \begin{cases} V_{OC,cell,dis}(SOC(t))\, y_{se} & for\ P_b \geq 0 \\ V_{OC,cell,chg}(SOC(t))\, y_{se} & else \end{cases} \quad (2\text{-}60)$$

where,

$V_{OC,cell,dis}(SOC(t))$ is the OCV of battery cells during discharge.

$V_{OC,cell,chg}(SOC(t))$ is the OCV of battery cells during charge.

Figure 2-10 shows the variation of the OCV of battery cells with the SOC.

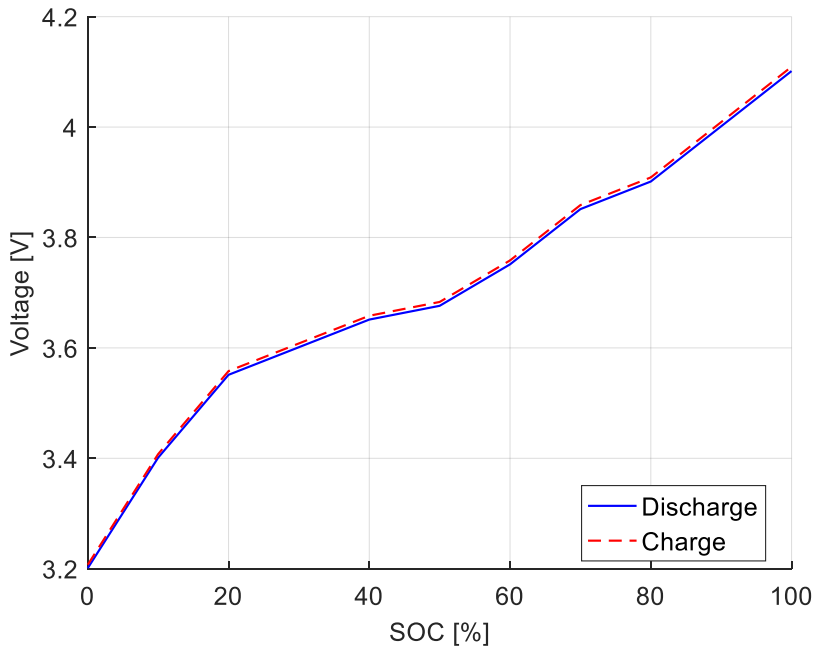

Figure 2-10. Cell OCV.

Instead, Figure 2-11 presents the cell internal resistance.

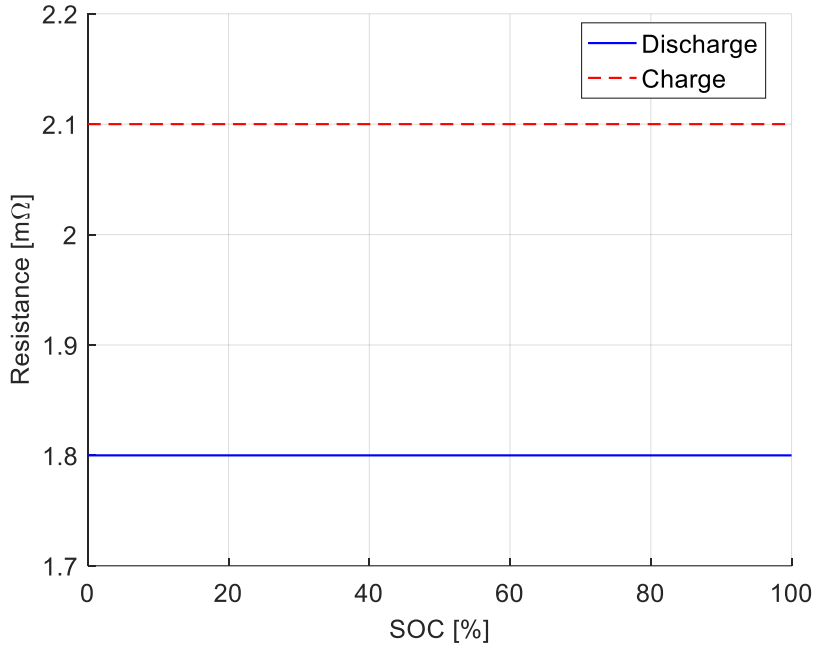

Figure 2-11. Cell internal resistance.

2.2.3.5 ICE

The HEV of interest is equipped with a 1.4 L in-line four-cylinder spark ignition gasoline engine with a maximum power output of 110 kW.

As for the EM, the ICE is modeled using torque and efficiency maps and the only dynamic element considered is the ICE inertia.

The torque needed to accelerate the engine is computed as:

$$T_{ICE,in}(t) = \dot{\omega}_{ICE}(t)\, J_{ICE} \tag{2-61}$$

When the quick-disconnect clutch is engaged, the ICE speed is assumed equal to that of the EM, i.e., $\omega_{ICE}(t) = \omega_{EM}(t)$. However, during ICE start events, the average speed considered is calculated in a different manner, as discussed in section 2.2.5.

The efficiency of the ICE is represented by means of the fuel consumption map presented in Figure 2-12 as a function of the ICE speed ω_{ICE} and torque request T_{ICE}:

$$\dot{m}_f(t) = f\left(\omega_{ICE}(t), T_{ICE}(t)\right) \tag{2-62}$$

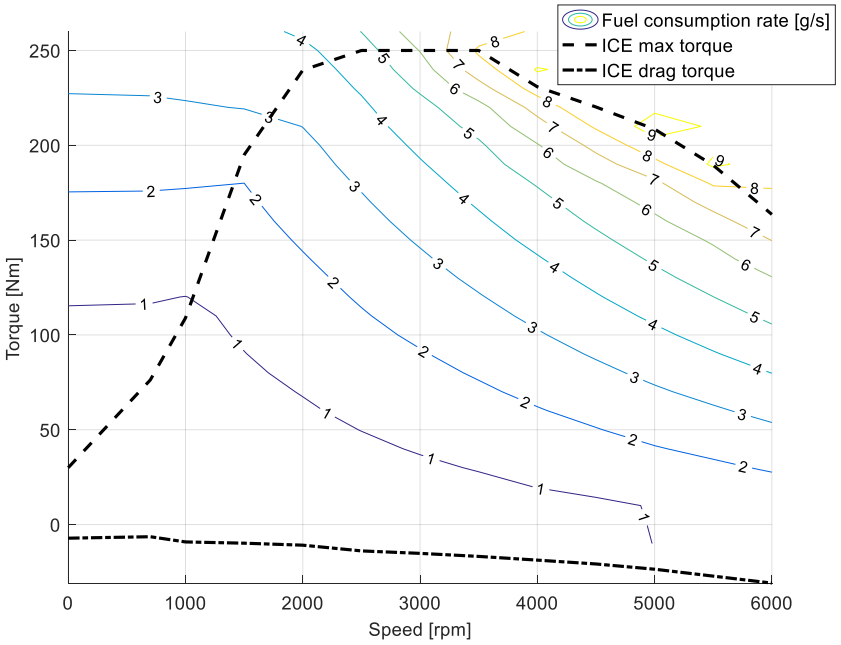

Figure 2-12. ICE fuel flow rate map.

ICE efficiency/consumption maps are built experimentally letting the component reach a steady-state condition and measuring power input/output. This procedure is repeated for several operating points until the desired map is built. As it can be inferred from the way the maps are created, the results obtained may not be accurate during transients. Nevertheless, this approach has been widely used because it allows to properly estimate fuel consumption during vehicle operation as confirmed by experimental experience [81]. The reason behind the effectiveness of such a simple model lies on the fact that most of the energy flows in a HEV are associated with the slower system dynamics [82].

Note that the torque request to the ICE is a control input determined as explained in chapter 5.

Figure 2-12 also allows appreciating the maximum ICE torque as a function of speed. The physical limitations of the ICE considered here are:

- Maximum torque (see Figure 2-12).
- Minimum torque: cut-off torque (5 Nm).

- Maximum angular speed: red line speed (6000 rpm).
- Minimum angular speed: idle speed (700 rpm).

In mathematical terms, the mentioned limits can be expressed as:

$$T_{ICE,min} \leq T_{ICE}(t) \leq T_{ICE,max}(t) \tag{2-63}$$

$$\omega_{ICE,idle} \leq \omega_{ICE}(t) \leq \omega_{ICE,max} \tag{2-64}$$

where,

$T_{ICE,min}$ is the minimum ICE torque.

$T_{ICE,max}(t)$ is the maximum ICE torque.

$\omega_{ICE,idle}$ is the ICE idle speed.

$\omega_{ICE,max}$ is the maximum ICE angular speed.

The maximum torque available from the ICE and its drag torque can be interpolated from the data indicated in Figure 2-12:

$$T_{ICE,max}(t) = f\big(\omega_{ICE}(t)\big) \tag{2-65}$$

$$T_{ICE,drag}(t) = f\big(\omega_{ICE}(t)\big) \tag{2-66}$$

2.2.4 DCT gearshift losses modeling

As it will be addressed later in section 4.7, frequently requesting transient events, such as gearshifts and ICE starts, negatively affects drive quality. The approach generally used to reduce the frequency and overall number of gearshifts maneuvers, resulting from the implementation of a certain EMS, is to introduce into the control algorithm a fixed cost associated to them [64], [65]. On the other hand, some studies have used physical considerations to achieve that same objective. For example, in [66] the energy losses of undertaking a gearshift process are computed for a HEV equipped with an AMT.

Properly accounting for the energy needed to perform gearshift operations allows to develop control strategies in which these maneuvers are undertaken when it is convenient in terms of the overall energy consumption with the extra benefit of

having an EMS that is not characterized by a gear hunting behavior that would have negative effects on vehicle drivability.

In this section, a simplified approach to estimate the energy losses when changing gears in the DCT of interest is described. This modeling of the energy dissipated is implemented into the EMSs developed in chapters 5 and 6 which, to the best of the author's knowledge, has not been done in previous studies for this type of transmissions.

2.2.4.1 Model overview

The estimation of the energy losses associated to gearshifts relies on a simplified model of the powertrain of interest. The same modeling assumptions discussed in section 2.2.2.1 apply, thus allowing to compute the energy dissipation of gearshift maneuvers without considerably increasing the computational burden of the calculations. In particular, it is worth mentioning that when solving the optimal control problem at hand by means of DP or ECMS, as explained in sections 4.4 and 4.6, several solution candidates are tested at each iteration, therefore, it is convenient to have tools that allow to perform each of these calculations as fast as possible while maintaining the desired level of accuracy.

A summary of the main inputs and outputs of the model developed to estimate the gearshift losses is presented below.

Main inputs:

- Torque request at the wheels.
- Vehicle speed.
- Vehicle acceleration.
- Oncoming gear number.
- Offgoing gear number.

Main outputs:

- EM speed.
- Total torque request to powertrain components.

In the following paragraphs, the mathematical formulation used is presented and then the assumptions made regarding the speed and torque trajectories of the DCT components are described.

2.2.4.2 Energy request calculation

In this paragrahp, the set of equations needed to estimate the energy request to the powertrain actuators during gearshifts is presented. The speed profiles of the EM and the two clutches togheter with the torque profiles of each clutch are assumed to be known inputs for the expressions presented in this section.

The simplified powertrain model for energy analysis shown in Figure 2-7 is used in Figure 2-13 to illustrate the calculations performed.

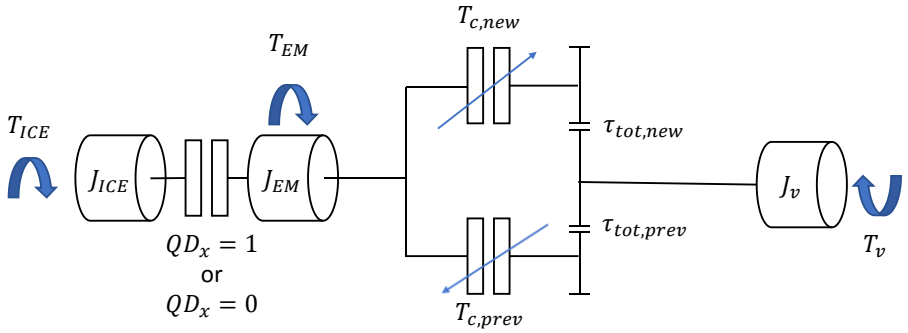

Figure 2-13. Powertrain model: gearshifts energy request.

Based on the developed model, the total torque passing through the DCU $T_c(t)$ and the torque applied to the wheels $T_{hs}(t)$ can be written as:

$$T_c(t) = T_{c,prev}(t) + T_{c,new}(t) \tag{2-67}$$

$$T_{hs}(t) = T_{c,prev}(t)\tau_{tot,prev}(t) + T_{c,new}(t)\tau_{tot,new}(t) \tag{2-68}$$

where,

$T_{c,prev}(t)$ is the torque passing by the offgoing clutch.

$T_{c,new}(t)$ is the torque passing by the incomimg clutch.

$\tau_{tot,prev}(t)$ is the total transmission ratio according to the offgoing gear.

$\tau_{tot,new}(t)$ is the total transmission ratio according to the oncoming gear.

The total transmission ratios are computed as:

$$\tau_{tot,prev}(t) = \tau_{prev}(t)\tau_{fd} \tag{2-69}$$

$$\tau_{tot,new}(t) = \tau_{new}(t)\tau_{fd} \tag{2-70}$$

Moreover, the total inertia torque considered depends on whether or not the quick-disconect clutch status QD_x is open ($QD_x = 0$) or closed ($QD_x = 1$), thus it can be written:

$$T_{in,tot}(t) = \begin{cases} T_{ICE,in}(t) + T_{EM,in}(t) & for\ QD_x = 1 \\ T_{EM,in}(t) & else \end{cases} \tag{2-71}$$

From the power equilibrium at the two clutches the following expressions are found:

$$T_{c,prev}(t)\omega_{EM}(t) = T_{c,prev}(t)\omega_{c,prev}(t) + P_{c,prev,loss}(t) \tag{2-72}$$

$$T_{c,new}(t)\omega_{EM}(t) = T_{c,new}(t)\omega_{c,new}(t) + P_{c,new,loss}(t) \tag{2-73}$$

Note that in Eq. (2-72) and Eq. (2-73) the fact that $\omega_{EM}(t) \neq \omega_{c,j}(t)$ implicates that a certain amount of energy is dissipated. Hence, $P_{c,prev,loss}(t)$ and $P_{c,new,loss}(t)$ represent the slip power losses of each of the two clutches which in general can be computed based on the clutch slip velocity $\omega_{c,j,slip}(t)$ as:

$$P_{c,j,loss}(t) = \omega_{c,j,slip}(t)T_{c,j}(t) \tag{2-74}$$

Finally, the total power request can be expressed as:

$$P_{tot,gs}(t) = T_{in,tot}(t)\omega_{EM}(t) + T_c(t)\omega_{EM}(t) \tag{2-75}$$

In Eq. (2-75) all the variables needed to compute the total power request are known since thanks to the torque and speed profiles assumed $T_{in,tot}(t)$ and $T_c(t)$ can be found trhough Eq. (2-71) and Eq. (2-67) respectevely. Hence, the total energy request is determined by integration:

$$E_{tot,gs}(t) = \int_0^{T_s} P_{tot,gs}(t)\, dt \tag{2-76}$$

Based on the overall energy needed to perform the gearshift maneuver, a mean torque request is elaborated and sent to the EMS in place which has the task of deciding how to divide it among the onboard power generation devices. Hence, the total torque request is:

$$T_{tot,gs}(t) = \frac{\frac{E_{tot,gs}(T_s)}{T_s}}{\bar{\omega}_{EM}} \tag{2-77}$$

where $\bar{\omega}_{EM}$ is the mean speed of the EM during the gearshift process. As mentioned in section 2.2.3.3, this value will be considered for $\omega_{EM}(t)$ instead of the speed computed in Eq. (2-42) each time a gearshift is requested by an EMS.

In the next paragraph, simulation results for downshift and upshift maneuvers are presented. This will allow to illustrate the assumptions made regarding the speed and torque trajectories of DCT components during both types of gearshifts.

2.2.4.3 Simulation results

Upshift and downshift maneuvers in DCTs are addressed in detail in chapter 3 where the level of complexity of the dynamic models described in section 2.1 enables their use for vehicle drivability assessment.

According to the quasi-static approach adopted for energy management purposes, a constant vehicle acceleration is assumed at each time step and shaft flexibility is neglected. Keeping in mind these modeling considerations and the observations made in chapter 3, the gearshift process is simplified here to obtain toque and speed profiles for the DCT components that allow to easily compute the energy consumption resulting from upshift and downshift maneuvers.

Downshifts

Figure 2-14 illustrates a 2nd to 1st downshift process. Since rigid shafts are assumed, the velocity of both clutches is given by the wheel speed. Furthermore, another linear profile is assumed for the EM shaft (DCU input shaft) considering that, at the end of the inertia phase, its speed increases until a small positive slip

velocity (5 rad/s) is reached. This allows to transmit positive power through both clutches during the torque phase.

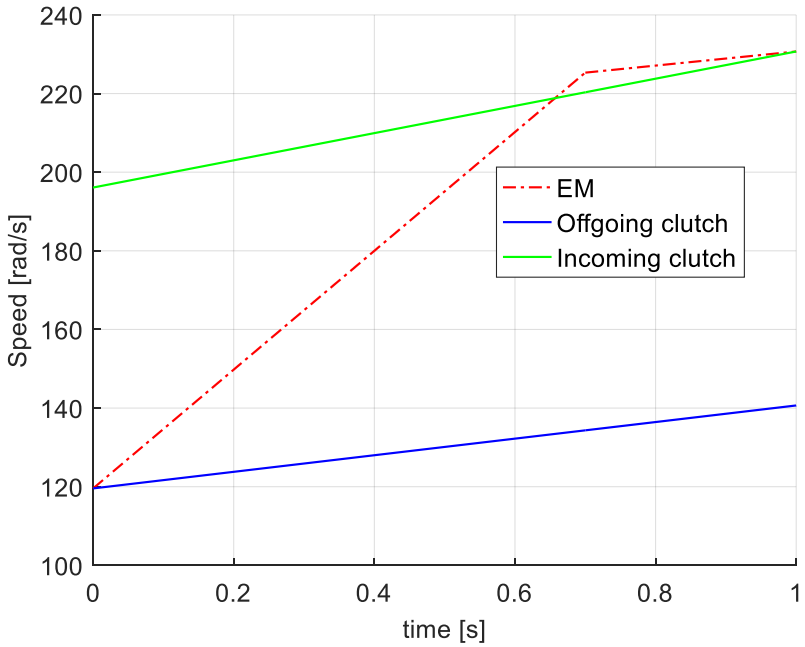

Figure 2-14. Gearshift speed profiles: downshift.

On the other hand, in Figure 2-15 the torque passing through the clutches is presented. During the inertia phase, the oncoming clutch is completely open and the torque requested at the wheels is transmitted by the offgoing clutch. Instead, during the torque phase, the latter is completely disengaged while the other is closed. Note that the torque trajectories assumed for the second part of the gearshift process are computed in order to satisfy the power request at the wheels at all times.

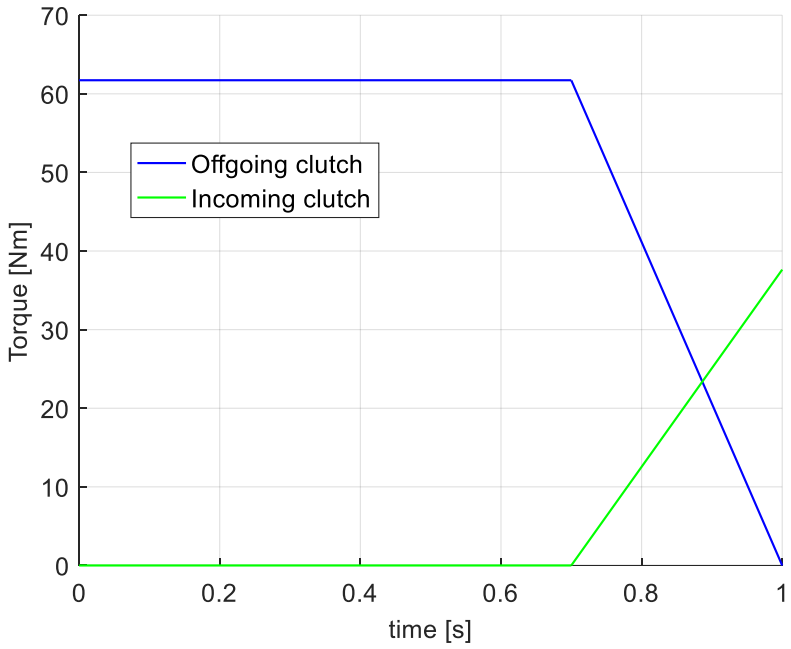

Figure 2-15. Gearshift torque profiles: downshift.

Based on the speed and torque profiles presented in the last two figures, it is possible to compute the energy consumed during the gearshift process using the set of equations provided in section 2.2.4.2. Figure 2-16 illustrates how this energy is distributed. It can be appreciated that the amount of energy dissipated due to clutch slip is not negligible. For this maneuver, it is slightly higher than the one needed to accelerate the powertrain components.

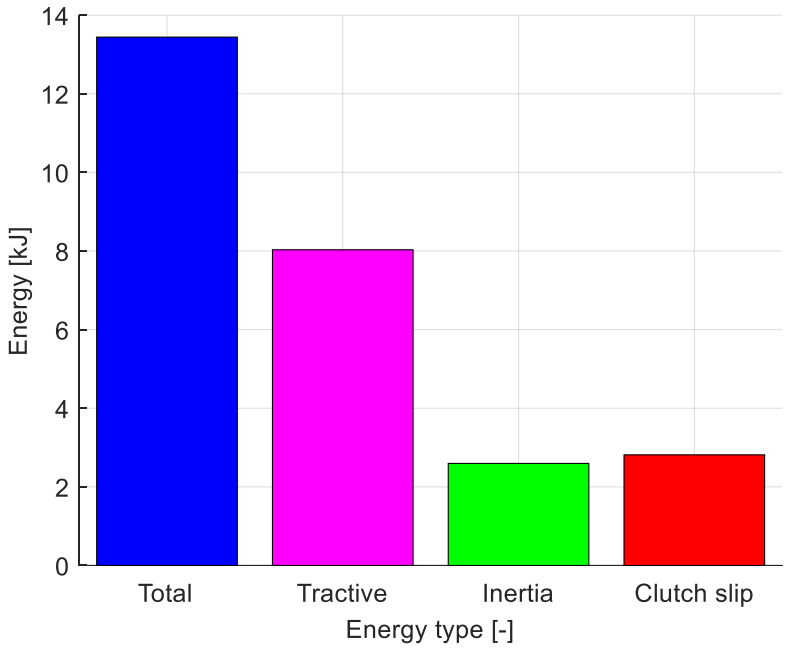

Figure 2-16. Gearshift energy: downshift.

Upshifts

Figure 2-17 depicts a 1st to 2nd upshift maneuver. Again, the velocity of the clutches can be estimated based on the wheel speed. On the other hand, during the torque phase, which happens before the inertia phase for an upshift, a small constant positive slip velocity (5 rad/s) is assumed for the EM shaft. Once the offgoing clutch is fully disengaged (see Figure 2-18), this speed is set to decrease linearly until it matches that of the oncoming clutch.

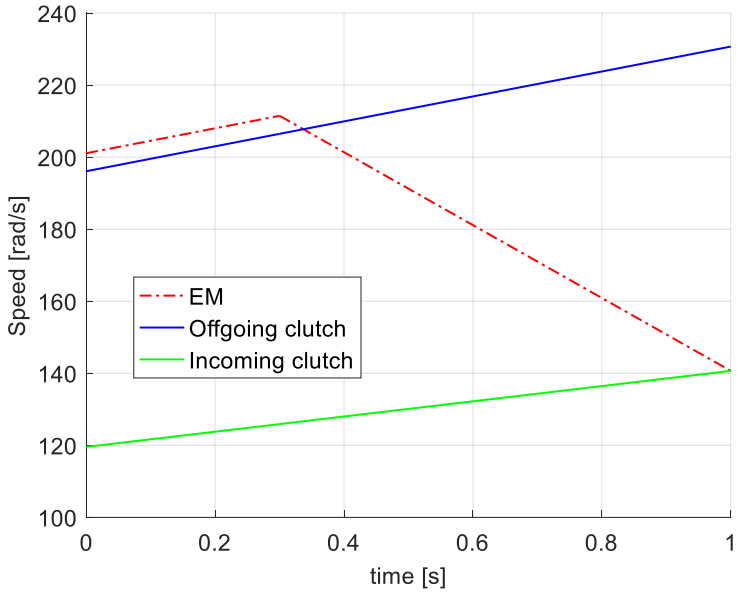

Figure 2-17. Gearshift speed profiles: upshift.

Besides the fact that the torque and inertia phase happen in a different order, the same considerations made for downshifts regarding the torque passing through the clutches still apply. Figure 2-18 presents the assumed torque profiles.

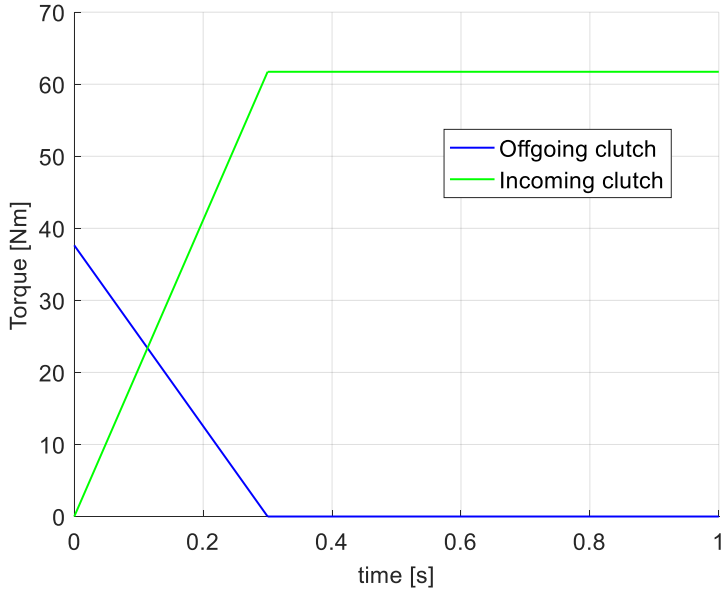

Figure 2-18. Gearshift torque profiles: upshift.

As shown in Figure 2-19, the need to decrease the speed of the EM shaft helps on reducing the total energy requested.

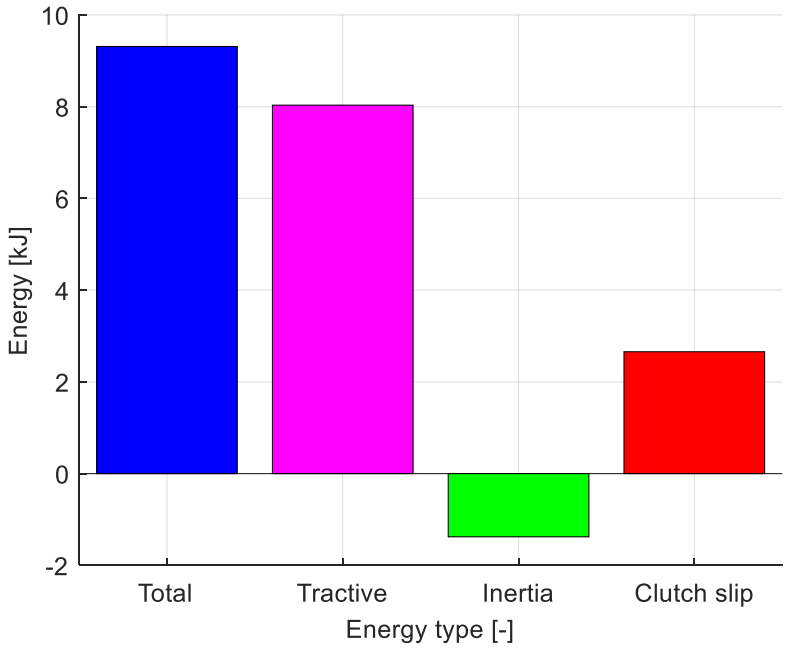

Figure 2-19. Gearshift energy: upshift.

A final remark is made here regarding the torque request at the wheels. Note that according to the speed profiles assumed for upshifts and downshifts, only positive torque can be transmitted through both clutches. To avoid complicating the calculations needed to determine the energy consumption of gearshifts, it is assumed that a negative torque request at the wheels will be provided by the mechanical brakes if a gearshift is being performed ($T_c(t) = 0$), i.e., regenerative braking with the EM is not possible during gearshifts. The implications of this fact are addressed in chapter 5.

2.2.5 ICE start losses modeling

As discussed in section 2.2.4 for gearshift maneuvers, requesting frequent transient events should be avoided since, in addition to deteriorate the vehicle drivability, there is an energy loss associated to them. This observation also applies to ICE starts.

Properly accounting for the energy needed to start the ICE enables model-based EMSs to determine when it is more convenient to perform these operations in order

to minimize fuel consumption. A similar approach to the one proposed in [66] is described here to estimate the amount of energy employed during ICE start events.

2.2.5.1 Model overview

The modeling of the energy required to start the ICE was performed with the objective of integrating this calculation into EMSs for HEVs. Hence, the level of complexity of the computations involved is limited based on a compromise between the necessity of evaluating several solution candidates to the energy management problem at hand and the desire to properly estimate the amount of energy being used.

The ICE start losses calculation is done dividing the whole process into two consecutive phases:

- Phase I: Accelerate the ICE to idle speed.
- Phase II: ICE and EM speed match.

Each of these phases is addressed in the next paragraph.

For simplicity, the following assumptions are made for ICE starts:

- There won't be a gearshift in the same time step in which the ICE is started.
- The ICE cannot be used to satisfy the torque request at the wheels during its start process.

A summary of the main inputs and outputs of the model for ICE start losses estimation is presented below.

Main inputs:

- Vehicle speed.
- Vehicle acceleration.
- Gear number.

Main outputs:

- ICE speed.
- Torque request to ICE.
- Extra torque request to EM.

In the following paragraphs, the mathematical formulation used is presented and then simulation results are provided to illustrate how the ICE start process is being modeled.

2.2.5.2 ICE start phases

Each of the two phases in which the ICE start process is divided are described in this section. As for the gearshift losses modeling, assumptions are made regarding the speed profiles of powertrain components (see section 2.2.5.4). For this reason, the speed of the ICE and the EM are considered as inputs for the equations presented here.

Phase I: Accelerate the ICE to idle speed

Since in the powertrain of intrest there is not a conventional starter, the ICE needs to be accelerated by the torque passing trough the quick-disconet clutch until its idle speed is reached ($P_{ICE}(t) = 0$ during this phase). This implies that the EM will be providing the necessary power.

The set of equations needed to model the first phase of the ICE start process is presented bellow. The expressions are written assuming positive slip velocity in the quick-disconnect clutch when the EM is spining faster than the ICE.

Since the ICE is off, its dynamics is given by:

$$J_{ICE}\dot{\omega}_{ICE}(t) = T_{QD}(t) - T_{ICE,drag}(t) \tag{2-78}$$

Considering that the quick-disconet clutch is slipping during this phase, the following expression holds for the torque transmitted through it:

$$T_{QD}(t) = T_{o,QD}(t)\, sgn\big(\omega_{EM}(t) - \omega_{ICE}(t)\big) \tag{2-79}$$

with $T_{o,QD}(t)$ being the clutch transmissible torque.

Note that the speed of the EM needs to be higher than that of the ICE for positive torque to be passing through the quick-disconnet clutch.

From the power equilibrium at the quick-disconet clutch, the power loss due to clutch slipping can be computed from:

$$T_{QD}(t)\omega_{EM}(t) = T_{QD}(t)\omega_{ICE}(t) + P_{QD,loss}(t) \quad (2\text{-}80)$$

The extra power request to the EM (to be added to the torque needed to move the vehicle) is determined using the next expression in which $T_{QD}(t)$ is calculated from Eq. (2-78) based on the speed profile assumed for the ICE.

$$P_{EM,es}(t) = T_{QD}(t)\omega_{EM}(t) \quad (2\text{-}81)$$

Phase II: ICE and EM speed match

Since by the beginning of phase II the ICE has reached its idle speed, this component could be used to speed match itself with the EM. Hence, the ICE dynamics is described as:

$$J_{ICE}\dot{\omega}_{ICE}(t) = T_{QD}\left(t_{p1,f}\right) + T_{ICE}(t) - T_{ICE,drag}(t) \quad (2\text{-}82)$$

with t_{p1f} being the time length of phase I.

The quick-disconnect clutch transmissible torque is kept constant until the speed of the EM and the ICE are equal, afterwards it is fully closed. Therefore, the power requests to the system prime movers are:

$$P_{ICE}(t) = T_{ICE}(t)\omega_{ICE}(t) \quad (2\text{-}83)$$

$$P_{EM,es}(t) = T_{QD}\left(t_{p1,f}\right)\omega_{EM}(t) \quad (2\text{-}84)$$

where $T_{ICE}(t)$ is computed using Eq. (2-82).

In case the torque passing through the clutch at the end of phase I is higher than the torque required for the speed match, instead of opening the clutch again (to keep $T_{ICE}(t)$ higher than zero), the ICE start process is undertaken using the EM, i.e.:

$$J_{ICE}\dot{\omega}_{ICE}(t) = T_{QD}(t) - T_{ICE,drag}(t) \quad (2\text{-}85)$$

$$P_{ICE}(t) = 0 \quad (2\text{-}86)$$

$$P_{EM,es}(t) = T_{QD}(t)\omega_{EM}(t) \quad (2\text{-}87)$$

2.2.5.3 Energy request calculation

In adition to the power requested at the wheels, a certain amount of energy is needed from the EM during ICE starts that can be estimated as:

$$E_{EM,es}(t) = \int_0^{T_s} P_{EM,es}(t)\, dt \tag{2-88}$$

from which a mean torque is computed:

$$T_{EM,es}(t) = \frac{\frac{E_{EM,es}(T_s)}{T_s}}{\bar{\omega}_{EM}} \tag{2-89}$$

where $\bar{\omega}_{EM}$ is the mean speed of the EM that can be derived from the wheel speed trhough the total gear ratio.

On the other hand, the total energy request to the ICE is:

$$E_{ICE}(t) = \int_0^{T_s} P_{ICE}(t)\, dt \tag{2-90}$$

The mean total torque request to the ICE is then:

$$T_{ICE}(t) = \frac{\frac{E_{ICE}(T_s)}{T_s}}{\bar{\omega}_{ICE}} \tag{2-91}$$

where $\bar{\omega}_{ICE}$ is the mean speed of the ICE. As mentioned in section 2.2.3.5, this value will be considered for $\omega_{ICE}(t)$ each time an ICE start is requested by an EMS.

In the next paragraph, simulation results are presented that will allow to illustrate the modeling of the ICE start process and the speed profiles assumed.

2.2.5.4 Simulation results

An ICE start process realized in 2nd gear is described here. Figure 2-20 shows the speed profiles of the ICE and the EM. For the ICE, a linear speed trajectory is assumed, that goes from zero to idle speed during phase I and from there to the EM speed at the end of the current time step.

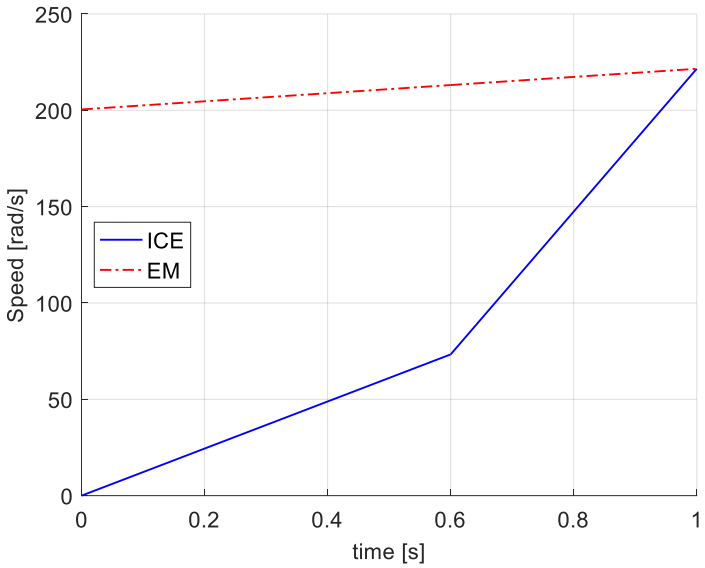

Figure 2-20. ICE start speed profiles.

Figure 2-21 shows how the total energy request is being distributed. The EM provides most of the energy while the ICE is used only in phase II. As in the gearshift simulation results presented in section 2.2.4, the energy dissipation due to clutch slip is not negligible.

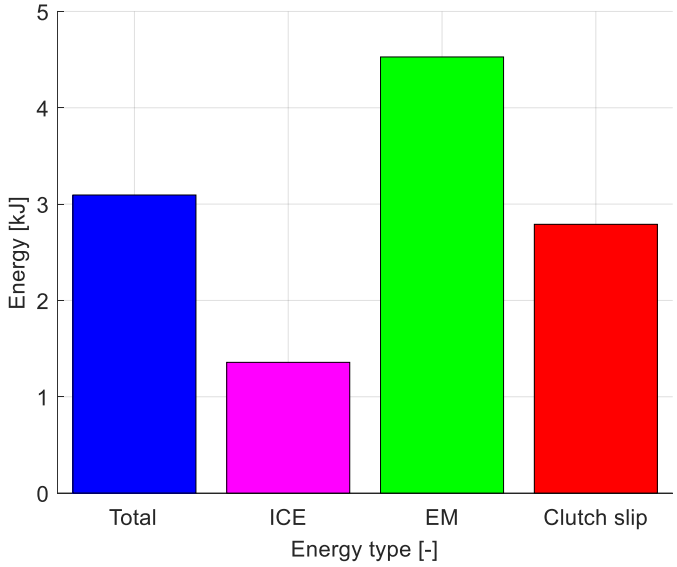

Figure 2-21. ICE start energy.

2.3 Summary

In this chapter, the modeling work undertaken in this dissertation is addressed in detail. The structure and capabilities of both the HEV powertrain architectures of interest are also described. The models here developed are designed to serve as a tool for one of these two main tasks:

- Vehicle dynamic performance assessment.
- Energy management of HEV.

For the assessment of gearshift quality and its impact on drivability, a nonlinear dynamic model of a series-parallel PHEV is developed. Two variants of this powertrain are studied, the main difference between them is in the type of transmission employed: AMT or DCT. In both vehicles, an EM is connected to the driveshaft through a mechanical coupler. This configuration enables full or partial compensation of the torque gap during gearshifts if the EM torque is properly managed as explained in chapter 3 where the model is used for the development of gearshift control strategies.

In the model, the compliance and damping of the main powertrain components is accounted for. Moreover, due to the way in which clutches and synchronizers are simulated, the models are able to deal with the change in the number of driveline kinematic DOF due to variations in the clutch status (engaged/disengaged) or in the synchronizers position. Thanks to these features, the first torsional mode of the driveline is correctly estimated and an assessment of the vehicle drivability during gearshift maneuvers can be conducted.

On the other hand, a low-order dynamic model of a parallel PHEV that considers the principal sources of energy dissipation present in the system is also developed. The mentioned model is used in chapters 5 and 6 for both solving the energy management problem and testing the performance of the designed control algorithms.

A backward quasi-static approach is adopted here to develop models for energy management purposes. This type of models is useful to assess and compare the performance of different control strategies in terms of the total energy consumption since simulation results are computed for a vehicle that follows the same trace every time. Moreover, considering that in most model-based control techniques it is

required to estimate the total power needed at the wheels to test several possible different ways of fulfilling such request, embedded backward-looking models become necessary to perform those calculations

Properly accounting for the energy needed to perform gearshift and ICE start operations allows to develop control strategies in which these maneuvers are undertaken when it is convenient in terms of the overall energy consumption with the extra benefit of having an EMS in which transient events are not frequently requested. As explained in this chapter, that would have negative effects on vehicle drivability. Therefore, a simplified approach to estimate the energy losses when changing gears in the DCT of interest is developed. This modeling of the energy dissipated is implemented into the EMSs developed in chapters 5 and 6 which, to the best of the author's knowledge, has not been done in previous studies for this type of transmissions. Furthermore, the model designed for the estimation of the energy consumption during ICE start events is also described. As for the gearshift losses, this model was integrated into the EMSs studied.

Chapter 3

3. Gearshift Control Strategies for Hybrid Electric Vehicle Powertrains Equipped with Automated Manual Transmissions or Dual-Clutch Transmissions

3.1 Metrics for gearshift quality assessment

The gearshift process must satisfy several and often conflicting requirements, *e.g.* short duration, smooth engagement and minimization of energy dissipation [7], [8]. Several previous studies have investigated gearshift quality for conventional and hybrid powertrains using a series of different metrics [24], [83], [84].

Considering the increasing demand for improved vehicle dynamic performance and reduced energy consumption that the automotive industry has experienced in recent years, the metrics employed in this dissertation to assess gearshift quality are selected to allow an objective evaluation of the developed control strategies performance regarding the fulfillment of the mentioned requirements.

In the following paragraphs each of the metrics used are described.

3.1.1 Shift comfort

Generally speaking, longitudinal acceleration is the main parameter used to evaluate vehicle drivability [36]. During gearshifts, the vehicle longitudinal acceleration variation should be as smooth as possible. Hence, the metric used to judge drive comfort will be jerk, *i.e.*, the derivative of acceleration [85], as done in [15], [8].

When evaluating vehicle drivability using its longitudinal acceleration, the usual practice is to only consider frequencies equal or lower than 10 Hz [86], [87]. This can be justified by the fact that the different parts of the human body have resonant frequencies in the 1 to 10 Hz range [88].

Based on the previous considerations, a filter is applied to the vehicle longitudinal acceleration before computing jerk. The filter used is a 3rd order lowpass digital Butterworth filter with a cutoff frequency of 10 Hz. Once jerk is computed, it is used to calculate the two parameters considered here to assess shift comfort:

- Jerk Root Mean Square (RMS) value: $Jerk_{RMS}$.
- Maximum and minimum jerk peak difference: $Jerk_{max/min}$.

The Jerk RMS value has been used in several studies to evaluate the effects of gearshift control strategies on vehicle drivability [19], [23]. This parameter can be computed as:

$$Jerk_{RMS}(t) = \sqrt{\frac{1}{t_f}\int_{t_0}^{t_f} Jerk^2(t)\, dt} \tag{3-1}$$

where,

$Jerk(t)$ is the derivative of the vehicle longitudinal acceleration.

t_f is the final time.

t_0 is the initial time.

In addition, another parameter used to assess the overall smoothness of the vehicle longitudinal acceleration is the maximum and minimum jerk peak difference seen during the entire gearshift process [15], i.e.:

$$Jerk_{max/min} = Jerk_{max} - Jerk_{min} \tag{3-2}$$

$Jerk_{max}$ is the maximum jerk value.

$Jerk_{min}$ is the minimum jerk value.

3.1.2 Vehicle performance

In terms of vehicle performance, it is desirable to complete the gearshift maneuver as fast as possible while satisfying the torque request expressed by the driver. Hence, three parameters are considered to assess the vehicle performance:

- Gearshift duration: t_{gs}.
- Mean vehicle longitudinal acceleration: $\bar{a}$.
- Mean torque error: $\overline{T}_{w,err}$.

To quantify how well is the torque request at the wheels being satisfied, the absolute difference between this value and the total torque at the transmission output reported at the wheels is computed as a percentage of the torque request. i.e.:

$$T_{w,err}(t) = \left| \frac{T_{w,req}(t) - T_{w,tot}(t)}{T_{w,req}(t)} \right| 100 \tag{3-3}$$

where,

$T_{w,req}(t)$ is the torque request at the wheels.

$T_{w,tot}(t)$ is the total torque at the transmission output reported at the wheels.

Note that a higher T_{err} means worse performance. Once this value is calculated, the mean can be taken and used to assess the gearshift performance.

As explained in section 2.1, two variants of the same powertrain are studied in this chapter. The main difference between the two is in the transmission system

employed: AMT or DCT. In Eq. (3-3), the total torque at the gearbox output reported at the wheels must be computed differently for each transmission layout.

For the powertrain variant with the AMT, it can be written:

$$T_{w,tot}(t) = \left(T_c(t)\tau_{GB}(t) + T_{syn}(t) + T_{EM}(t)\tau_{EM}\right)\tau_{fd} \tag{3-4}$$

where,

τ_{fd} is the final ratio.

$\tau_{GB}(t)$ is the transmission ratio of the current engaged gear.

τ_{EM} is the gear ratio of the mechanical coupler (see section 2.1.1).

$T_c(t)$ is the torque passing by the clutch.

$T_{EM}(t)$ is the EM torque.

$T_{syn}(t)$ is the torque transmitted through the synchronizers.

Instead, for the DCT variant:

$$T_{w,tot}(t) = \left(\sum_j T_{c,j}(t)\,\tau_j + T_{EM}(t)\tau_{EM}\right)\tau_{fd} \tag{3-5}$$

where,

j is the index identifying each transmission path (see section 2.1.3.4).

$\tau_j(t)$ is the transmission ratio of either the oncoming or the offgoing gear.

$T_{c,j}(t)$ is the torque passing by each clutch.

3.1.3 Shift efficiency

Energy dissipation in the form of heat during clutch slip should be limited to reduce fuel consumption and increase component life. Several control algorithms with the

objective of minimizing this form of energy dissipation during gearshift maneuvers can be found in literature [18], [20], [24], [25].

In the present work, the total clutch energy loss is considered as a parameter to assess shift efficiency. The energy dissipated by the clutch(es) is computed as the integral of the power loss:

$$E_{c,loss}(t) = \int_{t_0}^{t_f} \sum_j T_{c,j}(t)\omega_{c,slip,j}(t)\, dt \tag{3-6}$$

where $\omega_{c,slip,j}(t)$ is the clutch angular slip velocity.

Note that this parameter is also a measure of durability (clutch wear).

3.1.4 Torque fill energy consumption

As explained in section 2.1.1, in the PHEV of interest, an EM is connected to the driveshaft through a mechanical coupler. This configuration enables full or partial compensation of the torque gap during gearshifts if the EM torque is properly controlled [20], [21].

It was noticed in simulation that a significant variable to understand the differences between the capabilities of the two powertrain variants studied was the mechanical energy required to the EM in order to fulfil the torque request at the wheels. This will be further discussed in section 3.6.

The mechanical energy required to the EM is computed as:

$$E_{EM}(t) = \int_{t_0}^{t_f} T_{EM}(t)\omega_{EM}(t)\, dt \tag{3-7}$$

where $\omega_{EM}(t)$ is the EM angular speed.

3.2 Torque request during gearshifts

If the powertrain does not produce as much power as expected, this is perceived by the driver as a symptom of poor vehicle drivability [36]. During gearshift maneuvers, the torque delivered to the wheels should reflect the driver's intentions expressed in terms of the Accelerator Pedal Position (APP) [23].

In order to ensure a fast powertrain response to driver inputs, the torque request at the wheels is calculated as if the oncoming gear was engaged since the beginning of the gearshift, i.e.:

$$T_{w,req}(t) = T_{new}(t)\tau_{new}\tau_{fd} \tag{3-8}$$

where,

$T_{new}(t)$ is the torque request at the transmission input according to the oncoming gear.

τ_{new} is the transmission ratio of the oncoming gear.

In the remainder of this chapter, the variables related to the transmission path in which the oncoming gear is located will be identified with the subscript new, instead, for the ones related to the transmission path in which the offgoing gear is mounted, the subscript $prev$ is employed.

The torque request at the transmission input corresponds to the torque that would be provided by the ICE if the requested gear was already engaged. The Engine Control Unit (ECU) receives a percentage based torque request, e.g., APP, and processes this input to generate the actual torque request [89].

$$T_{new}(t) = ICE_{map}(APP(t), \omega_{ss}(t)\tau_{new}) \tag{3-9}$$

where,

$\omega_{ss}(t)$ is the speed of the transmission output shaft(s).

APP is the APP.

ICE_{map} is a stationary torque map in which the output is a function of the APP and crankshaft speed.

The transition between the torque request at the wheels computed considering the transmission ratio of the offgoing gear and the one determined in Eq. (3-8) is smoothed by means of a first order transfer function. As it is illustrated by the simulation results in section 3.6.3, the value of the time constant could be adjusted to modify the trade-off between powertrain responsiveness and jerk intensity.

3.3 Gearshift control for HEV powertrains equipped with AMTs

In this section, a gearshift control strategy designed for the PHEV powertrain equipped with an AMT described in section 2.1 is presented. First, a general description of the algorithm is provided in which its structure and main outputs are discussed. Then, each of the phases of the control strategy is explained in detail.

3.3.1 Algorithm overview

The gearshift control strategy for the AMT variant of the HEV powertrain of interest is designed aiming at reducing as much as possible the oscillations in the vehicle longitudinal acceleration while satisfying the driver's torque request in the shortest possible time.

The controller design in this study is carried out separating the entire gearshift process into six consecutive phases in analogy with what it is shown in [16] and [15] for a traditional AMT and a TGF-AMT respectively.

The mentioned gearshift phases are:

- Phase I: Go-to-slip.
- Phase II: Opening the clutch completely.
- Phase III: Disengage current gear / Speed synchronization / Engage new gear.
- Phase IV: Prepare to start closing the clutch.
- Phase V: Clutch slip control for engagement.
- Phase VI: Close the clutch completely.

Exit conditions for each of these phases are established and used to switch between consecutive phases.

The designed controller relies only on speed measurements that are usually available in commercial vehicles:

- ICE angular speed.
- Transmission input shaft angular speed.
- Transmission output shaft angular speed.

On the other hand, the controller output signals are:

- Torque request to EM.
- Torque request to ICE.
- Clutch transmissible torque request.
- Synchronizer position request.

In order to satisfy the request to the ICE, the BAS will produce the maximum torque; the remaining power necessary to fulfill the request will be supplied by the ICE. In addition, the clutch transmissible torque request is translated into a position command to the clutch actuator. Instead, a synchronizer position request will trigger the intervention of the low-level controllers responsible for either disengaging the offgoing gear or bringing the oncoming synchronizer to the sure engaged position (see section 3.3.2.3).

The maximum and minimum physical torque limitations of the ICE, BAS and EM are considered when creating the controller output signals. Furthermore, the response delay of powertrain actuators is also taken into account. In particular, for the ICE and the EMs, first order systems are considered [67], [89], [90], [91]. The time constant used for the ICE is significantly larger than those used for the EM and the BAS [67]. On the other hand, a rate limit is considered for the clutch transmissible torque variation [8]. The main parameters employed to model the mentioned response delays are:

- Rate limit for clutch transmissible torque variation: ±4000 Nm/s.
- Time constant for ICE: $2.7/\omega_{ICE}(t)$ with $\omega_{ICE}(t)$ being the ICE angular speed in rad/s.
- Time constant for EM and BAS: 0.0013 s.

3.3.2 Algorithm phases

In this section, each of the phases of the proposed control algorithm (see Figure 3-1) are described in detail. In particular, the main objective, control outputs and exit conditions established for each phase are discussed.

3.3.2.1 Phase I: Go-to-slip

The gearshift process starts once the gearshift request is validated by the Transmission Control Unit (TCU). The goal of this phase is to reduce the offgoing clutch transmissible torque until slippage starts while meeting the torque request.

This phase can be considered as a preparation stage before the actual gearshift maneuver starts. It was seen in simulation for the two powertrain architectures studied that requesting the torque computed in Eq. (3-9) before the offgoing clutch starts to slip could result in undesirable driveline oscillations. Hence, during phase I, the torque request at the transmission input is computed based on the transmission ratio of the offgoing gear as:

$$T_{prev}(t) = ICE_{map}\left(APP(t), \omega_{ss}(t)\tau_{prev}\right) \tag{3-10}$$

where τ_{prev} is the transmission ratio of the offgoing gear.

For all the other phases the torque request is computed as explained in section 3.2.

Control outputs

Clutch transmissible torque request

The clutch transmissible torque is ramped towards zero:

$$T_{o,c}(t) = T_{o,c,max} - \frac{T_{o,c,max}}{t_{p1}}t \tag{3-11}$$

where,

$T_{o,c,max}$ is the maximum clutch transmissible torque.

t_{p1} is the time length of the transmissible torque ramp (0.1 s). Its value is selected based on the capabilities of the clutch actuators.

EM and ICE torque request

For the simulations presented in section 3.6, it is assumed that the powertrain operates in ICE only mode before the gearshift control takes over. Hence:

$$T_{EM}(t) = 0 \tag{3-12}$$

$$T_{ICE,eq}(t) = T_{prev}(t) \tag{3-13}$$

where $T_{ICE,eq}(t)$ is the torque request supplied by the ICE and the BAS.

Synchronizer position request

No commands are given to the synchronizers.

Exit conditions

The exit condition for this phase:

- Clutch slips: $T_{o,c}(t) \leq T_c(t)$.

The torque passing through the clutch is computed with Eq. (2-1) based on the crankshaft speed measurements.

3.3.2.2 Phase II: Opening the clutch completely

The main goal of this phase is to open the clutch completely while meeting the torque request at the wheels.

Control outputs

Clutch transmissible torque request

The clutch transmissible torque request is computed as in Eq. (3-11).

EM torque request

Having an EM connected to the AMT output allows to compensate for the difference between the torque passing through the clutch and the request at the wheels. Hence:

$$T_{EM}(t) = \left(T_{new}(t)\tau_{new} - T_c(t)\tau_{prev}\right)\frac{1}{\tau_{EM}} \tag{3-14}$$

The EM torque is kept positive during all the phases of the control logic to avoid stressing the mechanical components of the transmission. This is also valid for the other powertrain variant studied.

Note that since the clutch is slipping, the torque passing through it is computed based on the transmissible torque using a Coulomb friction model [68].

ICE torque request

The torque request to the ICE is computed using a PI superimposed to a feedforward term:

$$T_{ICE,eq}(t) = PI\left(\omega_{ICE,ref}(t) - \omega_{ICE}(t)\right) + \left[T_c(t) + J_{ICE,eq}\dot{\omega}_{ICE,ref}(t)\right] \quad (3\text{-}15)$$

where,

$\omega_{ICE,ref}(t)$ is the ICE angular speed reference.

$J_{ICE,eq}$ is the equivalent inertia computed as in Eq. (2-2).

The ICE reference speed is computed to keep the clutch slip velocity positive:

$$\omega_{ICE,ref}(t) = \bar{\omega}_{ss}(t)\tau_{prev} + \Delta\omega_{th,p2} \quad (3\text{-}16)$$

where,

$\bar{\omega}_{ss}(t)$ is the mean secondary shaft speed.

$\Delta\omega_{th,p2}$ is the angular speed threshold (20 rad/s).

In order to avoid wasting energy forcing the crankshaft to follow the speed oscillations of the secondary shaft, the mean value of the transmission output shaft angular speed (calculated online) is used when creating the ICE speed reference.

A high enough speed threshold $\Delta\omega_{th,p2}$ is selected to force positive slip. When the clutch is slipping, the torque passing through it is equal to the transmissible torque and its sign corresponds to the one of the slip velocity [68], [69]. Hence, a linear trend of reduction of the clutch transmissible torque will imply a linear increase of the EM torque request which is preferred to other control signals with higher dynamics. The latter consideration arises from the fact that powertrain

actuators are not able to respond immediately to a given command, therefore, torque requests to the EM with lower dynamics are more likely to be fulfilled.

Synchronizer position request

No commands are given to the synchronizers.

Exit conditions

The exit condition for this phase:

- Clutch is open: $T_{o,c}(t) = 0$.

3.3.2.3 Phase III: Disengage current gear / Speed synchronization / Engage new gear

By the time phase III starts, there is no torque being transmitted through the clutch, therefore, the synchronizers can work has they would on a conventional AMT.

The objectives of this phase are to disengage the current gear and to use the oncoming synchronizer to force the speed of the primary shaft to match the speed of the secondary shaft with the new gear ratio so that the oncoming gear can be engaged.

Control outputs

Clutch transmissible torque request

The clutch is open during this phase ($T_{o,c}(t) = 0$).

EM torque request

Besides supplying for the torque request at the wheels, the EM torque needs to compensate for the torque that will be eventually be transmitted through the friction elements of the synchronizer, i.e.:

$$T_{EM}(t) = \left(T_{new}(t)\tau_{new} - T_{syn}(t)\right)\frac{1}{\tau_{EM}} \tag{3-17}$$

ICE torque request

The ICE torque is computed using a PI superimposed to a feedforward term as in Eq. (3-15). On the other hand, the ICE reference speed is ramped from the final value it had on the previous phase $\omega_{ICE,ref,f,p2}$ towards the speed that the primary shaft would have once the requested gear is engaged. As in the previous phase, a high enough angular speed threshold $\Delta\omega_{th,p3}$ is considered to pursue positive slip velocity at the end of this phase.

$$\begin{aligned}&\omega_{ICE,ref}(t)\\&= \omega_{ICE,ref,f,p2}\\&+ \frac{\omega_{ss}(t)\tau_{new} + \Delta\omega_{th,p3} - \omega_{ICE,ref,f,p2}}{t_{p3,1} + t_{p3,2}}\, t\end{aligned} \tag{3-18}$$

where,

$\omega_{ICE,ref,f,p2}$ is the ICE angular speed at the end of phase II.

$\Delta\omega_{th,p3}$ is the angular speed threshold (40 rad/s).

$t_{p3,1}$ is time to completely disengaged the outgoing synchronizer and for the ingoing one to move until its friction elements are in contact (0.1 s).

$t_{p3,2}$ is the time to reach maximum synchronizer transmissible friction torque (0.05 s).

At the end of the speed ramp the reference becomes:

$$\omega_{ICE,ref}(t) = \omega_{ss}(t)\tau_{new} + \Delta\omega_{th,p3} \tag{3-19}$$

Synchronizer position request

The first action undertaken during this phase is to completely disengage the outgoing synchronizer. Only then, the ingoing synchronizer is commanded to move until its friction elements are in contact. Note that the synchronizer transmissible torque is zero until the friction elements start touching each other. The friction torque is then ramped-up to its maximum value $T_{o,syn,max}$ and kept there for the whole speed synchronization process.

The synchronizer transmissible torque during this phase is therefore given by:

$$T_{o,syn}(t) = \begin{cases} 0 & for\ t - t_{0,p3} < t_{p3,1} \\ \dfrac{T_{o,syn,max}}{t_{p3,2}} t & for\ t - \left(t_{0,p3} + t_{p3,1}\right) \leq t_{p3,2} \\ T_{o,syn,max} & for\ t > t_{0,p3} + t_{p3,1} + t_{p3,2} \end{cases} \quad (3\text{-}20)$$

where,

$t_{in,p3}$ is the time when phase III starts.

$T_{o,syn,max}$ is the maximum synchronizers transmissible torque.

Exit conditions

The following exit conditions are established:

- Speeds of primary and secondary shaft are within a small threshold $\Delta\omega_{th,ex,p3}$ (0.5 rad/s): $\left|\omega_{ps}(t) - \omega_{ss}(t)\tau_{new}\right| \leq \Delta\omega_{th,ex,p3}$.
- Offgoing gear is disengaged and the ingoing synchronizer reaches the fully engaged position: $t \geq t_{0,p3} + t_{p3,1} + t_{p3,2}$.

3.3.2.4 Phase IV: Prepare to start closing the clutch

This phase is added to warranty there is positive slip velocity at the time in which the clutch starts to be closed. The main difference with respect to the previous phase is that gear engagement has already happened.

Control outputs

Clutch transmissible torque request

The clutch is open during this phase.

EM torque request

Because the clutch is open, no power can be transmitted from the ICE/BAS to the wheels. Therefore, the EM is responsible for supplying the torque request:

$$T_{EM}(t) = T_{new}(t)\tau_{new}\frac{1}{\tau_{EM}} \quad (3\text{-}21)$$

ICE torque request

The torque request to the ICE is computed using a PI superimposed to a feedforward term as in Eq. (3-15). The ICE reference speed is:

$$\omega_{ICE,ref}(t) = \overline{\omega}_{ss}(t)\tau_{new} + \Delta\omega_{th,p4} \quad (3\text{-}22)$$

where $\Delta\omega_{th,p4}$ is the speed threshold considered (40 rad/s).

Synchronizer position request

No commands are given to the synchronizers.

Exit conditions

For this phase, the exit condition is:

- The difference between the speeds of ICE and primary shaft is higher than a threshold $\Delta\omega_{th,ex,p4}$ (30 rad/s): $|\omega_{ICE}(t) - \omega_{ss}(t)\tau_{new}| \geq \Delta\omega_{th,ex,p4}$.

3.3.2.5 Phase V: Clutch slip control for engagement

In this phase the clutch re-engagement is performed. As explained in [22], the oscillations on the longitudinal vehicle acceleration generated at the clutch engagement, depend on the slip speed and acceleration at clutch lock-up, which should be as small as possible.

Control outputs

Clutch transmissible torque request

The clutch transmissible torque is ramped in open loop towards the current value of the torque request at the transmission input:

$$T_{o,c}(t) = \frac{T_{new}(t)}{t_{p5}} t \tag{3-23}$$

where,

t_{p5} is the time length of the transmissible torque ramp (0.1 s).

At the end of the torque ramp, the request becomes:

$$T_{o,c}(t) = T_{new}(t) \tag{3-24}$$

EM torque request

As in previous phases, the EM supplies the difference between the torque requested at the wheels and the one passing by the clutch:

$$T_{EM}(t) = \left(T_{new}(t) - T_c(t)\right) \frac{\tau_{new}}{\tau_{EM}} \tag{3-25}$$

ICE torque request

The ICE torque request is computed using a PI superimposed to a feedforward term as in Eq. (3-15). The ICE reference speed is computed to match the speed and acceleration of the primary shaft when the clutch is engaged.

As mentioned at the beginning of this section, a clutch engagement with both slip speed and acceleration equal to zero leads to minimum driveline oscillations [15], [20], [22]. Hence, a parabolic trend is used as a reference for the ICE speed [15]:

$$\omega_{ICE,ref}(t) = \omega_{ss}(t)\tau_{new} + \frac{\omega_{ICE,ref,f,p4} - \omega_{ss}(t)\tau_{new}}{t_{p5}^2} \left(t - t_{p5}\right)^2 \tag{3-26}$$

where,

t_{p5} is the time length of the parabolic fillet (0.1 s).

$\omega_{ICE,ref,f,p4}$ is the ICE speed reference at the end of phase IV.

In case the exit conditions are not satisfied at the end of the parabolic fillet, the speed reference is set to be equal to the speed of the primary shaft:

$$\omega_{ICE,ref}(t) = \omega_{ss}(t)\tau_{new} \tag{3-27}$$

Synchronizer position request

No commands are given to the synchronizers.

Exit conditions

The exit condition defined is:

- The difference between the speed of the ICE and primary shaft are within a certain small threshold $\Delta\omega_{th,ex,p5}$ (2 rad/s): $|\omega_{ICE}(t) - \omega_{ss}(t)\tau_{new}| \leq \Delta\omega_{th,ex,p5}$.

3.3.2.6 Phase VI: Close the clutch completely

In order to consider the gearshift maneuver as over, the clutch needs to be closed completely.

Control outputs

Clutch transmissible torque request

The clutch transmissible torque is ramped towards its maximum value:

$$T_{o,c}(t) = T_{o,c,f,p5} + \frac{T_{o,c,f,p5} - T_{o,c,max}}{t_{p6}}t \tag{3-28}$$

where,

t_{p6} is the time length of the transmissible torque ramp (0.05 s).

$T_{o,c,f,p5}$ is the value of the clutch transmissible torque at the end of phase V.

EM torque request

As in previous phases, the EM supplies the difference between the torque requested at the wheels and the one passing by the clutch (see Eq. (3-25)).

ICE torque request

The ICE is commanded to provide the torque being requested:

$$T_{ICE,eq}(t) = T_{new}(t) \tag{3-29}$$

Synchronizer position request

No commands are given to the synchronizers.

Exit conditions

The following exit condition is defined:

- Clutch is fully closed: $T_{o,c}(t) = T_{o,c,max}$.

3.4 Gearshift control for HEV powertrains equipped with DCTs: Upshift maneuvers

For the DCT variant of the powertrain architecture of interest, two different control strategies for upshift and downshift maneuvers are presented. The nonlinear torsional model used for their development is described in detail in section 2.1. The reader is referred to [8], [12], [11], [9], [10] for more information about the gearshift process for both conventional and hybrid DCTs.

In this section, the control logic designed to improve gearshift quality during upshifts is addressed. First, an overview of the algorithm is given. Then, each of the phases in which the strategy is divided are explained.

3.4.1 Algorithm overview

Similar to the gearshift control strategy presented for the AMT variant of the powertrain under consideration, the algorithm described in this section is designed aiming at reducing as much as possible the oscillations in the vehicle longitudinal acceleration while satisfying the driver's torque request as fast as possible.

As for the previous controller, the gearshift process is divided into six consecutive phases.

The mentioned gearshift phases are:

- Phase I: Go-to-slip.
- Phase II: Prepare for torque phase.
- Phase III: Torque phase.
- Phase IV: Inertia phase - Fast speed matching.
- Phase V: Inertia phase - Clutch slip control for engagement.
- Phase VI: Close the clutch completely.

Exit conditions for each of these phases are established and used to switch between consecutive phases.

The designed controller relies only on speed measurements that are usually available in commercial vehicles:

- ICE angular speed.
- Transmission output shaft angular speed (both secondary shafts are assumed to have the same speed, see section 2.1.3.4).

Instead, the controller output signals are:

- Torque request to EM.
- Torque request to ICE.
- Clutch transmissible torque request.

The same considerations maid for the AMT variant of the vehicle studied, regarding the use of the output signals and how the response delay of powertrain actuators (ICE, BAS, EM and clutches) is accounted for, still apply.

3.4.2 Algorithm phases

In this section, each of the phases of the proposed control algorithm (see Figure 3-1) are described in detail. In particular, the main objectives, control outputs and exit conditions established for each phase are discussed.

3.4.2.1 Phase I: Go-to-slip

The output signals and exit conditions of this phase are generated similar to what it is explained in section 3.3.2.1 for the AMT variant.

The clutch whose transmissible torque is ramped down is the offgoing one. Instead, the oncoming clutch is kept fully open.

3.4.2.2 Phase II: Prepare for torque phase

This phase can be regarded as a preparation stage for the torque phase. The main objective of phase II is to have enough torque available at the DCT input to enforce positive slip on the offgoing clutch in the next phase.

Control outputs

Offgoing clutch transmissible torque request

The transmissible torque of the offgoing clutch continues to be ramped towards zero as in the previous phase.

$$T_{o,c,prev}(t) = T_{o,c,prev,f,p1} - \frac{T_{o,c,max}}{t_{p2}} t \tag{3-30}$$

where,

t_{p2} is the time length of the transmissible torque ramp (0.1 s).

$T_{o,c,prev,f,p1}$ is the transmissible torque of the offgoing clutch at the end of phase I.

Oncoming clutch transmissible torque request

The oncoming clutch remains fully open ($T_{o,c}(t) = 0$).

EM torque request

The EM compensates the torque passing through the offgoing clutch to meet the torque request as in Eq. (3-14).

ICE torque request

The torque request is computed using a PI superimposed to a feedforward term:

$$T_{ICE,eq}(t) = PI\left(\omega_{ICE,ref}(t) - \omega_{ICE}(t)\right) + \left[T_{c,prev}(t) + T_{c,new}(t) + J_{ICE,eq}\dot{\omega}_{ICE,ref}(t)\right] \quad (3\text{-}31)$$

where,

$T_{c,prev}(t)$ is the torque of the offgoing clutch.

$T_{c,new}(t)$ is the torque of the oncoming clutch (zero in this case).

The ICE reference speed is computed to keep the clutch slip velocity positive. To do this, a high enough threshold $\Delta\omega_{th,p2}$ (20 rad/s) above the primary shaft speed is chosen as done in Eq. (3-16).

Exit conditions

The exit condition defined for this phase are:

- Offgoing clutch slips: $T_{o,c,prev}(t) \leq T_{c,prev}(t)$.
- Offgoing clutch transmissible torque is equal or lower than the minimum between the 70 % of the maximum available torque at the transmission input (ICE + BAS) and the actual torque request.

The latter condition is established to ensure there is enough available torque at the transmission input to warranty positive slip velocity at the offgoing clutch in the following phase where the oncoming one starts to be closed. This can be seen as a saturation of the torque transmitted by the offgoing clutch. In mathematical terms, such saturation is expressed as:

$$T_{o,c,prev} = \frac{min\left(0.7\ T_{ICE,eq,max}(t)\tau_{new}, T_{new}(t)\tau_{new}\right)}{\tau_{prev}} \quad (3\text{-}32)$$

with

$$T_{ICE,eq,max}(t) = T_{ICE,max}(t) + T_{BAS,max}(t) \quad (3\text{-}33)$$

where,

$T_{ICE,max}(t)$ is the maximum torque available from the ICE (see section 2.1.3.1).

$T_{BAS,max}(t)$ is the maximum torque available from the BAS (see section 2.1.3.1).

3.4.2.3 Phase III: Torque phase

The goal of this phase is to open completely the offgoing clutch and start transmitting power through the oncoming clutch while meeting the torque request at the wheels.

The control of the slip velocity at the offgoing clutch is the main challenge in this phase as it will be illustrated by the considerations made in the following paragraphs.

Control outputs

Offgoing clutch transmissible torque request

As explained in the previous phase, to ensure there is enough available torque at the transmission input to warranty positive slip velocity for the offgoing clutch, its transmissible torque is saturated. Instead of controlling both clutches to transmit the torque necessary to supply for the request $T_{new}(t)$, the minimum value between this quantity and the 70 % of the maximum available torque at the DCT input computed with Eq. (3-33) is considered. In addition, a PI is used to introduce a correction to the transmissible torque request aiming at achieving the desired slipping rate.

Based on the previous considerations, it can be written:

$$T_{o,c,prev}(t) = \frac{\left(min\left(0.7\,T_{ICE,eq,max}(t), T_{new}(t)\right) - T_{c,new}(t)\right)\tau_{new}}{\tau_p} + PI\left(\omega_{c,slip,ref}(t) - \omega_{c,slip}(t)\right) \quad (3\text{-}34)$$

The angular slip speed reference is ramped towards the desired value to avoid having discontinuities on the transmissible torque:

$$\omega_{c,slip,ref}(t) = \omega_{c,slip,f,p2} + \frac{\Delta\omega_{th,p3} - \omega_{c,slip,f,p2}}{t_{p3}}t \quad (3\text{-}35)$$

where,

t_{p3} is the time length of the speed ramp (0.1 s).

$\omega_{c,slip,f,p2}$ is the slip angular speed at the end of the previous phase.

$\Delta\omega_{th,p3}$ is the target slip angular speed (20 rad/s).

Finally, in order to regulate the action of the PI controller introduced, another saturation is in place to avoid increasing the transmissible torque above the value it had at the end of the previous phase or the one calculated in the first term on the right side of Eq. (3-34).

Oncoming clutch transmissible torque request

Transmissible torque of the oncoming clutch is ramped towards its target value in open loop:

$$T_{o,c,new}(t) = \frac{min\left(0.7\,T_{ICE,eq,max}(t), T_{new}(t)\right)}{t_{p3}}t \quad (3\text{-}36)$$

EM torque request

EM compensates the torque passing through both clutches to meet the torque request:

$$T_{EM}(t) = \left(T_{new}(t)\tau_{new} - T_{c,prev}(t)\tau_{prev} - T_{c,new}(t)\tau_{new}\right)\frac{1}{\tau_{EM}} \quad (3\text{-}37)$$

ICE torque request

The torque request to the ICE is computed using a PI superimposed to a feedforward term as in Eq. (3-31). The ICE angular speed reference is computed to keep the clutch slip velocity positive as in Eq. (3-16).

Exit conditions

The following exit condition is established:

- Offgoing clutch is open: $T_{o,c,prev}(t) = 0$.

3.4.2.4 Phase IV: Inertia phase - Fast speed matching

The goal of this phase is to decrease as fast as possible the speed of the ICE towards the speed of the oncoming clutch while meeting the torque request.

This phase ends once the slip speed on the oncoming is within a certain threshold. In the subsequent control stage, in order to perform a smooth clutch engagement, the speed difference between the ICE and the oncoming clutch is controlled more carefully.

Control outputs

Offgoing clutch transmissible torque request

The offgoing clutch is open since the beginning of this phase.

Oncoming clutch transmissible torque request

The transmissible torque is ramped towards its target value in open loop:

$$T_{o,c,new}(t) = T_{o,c,new,f,p3} + \frac{T_{new}(t) - T_{o,c,new,f,p3}}{t_{p4}} t \qquad (3\text{-}38)$$

where,

t_{p4} is the time length of the torque ramp (0.1 s).

$T_{o,c,new,f,p3}$ is the value of the oncoming clutch transmissible torque at the end of the previous phase.

After the end of the transmissible torque ramp, the request is:

$$T_{o,c,new}(t) = T_{new}(t) \qquad (3\text{-}39)$$

EM torque request

The EM compensates the torque passing through the oncoming clutch to meet the torque request. Hence, the torque request to the EM can be computed using Eq. (3-37).

ICE torque request

The ICE torque is computed using a PI superimposed to a feedforward term as in Eq. (3-31). The ICE reference speed is computed to match a certain threshold above the angular speed of the oncoming clutch. A ramp is imposed which makes the reference given to the ICE continuous.

$$\begin{aligned} &\omega_{ICE,ref}(t) \\ &= \omega_{ICE,ref,f,p3} \\ &+ \frac{\omega_{ss}(t)\tau_{new} + \Delta\omega_{th,p4} - \omega_{ICE,ref,f,p3}}{t_{ICE,p4}} t \end{aligned} \qquad (3\text{-}40)$$

Where,

$t_{ICE,p4}$ is the time length of the angular speed ramp (0.25 s).

$\omega_{ICE,ref,f,p3}$ is the ICE reference speed at the end of the previous phase.

$\Delta\omega_{th,p4}$ is the target speed threshold (40 rad/s).

After the speed ramp is undertaken, the reference is:

$$\omega_{ICE,ref}(t) = \omega_{ss}(t)\tau_{new} + \Delta\omega_{th,p4} \quad (3\text{-}41)$$

Exit conditions

The following exit condition is verified:

- The slip velocity is equal or lower than a certain threshold $\Delta\omega_{th,ex,p4}$ (45 rad/s): $\omega_{ICE}(t) - \omega_{ss}(t)\tau_{new} \leq \Delta\omega_{th,ex,p4}$.

3.4.2.5 Phase V: Inertia phase - Clutch slip control for engagement

The goal of this phase is to realize a very precise control of the slip velocity at the oncoming clutch in order to have a smooth clutch engagement while meeting the torque request. As explained for the AMT, this is achieved when the slip speed and acceleration at clutch lock-up are close to zero.

Control outputs

Offgoing clutch transmissible torque request

The offgoing clutch is open during this phase.

Oncoming clutch transmissible torque request

The oncoming clutch is controlled as in the previous phase.

EM torque request

The EM compensates the torque passing through the oncoming clutch to meet the torque request as described in Eq. (3-37).

ICE torque request

The ICE torque is computed using a PI superimposed to a feedforward term as in Eq. (3-31). The ICE angular speed reference is computed to match the speed of the oncoming clutch at the end of this phase. As for the AMT variant of the powertrain of interest, a parabolic fillet is imposed as a reference to the ICE speed

to induce the angular slip speed and acceleration to be zero at the time the clutch is engaged (see section 3.3.2.5).

Exit conditions

The exit condition is:

- Clutch slip velocity is within a small threshold $\Delta\omega_{th,ex,p5}$ (2 rad/s): $|\omega_{ICE}(t) - \omega_{ss}(t)\tau_{new}| \leq \Delta\omega_{th,ex,p5}$.

3.4.2.6 Phase VI: Close the clutch completely

In this phase, the output signals and exit conditions are designed in a similar way to what it is explained in section 3.3.2.6 for the AMT variant.

3.5 Gearshift control for HEV powertrains equipped with DCTs: Downshift maneuvers

In this section, the control logic designed to improve gearshift quality during downshifts for the H-DCT under consideration is addressed. First, an overview of the algorithm is given. Then, each of the phases in which the strategy is divided are explained.

As for the other control algorithms treated in this chapter, the model used to test the performance of the developed strategy, is the one described in section 2.1.

3.5.1 Algorithm overview

Similar to the control logic developed for upshift maneuvers, the control algorithm is designed aiming at reducing as much as possible the oscillations in the vehicle longitudinal acceleration while satisfying the driver's torque request as fast as possible.

The gearshift process is divided into four consecutive phases:

- Phase I: Go-to-slip.
- Phase II: Inertia phase - Fast speed matching.
- Phase III: Torque phase - Clutch slip control for engagement.
- Phase IV: Close the clutch completely.

Exit conditions for each of these phases are established and used to switch between consecutive phases.

The designed controller relies only on speed measurements that are usually available in commercial vehicles:

- ICE angular speed.
- Transmission output shaft angular speed (both secondary shafts are assumed to have the same speed, see section 2.1.3.4).

Instead, the controller output signals are:

- Torque request to EM.
- Torque request to ICE.
- Clutch transmissible torque request.

The same considerations maid for the other two gearshift control strategies presented before, regarding the use of the output signals and how the response delay of powertrain actuators (ICE, BAS, EM and clutches) is accounted for, still apply.

3.5.2 Algorithm phases

In this section, the main objectives, control outputs and exit conditions established for each phase are discussed. The phases described here are depicted in Figure 3-5.

3.5.2.1 Phase I: Go-to-slip

This phase is undertaken as explained for the upshifts (see section 3.4.2.1).

3.5.2.2 Phase II: Inertia phase - Fast speed matching

The goal of this phase is to increase as fast as possible the speed of the ICE towards a certain threshold above the speed of the oncoming clutch while meeting the torque request at the wheels.

Similar to phase IV of the strategy designed for the upshifts (see section 3.4.2.4), this is done in order to be able to perform a very precise angular slip speed control in the next phase with the objective of reducing driveline oscillations at clutch engagement.

Control outputs

Offgoing clutch transmissible torque request

Transmissible torque is ramped to compensate the difference between the maximum torque available from the EM and the actual torque request. Hence, it can be written:

$$\begin{aligned} & T_{o,c,prev}(t) \\ & = T_{o,c,prev,f,p1} \\ & + \frac{\frac{T_{new}(t)\tau_{new} - T_{EM,max}(t)\tau_{EM}}{\tau_{prev}} - T_{o,c,prev,f,p1}}{t_{p2}} t \end{aligned} \tag{3-42}$$

where,

t_{p2} is the time length of the transmissible torque ramp (0.1 s).

$T_{o,c,prev,f,p1}$ is the value of the offgoing clutch transmissible torque at the end of the previous phase.

$T_{EM,max}(t)$ is the maximum available torque from the EM (see Eq. (2-16)).

Once the transmissible torque ramp is undertaken, the request becomes:

$$T_{o,c,prev}(t) = \frac{T_{new}(t)\tau_{new} - T_{EM,max}(t)\tau_{EM}}{\tau_{prev}} \tag{3-43}$$

Note that controlling the offgoing clutch transmissible torque as explained above allows to minimize clutch slip losses since the mentioned component will eventually be fully open if the EM can handle the torque request by itself.

Oncoming clutch transmissible torque request

The oncoming clutch stays fully open.

EM torque request

EM compensates the torque passing through the offgoing clutch to meet the torque request (see Eq. (3-37)).

ICE torque request

The torque request to the ICE is computed using a PI superimposed to a feedforward term as described in Eq.(3-31). The ICE angular speed reference is computed to match a certain threshold above the speed of the oncoming clutch as fast as possible. A speed ramp is imposed whose duration was selected, after studying the results of several simulations, in order to provide a suitable reference for the crankshaft speed according to the capabilities of powertrain actuators.

$$\begin{aligned}&\omega_{ICE,ref}(t)\\&=\omega_{ICE,ref,f,p1}\\&+\frac{\omega_{ss}(t)\tau_{new}+\Delta\omega_{th,p2}-\omega_{ICE,ref,f,p1}}{t_{ICE,p2}}t\end{aligned} \tag{3-44}$$

where,

$t_{ICE,p2}$ is the duration of the ICE reference speed ramp (0.3 s).

$\omega_{ICE,ref,f,p1}$ is the ICE reference speed at the end of the previous phase.

$\Delta\omega_{th,p2}$ is the angular speed threshold considered (40 rad/s).

If the current phase last longer than the time estimated for the angular reference speed ramp, the output of the PI controller is computed based on:

$$\omega_{ICE,ref}(t)=\omega_{ss}(t)\tau_{new}+\Delta\omega_{th,p2} \tag{3-45}$$

Exit conditions

The exit condition is:

- The ongoing clutch slip velocity is equal or higher than a certain threshold $\Delta\omega_{th,ex,p2}$ (40 rad/s): $\omega_{ICE}(t)-\omega_{ss}(t)\tau_{new}\geq\ \Delta\omega_{th,ex,p2}$.

3.5.2.3 Phase III: Torque phase - Clutch slip control for engagement

The goal of this phase is to realize a very precise control of the slip velocity on the oncoming clutch in order to have a smooth clutch engagement while meeting the torque request.

The offgoing clutch must be completely disengaged at the end of this phase.

Control outputs

Offgoing clutch transmissible torque request

The offgoing clutch is required to compensate the difference between the torque request and the torque passing through the oncoming clutch:

$$T_{o,c,prev}(t) = \left(T_{new}(t) - T_{c,new}(t)\right)\frac{\tau_{new}}{\tau_{prev}} \tag{3-46}$$

The maximum value that the transmissible torque can take is the one at the end of the previous phase.

Oncoming clutch transmissible torque request

The oncoming clutch transmissible torque is ramped towards the value requested by the driver. In addition, a PI is used to introduce a correction to the transmissible torque to enforce the desired slipping rate:

$$T_{o,c,new}(t) = \frac{T_{new}(t)}{t_{p3}}t + PI\left(\omega_{ICE,ref}(t) - \omega_{ICE}(t)\right) \tag{3-47}$$

where,

t_{p3} is the duration of the transmissible torque ramp (0.1 s).

After t_{p3} the transmissible torque is:

$$T_{o,c,new}(t) = T_{new}(t) + PI\left(\omega_{ICE,ref}(t) - \omega_{ICE}(t)\right) \tag{3-48}$$

The speed reference seen in Eq. (3-47) and Eq. (3-48) is the same used to generate the ICE torque request (see section 3.4.2.5).

EM torque request

EM compensates the torque passing through the clutches to meet the torque request (see section (3-37)).

ICE torque request

The ICE torque request in this phase is computed as explained for phase V of the upshift control strategy (see section 3.4.2.5).

Exit conditions

The exit conditions defined are:

- The slip velocity is within a small threshold $\Delta\omega_{th,ex,p3}$ (2 rad/s): $|\omega_{ICE}(t) - \omega_{ss}(t)\tau_{new}| \leq \Delta\omega_{th,ex,p3}$.
- Previous clutch is open: $T_{o,c,prev}(t) = 0$.

3.5.2.4 Phase IV: Close the clutch completely

The last phase of the algorithm described in this section is undertaken as explained for the last phase of the upshift control strategy (see section 3.4.2.6).

3.6 Simulation results

In this section, simulation results are presented and analyzed to illustrate the effectiveness of the gearshift control strategies designed for the two variants of the powertrain of interest. In addition, the results are also used to establish the benefits and limitations of the two transmission systems studied.

For each of the gearshift maneuvers simulated, the powertrain model is initialized starting at a certain predefined speed from which the vehicle is driven using only the ICE to satisfy the torque request at the wheels. In all the simulations performed, the gearshift process starts after 2.5 s.

Moreover, the transmission ratios of the DCT and the AMT are set to be the same. In this way, the differences seen in the vehicle dynamic performance are more likely to be related to the functioning principle of each transmission technology.

3.6.1 Upshift maneuver: 1st to 2nd at 100% APP

Simulation results for a 1st to 2nd upshift performed at 100 % APP are presented for both the H-DCT and the H-AMT.

The upper plot of Figure 3-1 shows the speed of the main driveline components, including the ICE reference speed which is set to zero when the crankshaft speed is not being controlled. Instead, the lower plot shows the torque request to the ICE and the EM together with the clutch(es) and synchronizer transmissible torque. The actual torque passing through the clutch(es) is also presented.

Note that for the H-AMT, phase IV is skipped since the clutch slip speed at the end of phase III is above the specified threshold used as an exit condition for phase IV (see section 3.3.2.4).

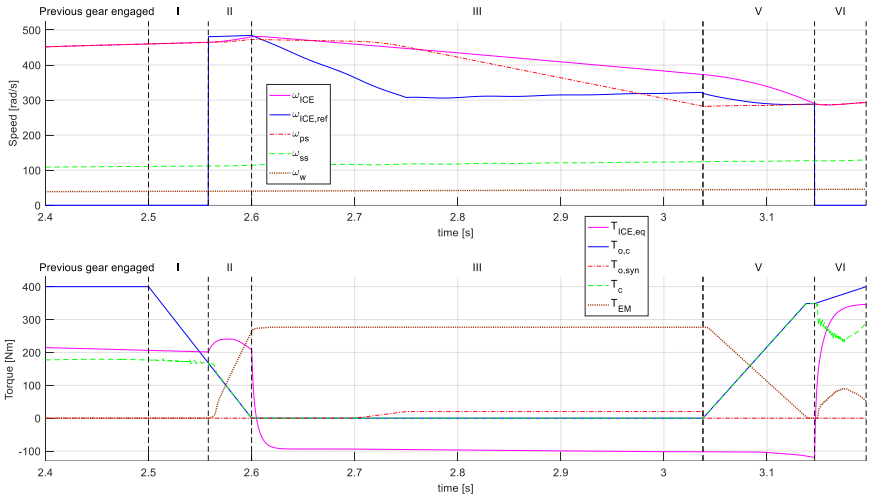

a) H-AMT

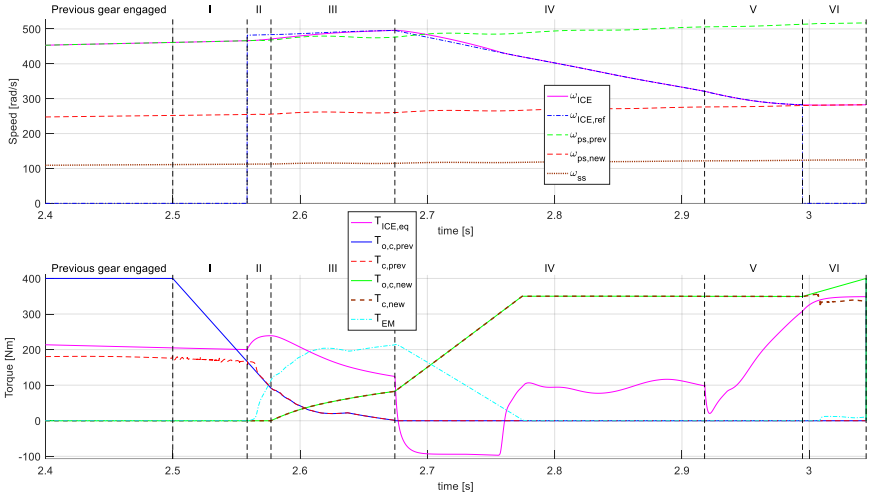

b) H-DCT

Figure 3-1. Speed and torque: 1st to 2nd at 100 % APP.

Due to the limited amount of braking torque that can be provided by the ICE and the BAS, for the H-AMT, during phases III and V the ICE speed does not properly follows its reference. This does not lead to undesired vibrations thanks to the way in which the EM is controlled. Instead, the H-DCT is able to properly follow the ICE speed reference.

On the other hand, Figure 3-2 shows the results of a 4th to 5th upshift performed at 100% APP by the H-AMT in which the powertrain is able to follow the imposed reference speed for the crankshaft considerably better. This translates into an almost linear decrease during phase II (or increase in phase V) of the torque passing by the clutch which makes the EM torque to have a very smooth change rate which is more likely to be provided by the motor.

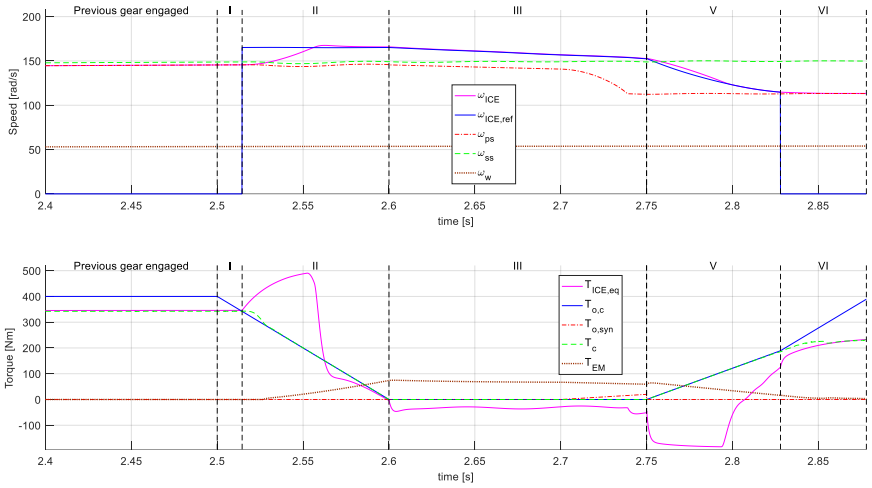

Figure 3-2. Speed and torque (H-AMT): 4th to 5th at 100% APP.

In a conventional (non-hybrid) AMT, oscillations in the primary shaft speed arise when the torque starts passing again through the clutch after the torque gap that occurs during the synchronization phase. In the H-AMT, thanks to the action of the EM, the secondary shaft is never unloaded. This reduces the input shaft vibrations at the beginning of phase V and enables the possibility of performing the clutch slip control while the transmissible torque is being ramped-up, making the gearshift process faster.

In addition, it is clear that the torque fill energy from the EM required by the H-AMT is considerably larger than that of the H-DCT (see Table 3-1). Note that, given the architecture of the AMT, during phase III, the EM has to supply the entire power request at the wheels.

Figure 3-3 shows how the total torque request at the wheels is fulfilled by the different powertrain actuators. Torque request at the wheels is satisfied better by the H-DCT as it is quantified by its mean torque error (see Table 3-1).

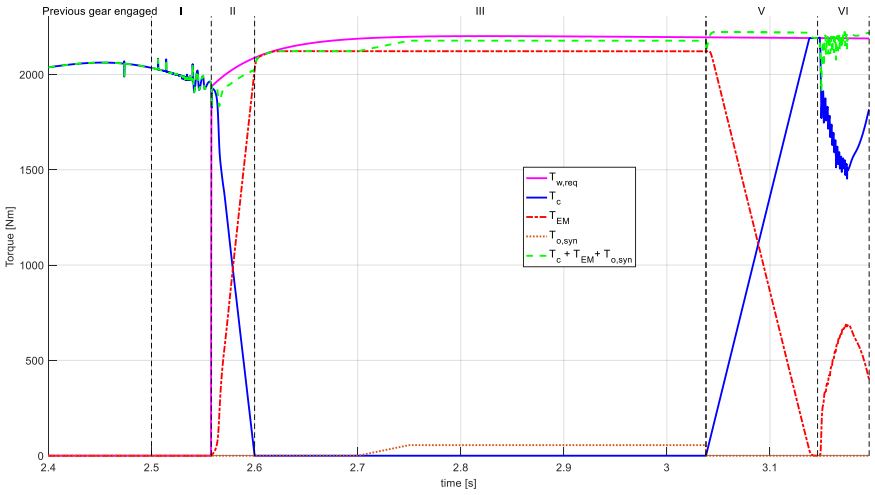

a) H-AMT

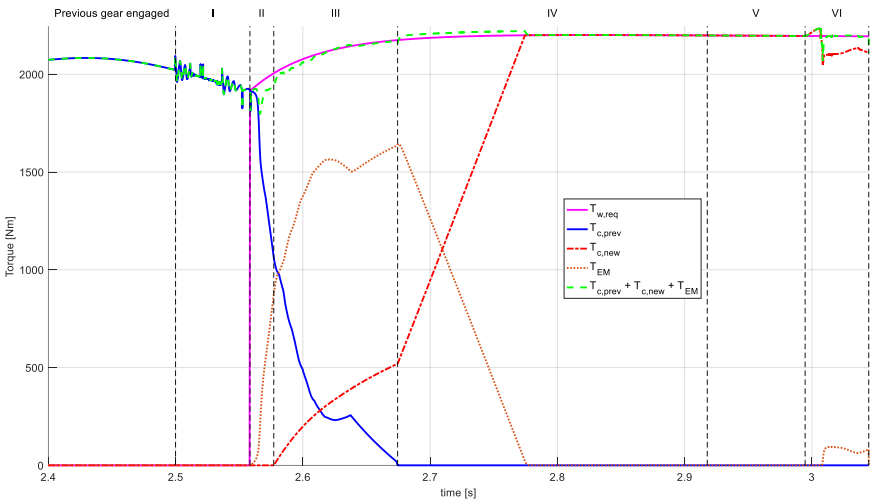

b) H-DCT

Figure 3-3. Torque at the wheels: 1st to 2nd at 100 % APP.

In Figure 3-4, the longitudinal acceleration and jerk seen during the gearshift maneuver are presented. A very smooth clutch engagement is achieved for both

powertrain architectures as indicated by the low jerk value seen right after the end of phase V. As expected, based on the fact that the H-DCT is able to follow better the given reference for the ICE speed, the maximum (absolute) jerk value seen for the H-AMT in phase VI is higher than that of the other powertrain (1.35 m/s^3 vs. 0.55 m/s^3).

Furthermore, Figure 3-4 shows that the main jerk peak is due to the increase in the torque delivered to the wheels to satisfy the request expressed by the driver. However, using a time constant of 0.05 s for the torque request transition, the maximum jerk value is always under 10 m/s^3. In [92], the experiments conducted shown than a value greater than 10 m/s^3 is perceived by the passengers as uncomfortable.

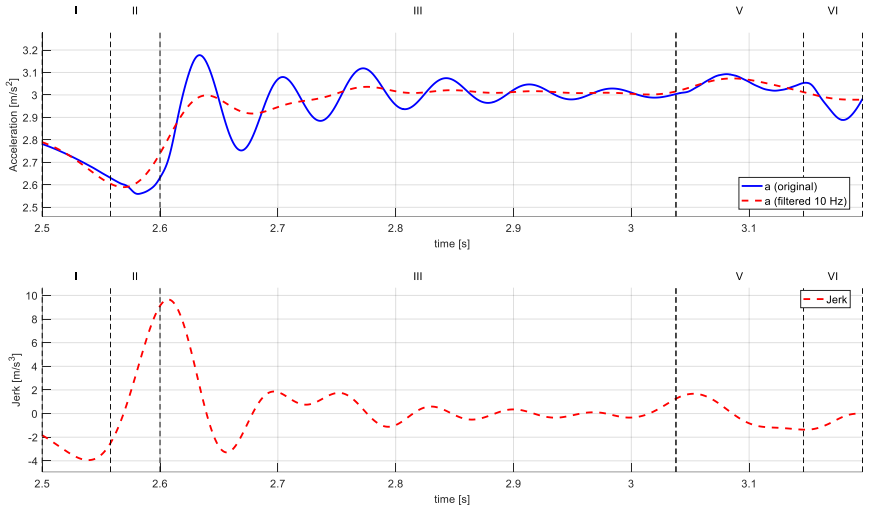

a) H-AMT

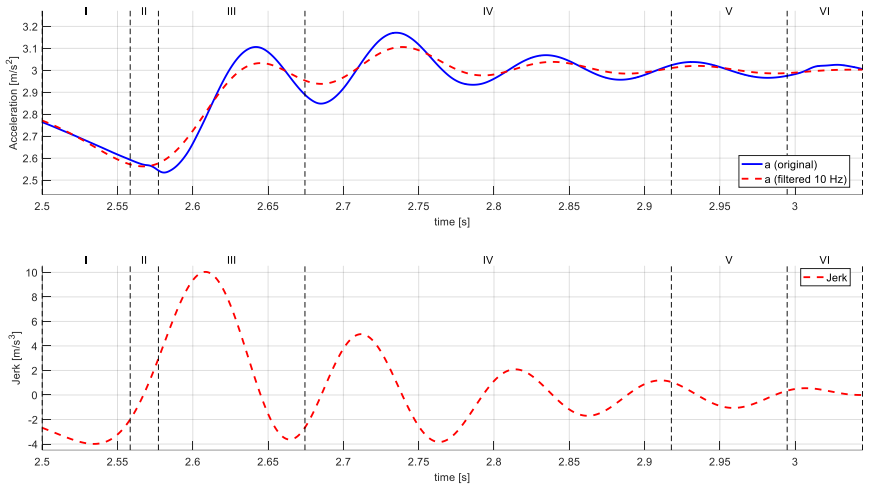

b) H-DCT

Figure 3-4. Acceleration and Jerk: 1st to 2nd at 100 % APP.

Table 3-1 presents the value of the gearshift quality metrics described in section 3.1. In terms of the vehicle performance and shift comfort, it can be seen that the results obtained for both powertrains are similar with the H-AMT indicators being slightly better. Instead, by looking at the energy consumption indicators, it can be noted that the H-DCT presents a significantly higher energy loss due to clutch slip (two clutches are slipping during the gearshift instead of one). On the other hand,

as explained when discussing Figure 3-1, the energy requested from the EM is larger for the H-AMT. The global energy balance made considering these two indicators shows that the H-DCT is more energy efficient during upshifts.

Table 3-1. Gearshift quality criteria: 1st to 2nd at 100 % APP.

Gearshift quality criteria	**Parameter**	**H-AMT**	**H-DCT**
Performance	t_{gs} [s]	0.696	0.545
	$\bar{a}$ [m/s^2]	2.942	2.933
	$\bar{T}_{w,err}$ [%]	1.680	0.742
Shift comfort	$Jerk_{RMS}$ [m/s^3]	2.482	3.290
	$Jerk_{max/min}$ [m/s^3]	13.596	14.028
Shift efficiency	$E_{c,loss}$ [kJ]	0.825	10.624
Torque fill energy consumption	E_{EM} [kJ]	47.702	9.839

3.6.2 Downshift maneuver: 4th to 3rd at 100% APP

Simulation results for a 4th to 3rd downshift at 100% APP are presented for both the H-DCT and the H-AMT.

Differently form the upshift maneuver, the ICE reference speed is followed well by the two powertrain architectures under consideration during the downshift as shown in Figure 3-5. Furthermore, it is worth noting that, to minimize clutch slip energy losses for the H-DCT, the EM works as a torque fill device in a similar manner than for the H-AMT (see section 3.5.2.2).

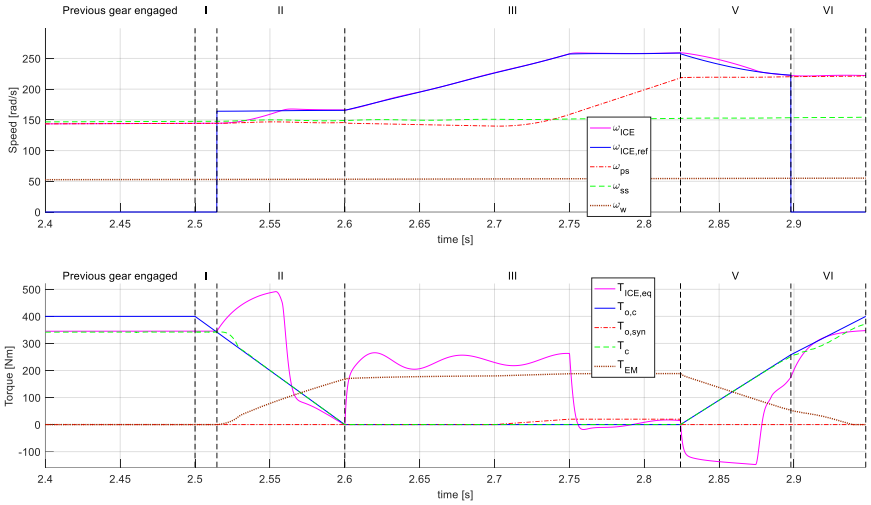

a) H-AMT

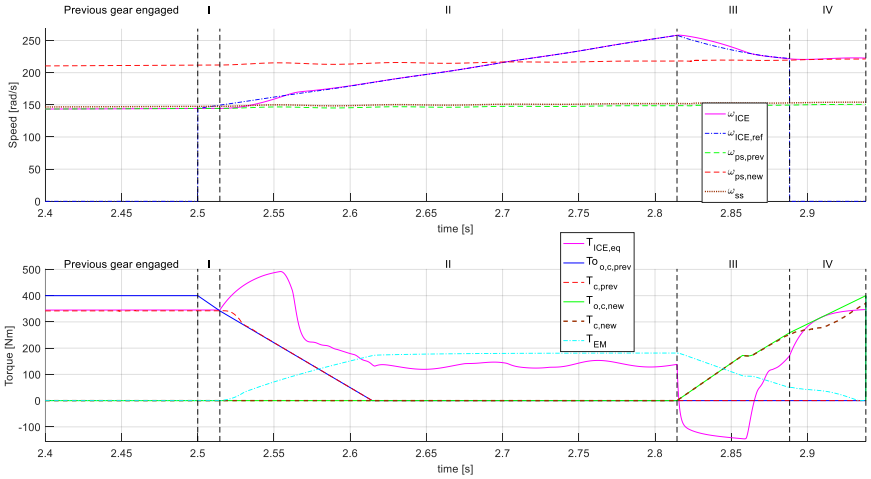

b) H-DCT

Figure 3-5. Speed and torque: 4th to 3rd at 100% APP.

Figure 3-6 shows that the torque request at the wheels is matched well by both powertrain variants. This is also expressed by the low torque mean errors reported in Table 3-2. Moreover, the effect of the actuation delay of the EM can be appreciated at the times in which the offgoing clutch is being opened or the oncoming one is being engaged. In those instances, the EM is not able to

compensate the torque passing through the transmission input in order to meet the exact request at the wheels.

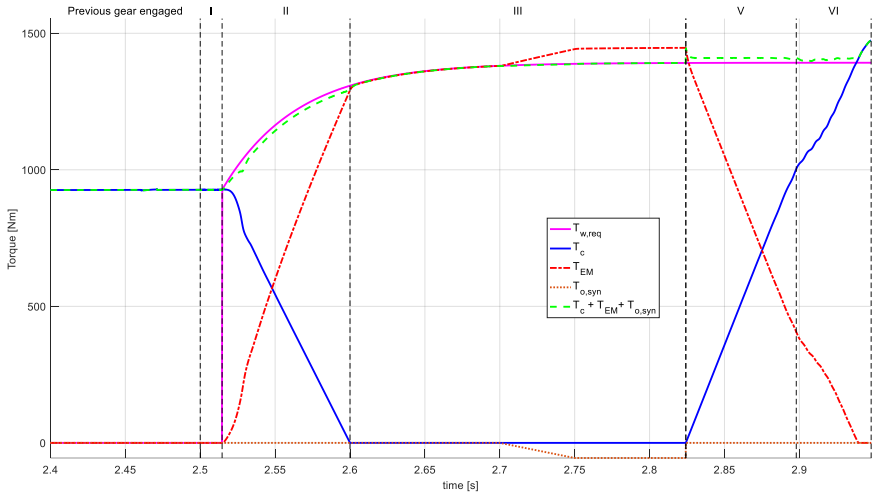

a) H-AMT

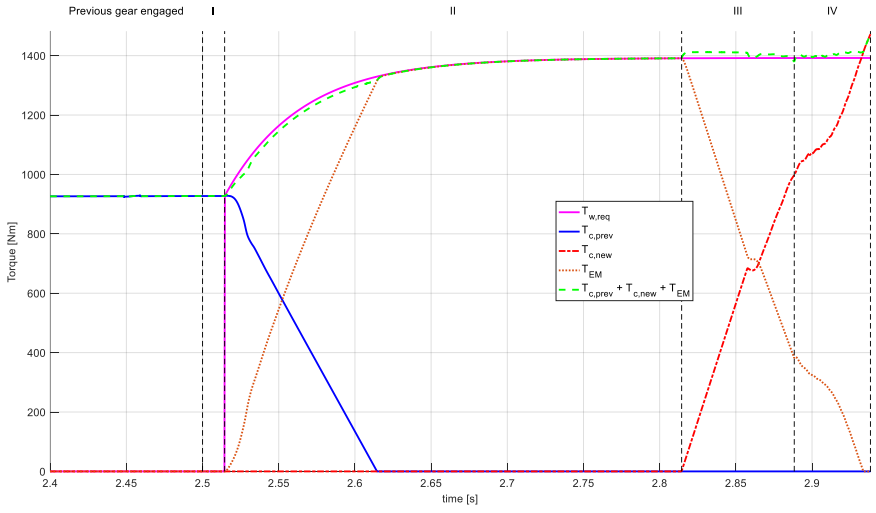

b) H-DCT

Figure 3-6. Torque at the wheels: 4th to 3rd at 100% APP.

As seen for the upshifts, Figure 3-7 shows that clutch engagement is done smoothly.

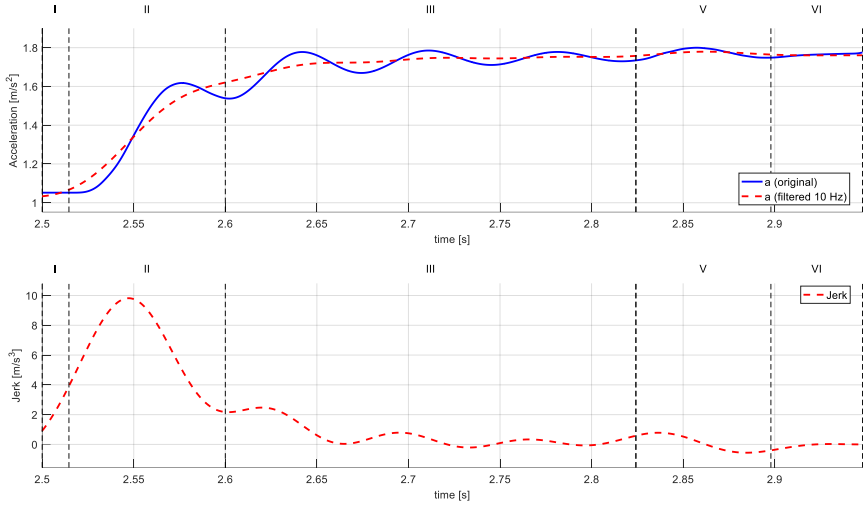

a) H-AMT

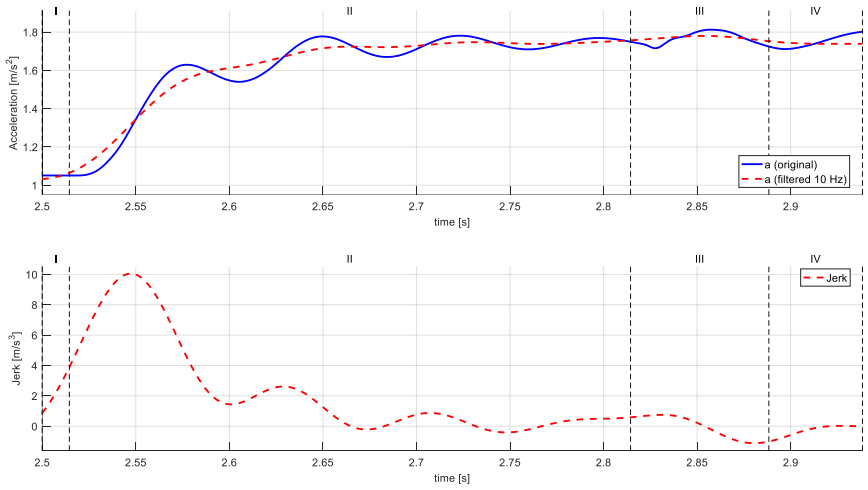

b) H-DCT

Figure 3-7. Acceleration and Jerk: 4th to 3rd at 100% APP.

Table 3-2 presents the values of the gearshift quality parameters for both powertrains. In terms of vehicle performance and shift comfort, the value of the selected indicators is almost the same for the H-AMT and the H-DCT. Moreover,

since the EM is used in a similar manner by both systems, the clutch slip losses and torque fill energy found are also comparable even though the H-DCT performs slightly better.

Table 3-2. Gearshift quality parameters: 4th to 3rd at 100% APP.

Gearshift quality criteria	Parameter	H-AMT	H-DCT
Performance	t_{gs} [s]	0.448	0.438
	$\bar{a}$ [m/s^2]	1.648	1.641
	$\bar{T}_{w,err}$ [%]	0.946	0.803
Shift comfort	$Jerk_{RMS}$ [m/s^3]	3.166	3.238
	$Jerk_{max/min}$ [m/s^3]	10.375	11.165
Shift efficiency	$E_{c,loss}$ [kJ]	0.272	0.352
Torque fill energy consumption	E_{EM} [kJ]	24.352	22.915

3.6.3 Effect of the torque request transition

As explained in section 3.2, the transition between the torque request at the wheels computed considering the transmission ratio of the offgoing gear and the one determined in Eq. (3-8) is smoothed by means of a first order transfer function.

Three different values of the time constant used for such transition are studied here:

- 0.1 s.
- 0.05 s.
- 0.01 s.

Figure 3-8 shows how the torque at the wheels changes with the time constant selected. The maneuver studied is the same 1st to 2nd upshift at 100 % APP performed with the H-DCT in section 3.4. As expected, the smaller the time constant, the faster the transition.

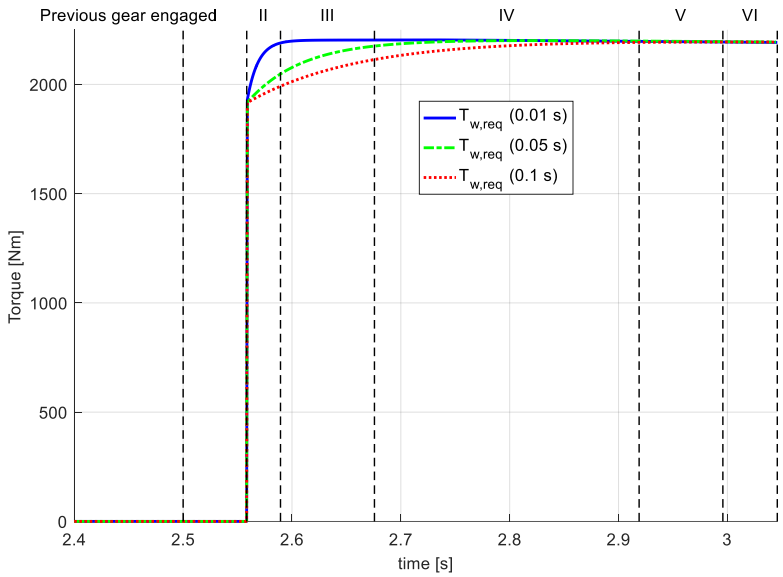

Figure 3-8. Torque request transition.

Instead, Figure 3-9 shows the effects of the different torque requests at the wheels in terms of acceleration and jerk. The results are intuitive in the sense that the performance in terms of vehicle drivability improves for smoother transitions of the torque delivered at the wheels (see Table 3-3).

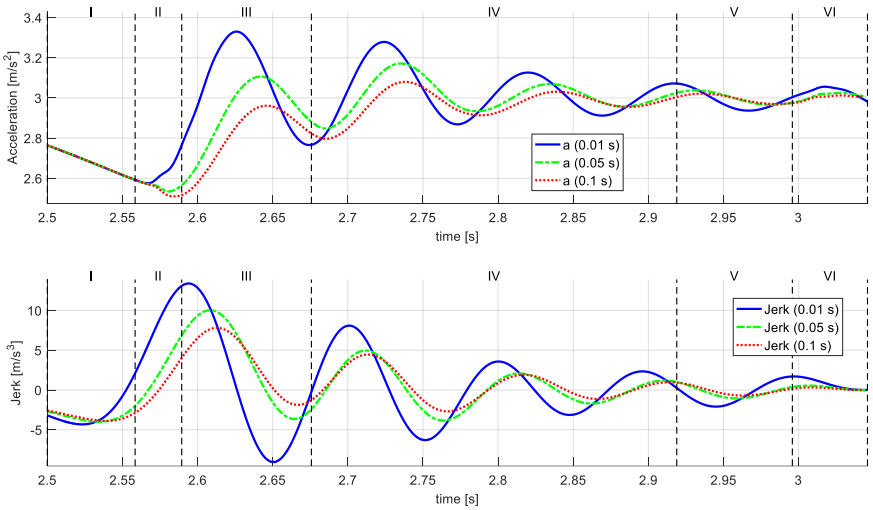

Figure 3-9. Torque request transition effects on drivability.

Table 3-3. Effects of the torque request transition.

Gearshift quality criteria	**Parameter**	**0.1 s**	**0.05 s**	**0.01**
Performance	a [m/s^2]	2.894	2.933	2.965
Shift comfort	$Jerk_{RMS}$ [m/s^3]	2.675	3.290	4.771
	$Jerk_{max/min}$ [m/s^3]	11.696	14.028	22.459

3.7 Summary

In this chapter, gearshift control strategies for the two variants of the powertrain described in section 2.1 are developed. The objectives of each of the algorithm phases, the equations for computing the ICE, BAS, clutch(es) and EM torque requests are reported together with the conditions that determine the passage from one phase to the next. In addition, simulation results are presented and analyzed to illustrate the effectiveness of the control strategies. These results are also used to establish the benefits and limitations of the two transmission systems studied.

The gearshift process must satisfy several and often conflicting requirements, *e.g.* short duration, smooth engagement and minimization of energy dissipation/consumption. The metrics employed to assess gearshift quality are selected to allow an objective evaluation of the developed control strategies performance regarding the fulfillment of the mentioned requirements.

The results obtained for both powertrains are promising in terms of vehicle dynamic performance. One fundamental implication of the previous remark is that the PHEV variant in which an AMT is employed has been proved capable of almost eliminating the torque gap during gearshifts while keeping the mechanical complexity of the system low with respect to its DCT counterpart.

In the simulations undertaken, the main differences in the performance of both architectures are seen during upshift maneuvers. When attention is focused on the

energy consumption indicators, it can be noted that the H-DCT presents a significantly higher energy loss due to clutch slip (two clutches are slipping during the gearshift instead of one). However, the energy requested from the EM is larger for the H-AMT. Note that, during the speed synchronization of the oncoming gear and the AMT output shaft, the EM is asked to supply the entire power request at the wheels. The global energy balance made considering these two sources of energy consumption shows that the H-DCT is more energy efficient during upshifts.

Instead, for the downshift maneuvers, in order to minimize the clutch slip energy losses for the H-DCT, the EM works as a torque fill device in a similar manner than it does for the H-AMT. Hence, the energy consumption indicators for both powertrains have similar values even though the H-DCT performs slightly better.

Furthermore, the effect of the time constant of the first order transfer function used to handle the transition from the torque request before the gearshift maneuver is undertaken and that computed based on the transmission ratio of the oncoming gear and the APP is also studied. Results are intuitive in the sense that the performance in terms of vehicle drivability is seen to improve for smoother transitions of the torque delivered at the wheels.

Finally, it is worth mentioning, that the developed strategies are very simple to implement and tune since they are based on the use of simple PI feedback controllers. Thus, transmission engineers without significant knowledge of advanced control theory will be able to use the developed tools.

Chapter 4

4. The Energy Management Problem in Hybrid Electric Vehicles

4.1 Energy management of HEVs

The energy management in hybrid vehicles consists in deciding the amount of power delivered at each time instant by the onboard energy sources [1], [26].

In a conventional vehicle the driver request is satisfied by the only mechanical power generation device available, i.e., ICE. In order for this to happen, the low-level controllers intervene to drive each of the powertrains components as intended by the driver [71]. These controllers are usually design using classical feedback control methods [1].

In HEVs an additional decision must be made regarding how the driver power request will be distributed among the different energy sources available. An Energy Management Strategy (EMS) is therefore necessary to determine the power split at each time instant [27]. This high-level control layer, often referred to as supervisory control, receives as inputs information coming from the vehicle (ICE speed, SOC, EM speed, etc.) together with the requests coming from the driver and process it to output a series of set-points to the powertrain actuators that are enforced by the low-level or component level control layer [1].

The design of the EMS is deeply related to the HEV architecture of interest and the predefined control objectives.

Depending on the powertrain configuration, a certain number of operational modes are available [93], e.g., EV-mode, ICE-only mode, Parallel hybrid mode, etc. The responsibility of deciding how and when to perform the transition among them lies also with the EMS [60].

In HEVs the control objectives are mostly integral in nature. Traditionally, EMSs are design with the goal of minimizing the total fuel consumption over a defined optimization horizon [28], [29]. However, other objectives could also be included as the reduction of pollutant emissions [30], [31] or the maximization of battery life [32], [33]. Furthermore, EMSs could be implemented to satisfy multiple and often conflicting requirements, arising the need of properly weighing the different objectives to obtain the desired vehicle performance. For example, in [34] a control strategy is developed aiming at optimally tradeoff between fuel consumption and battery capacity loss while in [35], [36] the compromised is established between fuel consumption and vehicle drivability.

In production vehicles, EMSs must be causal since real-time implementation is required. This implies that the control actions are local in time. Moreover, other than deciding the power split among onboard energy sources, depending on the vehicle architecture, other decisions might be taken, e.g., the current engaged gear, ICE state, clutches states, etc.

The energy management of HEVs involves respecting a series of constrains that can be either local or integral in nature. When making a control decision, the strategy implemented must be able to account for the physical limitations of powertrain components, e.g., maximum ICE torque or minimum battery current, which constitute local constrains. Furthermore, the value of a certain system state variable could be subjected as well to meet a predefined requirement. For instance, local constrains are often enforced aiming at maintaining the battery SOC within a prescribed range. On the other hand, most of the times a target SOC value at the end of the driving mission is required either for charge-sustaining [73] or charge-depleting [38] vehicle operation.

In the following sections, some of the most relevant EMSs discussed in literature will be addressed. This will set the basis for understanding the work on energy management for HEVs presented in the next two chapters.

4.2 Classification of energy management strategies for HEVs

The energy management problem in HEVs has been approached in literature using several different techniques, therefore, various families of EMSs have also been proposed. According to [1], [71], [41], [40] they can be classified as:

- Rule-based optimization methods.
- Model-based optimization methods.

The latter category can be subdivided in:

- Numerical approaches.
- Analytical approaches.

These types of EMSs will be briefly described in the following paragraphs.

4.2.1 Rule-based optimization methods

In rule-based approaches, a set of rules is employed to determine the set-points to the powertrain actuators that are enforced by the component level controllers at each time step.

The main advantage of these control techniques lies in their causal nature. Given that only past and present information is needed, rule-based approaches are suitable for real-time implementation. Furthermore, since no explicit optimization is involved, these methods are easy to implement and computationally cheap [71]. However, those same characteristics of rule-based techniques made the solutions obtained necessarily sub-optimal [1].

The rules employed are generally designed based on engineering intuition [26] or from the knowledge of the global optimal solution to the control problem, which is obtained offline using model-based approaches [27], [37], [38].

4.2.2 Model-based optimization methods

Model-based optimization strategies rely on a suitable mathematical model of the HEV powertrain of interest to provide a solution for the energy management problem. The level of complexity of the models employed depends on the control objectives and on the techniques used to obtain the desired solution. For example, in [34] a battery aging model is included in the control problem formulation since it is intended to reduce battery capacity degradation whilst in [38] a zero-th order

model is employed given that the only control objective is to reduce fuel consumption. Furthermore, in [77] simplified engine fuel rate and battery efficiency models are used to ease the introduction of an analytical formulation which allows to reduce the computational load with respect to the purely numerical solution.

Once an appropriate model is defined, the control trajectory is found minimizing a cost function over a known driving cycle. The need of the future driving information together with the computational burden involved makes this type of EMSs not suitable for online implementation if the global optimal solution is required. However, as stated before, the solutions obtained with these techniques can be used for the design of rule-based approaches or as a benchmark to evaluate the performance of other control strategies.

On the other hand, real-time implementable model-based techniques can also be found in literature which are able to provide results close to the global optimal solution under certain circumstances [94].

In the following, the two categories in which model-based methods could be divided will be addressed.

4.2.2.1 Numerical approaches

Numerical optimization methods are those in which the solution to the energy management problem in HEV is found numerically.

Some of the most relevant numerical approaches found in literature that have been implemented for the control of HEVs are: Dynamic Programming (DP) [26], [39], genetic algorithms [40] and stochastic dynamic programming [41].

In theory, by using numerical techniques like DP, there is no limit to the level of complexity of the problem. However, in practice, the limiting factor is the high number of computations required to find the solution [95], [96]. This numerical approach will be further discussed in section 4.4.

4.2.2.2 Analytical approaches

Analytical optimization methods use an analytical problem formulation to find a solution to the energy management problem in HEVs. Moreover, they can also be used to make the numerical solution faster than it would be by using a purely numerical method [66], [77].

As mentioned before, to be able to find a closed-form solution to the energy management problem, the level of complexity of the models employed is limited accordingly [97].

Pontryagin's Minimum Principle (PMP) [37] is one of the most widely used analytical control approaches applied to the energy management of HEVs [1]. It has been proved that, under certain conditions, PMP gives a non-causal solution which is globally optimal [42], [43].

In the field of real-time implementable model-based control methods, several research efforts have been dedicated to the Equivalent Consumption Minimization Strategy (ECMS) [27], [47]. This approach is real-time implementable since it is based on the minimization, at each time step, of a predefined cost function.

PMP and ECMS together with the connection that exists among them will be further addressed in sections 4.5 and 4.6.

In addition to the previously discussed techniques, researchers have recently show interest in the use of convex optimization [44] to solve the optimal energy management problem in HEVs [45], [46]. This approach can significantly reduce the computational time with respect to some numerical methods as DP. However, its use requires additional model approximations. Moreover, discrete control variables, e.g., ICE state or the engaged gear number, cannot be included in a convex formulation [45].

4.3 The optimal control problem in HEVs

The energy management in HEVs will be formalized here as an implementation of optimal control theory. In particular, it will be framed as a constrained-finite time horizon optimal control problem. This problem consists in finding the control law that minimizes a predefined performance index while meeting the dynamic state constraints, the local and global state constrains and the local control constraints [1].

Each of the quantities needed for a complete definition of the optimal control problem will be treated in the following sections. The reader is referred to [26], [37] for further details regarding the equations presented.

4.3.1 Performance index

The performance index to be minimized is defined as:

$$\Psi = \phi\left(\mathbf{x}(t_f)\right) + \int_{t_0}^{t_f} L\big(\mathbf{x}(t), \mathbf{u}(t)\big)\, dt \tag{4-1}$$

where,

$\mathbf{x}(t)$ is the state vector.

$\mathbf{u}(t)$ is the control vector.

$L\big(\mathbf{x}(t), \mathbf{u}(t)\big)$ is the instantaneous cost function.

$\phi\left(\mathbf{x}(t_f)\right)$ is the terminal cost.

t_f is the final time, end of the optimization horizon.

t_0 is the initial time.

$L\big(\mathbf{x}(t), \mathbf{u}(t)\big)$ is a generic cost function in which several objectives can be combined together by introducing properly calibrated weighting factors.

The terminal cost $\phi\left(\mathbf{x}(t_f)\right)$ is a penalty function used to induce the final value of state variables.

4.3.2 States and constrains

Depending on the developed model of the HEV of interest, a series of state variables are defined which will be subjected to dynamic constrains that can be represented in the form of:

$$\dot{\mathbf{x}}(t) = f\big(\mathbf{x}(t), \mathbf{u}(t)\big) \tag{4-2}$$

Global state constrains are conditions that the final value of state variables should satisfy. A state variable $x(t)$ should reach a predefined value $x_{req,f}$ at the final time t_f. This can be enforced as a hard constrain $\mathbf{x}(t_f) = \mathbf{x}_{req,f}$ or as a soft constrain introducing the penalty function $\phi\left(\mathbf{x}(t_f)\right)$ into the performance index, which is usually a function of the difference $\mathbf{x}(t_f) - \mathbf{x}_{req,f}$.

The function $\mathbf{G}\big(\mathbf{x}(t)\big)$ represents a set of inequalities that the state variables must satisfy. If the state variables are required to remain within a predefined range $[\mathbf{x}_{min}, \mathbf{x}_{max}]$ at all times, $\mathbf{G}\big(\mathbf{x}(t)\big)$ can be expressed as:

$$\mathbf{G}\big(\mathbf{x}(t)\big) \leq 0 \; \forall \; t \; \in [t_0, t_f] \tag{4-3}$$

$$G_1\big(\mathbf{x}(t)\big) \; = \; \mathbf{x}(t) \; - \; \mathbf{x}_{max} \; \leq \; 0 \tag{4-4}$$

$$G_2\big(\mathbf{x}(t)\big) \; = \; \mathbf{x}_{min} \; - \; \mathbf{x}(t) \; \leq \; 0 \tag{4-5}$$

4.3.3 Controls and constrains

The set of admissible controls are defined as:

$$\mathbf{u}(t) \in U(t) \; \forall \; t \; \in [t_0, t_f] \tag{4-6}$$

Where $U(t)$ indicates the set of admissible controls at each time step.

4.4 Dynamic programming

Dynamic programming (DP) [48], [49], [50] is a numerical method to solve problems in which a sequence of interrelated decisions have to be taken [51]. This approach yields a functional equation for which a solution can be found by using a digital computer [39].

DP is the only optimal control method capable of providing the optimal solution to problems of any complexity level within the accuracy limitations imposed by the discretization of problem variables [1], e.g., controls and states. The resolution of the vector of possible solution candidates U_k and states X_k come from a compromise between the computational burden of the calculations and the accuracy of the results [34].

When implementing DP, the optimal solution is found proceeding backwards, i.e.: starting from the final step, the sequence of controls which minimizes the sum of the costs from the current state to the end of the optimization horizon is found at each step [39].

Note that the above statement implies that in order to select the first control action, the backward solution of the entire problem needs to be found [34],

therefore, in the context of HEVs, the entire driving cycle must be known a priori, making DP a non-causal EMS.

Despite not being real-time implementable, DP yields the best available approximation of the optimal control policy for a certain HEV allowing to determine its maximum capabilities. Hence, the results obtained can be useful for:

- Optimizing the design of HEVs [98], [99].
- Designing of rule-based EMSs [100], [57], [101].
- Generating benchmark solutions for real-time implementable EMSs [35], [102], [31], [52], [53].

As stated before, one of the main practical limitations to the implementation of DP is the computational burden involved, which increases linearly with the final time and exponentially with the dimension of the state vector. This is referred to in literature as the curse of dimensionality [39].

In chapter 5, DP will be used to find the global optimal solution to the energy management of the HEV powertrain architecture described in chapter 2. Therefore, a study case won't be presented here. The reader is referred to [1] for an introductory example regarding the use of this technique for HEV control.

The theoretical aspects discussed in the next paragraphs are meant to set the basis for understanding the work presented in the following chapter.

4.4.1 The principle of optimality

The method of DP is based on Bellman's principle of optimality [48]. According to this intuitively appealing concept:

> An optimal policy has the property that whatever the initial state and initial decision are, the remaining decisions must constitute an optimal policy with regard to the state resulting from the first decision.

This implies that from any step on a discretized optimal trajectory, the remaining trajectory is optimal for the corresponding problem initiated at that step (and corresponding system states) [1], [103].

The mentioned principal will be described in mathematical terms in the next few lines.

Consider a discretized performance index for the optimal control problem starting at the initial state x_0:

$$\Psi_{0,N} = L_N(x_N) + \sum_{k=1}^{N-1} L_k(x_k, u_k) \tag{4-7}$$

where,

k indicates the time step k.

N indicates the final time step.

The corresponding optimal control trajectory is $u^* = \{u_1^*, u_2^*, \dots, u_{N-1}^*\}$.

Note that the instantaneous cost function $L_k(x_k)$, called arc cost in the context of DP, is equivalent to the integrand of the continuous formulation of the performance index presented in Eq. (4-1). Hence, $L_N(x_N)$ is the terminal cost which depends on the final state.

Let's also consider the performance index for the tail subproblem starting at time step j, i.e., the last part of the overall problem:

$$\Psi_{j,N} = L_N(x_N) + \sum_{k=j}^{N-1} L_k(x_k, u_k) \tag{4-8}$$

The implication of Bellman's principle of optimality is that the last part of the overall optimal control trajectory $\{u_j^*, u_{j+1}^*, \dots, u_{N-1}^*\}$ is the optimal solution of the tail subproblem. The analytical proof, which is based on the induction principal, can be found in [51].

4.4.2 A recurrence relation of DP

In order to show how the principle of optimality can be used to determine the solution to an optimal control problem, a recurrence relation is derived here. This will allow to illustrate the practical implementation of DP. The complete derivation can be found in [39].

The starting point is to consider a discretized version of the state dynamics described in Eq. (4-1):

$$x_{k+1} = x_k + f_k(x_k, u_k) = f_d(x_k, u_k) \tag{4-9}$$

Based on the discretized performance index defined in Eq. (4-7), the cost of reaching the final state is:

$$\Psi_{N,N}(x_N) = L_N(x_N) \tag{4-10}$$

Let's now consider a one-stage process starting at the initial state x_{N-1}:

$$\Psi_{N-1,N}(x_{N-1}, u_{N-1}) = L_{N-1}(x_{N-1}, u_{N-1}) + \Psi_{N,N}(x_N) \tag{4-11}$$

In the previous expression, the cost of driving the system from state x_{N-1} to x_N depends only on the state and control decision at the initial time step of this one-stage process since the final state can be expressed as a function of those variables through the state equation:

$$\begin{aligned} &\Psi_{N-1,N}(x_{N-1}, u_{N-1}) \\ &\qquad = L_{N-1}(x_{N-1}, u_{N-1}) \\ &\qquad + \Psi_{N,N}\big(f_d(x_{N-1}, u_{N-1})\big) \end{aligned} \tag{4-12}$$

Now it is possible to define the optimal cost as:

$$\begin{aligned} &\Psi^*_{N-1,N}(x_{N-1}) \\ &= arg\ min_{u_{N-1} \in U_{N-1}} \Big(L_{N-1}(x_{N-1}, u_{N-1}) \\ &+ \Psi_{N,N}\big(f_d(x_{N-1}, u_{N-1})\big)\Big) \end{aligned} \tag{4-13}$$

Note that only control candidates within the set of admissible controls are used when the minimization is performed [39].

Next, the optimal cost of a two-stage process will be derived. The cost of transitioning from state x_{N-2} to x_N can be described as:

$$\begin{aligned} &\Psi_{N-2,N}(x_{N-2}, u_{N-2}, u_{N-1}) \\ &\qquad = L_{N-2}(x_{N-2}, u_{N-2}) \\ &\qquad + L_{N-1}(x_{N-1}, u_{N-1}) \\ &\qquad + \Psi_{N,N}\big(f_d(x_{N-1}, u_{N-1})\big) \end{aligned} \tag{4-14}$$

It can be appreciated that the last two terms on the right side of Eq. (4-14) correspond to $\Psi_{N-1,N}(x_{N-1}, u_{N-1})$ from Eq. (4-12), hence:

$$\begin{aligned}\Psi_{N-2,N}(x_{N-2}, u_{N-2}, u_{N-1}) \\ = L_{N-2}(x_{N-2}, u_{N-2}) \\ + \Psi_{N-1,N}(x_{N-1}, u_{N-1})\end{aligned} \tag{4-15}$$

Applying the principle of optimality discussed in section 4.4.1 to this two-stage process implies that, for any initial state and control (x_{N-2} and u_{N-2}), the remaining decision must be optimal with respect to the system state resulting from the application of the control action u_{N-2}. Moreover, the state equation allows to express this resulting state x_{N-1} in terms of x_{N-2} and u_{N-2}. Based on these considerations, it is possible to rewrite Eq. (4-15) as:

$$\begin{aligned}&\Psi^*_{N-2,N}(x_{N-2}) \\ &= arg\ min_{u_{N-2} \in U_{N-2}} \Big(L_{N-2}(x_{N-2}, u_{N-2}) \\ &+ \Psi^*_{N-1,N}\big(f_d(x_{N-2}, u_{N-2})\big)\Big)\end{aligned} \tag{4-16}$$

Finally, for a j-stage process, the total cost to drive the system from a certain state x_{N-j} to the final state x_N, also called cost-to-go in the context of DP, can be expressed as:

$$\begin{aligned}&\Psi^*_{N-j,N}\big(x_{N-j}\big) \\ &= arg\ min_{u_{N-j} \in U_{N-j}} \Big(L_{N-j}\big(x_{N-j}, u_{N-j}\big) \\ &+ \Psi^*_{N-(j-1),N}\Big(f_d\big(x_{N-j}, u_{N-j}\big)\Big)\Big)\end{aligned} \tag{4-17}$$

Eq. (4-17) is the recurrence relation yield by the DP approach. This expression allows to appreciate how by proceeding backwards (starting at the final step) it is possible to find the optimal solution to the control problem at hand using model-based techniques.

One final consideration to be made here is that the application of a given control may drive the system into a state which does not exactly correspond to one of the discretized values of the state vector X_k. If this happens, the computation of the cost-to-go for each of the state grid values, which is necessary to find the solution as seen in the recurrence relation of Eq. (4-17), is done through interpolation [1].

Moreover, since only the range of admissible states is considered, the states resulting from the optimal control trajectory will never exceed the prescribed boundaries [34].

4.5 Pontryagin's minimum principle

Pontryagin's Minimum Principle (PMP) [37], [95], [104], [105], [54], constitutes a set of necessary conditions for optimality. This theorem is regarded by some authors as the beginning of modern optimal control theory [106].

Pontryagin's approach, which is a general case of the Euler-Lagrange equation in the calculus of variation [42], leads to a nonlinear TPBVP that must be solved to obtain an optimal control law [39]. In general, the problem cannot be solved analytically, thus iterative numerical techniques are employed to reach a solution [34]. Nevertheless, PMP requires less computational effort than numerical model-based optimization approaches like DP [35]. As mentioned before, the solution obtained is non-causal.

In the following paragraphs, a generic mathematical formulation of the minimum principal for problems with constrains on the state variables [1] is presented. After reviewing the most relevant characteristics of the analytical problem description obtained with PMP, its application to the energy management of HEVs will be discussed together with the methodology used to find the desired solution, i.e., a particular case of the generic optimal control problem defined in section 4.3 will be addressed.

4.5.1 Hamiltonian and co-state

To obtain the desired set of equations, the first step is to define the Hamiltonian function as:

$$\begin{aligned} H\big(\mathbf{x}(t), \mathbf{u}(t), \boldsymbol{\lambda}(t)\big) \\ &= L\big(\mathbf{x}(t), \mathbf{u}(t)\big) + \boldsymbol{\lambda}^T(t)\, f\big(\mathbf{x}(t), \mathbf{u}(t)\big) \\ &+ w(\mathbf{x})^T f\big(\mathbf{x}(t), \mathbf{u}(t)\big) \end{aligned} \tag{4-18}$$

where,

$f\big(\mathbf{x}(t), \mathbf{u}(t)\big)$ is the right-hand side of the system dynamic equation (Eq. (4-1)).

$\boldsymbol{\lambda}(t)$ is the vector of adjoint states or co-states.

$w(\mathbf{x})$ is an additive penalty function.

Next, the co-state equation is defined as:

$$\begin{aligned}\dot{\boldsymbol{\lambda}}(t) = & -\frac{\partial H}{\partial \mathbf{x}}\Big|_{\mathbf{u}(t)} \\ & = -\frac{\partial L}{\partial \mathbf{x}}\big(\mathbf{x}(t),\mathbf{u}(t)\big) \\ & -\big(\boldsymbol{\lambda}(t)+w(\mathbf{x})\big)\left[\frac{\partial f}{\partial \mathbf{x}}\big(\mathbf{x}(t),\mathbf{u}(t)\big)\right]^{T}\end{aligned} \tag{4-19}$$

Since it is required to enforce the system states to always remain within their admissible region, the Hamiltonian is modified by introducing a penalty (an extra cost) that is activated whenever the state boundaries are reached/violated [39], [95], [105], i.e.:

$$G_1\big(\mathbf{x}(t)\big) = \mathbf{x}(t) - \mathbf{x}_{max} > 0 \tag{4-20}$$

$$G_2\big(\mathbf{x}(t)\big) = \mathbf{x}_{min} - \mathbf{x}(t) > 0 \tag{4-21}$$

In order to introduce the mentioned cost into the Hamiltonian, the additive penalty function $w(\mathbf{x})$ that depends on the derivative of the constraint function must be defined [1]. To do so, the time derivatives of G_1 and G_2 are computed up to the order in which the control variables appear explicitly for the first time [58], [71]. For example, if the control $\mathbf{u}(t)$ appears in the first time derivative of G_1 and G_2:

$$\begin{aligned}&\dot{\mathbf{G}}\big(\mathbf{x}(t),\mathbf{u}(t)\big) \\ &= \begin{cases}\dot{G}_1\big(\mathbf{x}(t),\mathbf{u}(t)\big) = \dfrac{dG_1}{dt} = \dot{\mathbf{x}}(t) = f\big(\mathbf{x}(t),\mathbf{u}(t)\big) \\ \dot{G}_2\big(\mathbf{x}(t),\mathbf{u}(t)\big) = \dfrac{dG_2}{dt} = -\dot{\mathbf{x}}(t) = -f\big(\mathbf{x}(t),\mathbf{u}(t)\big)\end{cases}\end{aligned} \tag{4-22}$$

Thus, $w(\mathbf{x})$ can be defined so that solutions in which the selected control variables lead to state values outside of their admissible region are penalized:

$$w(\mathbf{x}) = \begin{cases} \sigma & if\ G_1(\mathbf{x}(t)) > 0 \text{ (upper constrains active)} \\ -\sigma & if\ G_2(\mathbf{x}(t)) > 0 \text{ (lower constrains active)} \\ 0 & if\ \mathbf{G}(\mathbf{x}(t)) < 0 \text{ (constrains not active)} \end{cases} \tag{4-23}$$

where σ is the cost of reaching/violating the state boundaries.

The value of the constant σ is arbitrary. In general, σ is selected high enough to guarantee that the introduced cost function is capable of enforcing the state constrains [107], [58].

This definition of the additive penalty function introduces discontinuities in the Hamiltonian at the times in which the state boundaries are reached/violated, this translates into discontinuities in the value of the co-state variables [108].

4.5.2 Necessary conditions for optimality

The set of necessary conditions for optimality provided by PMP [26], [37] will be addressed here.

1. Conditions on the states and co-states.

The states and co-states must satisfy the following conditions:

$$\dot{\mathbf{x}}^*(t) = \left.\frac{\partial H}{\partial \lambda}\right|_{\mathbf{u}^*(t)} \tag{4-24}$$

$$\dot{\boldsymbol{\lambda}}^*(t) = -\left.\frac{\partial H}{\partial \mathbf{x}}\right|_{\mathbf{u}^*(t)} \tag{4-25}$$

where $*$ indicates optimality.

2. Boundary conditions.

The initial conditions on the state variables are:

$$\mathbf{x}^*(t_0) = \mathbf{x}_0 \tag{4-26}$$

If only q final states are defined:

$$x_j^*(t_f) = x_{j,f} \quad j = 1, \dots, q \tag{4-27}$$

If no terminal conditions are imposed on the state, then the terminal condition is given on co-state, which must be:

$$\lambda_j^*(t_f) = \left.\frac{\partial \phi\left(\mathbf{x}(t_f)\right)}{\partial x_j}\right|_{t_f} \quad j = q+1, \dots, m \tag{4-28}$$

where m is the total number of states.

3. Conditions on the control variables.

The optimal solution $\mathbf{u}^*(t)$ at each time instant is such that:

$$\mathbf{u}^*(t) = arg\ min_{\mathbf{u}(t)\in U(t)} \left(H\left(\mathbf{u}(t), \mathbf{x}(t), \boldsymbol{\lambda}(t)\right)\right) \tag{4-29}$$

Therefore,

$$\begin{aligned} H\left(\mathbf{u}(t), \mathbf{x}^*(t), \boldsymbol{\lambda}^*(t)\right) \\ \geq H\left(\mathbf{u}^*(t), \mathbf{x}^*(t), \boldsymbol{\lambda}^*(t)\right), \forall\, \mathbf{u}(t) \\ \in U(t), \forall\, t \in [t0, tf\,] \end{aligned} \tag{4-30}$$

A control law that respects the conditions established by the minimum principle is called extremal. Since these conditions are only necessary, the optimal solution, if exists, must be an extremal control. On the other hand, not all extremal controls are optimal [37].

As it can be appreciated in the previous set of equations, PMP allows redefining an optimal control problem in terms of local conditions that must be respected at each time instant. However, the global nature of the problem does not disappear since boundary conditions are given at the initial and final time [1].

In general, solving the TPBVP yield by the conditions provided by the minimum principal implies properly selecting q initial values of the co-states so that the conditions imposed at the final time for the state variables are satisfied [26].

Hence, in order to solve the problem numerically, an iterative procedure must be used [1].

4.5.4 Application to HEVs

Having discussed a general formulation of the minimum principle applicable to problems with constrains on the state variables, the optimal solution to the energy management problem for a generic parallel HEV is obtained here by applying PMP. This will set the basis for understanding the relationship that the real-time implementable instantaneous minimization methods discussed in section 4.6 have with the optimal solution.

PMP has been extensively employed in literature to obtain the optimal EMS for several HEVs architectures [1], [26], [42], [109]–[111].

4.5.4.1 Performance index

The control objective is to minimize fuel consumption. The performance index is thus defined:

$$\Psi = \int_{t_0}^{t_f} \dot{m}_f\big(P_{EM}(t)\big)\, dt \tag{4-31}$$

where,

$\dot{m}_f\big(P_{EM}(t)\big)$ is the fuel consumption rate.

$P_{EM}(t)$ is the power request to the electrical path (EM).

The fuel mass rate $\dot{m}_f\big(P_{EM}(t)\big)$ in Eq. (4-31) corresponds to the instantaneous cost function $L\big(\mathbf{x}(t), \mathbf{u}(t)\big)$ in Eq. (4-1).

The terminal cost is excluded from the performance index since the final value of state variables is enforced as a hard constrain.

4.5.4.2 States and constrains

In general, when minimizing fuel consumption is the only concern, the only state variable considered is the SOC [34]. Instead, in this section, the State of Energy (SOE) is used as the state variable. This allows to have the battery charge-effectiveness factor explicitly in the Hamiltonian, providing clear insights about the physical meaning of the instantaneous minimization performed at each time instant.

For the definitions of variables related to the battery model, the reader is referred to section 2.2.3.4.

To derive an equation for the SOE, the first step is to define the battery electrochemical energy variation. As it can be seen in the next equation, this variable represents the amount of energy provided by the battery in a certain time window [1].

$$E_{ech}(t) = -\int_{t_0}^{t_f} P_{ech}(t)\, dt \tag{4-32}$$

where P_{ech} is the battery electrochemical power.

Note that when the battery is being discharged (positive battery electrochemical power) the energy stored in the battery reduces, thus explaining the minus sign in the previous equation.

The definition of the electrochemical power is:

$$P_{ech}(t) = V_{OC}\big(SOC(t)\big)\, I(t) \tag{4-33}$$

where,

$V_{OC}\big(SOC(t)\big)$ is the OCV.

$I(t)$ is the battery current.

The SOE is defined as the amount of energy stored E_{ech}, relative to the maximum amount of energy that the battery can hold E_b. The latter is equal to the product of the nominal charge capacity Q_{nom} and the nominal value of the OCV $V_{OC,nom}$ [112]. Thus:

$$E_b = Q_{nom} V_{OC,nom} \tag{4-34}$$

$$SOE(t) = \frac{E_{ech}(t)}{E_b} \tag{4-35}$$

The time derivative of SOE can be written as:

$$S\dot{O}E(t) = -\frac{1}{E_b} P_{ech}(t) \tag{4-36}$$

The battery charge-effectiveness factor is then defined as:

$$\varepsilon_b\big(SOC(t), P_b(t)\big) = \frac{P_b(t) + R_b\big(SOC(t)\big)I^2(t)}{P_b(t)} \tag{4-37}$$

where,

$P_b(t)$ is the power at battery terminals.

$R_b\big(SOC(t)\big)$ is the battery internal resistance.

From the zero-th order circuit model adopted in section 2.2.3.4:

$$P_{ech}(t) = P_b(t) + R_b\big(SOC(t)\big)I^2(t) \tag{4-38}$$

Finally, the state equation can be rewritten as:

$$\begin{aligned} S\dot{O}E(t) &= -\frac{1}{E_b}\left[\frac{P_b(t) + R_b\big(SOC(t)\big)I^2(t)}{P_b(t)}\right] P_b(t) \\ &= -\frac{1}{E_b}\varepsilon_b\big(SOC(t), P_b(t)\big)\, P_b(t) \end{aligned} \tag{4-39}$$

The local constraints on the state are enforced in terms of the battery SOC. Its relationship with the SOE is addressed further ahead in section 4.6.2.2. The constrains, reflect the fact that the SOC is required to remain within a certain range. This is to make the battery work at high efficiency and preserve its cycle life [112].

Analogous to Eq. (4-4) and Eq. (4-5) of the general problem formulation, it can be written that:

$$G_1\big(SOC(t)\big) = SOC(t) - SOC_{max} \leq 0 \tag{4-40}$$

$$G_2\big(SOC(t)\big) = SOC_{min} - SOC(t) \leq 0 \tag{4-41}$$

Thus $w(x)$ can be defined as:

$$w\big(SOC(t)\big) = \begin{cases} \sigma & if\ SOC(t) \geq SOC_{max} \\ -\sigma & if\ SOC(t) \leq SOC_{min} \\ 0 & else \end{cases} \tag{4-42}$$

4.5.4.3 Controls and constrains

The control variable is the power request to the electrical path.

$$u(t) = P_{EM}(t) \tag{4-43}$$

Local constraints on the control variables are imposed to guarantee that the physical operation limits of powertrain actuators are respected by the solution, e.g., maximum and minimum ICE and EM torque and speed, and battery power.

4.5.4.4 Hamiltonian and co-state

Using the variables defined above, the Hamiltonian of the system in Eq. (4-18) can be written as:

$$\begin{aligned} &H\big(SOE(t), P_{EM}(t), \lambda(t)\big) \\ &= \dot{m}_f\big(P_{EM}(t)\big) \\ &- \Big(\lambda(t) + w\big(SOC(t)\big)\Big)\left(\frac{1}{E_b}\varepsilon_b\big(SOC(t), P_b(t)\big)P_b(t)\right) \end{aligned} \tag{4-44}$$

Note that the power at battery terminals $P_b(t)$ will depend on the power requested to the electrical path $P_{EM}(t)$.

The co-state equation is defined as:

$$\begin{aligned} &\dot{\lambda}(t) \\ &= \Big(\lambda(t) \\ &+ w\big(SOC(t)\big)\Big)\left(\frac{1}{E_b}\frac{\partial\varepsilon_b\big(SOC(t), P_b(t)\big)}{\partial SOE}\ P_b(t)\right) \end{aligned} \tag{4-45}$$

The co-state has the function of relative weight of the terms in the Hamiltonian. Thanks to the selection of the SOE as the state variable, it can be seen that the

instantaneous minimization of the Hamiltonian implies minimizing the sum of the actual fuel consumed and a term that is related to the efficiency of the electrical path. This implies that even though the electrical energy is not included into the performance index, the optimal solution won't reflect an arbitrary use of it.

The units of $\lambda(t)$ are grams when the fuel consumption is computed in those same units.

4.5.4.5 Existence of the solution and sufficient conditions for optimality

An optimal EMS is assumed to exist for the HEV of interest. It is intuitive that there is at least one control trajectory that allows to minimize fuel consumption.

On the other hand, the uniqueness of the solution is not guaranteed by the theorem. If there is only one solution that satisfies the necessary conditions established by PMP, that solution must be optimal [42]. However, even if multiple controls are found, all of them could be tested to identify the one yielding the minimum cost [1].

The optimality of the solution found using PMP and its relation with the battery characteristics is discussed in [42], [43].

4.5.4.6 Solution of the optimal control problem

As stated at the beginning of section 4.5, the solution obtained with PMP is non-causal. The reason being that the initial value of the co-state that yields the optimal solution is unknow [34].

An iterative procedure that has been successfully implemented to solve the optimal control problem for HEVs using PMP is the so-called shooting method. Examples can be found in [1], [34], [71].

The mentioned procedure can be summarized in the next few steps:

1. Assume an arbitrary value for the initial co-state $\lambda(t_0)$.
2. Solve the problem finding the sequence of controls that minimizes the Hamiltonian.

   In every iteration, a control is found by:

   2.1. Define the set of admissible control values.

2.2.Compute the Hamiltonian for each control candidate.

2.3.Select the control candidate that minimizes the Hamiltonian.

3. Integrate the dynamic equations to calculate the final values $SOE(t_f)$ and $\lambda(t_f)$.
4. Repeat the above steps if the boundary conditions are not satisfied, i.e., the final value of the state variable is different than its reference (by more than a certain threshold).

4.6 Instantaneous minimization methods

Even though both PMP and DP are techniques able to provide the optimal solution to the energy management problem in HEVs, the requirement of knowing a priori the future driving conditions generates the need of searching for other EMSs that are real-time implementable.

As mentioned in section 4.2.2.2, approaches based on the minimization, at each time instant, of a predefined cost function have received a lot of attention in literature due to their causal nature.

Instantaneous minimization methods have been shown to be able to obtain results which are close to the global optimal solution [27], [94]. Moreover, the local nature of the operations performed makes these approaches computationally less demanding than other methods like DP.

In this section, ECMS, which is the most important and well-known technique among the instantaneous minimization methods, and a variant of it referred to as A-ECMS are addressed in detail to provide the theoretical foundations for the work presented in chapter 6 regarding online implementable EMSs, where their application is illustrated. In particular, their relationship with the optimal solution is discussed in section 4.6.2.

4.6.1 ECMS

The Equivalent Consumption Minimization Strategy (ECMS) [47], [113], [114], [115] is a model-based method that allows solving optimal control problems in which the control objectives are integral in nature, e.g., reducing as much as possible the total fuel consumption over a defined optimization horizon, through a succession of instantaneous minimizations of a certain cost function.

The idea at the core of the ECMS is that an equivalent fuel consumption can be associated with the use of electrical energy [116], i.e., electrical energy has a cost associated to it even when the main objective is to minimize fuel usage. This idea finds its justification in the intuitive realization that in a charge-sustaining HEV, since the SOC does not change significantly during a single driving mission, the energy storage system can be regarded as an energy buffer where all the energy ultimately comes from fuel [115], [117]. Therefore, when the EM is used, the battery will have to be recharged on a later stage, implying an instantaneous fuel consumption. On the other hand, when the battery SOC increases, considering that the energy stored could be used in the future to reduce the ICE load, this can be seen as an instantaneous fuel saving.

Based on these considerations, the ECMS algorithm, using an appropriate model of the system, estimates the fuel and electrical energy consumption resulting for each of the possible control candidates and makes a decision aiming at locally minimizing an equivalent fuel consumption given by:

$$\dot{m}_{f,eq}(t) = \dot{m}_f(t) + \dot{m}_e(t) = \dot{m}_f(t) + s(t)\frac{P_b}{LHV} \tag{4-46}$$

where,

$\dot{m}_e(t)$ is the fuel consumption rate associated with the use of electrical energy.

$s(t)$ is the ECMS equivalence factor.

LHV is the fuel lower heating value.

In order to guarantee that the EMS respects the physical limitations of powertrain components, only control candidates within the set of admissible values are used when the minimization is performed [58].

As it can be appreciated in Eq. (4-46), the equivalence factor $s(t)$ allows converting electrical power into an equivalent amount of chemical fuel power which is translated into fuel mass flow through its LHV. Note that depending on the sign of the power request to the battery, the equivalent fuel consumption can be either higher or lower than the actual fuel usage.

It is quite obvious at this point, that selecting the most appropriate value of equivalence factor is fundamental to the effectiveness of the strategy. This aspect is treated in section 4.6.2 together with the practical issues that it involves.

4.6.2 Equivalence between PMP and the ECMS

Even though ECMS was first introduced in [47] as a heuristic method derived from engineering intuition, it was later shown that under certain conditions it is equivalent to PMP [58], i.e., ECMS is able to provide the optimal solution to the energy management of HEVs.

The mathematical formulation presented in this section is meant to illustrate the relationship between ECMS and PMP, allowing to have insights about the meaning of the equivalence factor and some practical implementation issues.

4.6.2.1 Relation between the co-state and the equivalence factor

The next few lines will serve to derive an expression of the ECMS equivalence factor in terms of the co-state variable from the PMP formulation.

The expressions derived before for the Hamiltonian (Eq. (4-44)) and the equivalent fuel consumption (Eq. (4-46)) will be reported here for convenience:

$$\begin{aligned} &H\big(SOE(t), P_{EM}(t), \lambda(t)\big) \\ &= \dot{m}_f\big(P_{EM}(t)\big) \\ &- \Big(\lambda(t) + w\big(SOC(t)\big)\Big)\frac{1}{E_b}\varepsilon_b\big(SOC(t), P_b(t)\big)P_b(t) \end{aligned}$$

$$\dot{m}_{f,eq}(t) = \dot{m}_f(t) + \dot{m}_e(t) = \dot{m}_f(t) + s(t)\frac{P_b}{LHV}$$

The similarity in the form of these two equations is evident. Both expressions represent the sum of the actual fuel consumption and a term that is proportional to the energy request to the electrical path. For the former equations to be equal:

$$\begin{aligned} &s(t) \\ &= -\Big(\lambda(t) + w\big(SOC(t)\big)\Big)\,\varepsilon_b\big(SOC(t), P_b(t)\big)\,\frac{LHV}{E_b} \end{aligned} \qquad (4\text{-}47)$$

Eq. (4-47) shows that ECMS is equivalent to PMP if the equivalence factor is defined as a time-varying parameter that depends on the battery charge-

effectiveness factor, i.e., the equivalence factor is related to the efficiency of the electrical path and is not in general a constant. The fundamental implication of this fact is that a real-time implementable strategy like ECMS is also formally optimal [71].

Based on the previous considerations it should be noticed that, despite of its instantaneous formulation, the optimal solution when applying ECMS can only be guaranteed by means of an iterative procedure that relies on the future driving conditions [27], as described for PMP in section 4.5.4.6. Moreover, also in this case the function $w\big(SOC(t)\big)$ allows to maintain the SOC within its desired range.

As explained before, both the co-state and the equivalence factor allow to convert electrical power into fuel power serving as a weighting factor when minimizing the equivalent fuel consumption (or the Hamiltonian given the analogy made). The initial value selected for this variable defines how close the final state will be from its target. Since for real-time implementation an offline calibration is required, the optimal equivalence factor may different from the one for which ECMS is tuned, the strategy still works but the its potential is not fully realized.

4.6.2.2 Constant co-state assumption

It is often the case that the OCV and internal resistance characteristics of the battery are such that their dependence on SOC (over the SOC range of operation) can be neglected [1].

This implies that:

$$V_{OC}\big(SOC(t)\big) = V_{OC,eq} \tag{4-48}$$

where $V_{OC,eq}$ is the constant value of the OCV considered for a certain SOC range.

In the case in which the OCV can be considered a constant, the relationship between the SOE and the SOC can be described starting from Eq. (4-33) and Eq. (4-35) as:

$$SOE(t) = -\frac{\int_{t_0}^{t_f} V_{OC}\big(SOC(t)\big)\, I(t)\, dt}{E_b} = \frac{V_{OC,eq}}{V_{OC,nom}}\frac{Q(t)}{Q_{nom}} = \frac{V_{OC,eq}}{V_{OC,nom}}\, SOC(t) \tag{4-49}$$

In addition, the derivative of the charge-effectives factor with respect to SOC is:

$$\frac{\partial \varepsilon_b\big(SOC(t), P_b(t)\big)}{\partial SOC} = \frac{1}{P_b^2(t)}\left(\left(\frac{\partial P_b(t)}{\partial SOC} + \frac{\partial R_b(SOC(t))}{\partial SOC} I^2(t) + 2\frac{\partial I(t)}{\partial SOC}\right) P_b(t) - \Big(P_b(t) + R_b\big(SOC(t)\big) I^2(t)\Big)\frac{\partial P_b(t)}{\partial SOC}\right) \tag{4-50}$$

with:

$$\frac{\partial I(t)}{\partial SOC} = \frac{\partial I(t)}{\partial V_{OC}}\frac{\partial V_{OC}\big(SOC(t)\big)}{\partial SOC} + \frac{\partial I(t)}{\partial R_b}\frac{\partial R_b\big(SOC(t)\big)}{\partial SOC} \tag{4-51}$$

Therefore, under the assumptions:

$$\frac{\partial V_{OC}(SOC(t))}{\partial SOC} \approx 0 \tag{4-52}$$

$$\frac{\partial R_b(SOC(t))}{\partial SOC} \approx 0 \tag{4-53}$$

It can be concluded that:

$$\frac{\partial \varepsilon_b(SOC(t), P_b(t))}{\partial SOE} \approx \frac{\partial \varepsilon_b(SOC(t), P_b(t))}{\partial SOC} \approx 0 \tag{4-54}$$

This means that the co-state equation can be approximated to:

$$\dot{\lambda}(t) = \big(\lambda(t) + w(x)\big)\left[\frac{1}{E_b}\frac{\partial \varepsilon_b\big(SOC(t), P_b(t)\big)}{\partial SOE}\, P_b(t)\right] \approx 0 \tag{4-55}$$

Meaning the co-state has a constant value:

$$\lambda(t) = \lambda(t_0) \tag{4-56}$$

Eq. (4-56) implies that the equivalence between ECMS and PMP can be exploited without having to integrate the co-state equation, which reduces the computational load. Hence, the quality of the results is directly linked to the selection of the initial co-state, which, as stated before, serves as a weighting factor when minimizing the equivalent fuel consumption. Therefore, if the selected value is too high, the cost of using electrical energy would be excessively elevated making the electrical path capabilities not fully exploited. On the other hand, if it is too low, the battery would be depleted fast implying that the EM won't be necessarily used when it is most convenient.

The constant co-state assumption has shown in simulations to yield results close to the optimal solution obtain with a dynamic co-state [71], [42].

4.6.2.3 Notes on the co-state

Having explained the physical meaning of the co-state for the optimal control of HEVs, in this paragraph, some of the most relevant remarks to the work that will be presented in chapter 6 about its behavior are presented.

For the case in which road grade is not considered, the following observations regarding the co-state can be found in literature:

- The co-state is a function of both the HEV powertrain and driving cycle features [26]. In particular, the energy characteristics of driving cycles, i.e., the amount of potential regenerative braking relative to the total tractive energy request, has been identified to be linked to the optimal co-state value [71].

- The dependency of the optimal initial co-state on the driving cycle characteristics implies that the optimal EMS for HEVs can only be warranted by PMP/ECMS when the method is applied offline [34].
- Simulations results have shown that, depending on some characteristics of the energy storage system, the co-state could be approximated by its initial value since it presents very small variations during the whole driving cycle [1], [53], [118], [119].
- For a given driving cycle, the optimal co-state increases with the trip length [60], [118]. However, after a certain distance is traveled, the mentioned trend becomes less evident [38].

4.6.3 A-ECMS

In section 4.6.2 the most relevant characteristics of the equivalence factor were discussed. In particular, it was addressed how the selection of its value affects the quality of the results obtained with ECMS in terms of reaching the target SOC at the end of the driving mission.

Considering that a real-time implementable strategy cannot retain the future driving conditions as known, an adaptation scheme for the equivalence factor should be in place to adjust the value of this parameter as driving conditions change. EMSs that perform this kind of adaptation online are referred to in literature as Adaptive Equivalent Consumption Minimization Strategy (A-ECMS).

Based on the adaptation techniques, A-ECMS implementations can be divided in the following categories:

- Adaptation based on driving cycle prediction [29], [120], [121].
- Adaptation based on driving pattern recognition [122], [59].
- Adaptation based on feedback from SOC [60], [73], [61], [72].

The methods in the first of the three aforementioned categories use estimates of the future driving conditions to perform a periodic recalculation/optimization of the equivalence factor. On the other hand, techniques based on driving pattern recognition select the most suitable value from data stored offline based on an analysis of the past driving conditions. Therefore, the later method takes advantage

of the fact that similar optimal equivalence factors are required for driving schedules with similar characteristics.

In the following paragraph, A-ECMS variants in which the equivalence factor is adapted based on feedback from SOC will be treated in more detail since they are at the basis of the real-time implementable strategies developed in chapter 6.

The various implementations of A-ECMS available in literature have shown that this causal strategy, despite being suboptimal, can generate results close to the optimal solution [60], [73].

4.6.3.1 Adaptation based on feedback from SOC

In A-ECMS approaches that use SOC feedback, the main idea is to dynamically update the value of the equivalence factor using classical feedback control methods based on the difference between the current SOC and a predefined reference [1].

For charge-sustaining operation, the SOC reference is usually regarded as a constant [73]. Instead, for a charge-depleting operation, as generally seen in PHEVs, the optimal SOC trajectory is a quasi-linear decreasing function of the traveled distance, which is referred to as a blended strategy [60], [118], [123], [124].

The main advantages of A-ECMS approaches based on feedback from SOC is their robustness and low computational burden when compared to other control techniques. However, its full potential can only be realized if the parameters of the adaptation law are properly tuned.

A possible adaptation scheme is to update the value of the equivalence factor at each instant according to [61]:

$$s(t) = s_0 + K_p\left(SOC_{ref}(t) - SOC(t)\right) + K_I\int_{t_0}^{t_f}\left(SOC_{ref}(t) - SOC(t)\right)dt \tag{4-57}$$

where,

s_0 is the initial equivalence factor.

K_p is the proportional gain of the adaptation law.

K_I is the integral gain of the adaptation law.

SOC_{ref} is the reference trajectory for the SOC.

In Eq. (4-57) the integral action is added to guarantee better performance when tracking a constant reference value, at the price of having an extra tuning parameter. This continuous adaptation scheme may not always be desirable since it would prevent using the battery over its entire SOC range. This is due to the fact that even small deviations from the reference value will be corrected right away [1].

In alternative to performing a continuous adaptation of the equivalence factor, a discrete adaptation law could be implemented. For example, in [73] the update is performed in regular intervals of time length T_s:

$$s(t+T_s) = \frac{s(t)+s(t-T_s)}{2} + K_p\left(SOC_{ref}(t) - SOC(t)\right) \tag{4-58}$$

or after a certain distance is traveled as in [60]:

$$s(D+D_s) = \frac{s(D)+s(D-D_s)}{2} + K_p\left(SOC_{ref}(D) - SOC(D)\right) \tag{4-59}$$

where,

T_s is the sampling time.

D_s is the sampling distance.

D is the current covered distance.

In the former two equations, the two previous values of the equivalence factor are used to stabilize the output. This expression corresponds to an Autoregressive Moving Average (ARMA) filter [60].

As stated before, in order to get proper results, the adaptation law parameters must be calibrated correctly. In [125] the sampling distance and the proportional gain have been shown to have small influence on the quality of the results. Hence,

a constant value can be used for different driving missions, which can be selected during offline calibration [34]. On the other hand, a parameter that has an elevated impact on the results obtained is the initial value of the equivalence factor.

In order to properly initialize the equivalence factor, a pre-computed offline map (see Figure 4-1) can be used in which the optimal values are stored for several different cycles based on the total traveled distance and the average speed as done in [60]. This finds its justification in the observations made about the co-state behavior in section 4.6.2.3.

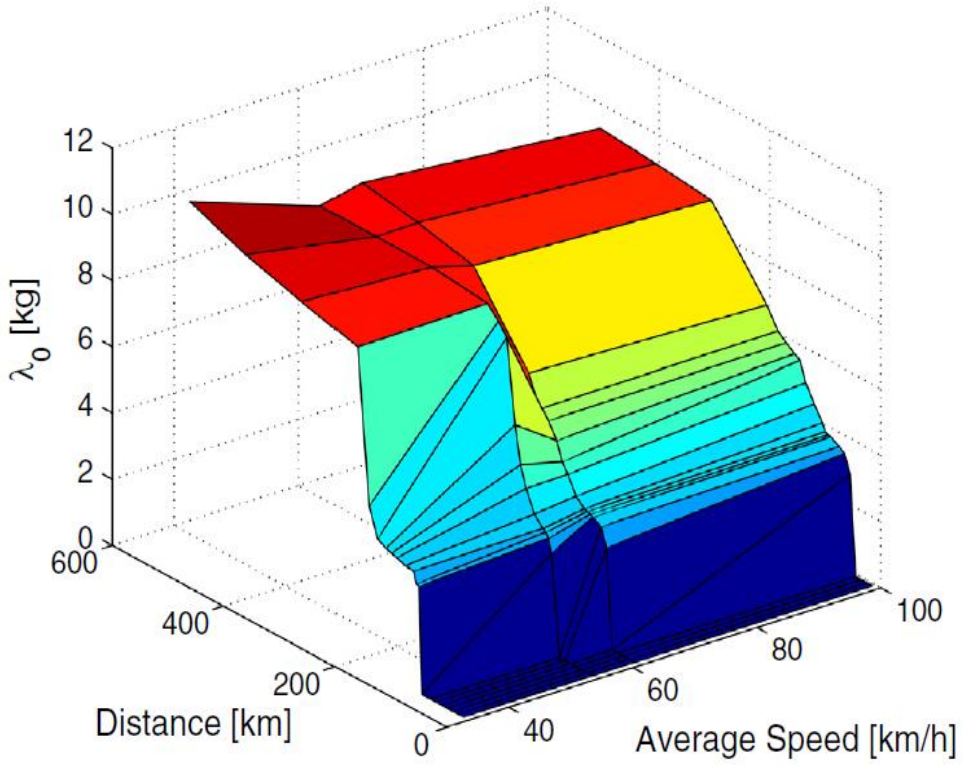

Figure 4-1. Optimal co-state value as a function of distance and average speed [60].

4.7 Drivability concerns in energy management strategies for HEVs

A common issue found in EMSs that do not explicitly incorporate drivability metrics in their performance index, is that the requests sent to the powertrain actuators aiming at optimizing the onboard energy consumption may have negative effects on vehicle drivability [36].

In particular, two of the most relevant type of decisions that can potentially cause drivability issues in HEVs are [62], [63]:

- High frequency switching among powertrain operating points/modes, e.g., from ICE-only mode to EV-mode.
- Frequent gearshifts.

These types of behavior can potentially reduce the vehicle dynamic performance by inducing oscillations in the powertrain which will cause discomfort to the vehicle occupants [36].

Because of the way in which they are formulated, instantaneous minimization methods are especially inclined to provide control requests that would generate high frequency switching between powertrain components operating points. The reason for this is that the cost related to several control candidates may be very similar, which makes it possible for small variations in the driving conditions to continuously favor the selection of substantially different operating points based on neglectable improvements in the cost function of interest.

In [36], [87] this problem is handled by only searching among controls corresponding to operating points which are close to the one from the previous iteration. This procedure has the extra benefit of reducing the computational burden of the calculations needed for the implementation of ECMS. Another approach would be to introduce some hysteresis into the ECMS formulation, preventing the EMS from inducing changes in the powertrain operating conditions if the gain in terms of equivalent fuel consumption is below a certain value [126].

When fuel consumption is the main concern, requesting transient events such as gearshifts and ICE starts that would result in little to no improvement in this regard should be avoided since, in addition to the drivability issues discussed above, there is an energy loss associated to them.

Several research efforts have been dedicated to solve these issues using different approaches. In [64], [65] minimizing the overall number of ICE starts and gearshifts was included as one of the control objectives of a stochastic dynamic programming algorithm. Instead, in [27] to prevent frequent ICE starts/stops as a result of implementing ECMS, the cost function is incremented considering the fuel equivalent energy (electrical energy used to power the starter) that is required to accelerate the ICE from rest to idle speed. In addition to the energy needed to go through the ICE start process, the energy losses of ICE starts and gearshifts are considered in [66]. Properly accounting for the energy needed to perform these operations allowed the developed DP formulation to minimize fuel consumption without providing a solution with frequent start/stops or the presence of gear hunting behavior.

A detailed explanation of the considerations made to exclude frequent ICE start events and gearshifts from the solutions obtained with the developed EMSs is provided chapters 5 and 6.

4.8 Summary

The energy management in hybrid vehicles consists in deciding the amount of power delivered at each time instant by the onboard energy sources. In production vehicles, EMSs must be causal since real-time implementation is required. In this chapter, some of the most relevant EMSs for HEVs having as the main objective the task of reducing the overall fuel consumption during a driving mission are reviewed, setting the theoretical basis for understanding the work presented in chapters 5 and 6.

The energy management problem in HEVs is formalized here as an implementation of optimal control theory and the procedure to obtain the optimal solution using PMP is addressed. This allowed to demonstrate the equivalence between ECMS and PMP, which implies that a real-time implementable EMS can also be regarded as formally optimal. In addition, the main characteristics of the equivalence factor are addressed. It is explained that the quality of the results obtained with ECMS in terms of reaching the target SOC depends directly on the selection of its value. Since the optimal co-state is a function of the driving cycle features and a real-time implementable strategy cannot retain this information as known, an adaptation scheme for the equivalence factor should be in place to adjust the value of this parameter as driving conditions change. Hence, A-ECMS variants in which the equivalence factor is adapted based on feedback from SOC are treated

in detail. As found in literature, these algorithms can be properly tuned only knowing the total trip length and the average speed.

On the other hand, DP is also addressed because it is the only optimal control method capable of providing the optimal solution to problems of any complexity level within the accuracy limitations imposed by the discretization of problem variables. Despite being non-causal, its results are useful for designing rule-based EMSs and generating benchmark solutions.

Finally, it is explained how EMSs that do not explicitly incorporate drive quality metrics in their performance index may have negative effects on the vehicle drivability while aiming at optimizing the onboard energy consumption. Some of the solutions that have been proposed to avoid high frequency switching among powertrain operating points/modes and frequent gearshift requests are discussed.

Chapter 5

5. Dynamic Programming Solution for the Energy Management Problem in Hybrid Electric Vehicle powertrains equipped with Dual-Clutch Transmissions

5.1. Problem formulation

The energy management problem in HEVs is formalized in chapter 2 as an implementation of optimal control theory. In particular, it is framed as a constrained-finite time horizon optimal control problem that consists in finding the control law that minimizes a predefined performance index while meeting the dynamic state constraints, the local and global state constrains and the local control constraints.

In this chapter, DP (see section 4.4) is used to find the global optimal solution to the energy management of the HEV powertrain architecture described in section 2.2. In the current section, the general problem formulation used is given in a discretized form as it is solved by the DP algorithm.

5.1.1 Arc cost

The control objective is to minimize the overall fuel consumption during a certain driving cycle. The performance index is thus defined:

$$\Psi_{0,N} = \sum_{k=0}^{N-1} \dot{m}_{f,tot,k} \mathrm{T}_s \tag{5-1}$$

where,

k indicates the time step k.

N indicates the final time step.

$\dot{m}_{f,tot,k}$ is the total fuel consumption rate which considers the fuel penalties discussed in section 5.3.

T_s is the fixed time step used by the DP algorithm (1 s).

Note that the instantaneous fuel consumption in Eq. (5-1) corresponds to the arc cost of the generic performance index defined in Eq. (4-7).

5.1.2 Driving cycle information

According to the backward quasi-static modeling approach (see section 2.2.2.1) adopted for the development of EMSs for HEVs, the DP implementation used requires as inputs from the driving cycle data:

- Mean vehicle speed: v_k
- Vehicle acceleration: a_k

At each iteration, the mean vehicle speed between consecutive points in the given speed profile (v_j and v_{j+1}) is computed:

$$v_k = \frac{v_{j+1} + v_j}{2} \tag{5-2}$$

As explained in section 2.2.2.1, it is assumed that during each time step the vehicle acceleration is constant:

$$a_k = \frac{v_{j+1} - v_j}{\mathrm{T}_s} \tag{5-3}$$

5.1.3 States discretization and constrains

In the DP formulation developed to solve the energy management problem at hand, a total of five state variables are defined:

- SOC.
- Gear number.
- Quick-disconnect clutch state.
- ICE state.
- EM torque counter state.

Each of these variables is defined here in a discretized form. The local and global state constrains imposed together with the resolution of the state grid (vectors composed by all the possible values the states can have, see section 4.4) are also reported.

As mentioned in chapter 2, in general, when minimizing the overall fuel consumption is the main control objective, the battery SOC is used as the only state variable [34]. However, when solving an optimal control problem by means of DP, the only way to pass information from one iteration to the next is using state variables. As a consequence, for the DP solution to account for the gearshift and ICE start losses, the fuel cut-off functionality and the limitation described in section 2.2.3.3 regarding the EM torque, four additional state variables are needed.

5.1.3.1 SOC

Since the SOC is a dynamic variable, it is defined as a state. Being able to estimate the value of the SOC at each iteration enables the algorithm to account for the physical limitations of the energy storage system and to impose a final target for it.

The SOC is defined here using a discretized version of Eq. (2-50):

$$SOC_k = SOC_{k-1} - \frac{I_k}{Q_{nom}} \mathrm{T}_s \tag{5-4}$$

where,

Q_{nom} is the nominal charge capacity.

I_k is the battery current.

Note that Eq. (5-4) implies that the state dynamics depends on the state itself and on the control inputs, i.e.:

$$SOC_k = SOC_{k-1} + f_k(SOC_{k-1}, \mathbf{u}_k) \tag{5-5}$$

where $\mathbf{u}_k$ is the control vector.

For the charge-depleting simulations presented in section 5.5, a specific final value is not required. On the other hand, an initial condition is given:

$$SOC_0 = 0.905 \tag{5-6}$$

Instead, for charge-sustaining simulations:

$$SOC_0 = 0.5 \tag{5-7}$$

$$SOC_N \in [0.505, 0.495] \tag{5-8}$$

For the practical implementation of the DP formulation developed, the constrains on the final value of the state variables must be given as a range instead of as a single value. As seen in Eq. (5-8), charge sustainability is considered to be achieved if the final SOC value is within a 10 % range around its initial value.

According to the characteristics of the energy storage system present in the vehicle of interest, the local state constrains are defined as:

$$SOC_{max} = 0.93 \tag{5-9}$$

$$SOC_{min} = 0.32 \tag{5-10}$$

A final remark is made regarding the discretization of the SOC. The resolution selected for the SOC grid is 0.1 %. As seen in simulation, a high SOC discretization

helps to reduce the influence of numerical errors in the DP solution at the cost of an increased computational effort.

5.1.3.2 Gear number

In order to introduce the modeling of the gearshift losses (see section 2.2.4) into the DP formulation, the gear number is defined as a state. In this way, by comparing the value of this variable at the previous iteration with the gear command being given at the current step, gearshift maneuvers are detected, and the corresponding losses can be estimated.

For the gear number, the state dynamics depends only on the control inputs:

$$gn_{x,k} = gn_{u,k} \tag{5-11}$$

where $gn_{u,k}$ is the gear command.

Since the PHEV of interest is equipped with a 6-speed DCT, seven discrete values (state grid resolution equal to 1) are possible for the gear number state:

$$gn_{x,max} = 6 \tag{5-12}$$

$$gn_{x,min} = 0 \tag{5-13}$$

The neutral gear ($gn_x = 0$) is forced when the torque request to the vehicle is zero.

For the gear number, there are no boundary conditions.

5.1.3.3 Quick-disconnect clutch state

In order to introduce the modeling of the ICE start losses (see section 2.2.5) into the DP formulation, the quick-disconnect clutch state is defined. In this way, by comparing the value of this variable at the previous iteration with the clutch command being given at the current step, ICE start maneuvers are detected, and the corresponding losses can be estimated. Note that it is considered that each time the quick-disconnect clutch state goes from open (disengaged) to closed (engaged), an ICE start is undertaken.

As it can be inferred from the previous remarks, the quick-disconnect clutch state is a binary variable (state grid resolution equal to 1) that can assume one of two values: open ($QD_{x,k} = 0$) or closed ($QD_{x,k} = 1$). Thus, it can be written:

$$QD_{x,max} = 1 \tag{5-14}$$

$$QD_{x,min} = 0 \tag{5-15}$$

As for the gear number, the state dynamics depends only on the control inputs:

$$QD_{x,k} = QD_{u,k} \tag{5-16}$$

where $QD_{u,k}$ is the quick-disconnect clutch command.

For this state, there are no boundary conditions.

5.1.3.4 ICE state

Similar to the quick-disconnect clutch state, the ICE state is a binary variable (state grid resolution equal to 1) that can assume one of two values: off ($ICE_{x,k} = 0$) or on ($ICE_{x,k} = 1$).

Therefore, it can be written:

$$ICE_{x,max} = 1 \tag{5-17}$$

$$ICE_{x,min} = 0 \tag{5-18}$$

Moreover, the state dynamics depends only on the control inputs. The ICE state is determined by the torque request resulting from the torque split control input:

$$ICE_{x,k} = \begin{cases} 1 & for\ T_{ICE,k} > 0 \\ 0 & else \end{cases} \tag{5-19}$$

where $T_{ICE,k}$ is the torque request to the ICE decided by the EMS.

For this state, there are no boundary conditions.

The reason behind the definition of this state is that the quick-disconnect clutch status is not enough to determine if the ICE is being used or not since the fuel cut-off functionality is introduced, i.e., it is possible to turn off the ICE without opening

the quick-disconnect clutch, and therefore, without having to perform an ICE start event the next time this component is needed. Note that not disconnecting the ICE from the rest of the driveline means that the EM will be obligated to drag its inertia and also to compensate for its losses.

5.1.3.5 EM torque counter state

As explained in section 2.2.3.3, a counter is needed to assess for how many consecutive time steps the EM torque request has been higher (in absolute value) than its continuous torque limit. This information is crucial to establish whether to enforce the continuous or peak torque limits when defining the set of admissible control inputs to the EM. In particular, from experimental experience it was determined that: if the continuous torque limit is breached for 7 consecutive seconds, at least 13 s must pass before the EM torque can go again above its continuous boundary. This condition is set to ensure that the EM components operate on a desirable temperature range. Hence, a counter is designed in which each time the torque request is within the continuous limit and its value is lower than 7, a reset is enforced. On the other hand, when the counter reaches a value of 7, it is reset only after 13 additional time steps have passed.

Based on the previous considerations, the following local conditions are established:

$$\mathrm{T}_{EM,lim,max} = 20 \tag{5-20}$$

$$\mathrm{T}_{EM,lim,min} = 0 \tag{5-21}$$

In section 5.4, the limitations imposed on the EM torque request are described together with an explanation of how the aforementioned counter is used to enforce those limits.

Furthermore, it is also clear than the state dynamics depends on the state and the control inputs, i.e.:

$$\mathrm{T}_{EM,lim,k} = \mathrm{T}_{EM,lim,k-1} + f_k(\mathrm{T}_{EM,lim,k-1}, \mathbf{u}_k) \tag{5-22}$$

Note that being this state a counter, the resolution of the state grid is equal to 1. Quite obviously, the initial state constrain is:

$$\mathrm{T}_{EM,lim,0} = 0 \tag{5-23}$$

5.1.4 Controls discretization and constrains

According to the architecture of the powertrain system studied, three control variables are needed:

- Torque split factor.
- Gear command.
- Quick-disconnect clutch command.

In the following, the physical meaning of each of these variables is addressed. The local control constrains imposed together with the resolution of the control grid (vectors composed by all the possible values the control variables can have, see section 4.4) are also reported.

5.1.4.1 Torque split factor

As explained in section 4.1, the main task of any EMS for HEVs consists in deciding the amount of power delivered at each time instant by the onboard energy sources. Hence, the Torque Split Factor (TSF) is a control variable introduced to indicate to powertrain actuators how the total power request at the wheels is distributed between the ICE and the EM.

The TSF is defined as the ratio between the EM torque request $T_{EM,k}$ and the total torque request at the transmission input $T_{tot,k}$:

$$TSF_k = \frac{T_{EM,k}}{T_{tot,k}} \tag{5-24}$$

The local constrains on the TSF are:

$$TSF_{max} = 1 \tag{5-25}$$

$$TSF_{min} = -1 \tag{5-26}$$

Given the definition presented in Eq. (5-24), the physical meaning of the values the TSF can take is summarized as:

- $TSF_k = 1$ implies operation in EV-mode.
- $TSF_k \in (0,1)$ implies operation in parallel hybrid mode.

- $TSF_k = 0$ implies operation in ICE-only mode.
- $TSF_k \in [-1,0)$ implies operation in parallel hybrid mode. In this case, additional power, with respect to the tractive energy needed, is requested to the ICE to recharge the battery.

It was seen in simulation, that increasing the resolution of the TSF grid allows to have better results. A value of 0.05 is selected.

5.1.4.2 Gear command

At each time step, the EMS must select the engaged gear on the DCT. As described in section 2.2.3.2, there are six possible gears to choose from, hence:

$$gn_{u,max} = 6 \tag{5-27}$$

$$gn_{u,min} = 1 \tag{5-28}$$

As explained for the gear number state, the neutral position is enforced based on the torque request at the wheels (see section 5.1.3.2).

Being the gear number a discrete variable, the resolution of the control grid is equal to 1.

5.1.4.3 Quick-disconnect clutch command

According to the definition given for the quick-disconnect clutch state in section 5.1.3.3, the corresponding control is also a binary variable (grid resolution equal to 1) that can assume one of two values:

$$QD_{u,max} = 1 \tag{5-29}$$

$$QD_{u,min} = 0 \tag{5-30}$$

The physical meaning of these values is:

- $QD_{u,k} = 1$ implies that the clutch is closed or kept closed.
- $QD_{u,k} = 0$ implies that the clutch is open or kept open.

5.2 Introduction of gearshift and ICE start losses

In this section, the way in which the modeling of the gearshift and ICE start losses (see sections 2.2.4 and 2.2.5) are integrated into the DP formulation is described. In particular, the computation of the total torque request to powertrain actuators and its distribution among the ICE and the EM are described while explaining how the outputs of the mentioned loss models are employed.

As anticipated in chapter 2, properly accounting for the energy needed to perform gearshift and ICE start operations allows to develop control strategies in which these maneuvers are undertaken when it is convenient in terms of the overall energy consumption. In the simulation results presented in section 5.5.2.2, the effects of integrating the loss models developed for the mentioned transient events are illustrated.

5.2.1 Total torque request

The use of the quantities estimated by the models described in chapter 2 to generate the total torque request at the EM shaft is discussed in this paragraph.

The total torque request at the EM shaft when there is no gearshift is:

$$T_{tot,ngs,k} = \begin{cases} T_{ICE,in,k} + T_{ICE,drag,k} + T_{EM,in,k} + T_{GB,inp,k} & for\ es_k \neq 1\ and\ QD_{u,k} \neq 0 \\ T_{EM,in,k} + T_{GB,inp,k} & for\ es_k = 1\ or\ QD_{u,k} = 0 \end{cases} \quad (5\text{-}31)$$

where,

$T_{ICE,in,k}$ is the ICE inertia torque (see Eq. (2-61)).

$T_{ICE,drag,k}$ is the ICE drag torque (see Eq. (2-66)).

$T_{EM,in,k}$ is the EM inertia torque (see Eq. (2-41)).

$T_{GB,inp,k}$ is the torque request at the wheels reported to the EM shaft (see Eq. (2-39)).

es_k is the ICE start status.

When there is an ICE start, i.e., the state of the quick-disconnect clutch goes from open to closed, the ICE start status es is 1, otherwise, it is set to 0.

In Eq. (5-31) the ICE drag torque and its inertia are considered only when the quick-disconnect clutch is closed and when an ICE start is not being undertaken. These contributions are already considered in the ICE start loss model.

On the other hand, when a gearshift event occurs, the total torque request at the EM shaft is computed based on the output of the DCT gearshift loss model. Therefore, in general, it can be written:

$$T_{tot,k} = \begin{cases} T_{tot,ngs,k} & for\ gs_k = 0 \\ T_{tot,gs,k} & for\ gs_k = 1\ and\ QD_{u,k} = 0 \\ T_{tot,gs,k} + T_{ICE,drag,k} & for\ gs_k = 1\ and\ QD_{u,k} \neq 0 \end{cases} \quad (5\text{-}32)$$

where,

$T_{tot,gs,k}$ is the total torque request during gearshift maneuvers, i.e., the output of the gearshift loss model presented in section 2.2.4.

gs_k is the gearshift status.

The gearshift status is set to 1 when the current gear number is different from the previous one, otherwise, its value is equal to 0. This excludes the case when going to/from neutral in which there is no need to compute the gearshift losses.

Note that the ICE drag torque is added to the output of the gearshift loss model since this source of dissipation is not considered when generating $T_{tot,gs,k}$.

As it was explained in section 2.2.5, a gearshift maneuver and an ICE start event are not undertaken during the same time step.

5.2.2 Torque request to ICE

The ICE torque request is elaborated here based on the TSF and the ICE start status.

It is assumed that the ICE will be requested to provide positive torque. Therefore, considering the TSF, it can be written:

$$T_{ICE,k} = \begin{cases} T_{tot,k}(1 - TSF_k) & for\ T_{tot,k} > 0 \\ 0 & else \end{cases} \quad (5\text{-}33)$$

where $T_{ICE,k}$ is the torque request to the ICE.

On the other hand, in case of a negative request to the thermal path, mechanical braking is employed:

$$T_{br,k} = \begin{cases} T_{tot,k}(1 - TSF_k) & for\ T_{tot,k} < 0 \\ 0 & else \end{cases} \quad (5\text{-}34)$$

where $T_{br,k}$ is the torque request to the mechanical brakes reported at the EM shaft.

However, in case of an ICE start, the ICE torque request and angular speed are overwritten by the outputs of the ICE start loss model as explained in section 2.2.5.

5.2.3 Torque request to EM

Similar to the ICE torque request, the torque that the EM must provide is computed based on the TSF and the ICE start status.

Considering the extra torque request computed by the ICE start loss model (see Eq. (2-89)), the EM torque is:

$$T_{EM,k} = \begin{cases} T_{tot,k} TSF_k & for\ es_k = 0 \\ T_{tot,k} TSF_k + T_{EM,es,k} & else \end{cases} \quad (5\text{-}35)$$

where $T_{EM,es,k}$ is the additional torque request to the EM computed by the ICE start loss model.

5.3 Introduction of fuel penalties

In section 5.1.3.4, it is discussed how the introduction of a state variable for the ICE allowed the developed DP formulation to account for the possibility of not utilizing this component even when the quick-disconnect clutch is closed, which it is referred to here as the fuel cut-off functionality.

To account for the fact that the ICE will cool down during the time steps in which there is a fuel cut-off or when the quick-disconnect clutch is disengaged, meaning that an extra quantity of fuel will have to be used to compensate for it, a fuel penalty is introduced. For simplicity, a constant value is considered.

Therefore, the total fuel consumption rate is:

$$\dot{m}_{f,tot,k} = \begin{cases} \dot{m}_{f,k} + \dot{m}_{f,cds} & for\ es_k = 1\ or\ fco_k = 1 \\ \dot{m}_{f,k} & else \end{cases} \quad (5\text{-}36)$$

where,

$\dot{m}_{f,k}$ is interpolated from the ICE fuel rate map (see Eq. (2-62)).

$\dot{m}_{f,cds}$ is the fuel penalty for ICE cold starts (0.1 g/s).

fco_k is the ICE fuel cut-off status.

When the ICE state goes from 0 to 1, i.e., from off to on, the ICE fuel cut-off status is equal to 1, otherwise, it is set to be 0.

5.4 Infeasible working conditions

The solution candidates that lead the system to infeasible working situations are identified by verifying a series of conditions related to the physical limitations of the powertrain components.

Infeasible operating conditions are summarized by grouping them into different categories according to the variables being constrained. If any of the conditions stated below is verified, the corresponding solution candidate will be discarded by assigning a high enough cost to it.

es and gs

In order to avoid further complicating the gearshift and ICE start loss models, it is assumed that these events are not performed in the same time step.

Therefore, the corresponding infeasible condition could be expressed as:

$$es_k = 1\ and\ gs_k = 1 \quad (5\text{-}37)$$

EM speed during ICE start

As explained in section 2.2.5, the EM speed during ICE starts must be greater than the ICE speed at all times (except at the end of the process).

Gear selection

Given that multiple shifts in DCTs in which the gears involved are related to the same primary shaft (and clutch) would have to be modeled differently than single shifts, the offgoing and oncoming gear cannot both be even or odd gears. This condition eliminates the need to introduce an additional model for the estimation of gearshift process energy consumption.

Mechanical braking during gearshifts

Note that according to the speed profiles assumed for upshifts and downshifts when computing the energy consumption of the gearshift process (see section 2.2.4.3), only positive torque can be transmitted through both clutches. Hence, it is assumed that a negative torque request at the wheels will be provided by the mechanical brakes when changing gears.

This implies that the total torque request computed based on the output of the gearshift loss model in Eq. (5-32) must not be fulfilled by attributing part of it to the mechanical brakes, that will only be responsible for the request at the wheels. Then, the corresponding infeasible condition can be expressed as:

$$T_{br,k} \neq 0 \; and \; gs_k = 1 \; and \; T_{v,k} < 0 \tag{5-38}$$

where $T_{v,k}$ is the torque request at the wheels (see section 2.2.3.1).

Note that $T_{br,k}$, as defined in Eq. (5-34), represents the part of the total torque request at the EM shaft attributed to the mechanical brakes. Therefore, it does not account for the torque request at the wheels during gearshifts performed while braking.

ICE torque request

In the next few lines, the constrains on the ICE torque request are presented.

As explained in section 2.2.5, the ICE cannot be used to satisfy the wheel torque request during ICE starts. Hence, the infeasible operating condition can be represented as:

$$es_k = 1 \; and \; TSF_k \neq 1 \tag{5-39}$$

Differently from the PHEV architecture described in section 2.1, the powertrain studied for energy management purposes does not have a BAS, therefore, when the quick-disconnect clutch is commanded to be open, it makes no sense to use the ICE. Hence:

$$QD_{u,k} = 0 \; and \; TSF_k \neq 1 \tag{5-40}$$

One last set of infeasible operating conditions regarding the ICE torque request can be written considering its maximum and minimum limits:

$$T_{ICE,k} > T_{ICE,max,k} \tag{5-41}$$

$$T_{ICE,k} < T_{ICE,min} \; es_k = 0 \tag{5-42}$$

where,

$T_{ICE,max,k}$ is the maximum ICE torque (see section 2.2.3.5).

$T_{ICE,min}$ is the minimum ICE torque (see section 2.2.3.5).

Note that the condition on the minimum torque request is not enforced during ICE start events. Further note that the output of the ICE start loss model is designed to avoid requesting negative values.

ICE speed

As for the torque request, there are also infeasible operating conditions that regard the ICE speed.

In general, the crankshaft speed cannot exceed its maximum limit, hence, it is not allowed that:

$$\omega_{ICE,k} > \omega_{ICE,max} \; and \; QD_{x,k} = 1 \tag{5-43}$$

where,

$\omega_{ICE,k}$ is the crankshaft angular speed.

$\omega_{ICE,max}$ is the maximum value of the ICE angular speed (see section 2.2.3.5).

Same applies to its minimum speed limit when ICE is on:

$$\omega_{ICE,k} < \omega_{ICE,idle} \; and \; QD_{x,k} = 1 \; and \; T_{ICE,k} > 0 \tag{5-44}$$

where $\omega_{ICE,idle}$ represents the idle speed.

Note that the speed limits are only meaningful when the quick-disconnect clutch is closed.

EM torque

As mentioned in section 5.1.3.5, the selection of whether to enforce the EM continuous torque limit or the peak torque limit depends on the value of the counter introduced as a state.

Whenever the value of the EM torque counter is higher than 7, the continuous torque limit is enforced. Accordingly, the infeasible conditions can be described by:

$$T_{EM,k} > T_{EM,max,k} \tag{5-45}$$

$$T_{EM,k} < T_{EM,min,k} \tag{5-46}$$

where,

$T_{EM,min,k}$ is the minimum EM torque.

$T_{EM,max,k}$ is the maximum EM torque.

EM speed

It is required that the EM must not exceed its maximum angular speed limit. Hence, the infeasible condition is:

$$\omega_{EM,k} > \omega_{EM,max} \tag{5-47}$$

where,

$\omega_{EM,k}$ is the EM angular speed.

$\omega_{EM,max}$ is the maximum EM angular speed (see section 2.2.3.3).

Battery power

From the battery power limits discussed in section 2.2.3.4, it is clear that, if the following conditions are verified, the corresponding solution candidate must be discarded:

$$P_{b,k} > P_{b,max,k} \tag{5-48}$$

$$I_{b,k} < I_{min,k} \tag{5-49}$$

where,

$I_{min,k}$ is the minimum charge current (see Eq. (2-56)).

$P_{b,max,k}$ is the maximum battery power (see Eq. (2-55)).

5.5 Simulation results

As stated in the previous chapter, despite not being real-time implementable, DP is able to yield the best available approximation of the optimal control policy for problems of any complexity level within the accuracy limitations imposed by the discretization of problem variables [1].

In this section, DP is used to find the global optimal solution to the energy management of the HEV powertrain architecture described in section 2.2. Simulation results are presented for two different cases:

- Charge-sustaining operation.
- Charge-depleting operation.

These simulation results are used to assess the effect of the gearshift and ICE start losses in the obtained solutions. Furthermore, practical implementation issues related to the computational burden of the calculations are also discussed.

The reader is referred to [127], [128] for a detailed description of a general-purpose DP algorithm that is used here to find a solution for the optimal control problem formulation described in this chapter. The mentioned routine is available for download at [129].

5.5.1 Driving cycle

The World-wide harmonized Light duty Test Cycle (WLTC) was developed under the Working Party on Pollution and Energy (GRPE) and sponsored by the European Union and Japan with contributions from Switzerland, India, Korea and the USA [130].

In order to build the WLTC, driving data and traffic statistics of light duty vehicles from different regions were analyzed. The resulting cycle can be divided in four speed phases according to their average speed values as defined in [130]: low (< 60 km/h), medium (< 80 km/h), high (< 110 km/h) and extra-high (> 110 km/h). The presence of these driving portions with very different characteristics is a consequence of the cycle being designed to represent average driving conditions from all around the globe [130].

During its development, it was determined that for some vehicles, the WLTC was impossible to follow. Therefore, the cycle was adapted to three vehicle classes (class 1, class 2 and class 3) with different Power-to-Mass Ratio (PMR) [131]. Moreover, the WLTC class 3, defined for vehicles with a PMR higher than 34 kW/ton, has two variants according to the maximum speed of the car under testing. In this dissertation, the WLTC class 3, version 3.2, is studied since the PHEV of interest has a maximum speed higher than 120 km/h. Table 5-1 summarizes the main characteristic of this cycle.

Table 5-1. Driving cycle characteristics: WLTC class 3, version 3.2.

Parameter	**Value**
Duration	1800 s
Distance	23.27 km
Average speed	46.5 km/h
Maximum speed	131.3 km/h

In Figure 5-1 and Figure 5-2, the speed and acceleration profiles used for the development and testing of EMSs are presented (see section 5.1.2). These profiles were measured during vehicle testing.

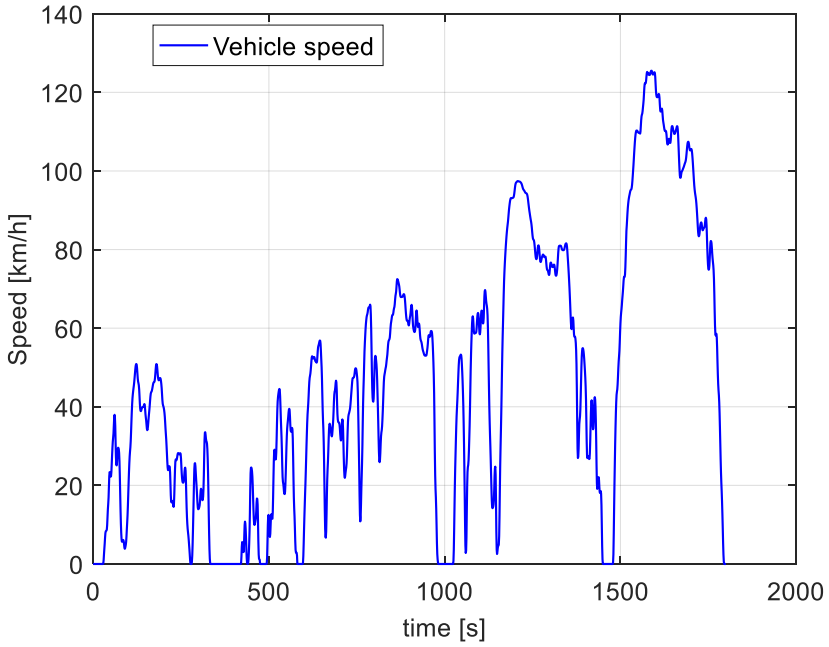

Figure 5-1. Speed profile (experimental): WLTC class 3, version 3.2.

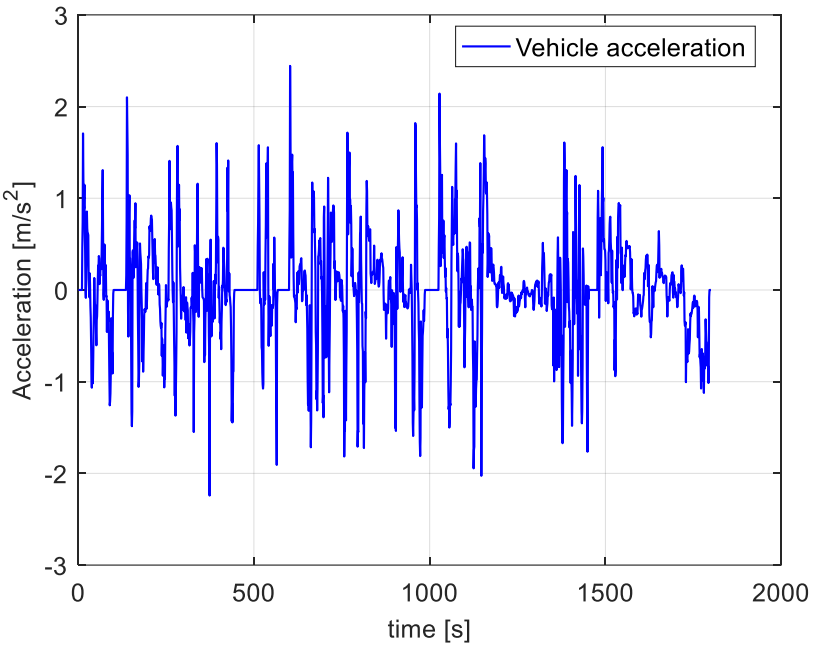

Figure 5-2. Acceleration profile (experimental): WLTC class 3, version 3.2.

It has been argued that the New European Driving Cycle (NEDC) is not representative of real driving conditions, therefore, it does not properly reflect the actual amount pollutant emissions and fuel consumption seen during vehicle operation [132]. To address this issue, starting on September 2017, the NEDC lab test will be gradually replaced by the World-wide harmonized Light-duty Test Procedure (WLTP) [133]. Even though the acronyms WLTP and WLTC are sometimes used interchangeably, the WLTP refers to a series of procedures that, in addition to the WLTC, will be needed to type approve a vehicle [131].

5.5.2 Charge-sustaining case

A charge-sustaining vehicle operation is studied here, i.e., the SOC at the end of the cycle is required to be equal to its initial value.

As explained in section 5.1.3.1, for the practical implementation of the DP formulation it is required to set a range of valid values as a final state constrain rather than a single value. A 10 % range around the initial value is considered.

In the following, simulation results are presented and then used to assess the effects of the gearshift and ICE start losses in the obtained solutions.

5.5.2.1 DP solution

Simulation results for charge-sustaining operation over three repetitions of the driving cycle described in section 5.5.1 are discussed here.

The DP solution is able to comply with the final constrain imposed to the SOC since its final value is 50.01 %. In Figure 5-3, it can be seen that the SOC almost repeats itself for each of the three WLTCs undertaken by the vehicle. Moreover, the optimal solution shows that keeping the SOC within a narrow range (less than 2 % in this case) around the required final value is the best way to proceed in terms of reducing the overall fuel consumption. These observations are in agreement with the results presented in previous works [73].

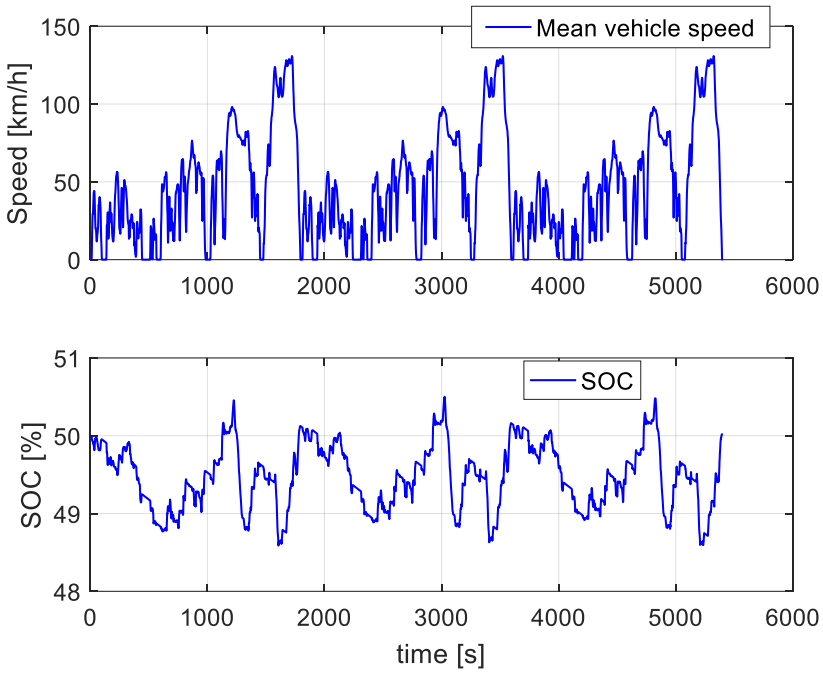

Figure 5-3. SOC.

Figure 5-4 shows how the total torque request at the EM shaft is distributed during the last repetition of the driving schedule. An interesting observation to be made is that torque assist with the EM is used just in a few occasions. The vehicle operates mostly in ICE-only mode or EV-mode. Thus, parallel hybrid mode is mainly seen in the form of the ICE power being used to recharge the battery cells.

The same conclusions can be drawn by looking at the TSF values presented in Figure 5-5. It can also be appreciated that the ICE torque is generally higher than 50 Nm, instead, lower requests are seen for the EM.

Moreover, no mechanical braking is needed during the entire simulation, i.e., the electrical path powertrain components are capable of regenerating all the energy needed to decelerate the vehicle. Mechanical braking can be present in the results obtained, near the end of the driving cycle, if the SOC resolution is low enough due to numerical errors. An SOC grid resolution of 1 % is already too low to get good results.

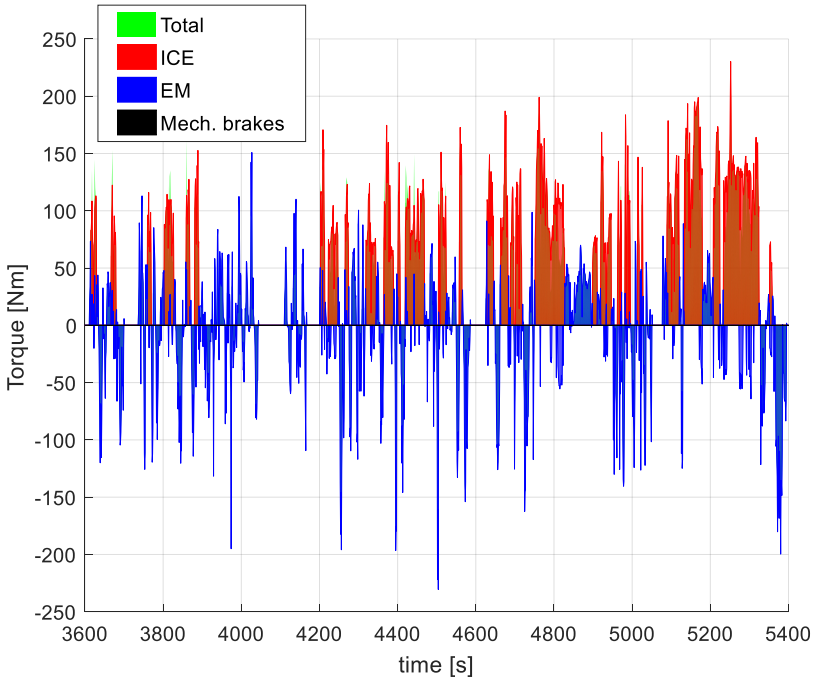

Figure 5-4. Torque split (3rd repetition).

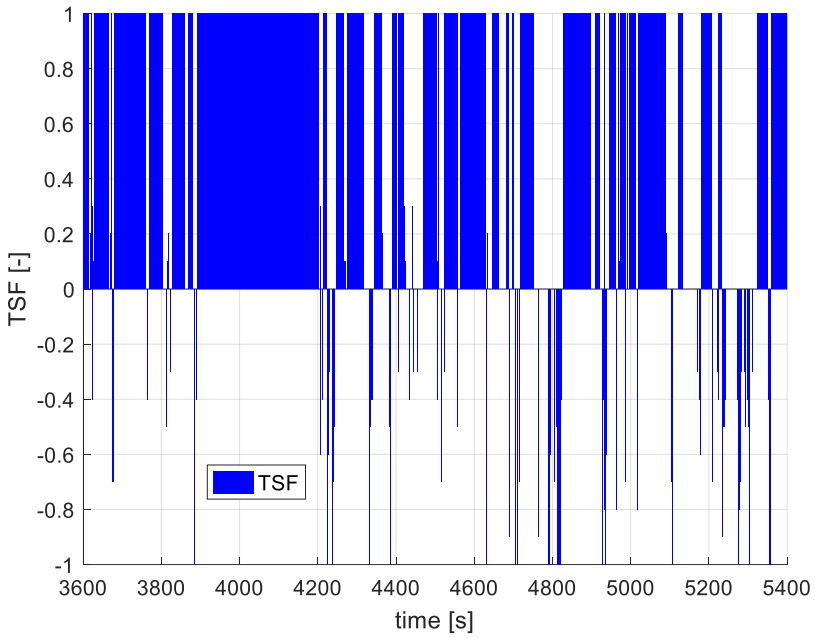

Figure 5-5. TSF (3rd repetition).

The energy request distribution can be seen in terms of power in Figure 5-6. In general, the power request to the EM is lower than 20 kW. Higher power requests are handled by the ICE.

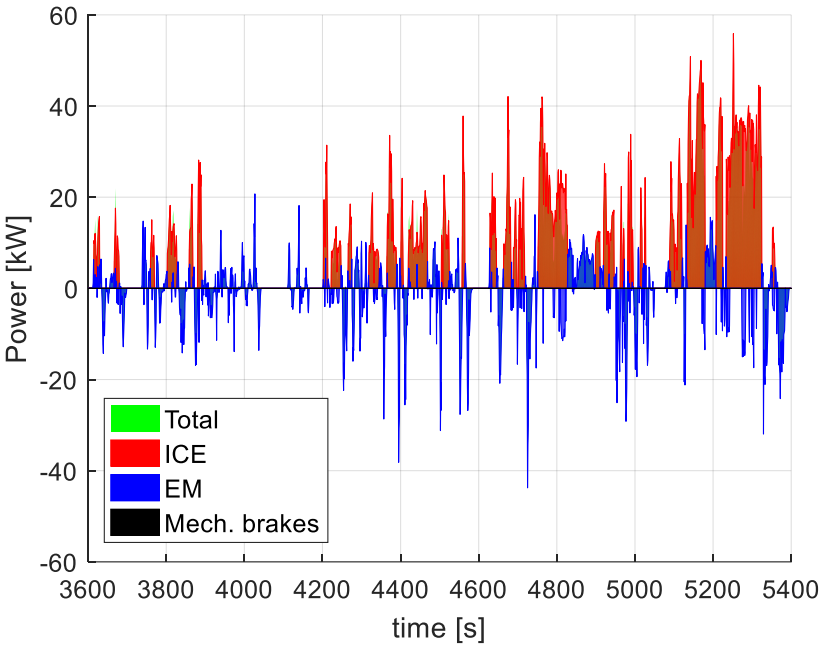

Figure 5-6. Power split (3rd repetition).

Figure 5-7 shows the optimal shifting schedule for the last part of the cycle. The total number of shifts is 446. As it can be better appreciated in Figure 5-8, where a zoom is made, the results do not present any gear hunting behavior. Generally speaking, when a gearshift is made, the new gear is maintained for at least 3 s.

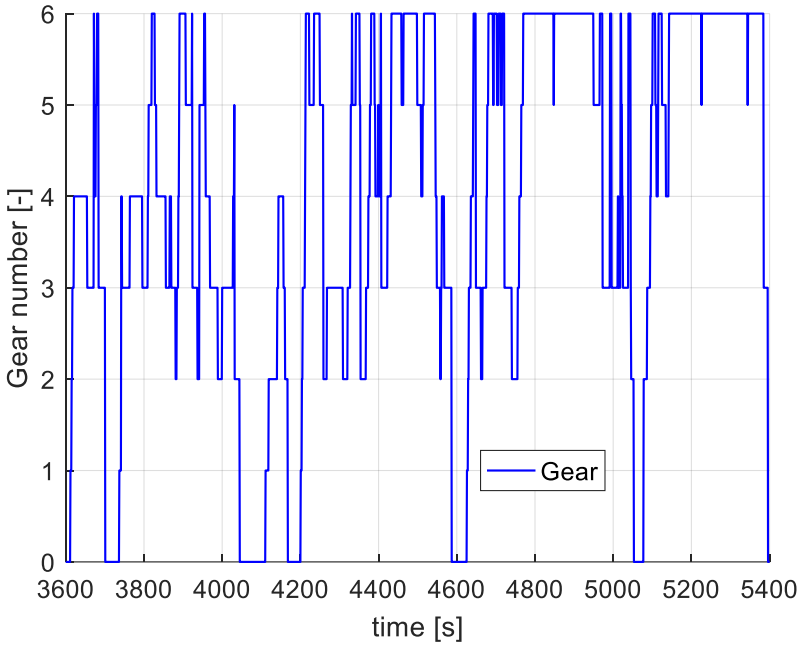

Figure 5-7. Gear number (3rd repetition).

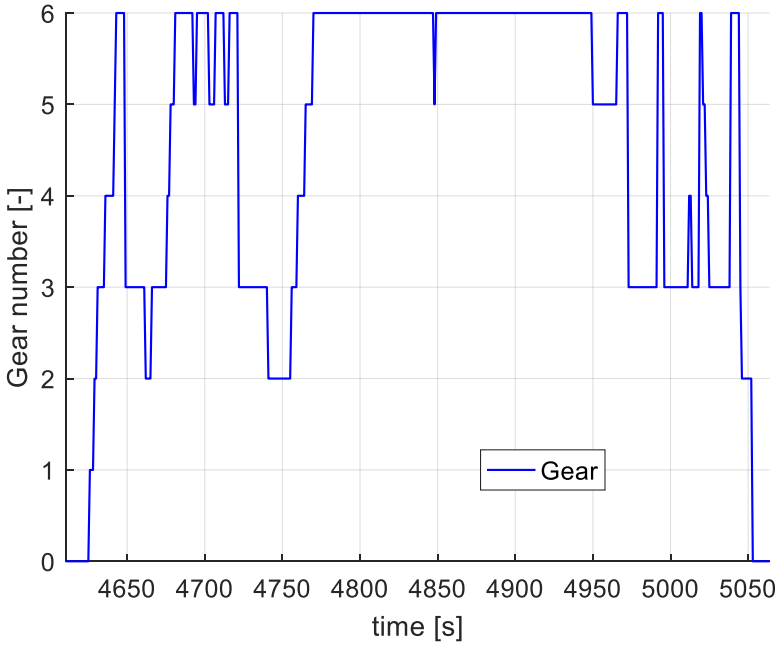

Figure 5-8. Gear number (zoom of 3rd repetition).

The ICE operating points are shown in Figure 5-9. These points are concentrated in the ICE map region that corresponds to the lowest fuel consumption. This is expected considering that the arc cost defined in Eq. (5-1) represents the instantaneous fuel flow rate. Moreover, since the cost to be minimized depends directly on the used made of the ICE, it is also reasonable for the mean efficiency of the selected operating points to be close to the maximum possible value. The mean ICE efficiency is 31.87 % while the highest possible value is around 35 %. This trend of selecting the best working conditions is further discussed in section 6.1.

Figure 5-9 also illustrates the 82 ICE starts present in the results. Furthermore, it is worth mentioning that the fuel cut-off functionality is used several times during vehicle operation.

Note that the torque and speed limitations imposed are respected by the DP solution.

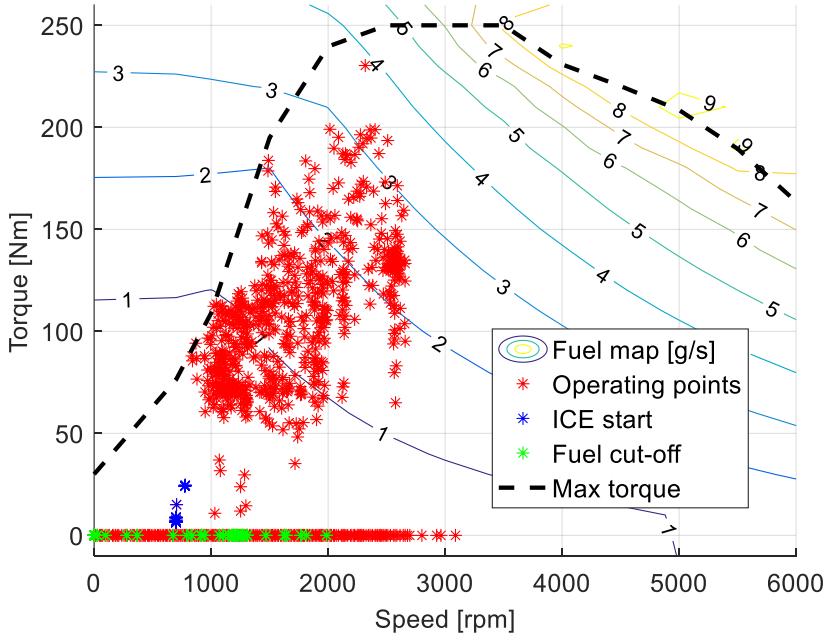

Figure 5-9. ICE operating points.

On the other hand, the EM operating points can be seen in Figure 5-10. Note that the continuous torque limit is only breached to maximize the quantity of regenerative braking energy. The mean efficiency of the EM during the cycle was 83.32 %.

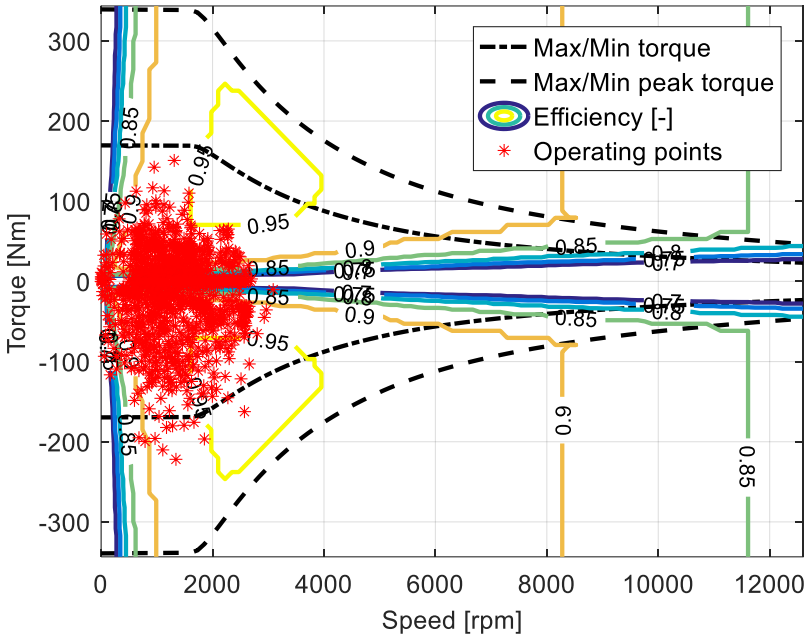

Figure 5-10. EM operating points.

Finally, as a result of the EMS found with the DP technique, the total fuel consumption is 2643 g (see Figure 5-11).

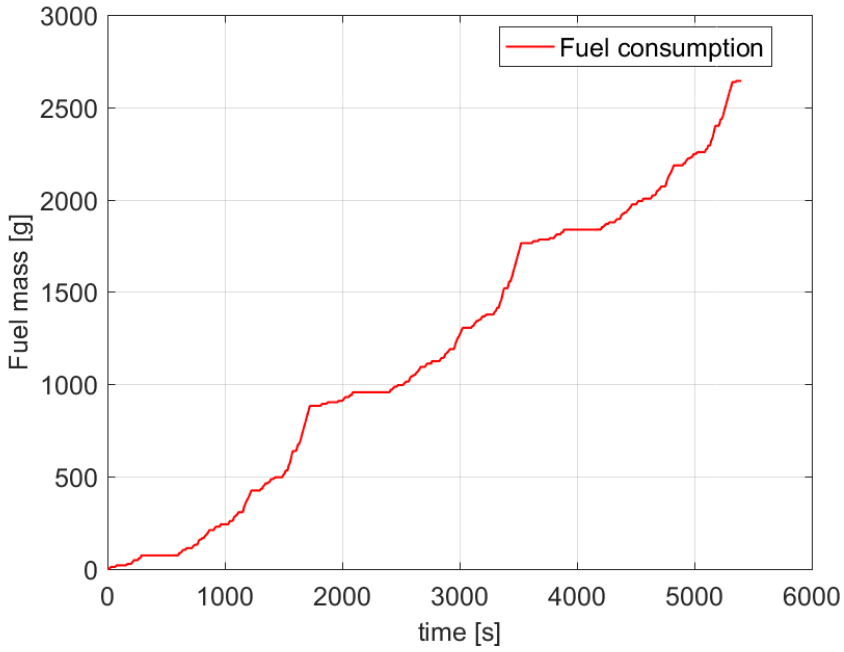

Figure 5-11. Fuel consumption.

5.5.2.2 Effect of the gearshift and ICE start losses

To assess the effects of the ICE start and gearshift losses in the solutions obtained, the results of a simulation of three repetitions of the cycle described in section 5.5.1 are compared for different cases:

- Considering both ICE start and gearshift losses.
- Considering only the gearshift losses.
- Neglecting both gearshift and ICE start losses (including the fuel penalties discussed in section 5.3).

Table 5-2 shows the total number of gearshifts and ICE starts events together with the cumulative fuel consumption for all the cases considered. In parenthesis, the percentage difference w.r.t the solution that accounts for both sources of dissipation is reported.

Table 5-2. Effect of gearshift and ICE start losses.

	Gearshift + ICE start losses	**Gearshift losses**	**No losses**
Gearshifts	446	550 (+23 %)	1504 (+237 %)
ICE start	82	317 (+287 %)	256 (+216 %)
Fuel consumption	2643	2540 (-3.4 %)	2524 (-4.5 %)

Considering both types of losses, the fuel consumption becomes higher than for the other two cases. The effect of the ICE start losses on fuel consumption is higher than the one of the gearshift losses as shown in Figure 5-12.

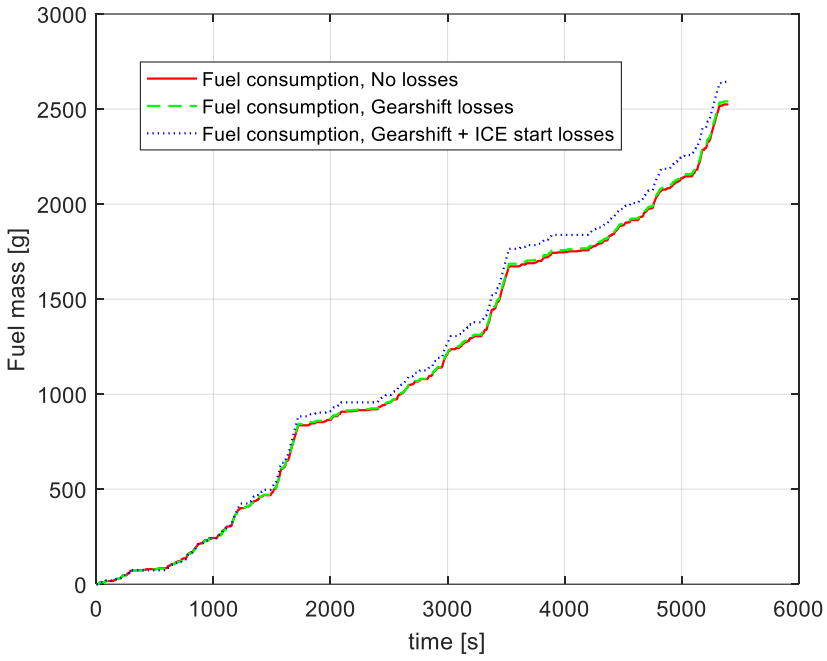

Figure 5-12. Effect of gearshift and ICE start losses: fuel consumption.

According to the data presented in Table 5-2, the number of gearshift maneuvers increases significantly when the losses associated with them are neglected. This is clearly seen in Figure 5-13.

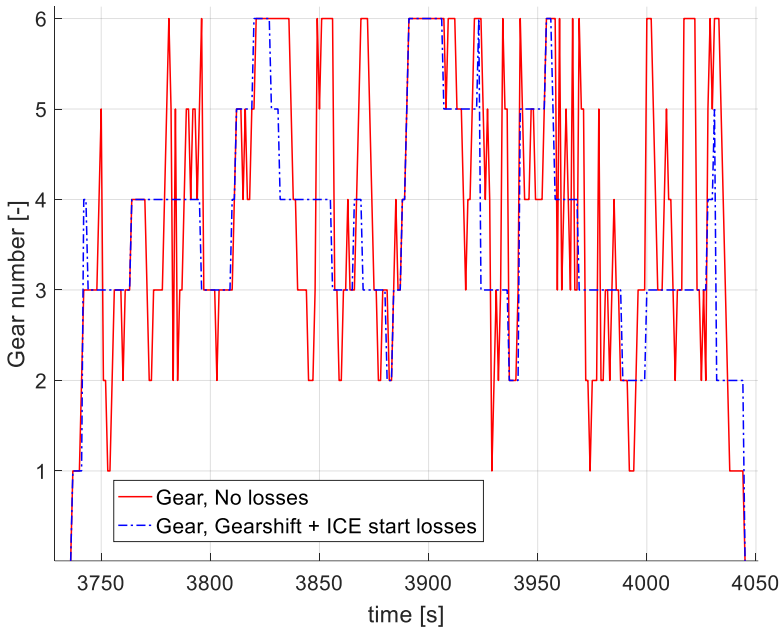

Figure 5-13. Gearshift schedule: Gearshift + ICE start losses vs. No losses.

On the other hand, Figure 5-14 helps to understand the relationship between the ICE start events and the gearshift losses. Looking at the results of the case in which only the gearshift losses are considered, at 3895 s, an ICE start event can be seen even tough in the next few seconds this component is not used to propel the vehicle. The very next second, a 1st to 6th gearshift is performed. During this upshift, having the quick-disconnect clutch engaged implies decelerating a higher inertia which increases the power available for regeneration, that in this case amounts to 20.86 kW. If the mentioned clutch were not engaged, the available power for regeneration would only be 2100 W.

This shows that neglecting the ICE start losses could lead to an unrealistic use of the ICE inertia to overcome gearshift losses. Therefore, the decrease in the total number of ICE start events seen in Table 5-2 when the gearshift losses are also neglected can be explained.

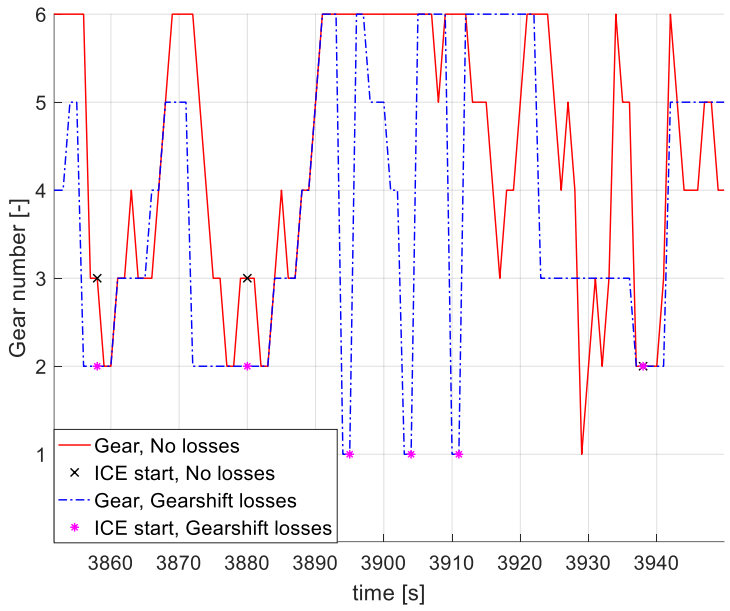

Figure 5-14. Gearshift schedule: Gearshift losses vs. No losses.

Finally, Figure 5-15 shows statistics regarding the ICE state during the simulations performed. The number of instances in which the ICE is on, disengage and engaged but not on (fuel cut-off) for less than 5 s is reported.

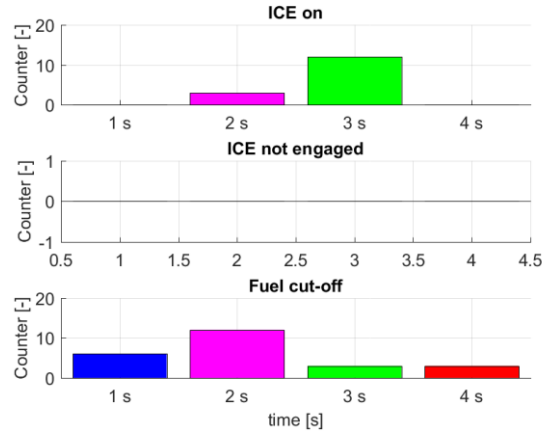

a) Gearshift + ICE start losses

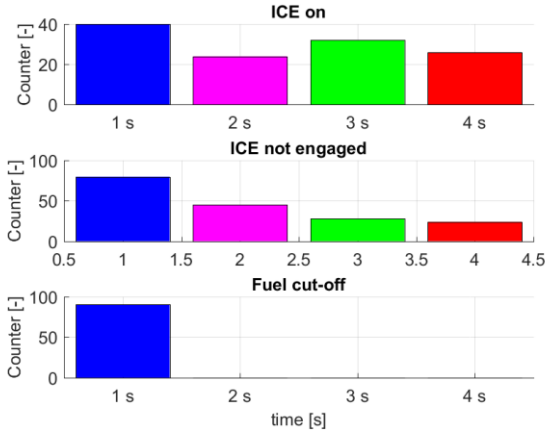

b) Gearshift losses

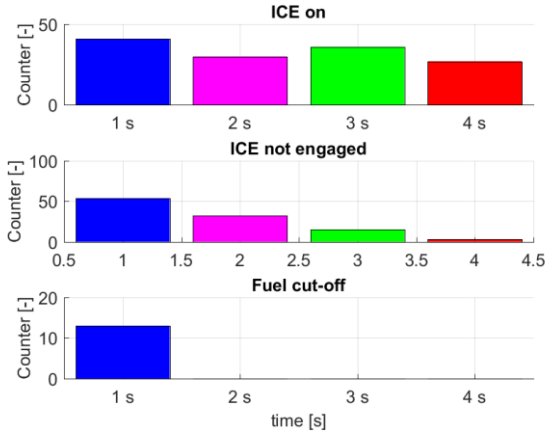

c) No losses

Figure 5-15. Effect of Gearshift and ICE start losses: ICE state.

Results show that a more intermittent use of the ICE is encountered when the outputs from the loss models developed for the transient events mentioned before are not integrated into the DP formulation.

In Figure 5-15, it can be appreciated that, when all the losses are accounted for, the ICE is never disengaged for less than 5 s. Moreover, only in a few instances this component is on for 2 or 3 s. Instead, for the other two cases, the number of times in which the ICE is on for less than 5 s is considerably higher. For example, the ICE is on for just 1 s around 40 times for both cases. This follows from the fact that removing the ICE start losses implies that this component can be started without consuming any energy. On the other hand, the quantity of instances in which the ICE is disengaged for a short period of time also rises significantly. The increase is higher for the case in which only gearshift losses are considered which can be explained by the observations made regarding Figure 5-14. Furthermore, these considerations also justify the higher amount of 1 s fuel cut-offs seen: 90 when neglecting the ICE start losses and 13 when gearshift losses are also not taken into account.

5.5.3 Charge-depleting case

The results obtained in simulation for charge-depleting operation over one repetition of the same driving cycle considered for the charge-sustaining case are presented.

As stated before, one of the main practical limitations to the implementation of DP is the computational burden involved, which increases exponentially with the dimension of the state vector. The results presented for the charge-sustaining case were produced without including the EM torque counter state. The complete DP formulation is not needed since the solution obtained does not breach the EM continuous torque limit for more than 7 s. However, for the charge-depleting case the counter is necessary and its effects on the solution are addressed here. Hence, instead of simulating three repetitions of the driving cycle, only one is considered.

In order to compute the minimum amount of fuel necessary to complete the driving schedule of interest, a final SOC target is not established. The SOC profile obtained is presented in Figure 5-16. Since the cycle can be driven almost entirely in EV-mode, as seen in Figure 5-17, the battery is continuously discharged while regenerative braking energy is absorbed when available (the mechanical brakes are never employed). This type of operation is possible thanks to the dimensions of the

energy storage system and capabilities of the EM mounted into the powertrain of the PHEV of interest. The SOC at the end of the cycle is 53.06 %.

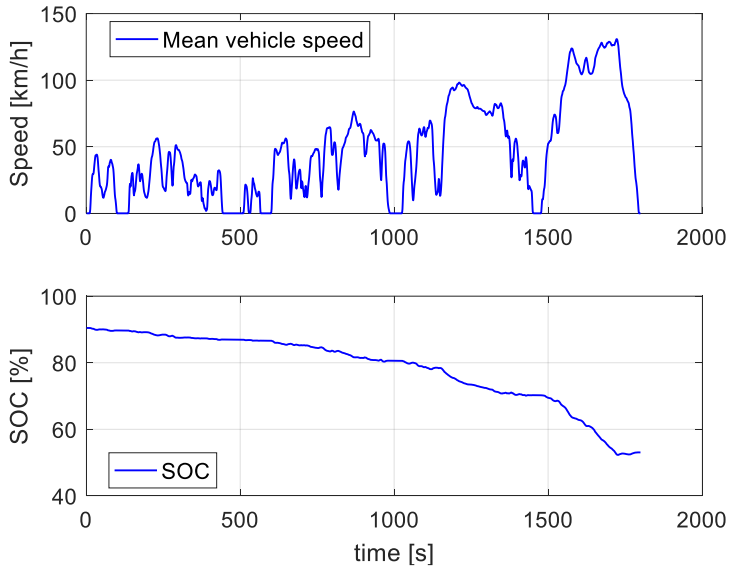

Figure 5-16. SOC.

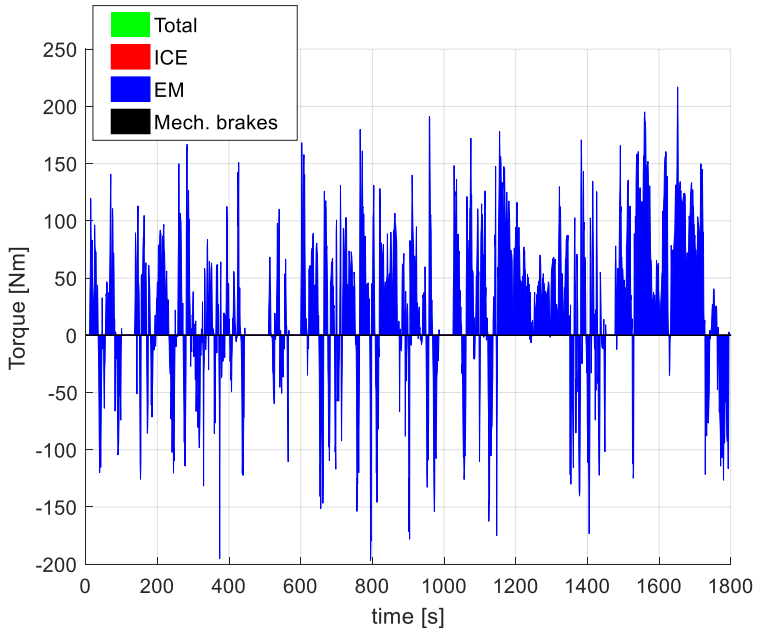

Figure 5-17. Torque split.

The effects of including the EM torque counter state into the DP formulation are seen in Figure 5-18 where the counter value is presented together with a zoom of the torque split time history around the only point in which the ICE is used to propel the vehicle. At 1564 s the ICE is used to supply part of the torque needed, allowing the EM to operate within its continuous torque limit for 1 s. As a consequence, the peak torque limit is enforced in the following 6 s and no further fuel is consumed. This shows the main limitation of the counter implemented, i.e., 1 s operating within the continuous torque limit provides the possibility of breaching it for 7 s more. However, in the several simulations performed, this situation is not very common. Furthermore, the counter introduced showed to be useful to enforce mechanical braking after high amounts of negative torque are requested to the EM (see section 6.3.2). Note that to improve the way in which the EM torque limits are imposed, physical consideration may have to be introduced into the DP formulation, thus further complicating the vehicle model.

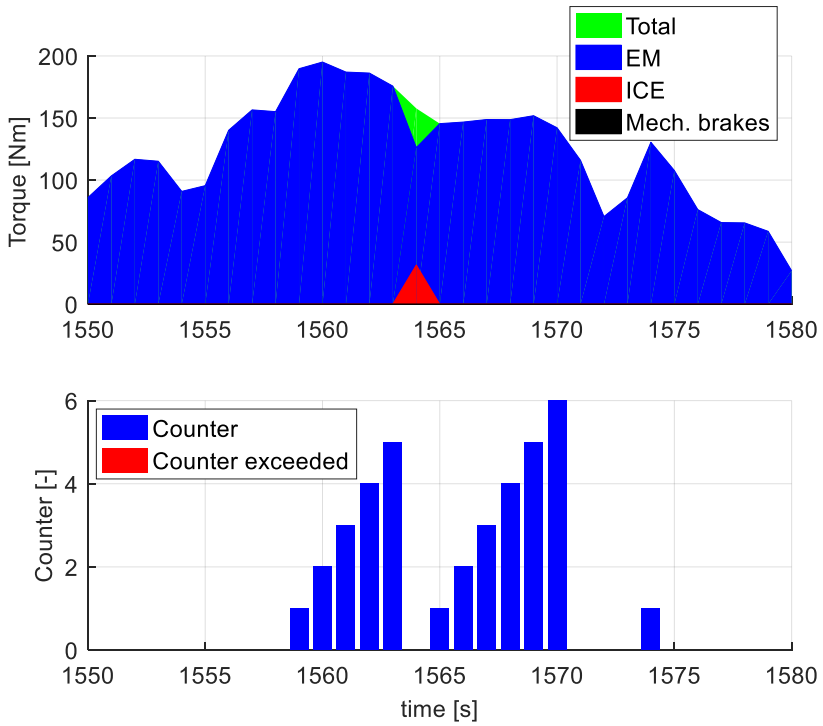

Figure 5-18. Effect of the EM counter state.

As it can be appreciated in Figure 5-19, where the gearshift schedule is presented, the results do not present any gear hunting behavior. The total number of shifts is 95.

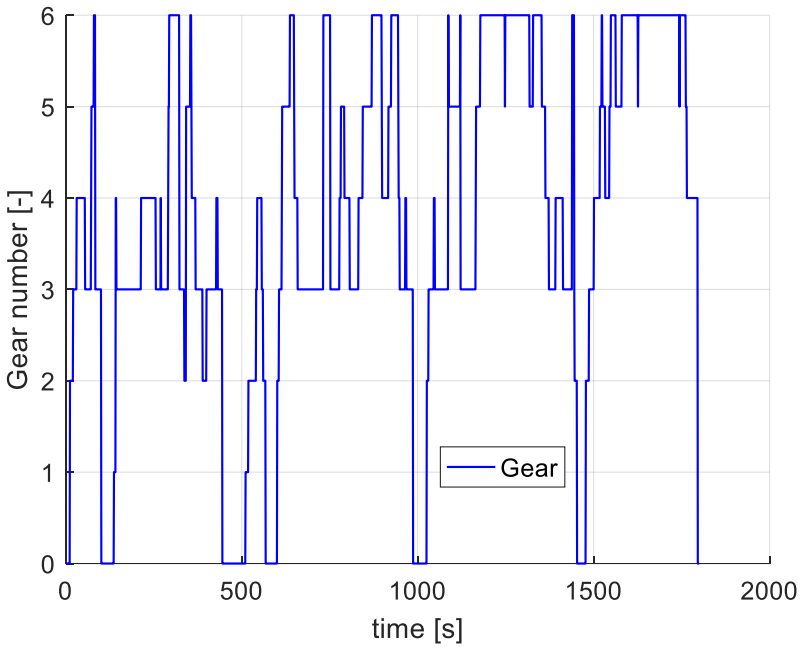

Figure 5-19. Gear number.

The EM operating points are presented in Figure 5-20. Differently from the results seen for the charge-sustaining run, the continuous torque limit is breached also when providing tractive torque. The mean efficiency of the EM working points is 86.58 %, thus, higher than for the previous case. This is reasonable when considering that the EM does not need to accommodate for the ICE being in the best possible operating conditions.

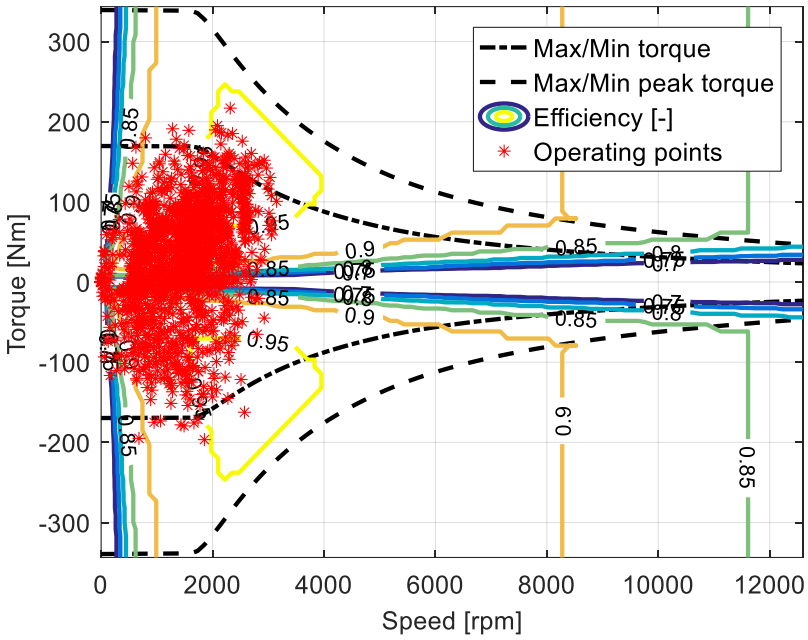

Figure 5-20. EM operating points.

Finally, the total fuel consumption is given by a unique ICE start process and the only point in which the thermal path is used to fulfill the torque request at the wheels.

5.6 Summary

In this chapter, DP is used to find the global optimal solution to the energy management of the PHEV described in section 2.2. The general problem formulation is given. Each state and control variable are defined and the reasons behind their introduction are explored. Moreover, the constrains imposed together with the characteristic of the state and control grids are also reported. In addition, the way in which the modeling of the gearshift and ICE start losses (see sections 2.2.4 and 2.2.5) are integrated into the DP formulation is described.

The WLTC class 3, version 3.2, is considered for the simulations performed. This cycle was designed to represent average driving characteristics from all around the globe. Hence, it is composed of different speed phases [130]: low, medium, high and extra-high. The presence of these driving portions make the cycle more representative of real driving conditions than the NEDC [132], which is one of the main motivations behind the decision of, starting on September 2017, gradually replacing the latter lab test by the WLTP [133].

The simulation results obtained with the described DP formulation are presented for two different cases:

- Charge-sustaining operation.
- Charge-depleting operation.

In the charge-sustaining results, the optimal solution shows that keeping the SOC within a narrow range around the required final value is the best way to proceed. Another interesting observation to be made is that torque assist with the EM is used just in a few occasions. The vehicle operates mostly in ICE-only mode or EV-mode. Thus, parallel hybrid mode is mainly seen in the form of the ICE being used to recharge the battery. In general, the power request to the EM is lower than 20 kW while higher power requests are handled by the ICE. Regarding the ICE operating points, it can be appreciated that they are concentrated in the ICE map region that corresponds to the lowest fuel consumption and that their mean efficiency is kept high during vehicle operation. This last remark can be justified considering that the cost to be minimized depends directly on the used made of the ICE.

Since the vehicle of interest corresponds to a PHEV, the dimensions and capabilities of the electrical path components enable the possibility of regenerating all the energy needed to decelerate the vehicle and to provide the necessary tractive energy to follow the driving schedule. This is clearly shown by the charge-depleting results that are used in section 6.1.4 to extract a set of rules for the gear selection in EV-mode.

In the simulation results presented in section 5.5.2.2, the effects of integrating into the DP formulation the loss models developed for gearshift and ICE start events are studied in terms of the overall fuel consumption, the number of gearshifts and the quantity of ICE start events. Accounting through physical considerations for these sources of dissipation enables the DP algorithm to decide when it is more convenient, in terms of minimizing the fuel consumption, to perform these transient events. This capability differentiates the developed DP formulation from those presented in previous studies. In particular, the author is not aware of any other DP code that includes a similar modeling approach to account for the energy consumption of gearshifts in DCTs.

The analysis made shows that considering both sources of energy dissipation, the fuel consumption increases with respect to the case in which they are neglected. Furthermore, it is seen that the effect of the ICE start losses on fuel consumption is higher than that of the gearshift losses.

On the other hand, the number of gearshifts increases significantly when the losses associated with them are neglected. In addition, another important conclusion that can be drawn is that neglecting the ICE start losses could lead to an unrealistic use of the ICE inertia to overcome gearshift losses. It is noted that when all losses are considered, there is no gear hunting behavior in the results.

Regarding the ICE state, the optimal solution shows a more intermittent use of this component when the outputs from the loss models are not employed.

In the next chapter, the DP formulation described here is used to generate benchmark solutions for real-time implementable EMSs.

Chapter 6

6. Real-time Energy Management Strategies for Hybrid Electric Vehicle Powertrains Equipped with Dual-Clutch Transmissions

6.1 A-ECMS with rule-based gear selection

As discussed in chapter 4, PMP and DP are model-based techniques able to provide the optimal solution to the energy management problem in HEVs. However, the requirement of knowing the future driving conditions beforehand generates the need of searching for other EMSs that are real-time implementable.

The various implementations of A-ECMS available in literature have shown that this causal strategy, despite being suboptimal, can generate results close to the optimal solution [60], [73].

On the other hand, the results obtained with DP can be analyzed to extract rules that would allow to generate a control trajectory similar to that of the global optimal solution in real-time. This approach has been successfully applied in literature for the energy management of HEVs [31], [55]–[57].

Based in these previous studies, a real-time EMS is designed in this chapter that combines the aforementioned techniques:

- DP results are used to derive a set of rules aiming at reproducing the optimal gearshift schedule in EV-mode.
- A-ECMS is used to decide the powertrain operating mode (through the selection of the TSF) and the current gear if power from the ICE is needed.

In the following paragraphs, a detailed description of the algorithm is given, including insights on the rule extraction and strategy calibration processes. Then, the DP formulation presented in chapter 5, is used to benchmark the results of the developed EMS and those of the A-ECMS. Note that, besides realizing how close the results are from those of the optimal solution, this also allows to compare the performance of the designed algorithm with that of a well-known real-time implementable EMS.

6.1.1 Algorithm overview

After performing several simulations using DP, it was observed that the gearshift schedule obtained when increasing the value of the final SOC target, thus forcing a more charge-sustaining operation, could be interpreted as the one obtained when the vehicle operates in EV-mode with some deviations. The mentioned deviations, corresponded, most of the times, to gearshifts performed when the intervention of the ICE was required. This can be clearly seen in Figure 6-1, where the gear number state trajectory in EV-mode, obtained without imposing a constrain for the final SOC value (see section 5.5.3), and that resulting from a simulation in which the final SOC is required to be 75 % are compared. The driving cycle considered is the WLTC class 3, version 3.2.

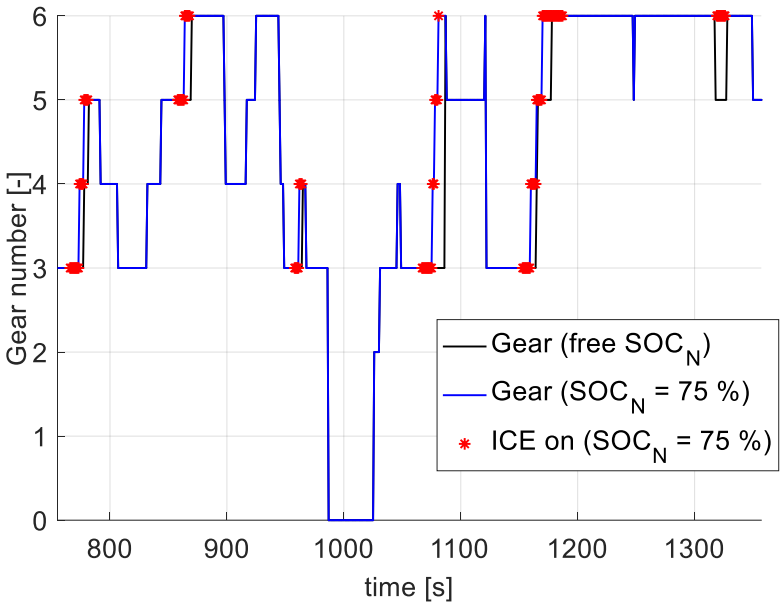

Figure 6-1. Gearshift schedule variation with final SOC target.

As a consequence of the previous observations, the issue of determining how the optimal solution is choosing the ICE operating points presents itself. Hence, a set of simulations are undertaken in which the final SOC constrain is continuously increased.

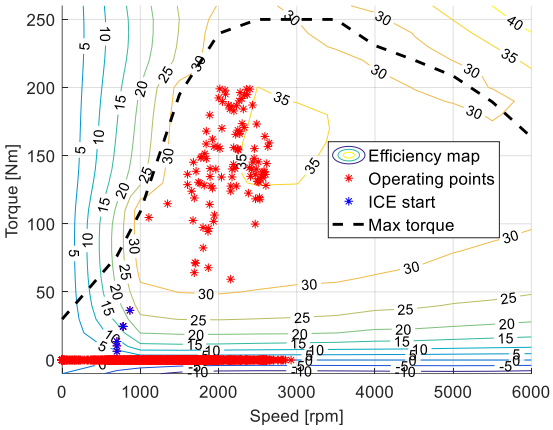

a) $SOC_N = 65\ \%$

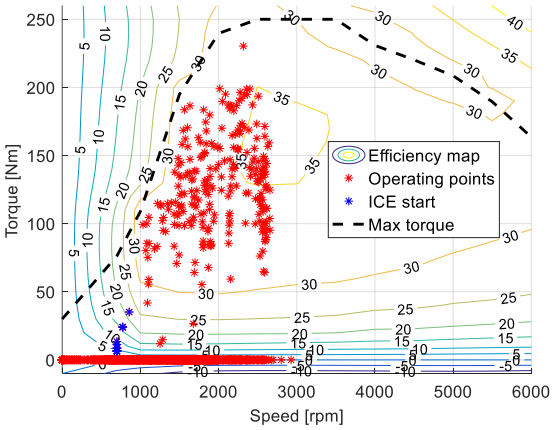

b) $SOC_N = 75\ \%$

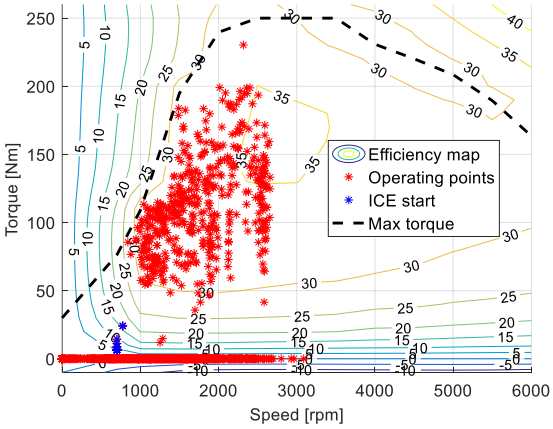

c) $SOC_N = 85\ \%$

Figure 6-2. ICE operating points variation with final SOC target.

The optimal solution seems to indicate that the most efficient operating points for the ICE are selected first and the other areas of the map with lower efficiencies are covered gradually as the use of the ICE to satisfy the final SOC constrain becomes more frequent. Note that area populated in the map corresponds to that associated with lower fuel consumption values (see section 5.5.2).

Hence, the idea behind the proposed approach is that if it can be understood how the optimal solution selects the gear in EV-mode, when the ICE is needed, gear selection is simply a matter of minimizing the equivalent fuel consumption as defined in the context of the ECMS (see section 4.6). Note that reducing the overall fuel consumption is the main objective of the designed EMS.

The developed algorithm is composed of the following phases:

- Phase I: Gear selection in EV-mode.
- Phase II: Equivalence factor calculation.
- Phase III: TSF selection.
    - Phase III-1: TSF selection – EV-mode gear.
    - Phase III-2: TSF – ICE on.
        - Phase III-2.1: TSF selection – ICE on – ICE start.
        - Phase III-2.2: TSF selection – ICE on.
- Phase IV: Define inputs for the next time step.

Each of these phases is described in section 6.1.2, where the main assumptions made and the conditions that determine the transition among different phases are reported.

In Figure 6-3, a flow chart of the developed algorithm is presented.

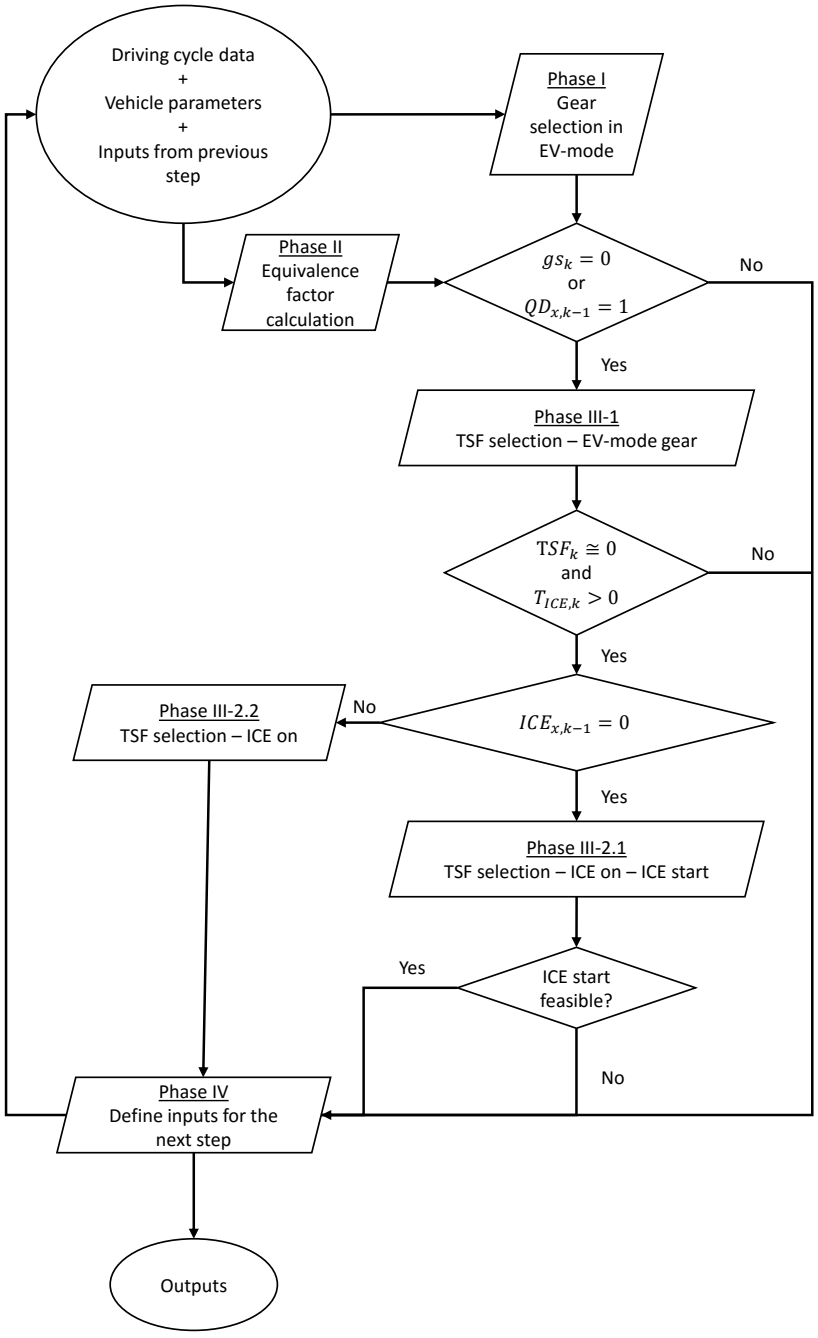

Figure 6-3. A-ECMS with rule-based gear selection flow chart.

where,

gs_k is the gearshift status.

$QD_{x,k-1}$ is the quick-disconnect clutch state at the previous time step.

TSF_k is the TSF.

$T_{ICE,k}$ is the ICE torque request.

$ICE_{x,k-1}$ is the ICE state at the previous time step.

When any of the conditions checked during the execution of the algorithm is not verified, excepting the one related to the ICE state, the vehicle will work in EV-mode. The process shown in Figure 6-3 is repeated at every time step.

A summary of the main algorithm inputs and outputs is presented below.

Main inputs:

- Vehicle parameters.
- Driving cycle information.
  - Vehicle longitudinal speed.
  - Vehicle longitudinal acceleration.
  - Mean speed of the driving cycle.
  - Total distance to be traveled.
  - Time length of the driving mission.
- System states.
  - SOC.
  - Gear number.
  - Quick-disconnect clutch state.
  - ICE state.
  - EM torque counter state.
- SOC constrains.
  - Initial SOC.
  - Final SOC.
  - Maximum SOC.
  - Minimum SOC.
- A-ECMS parameters.
  - Distance traveled.
  - Initial value of the equivalence factor (see section 6.1.5).

    - Sampling distance for equivalence factor adaptation (see section 6.1.5).
    - Proportional gain for equivalence factor adaptation (see section 6.1.5).
- EV-mode gearshift rules parameters (see section 6.1.4).
- Parameters for the introduced penalties (see section 6.1.3.2).

Note that all the inputs to the algorithm regard data coming from either the previous and current time step, thus making the proposed EMS causal. The only a-priori information needed related to the driving cycle characteristics are the estimated mean speed, distance to be traveled and duration of the driving mission.

Main outputs:

- Controls.
    - TSF.
    - Gear command.
    - Quick-disconnect clutch command.

These outputs are computed in certain algorithm phase that is chosen according to the transition conditions illustrated in Figure 6-3 (see section 6.1.2).

In order for the results obtained to be comparable with those of the DP formulation described in chapter 5, the real-time EMS developed here relies on the same powertrain model used to obtain the optimal solution (see section 2.2). Hence, the energy consumption during gearshifts and ICE start events are accounted for together with the same fuel penalties introduced in section 5.3. Moreover, this also implies that the same state and control variables are used (see section 5.1).

It is worth noting that the mentioned vehicle model is not only used to assess the effects of the control decisions made by the EMS on the system states but also for their generation. As explained in section 4.6, instantaneous minimization methods, as the one presented in this chapter, usually rely on a suitable model of the system to test several solution candidates and select the one yielding the lower cost.

Finally, an important aspect to address is the fact that, differently from the work presented in the previous chapter, the fuel cut-off functionality is not considered here for practical implementation reasons. This means that if the quick-disconnect

clutch is engaged, the ICE is either being used to supply for the power request at the wheels (or part of it) or to recharge the battery.

The equations in this chapter are presented in a discretized form as they are solved by the EMS. As for the vehicle model, the time step considered is 1 s.

6.1.2 Algorithm phases

In this section, the main objectives and assumptions made in each of the algorithm phases are described. Moreover, the conditions that determine the transition among them are also reported.

6.1.2.1 Phase I: Gear selection in EV-mode

As discussed at the beginning of this chapter, DP results are used to derive a set of rules aiming at reproducing the optimal gearshift schedule in EV-mode. In this phase, based on the algorithm inputs and the vehicle model, the mentioned set of rules is employed to select the current gear. The rule-based gear selection process is discussed in detail in section 6.1.4.

The general assumptions made when using the vehicle model to assess the effects of the controls selected can be summarized as:

- EV-mode is assumed ($TSF_k = 1$).
- The quick-disconnect clutch is considered open ($QD_{x,k} = 0$).

On the other hand, the main outputs of the current phase are:

- TSF ($TSF_k = 1$).
- Gear command.
- Quick-disconnect clutch command ($QD_{u,k} = 0$).

6.1.2.2 Phase II: Equivalence factor calculation

In this phase, the A-ECMS equivalence factor is updated according to Eq. (4-59). Hence, an adaptation based on feedback from SOC is performed each time a certain distance is traveled by the vehicle. The reader is referred to section 6.1.3 for more details.

6.1.2.3 Phase III: TSF selection

As discussed in section 4.6, in the context of the ECMS, the TSF is selected searching for the one that minimizes the instantaneous equivalent fuel consumption. In this phase, the TSF selection is divided in two consecutive steps:

1. Based on the gear chosen in the previous phase, it is verified that the current value of the equivalence factor suggests operation in EV-mode.
2. If the computations made in step 1 indicate that it is convenient to use the ICE, the A-ECMS is employed to select the best values for the gear number and the TSF.

These calculations are undertaken in the sub-phases discussed in the following paragraphs. The A-ECMS formulation employed is described in section 6.1.3.

Note that the possibility of using the ICE is considered only when a gearshift is not suggested in the previous phase or when the quick-disconnect clutch was engaged/closed in the preceding time step. This is because, as explained in section 2.2.5, a gearshift and an ICE start event cannot occur in the same time step. If these computations are skipped, the outputs from phase I are considered.

Phase III-1: TSF selection - EV-mode gear

The TSF that minimizes the equivalent fuel consumption is identified based in the following considerations using the embedded vehicle model:

- The gear selected in phase I is considered.
- For $TSF_k \neq 1$ it is assumed that the ICE is ready to be used when computing the equivalent fuel consumption, i.e., it is considered that $QD_{x,k} = 1$.

If the TSF that minimizes the equivalent fuel consumption corresponds to operating in EV-mode, the outputs from phase I are considered. Instead, if the TSF indicates that the ICE should be employed, phase III-2 is undertaken.

Phase III-2: TSF selection – ICE on

If the TSF selected in the previous calculation step indicates that the ICE should be used, one of two possible sub-phases are undertaken according to the ICE state at the previous time instant:

- Phase III-2.1: TSF – ICE on – ICE start.
- Phase III-2.2: TSF – ICE on.

Phase III-2.1: TSF selection – ICE on – ICE start

This phase is active if the ICE was off in the previous step ($ICE_{x,k-1} = 0$), meaning that in order to use this component, an ICE start process needs to be undertaken. This implies that when computing the system states resulting from the control decisions made here, the ICE start loss model discussed in section 2.2.5 is used.

The main outputs of the current phase are:

- TSF ($TSF_k = 0$).
- Gear command ($gn_{u,k} = gn_{x,k-1}$).
- Quick-disconnect clutch command ($QD_{u,k} = 1$).

Note that if the ICE start process is not feasible, which is determine based on the considerations reported in section 5.4, the outputs of phase I are considered.

Phase III-2.2: Torque split selection – ICE on

Phase III-2.2 is active when the ICE was already on in the previous time step ($ICE_{x,k-1} = 1$).

Based on the observations made from the DP results presented in section 6.1.1, since the ICE is employed in this phase, i.e., fuel is consumed, both the TSF and the gear number are selected to minimize the equivalent fuel consumption. Therefore, the control signals generated are:

- TSF.
- Gear command.
- Quick-disconnect clutch command ($QD_{u,k} = 1$).

6.1.2.4 Phase IV: Define inputs for the next time step

Phase IV serves to define the inputs for the next iteration of the algorithm. In particular, the equivalence factor and the system states are updated.

Since the algorithm has been implemented in a simulation environment, the control outputs of the EMS, generated in the computation phase determined by the transition conditions described in the preceding paragraphs, are applied to the

vehicle model to obtain the resulting system states that will be used in the next iteration.

6.1.3 A-ECMS formulation

In section 4.6, it is explained that even though ECMS was first introduced in [47] as a heuristic method derived from engineering intuition, it was later shown that under certain conditions it is equivalent to PMP [58]. The fundamental implication of this fact is that a real-time implementable strategy like ECMS can also be formally optimal [71].

In section 4.6.2, the equivalence between PMP and ECMS is illustrated by expressing the equivalence factor as a function of the co-state variable (see Eq. (4-47)) for the simple mathematical model of a generic parallel HEV presented in section 4.5.4. However, since the PHEV model described in section 2.2 introduces discrete variables, e.g., the quick-disconnect clutch and gear states/commands, into the optimal control problem formulation, making it a Hybrid Dynamic System (HDS) [134], proving the mentioned equivalence is not as straightforward. Demonstrating this is out of the scope of the dissertation, the interested reader is referred to [135], [136] for more information about the application of optimal control techniques to HDSs.

In this section, the ECMS formulation employed is described paying particular attention to the penalties introduced and the adaptation approach used to update online the value of the equivalence factor.

6.1.3.1 Instantaneous minimization

The idea at the core of the ECMS is that an equivalent fuel consumption can be associated with the use of electrical energy [116]. As explained in section 4.6, using an appropriate model of the system, the ECMS algorithm estimates the fuel and electrical energy consumption resulting for each of the possible control candidates and makes a decision aiming at locally minimizing an equivalent fuel consumption.

For the development of the EMS presented here, the mentioned instantaneous equivalent fuel consumption rate is computed as [43], [60]:

$$\dot{m}_{f,eq,k} = \dot{m}_{f,k} + s_k \, S\dot{O}C_k \tag{6-1}$$

where,

$m_{f,eq,k}$ is the equivalent fuel consumption.

$m_{f,k}$ is the actual fuel consumption.

s_k is the equivalence factor.

SOC_k is the SOC.

Note that in this formulation, the equivalence factor has the same meaning than in Eq. (4-46), i.e., it allows converting electrical power into an equivalent amount of fuel mass flow. Note that its units are grams.

In Eq. (6-1), if the equivalence factor is positive, the instantaneous minimization approach that characterizes the ECMS points towards selecting the TSF that maximizes the power request at the battery terminals, as it is clear from the battery model described in section 2.2.3.4. Quite obviously, this is not the solution that can satisfy the constrain on the final SOC target, implying that the equivalence factor shall have a negative value [43]. For convenience, the equivalence factor is reported in the rest of this chapter as a positive quantity, which is more intuitive, since it implies that this variable acts as a weighting factor in the cost function to be minimized at each iteration, i.e., the higher its value, the higher the cost of electrical energy in terms of fuel. Hence, to accommodate for this, Eq. (6-1) is re-written as:

$$\dot{m}_{f,eq,k} = \dot{m}_{f,k} - s_k \, S\dot{O}C_k \tag{6-2}$$

Note that depending on the sign of the power request to the battery, the equivalent fuel consumption can be either higher or lower than the actual fuel usage.

6.1.3.2 Penalties introduced

The penalties that could be assigned to solution candidates when undertaking the minimization of the equivalent fuel consumption in Eq. (6-2) are divided here in four different categories and described.

Penalties to discard infeasible working conditions

The solution candidates that lead the system to infeasible working conditions are discarded by assigning a high enough cost to them, i.e., the equivalent fuel consumption is increased by a large quantity.

Since the PHEV analyzed here corresponds to that studied when developing the DP formulation presented in chapter 5, the same infeasible working conditions described in section 5.4 are considered.

In addition, solution candidates that yield to a SOC value which is not between its allowable range are also penalized. Hence, the infeasible conditions can be expressed as:

$$SOC_k > SOC_{max} \tag{6-3}$$

$$SOC_k < SOC_{min} \tag{6-4}$$

where,

SOC_{max} is the maximum SOC allowed.

SOC_{min} is the minimum SOC allowed.

Penalties to introduce restrictions on the ICE state

Given that in phase III of the algorithm, the TSF is selected assuming that the ICE is ready to be used, i.e., the ICE start losses are not considered, a series of fuel penalties are introduced to avoid frequent changes in the ICE state.

The first of the mentioned fuel penalties (1 g) is applied when:

- ICE is turned on before being off at least 4 s.
- ICE is turned off before being on at least 3 s.

Moreover, when there is a change in the ICE state, a certain reduction in terms of instantaneous equivalent fuel consumption is required. A value of 0.35 g is requested to turn on the ICE. Instead, 0.2 g are considered when turning it off.

Penalties to introduce restrictions on the gear number state

Due to the instantaneous minimization approach for gear selection used in phase III-2, it was seen during the calibration phase of the developed EMS, that it is convenient to introduce a fuel penalty (1 g) aiming at inducing gearshift hysteresis.

Hence, the equivalent fuel consumption is increased if an upshift is performed before a certain time has passed since the last downshift or vice versa. The time frame considered is 4 s.

Penalties to induce the TSF selection

A penalty is introduced to discourage the use of the fuel energy to recharge the battery cells. This was seen to be opportune when calibrating the strategy.

Therefore, the equivalent fuel consumption rate is increased by 0.2 g/s when the TSF is negative.

6.1.3.3 Equivalence factor adaptation

As explained in section 4.6, the optimal equivalence factor is a function of both the HEV powertrain and driving cycle features. Since a real-time implementable strategy cannot retain the future driving conditions as known, an adaptation scheme for the equivalence factor is necessary to adjust the value of this parameter as driving conditions change.

For the EMS developed here, the discrete adaptation scheme based on feedback from SOC discussed in section 4.6.3.1 is employed. As it is mentioned there, for a charge-depleting operation, typical of PHEVs, the optimal SOC trajectory is approximately a quasi-linear decreasing function of the traveled distance, which is referred to as a blended strategy [124]. This can be clearly appreciated in Figure 6-4 where the optimal SOC trajectory obtained with DP for a charge-depleting run of the WLTC is presented in the distance domain.

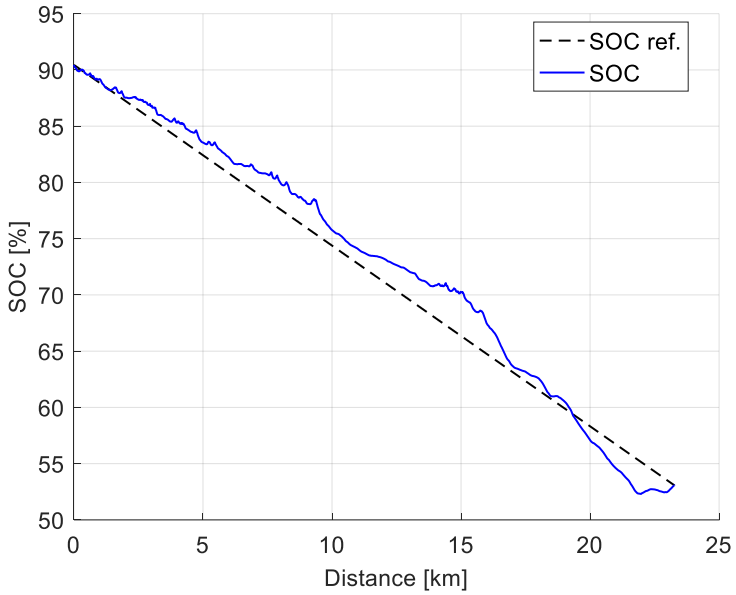

Figure 6-4. SOC (distance domain).

However, when the final SOC target is set higher with respect to that encountered when solving for the global optimal solution in terms of fuel consumption, i.e., when the DP algorithm is free to exploit all the energy available in the battery cells, it is seen for some driving cycles that a linear SOC reference defined in the time domain is more representative of the optimal solution. This can be appreciated in Figure 6-5 where the results obtained with DP while requiring to complete the WLTC with a final SOC of 75 % are presented in both the time and distance domains.

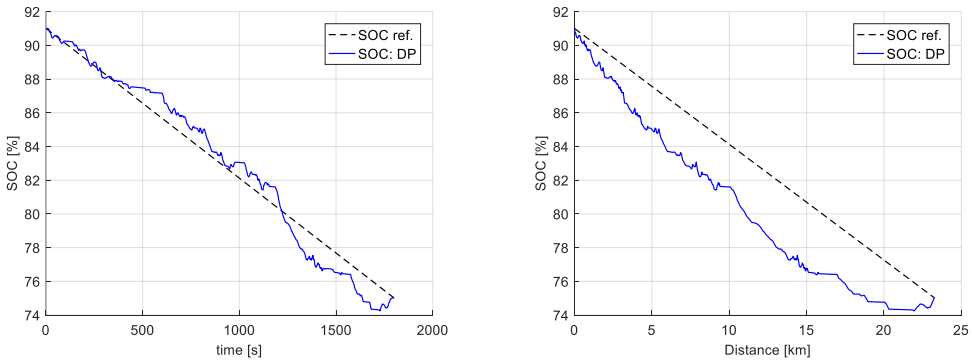

a) Time domain b) Distance domain

Figure 6-5. SOC reference: time domain vs. distance domain.

Based on the previous considerations, the SOC reference used for the equivalent factor adaptation in Eq. (4-59) is computed as:

$$SOC_{ref,k} = SOC_0 + \frac{SOC_{ref,N} - SOC_0}{N\ \mathrm{T}_s} k\mathrm{T}_s \tag{6-5}$$

where,

T_s is the sampling time (1 s).

N is the final discrete step.

k is the current discrete step.

SOC_0 is the initial SOC.

$SOC_{ref,N}$ is the final SOC target.

It is quite obvious at this point, that selecting the most appropriate value of equivalence factor is fundamental to the effectiveness of the strategy. This aspect is treated in section 4.6.2.

As for the DP formulation developed in chapter 5, the road grade variations are not considered.

6.1.4 Rule-based gear selection in EV-mode

As discussed in previous sections, to integrate a set of rules for gear selection with the A-ECMS approach, the first step is to be able to reproduce the optimal gear schedule in EV-mode obtained with DP. In the following, the rule extraction process undertaken is described and the results obtained by applying the derived set of rules are discussed.

6.1.4.1 Rule extraction process

In this section, the rule extraction process is illustrated by reviewing the main observations made from the DP results.

In Figure 6-6, the optimal gearshift schedule in EV-mode obtained for the charge-depleting run analyzed in chapter 5 is presented identifying the gearshift points in which the EM operates more efficiently after switching gears. As it can be appreciated, a local improvement in the EM efficiency is not always the reason behind the decision of changing gears. Hence, a more detailed study of the optimal solution needs to be undertaken.

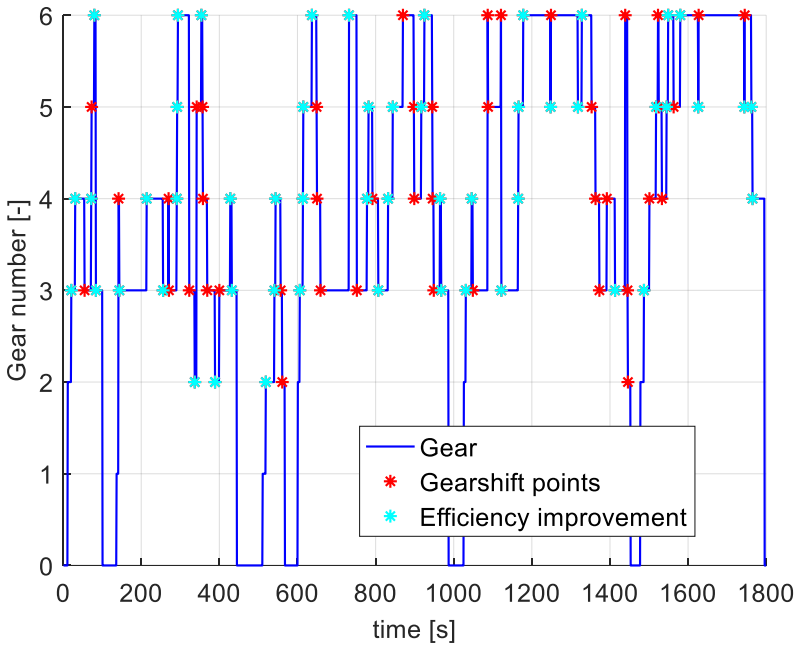

Figure 6-6. Gear number.

Rule extraction process overview

In order to derive rule-based EMSs for HEVs from DP, simulations results representative of several different driving conditions can be studied to identify certain behaviors in the optimal solution that can be tuned into rules.

Since, as described in section 5.5.1, the WLTC is constituted by driving portions with very different characteristics, it will be considered here for the rule extraction process. The idea behind this choice, is that rules designed from the analysis of the optimal EMS for a cycle that is representative of various driving conditions should also provide, after some tuning, adequate results when applied to other driving schedules.

Hence, the DP results obtained for the charge-depleting case in section 5.5.3, are studied since the vehicle can follow the requested velocity profile almost entirely in EV-mode. Such analysis is focused on the points in which gearshifts are performed. The objective is to understand how the DP algorithm is choosing whether to do a downshift or an upshift and the gear number itself.

The Rule extraction process followed for the design of the mentioned set of rules could be summarize in the following steps:

1. DP is used to find the optimal solution for driving cycles that can be completed in EV-mode.

Based on those results:

2. Speed ranges are identified for each new gear after a gearshift event.

3. Rules for single gearshifts are extracted.

   3.1. General rules are extracted from the EM power and vehicle speed plane.

   3.2. Detailed rules are extracted considering: vehicle speed and acceleration, EM power, EM power rate and the energy consumption with respect to the no gearshift case.

4. Rules for multiple upshifts are extracted based on the EM power request and vehicle acceleration.

5. Rules for gearshifts prior to significant braking events are extracted considering: vehicle speed and acceleration, EM power, EM power rate and the energy consumption with respect to the no gearshift case.

The main observations made from the DP results are reviewed below.

Speed range analysis

The speed profile of the driving cycle of interest is studied looking for general trends in the optimal solution relating the gear number selection to the vehicle longitudinal speed.

Figure 6-7 presents the vehicle speed and the gear engaged after each gearshift maneuver.

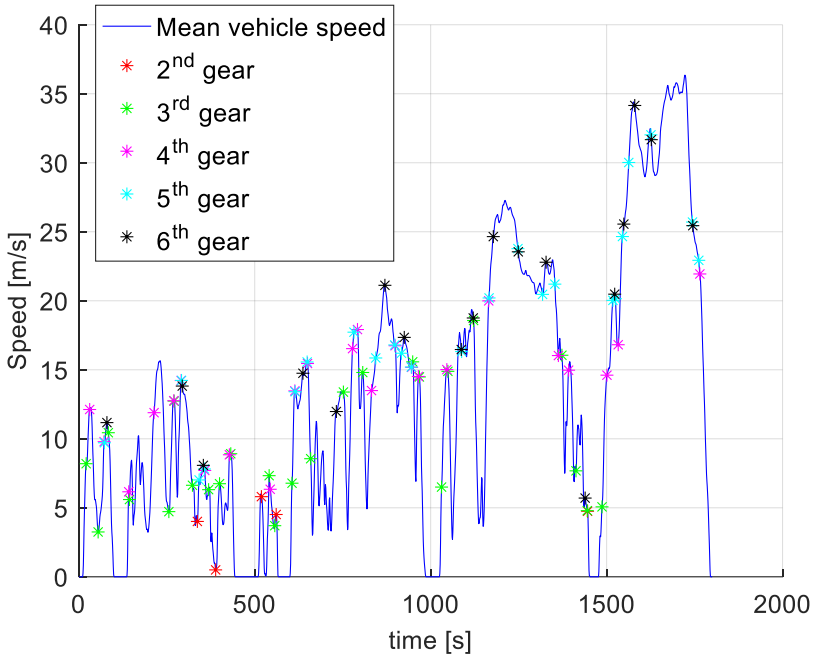

Figure 6-7. Vehicle speed and gear selection.

In Table 6-1, the speed ranges identified regarding the engaged gear after a gearshift are presented. Note that these ranges are not strictly respected for all gearshift events but rather represent a general trend observed in the simulation results.

Table 6-1. Speed range for gear selection.

New gear number	**Speed range [m/s]**
2	< 6
3	4 to 17
4	6 to 20
5 and 6	> 6

Single gearshifts analysis

The following figures show the downshifts and upshifts performed in the EM power and vehicle speed plane.

From the data presented in Figure 6-8, the following observations can be made about the downshift maneuvers:

- Most gearshifts are performed for EM power requests lower than 7 kW.
- No gearshifts are performed for EM power requests lower than 450 W.
- No downshifts to 1st gear are performed.
- Downshifts to 4th and 5th gear are mostly undertaken for speeds higher than 15 m/s.
- Downshifts to 3rd gear are mostly undertaken for speeds between 5 and 15 m/s.
- For speeds lower than 5 m/s, only downshifts to 2nd and 3rd gear are performed.

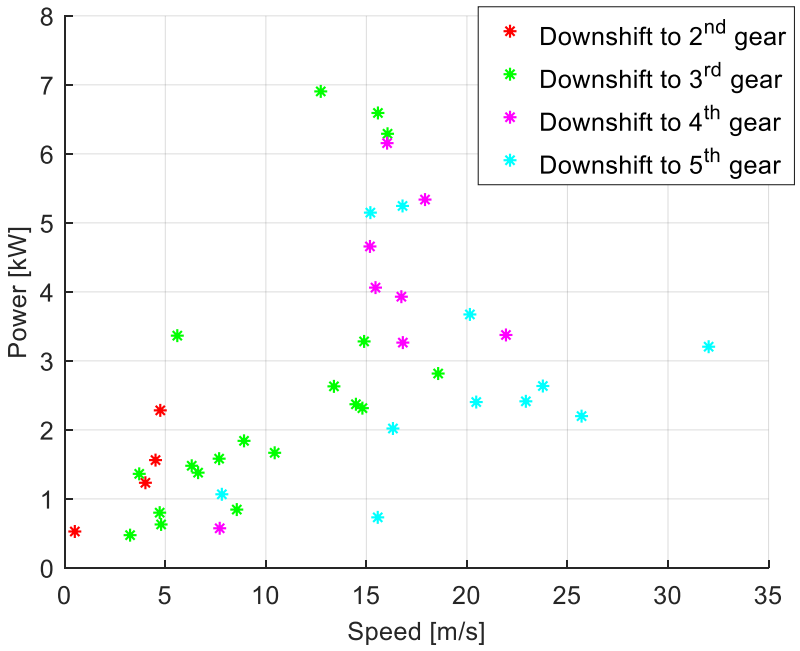

Figure 6-8. EM power and vehicle speed plane: downshifts (zoom).

Instead, for the upshift maneuvers (see Figure 6-9):

- Most gearshifts are performed for EM power requests lower than 20 kW.

- No gearshifts are performed for EM power requests lower than 250 W.
- For speeds higher than 17 m/s, most gearshifts correspond to upshifts towards 5th and 6th gear.
- Upshifts to 3rd and 2nd gear are only performed for speeds lower than 9 m/s.

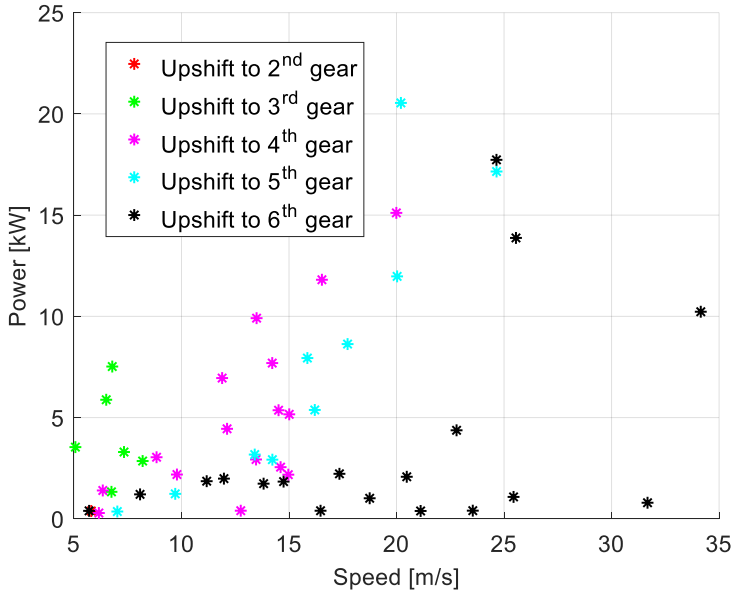

Figure 6-9. EM power and vehicle speed plane: upshifts.

After this first set of observations, the optimal gearshift schedule was studied in detail. To illustrate this process, the characteristics of the gearshift points found in a section of the driving cycle will be discussed (see Figure 6-10).

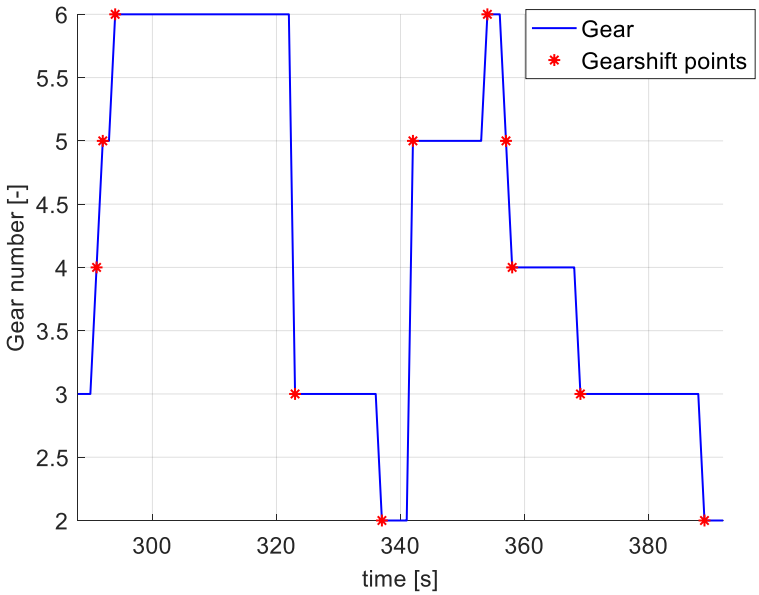

Figure 6-10. Gear number (zoom).

The characteristics of the gearshift points seen in Figure 6-10 are reported in Table 6-2.

Table 6-2. Gearshift points data.

Time [s]	Offgoing gear [-]	Oncoming gear [-]	Speed [m/s]	EM power [kW]	EM power loss [W]	Filtered acceleration [m/s^2]	Filtered EM power rate [kW/s]
291	3	4	14.22	7.692	555	0.37	-9.817
292	4	5	14.23	2.922	67	0.09	-4.182
294	5	6	13.82	1.737	-39	-0.20	-0.539
337	3	2	4.00	1.234	237	-0.15	0.667
357	6	5	7.81	1.067	106	-0.09	-0.044
358	5	4	7.71	0.574	190	-0.10	-0.314

The filtered acceleration and EM power rate presented in Table 6-2 are defined, respectively, as the derivative of the vehicle longitudinal speed and EM power computed every two time steps, i.e.:

$$a_{fil,k} = \frac{v_k - v_{k-2}}{2\ \mathrm{T}_s} \tag{6-6}$$

$$P_{EM,fil,k} = \frac{P_{EM,k} - P_{EM,k-2}}{2\ \mathrm{T}_s} \tag{6-7}$$

Moreover, the EM power loss is computed as the difference between the actual EM power request (considering the gearshift losses) and the power consumption of the no gearshift case. Hence, negatives values of this quantity imply energy savings as a consequence of going through with the gearshift process.

In Figure 6-11 and Figure 6-12, the speed and EM power profiles for the section of the driving cycle under analysis are presented.

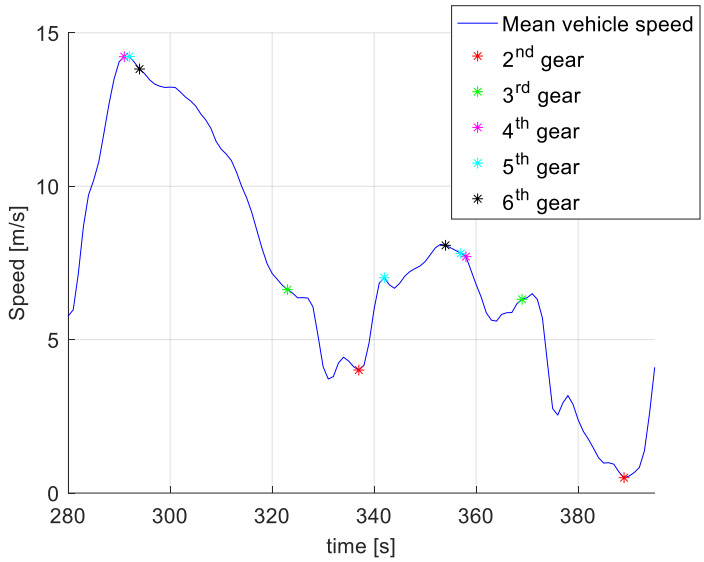

Figure 6-11. Vehicle mean speed (zoom).

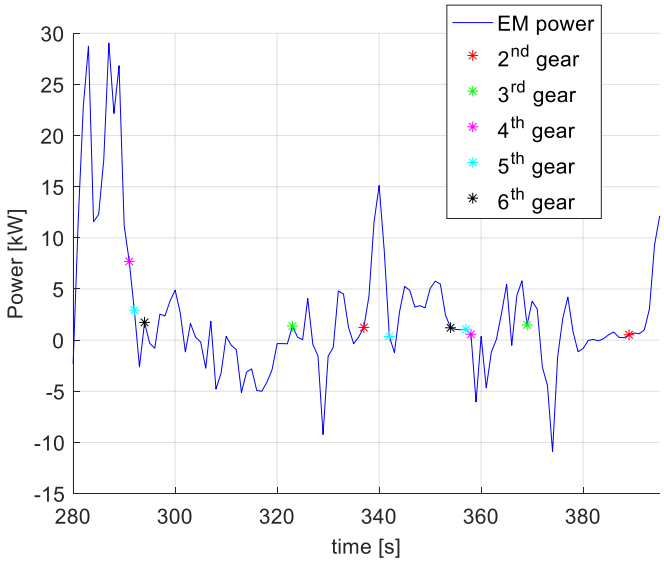

Figure 6-12. EM power (zoom).

As it can be seen in the previous two figures, at 291 and 292 s, two consecutives upshifts are made in which the vehicle speed is increasing and the EM power request is decreasing.

Another observation that can be made concerns the 5^{th} to 6^{th} upshift seen at 294 s. Similar gear changes are seen through the cycle when the EM power consumption is lower than that of the no gearshift case. This pattern presents itself for vehicle speeds lower than 20 m/s. Note that this maneuver allows to perform a 6^{th} to 3^{rd} downshift before the braking event that occurs at 323 s which helps to regenerate energy more efficiently.

At 337s, where the speed is low and the EM power request is increasing, a downshift to 2^{nd} gear is undertaken.

In addition, when analyzing the downshifts at 357 and 358 s, it is noticed that in both cases the vehicle speed decreases and the EM power request also reduces.

The previous observations can be summarized as:

- If the vehicle speed is increasing and the EM power request decreases, upshifts are performed.
- 5^{th} to 6^{th} upshifts are performed for speeds lower than 20 m/s and negative EM power loss.
- At speeds lower than 5 m/s with increasing power request, downshifts to 2^{nd} gear are performed.
- If the vehicle speed decreases and the EM power request also diminishes, a downshift is undertaken.

Another particular trend observed is that once it is decided whether to do an upshift or a downshift, the gear chosen corresponds to the one involving the lowest power consumption. This can be appreciated in Figure 6-13 and Figure 6-14 where the EM power request for all possible gears is presented.

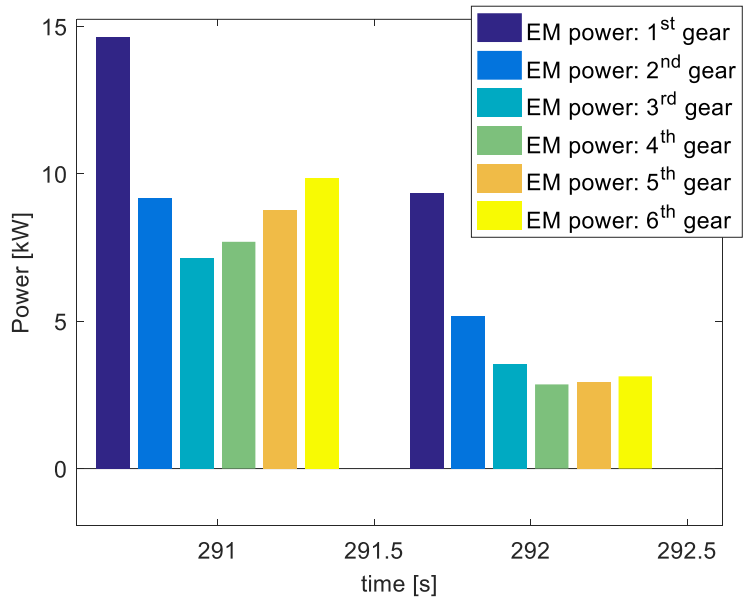

Figure 6-13. EM power request for all gears: 291 and 292 s.

For 357 (6^{th} to 5^{th}) and 358 (5^{th} to 4^{th}) s:

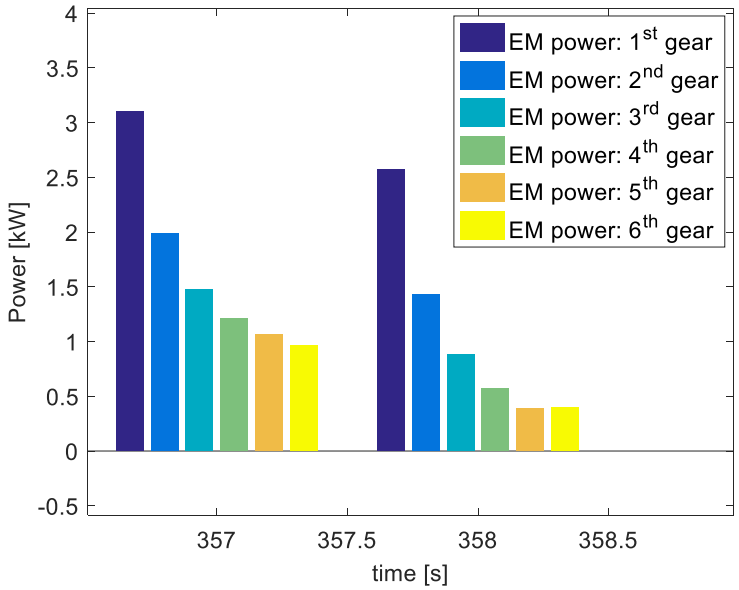

Figure 6-14. EM power request for all gears: 357 and 358 s.

By looking at the same variables studied here, other portions of the cycle were also analyzed to define a complete set of rules for single gearshifts.

Multiple upshifts analysis

By studying the optimal gear schedule, it is observed that, when the vehicle speed increases, multiple upshifts are performed if the EM power request is very close (within 300 W) to that of the single gearshift. An example of this is the 3rd to 6th upshift made at 732 s for which the power consumption is reported in Figure 6-15.

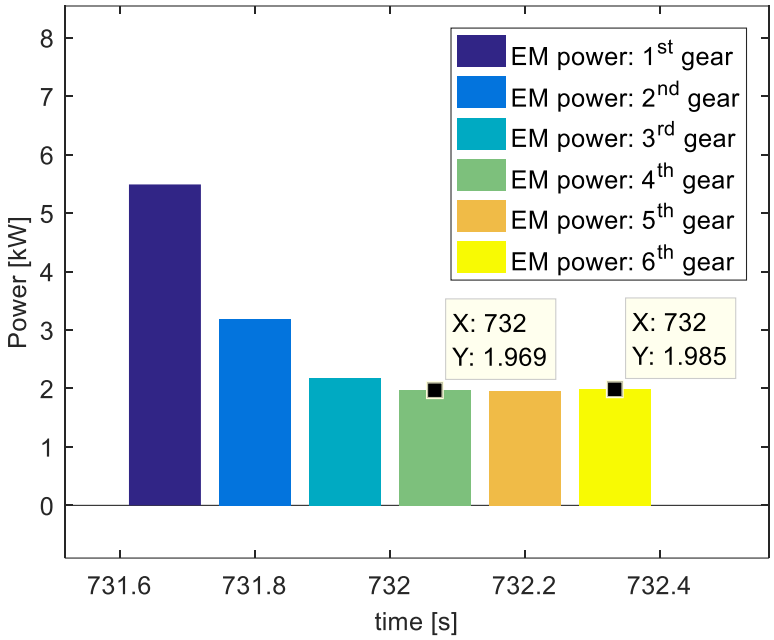

Figure 6-15. EM power request for all gears: 732 s.

Braking events analysis

The analysis of all the gearshift maneuvers performed revealed that only a small amount of them involved and EM power loss higher than 20 % with respect to the power consumption of the no gearshift case. If the points in which such power is lower than 350 W are excluded, almost all the remaining gearshifts correspond to downshifts that occurred right before a braking event.

Note that choosing the appropriate gear when decelerating the vehicle is crucial since it allows to maximize the energy regenerated with the EM that otherwise will be dissipated by the mechanical brakes. Further note that, because of the characteristics of the gearshift loss model discussed in section 2.2.4, while

switching gears, it is not possible to recharge the battery using the vehicle kinetic energy, i.e., it is convenient to engage the most suitable gear before the braking event starts.

An example of the mentioned downshifts is seen in Figure 6-16. In the figure, a 6th to 3rd gearshift that happens right before an important deceleration event (EM power around -25 kW) is presented.

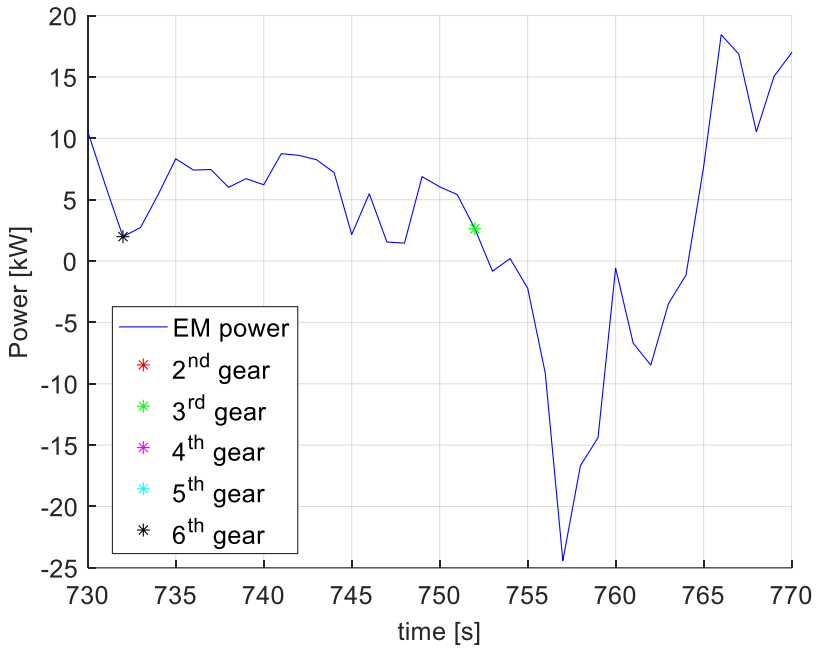

Figure 6-16. Gearshifts before braking events: 752 s.

After reviewing each of the gearshifts undertaken before braking events, the following trends were observed in the optimal solution:

- In 6th to 3rd gearshifts:
  - EM power rate is lower than -1 kW/s.
  - EM power loss is lower than 1.1 kW.
- In 5th to 4th gearshifts:
  - Vehicle speed is higher than 17 m/s.
  - EM power loss is lower than 600 W.
- In 4th to 3rd gearshifts:
  - Vehicle speed is higher than 14 m/s.

- EM power rate is lower than -1.3 kW/s.
- EM power loss is lower than 1.1 kW.

6.1.4.2 Rule extraction results

From the observations made in section 6.1.4.1, a set of rules for the gear selection in EV-mode was designed. The rules were then tuned by running simulations for several driving cycles with different characteristics. This allowed to choose the most suitable values for the speed and power related thresholds used. For each current gear, a different set of rules is designed.

Figure 6-17 shows the gearshift schedule obtained after implementing the EV-mode gearshift rules. It can be seen that, generally speaking, the optimal gear number state trajectory is reproduced. However, there are also several instances in which different decisions are taken.

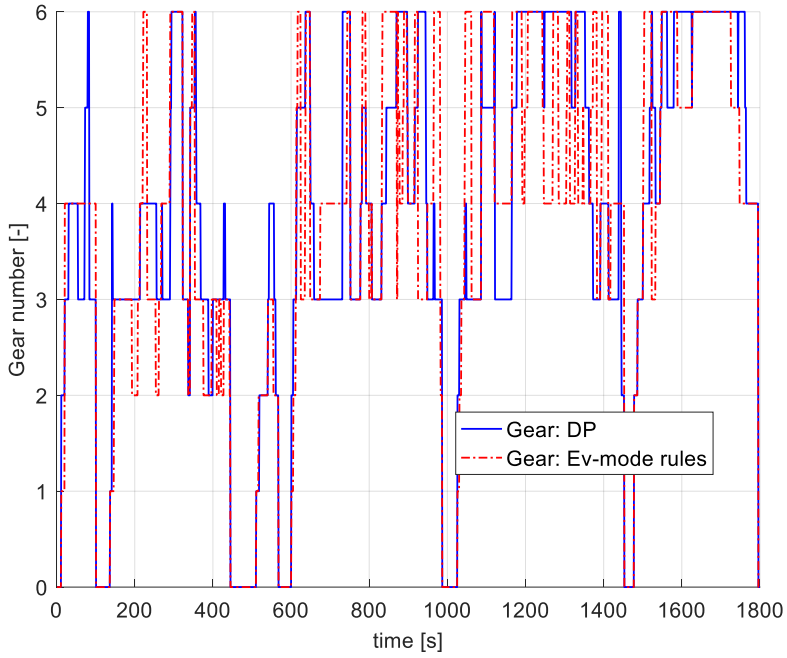

Figure 6-17. EV-mode: gearshift schedule.

In Figure 6-18, it can be seen that, since the rules do not rely on the knowledge of the future driving conditions, when certain speed and power trends are present in the driving cycle, the rule-based approach tends to anticipate the decisions made with DP.

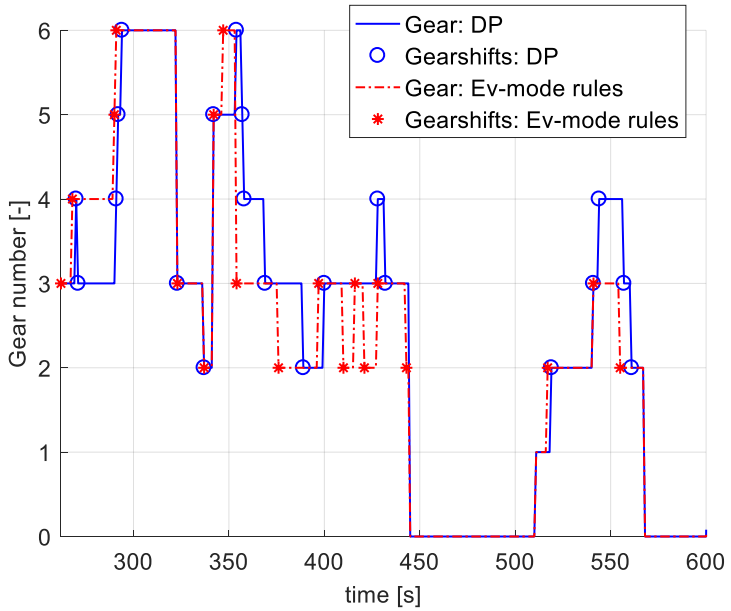

Figure 6-18. EV-mode: gearshift schedule (zoom).

This can also be seen in the last portion of the cycle for higher speeds:

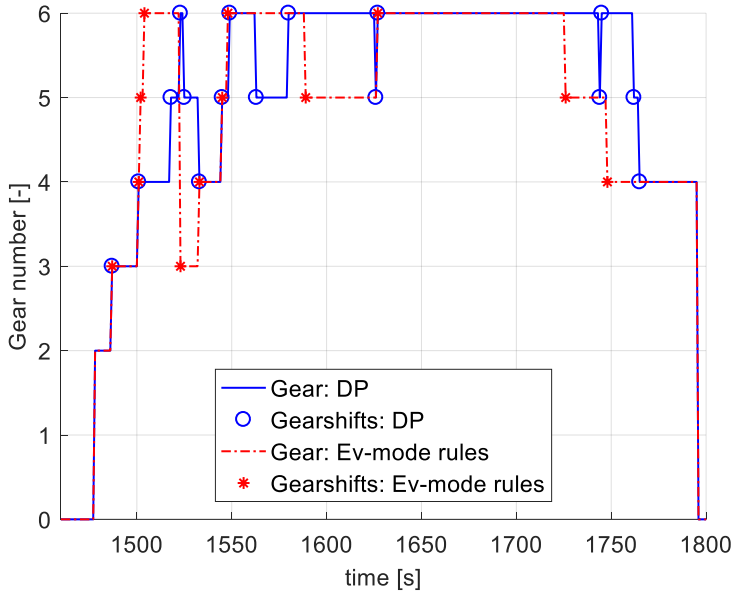

Figure 6-19. EV-mode: gearshift schedule (2nd zoom).

Even though several different gearshift decisions are seen when comparing the gearshift schedule obtained with the DP solution, the SOC profile is well reproduced as illustrated in Figure 6-20.

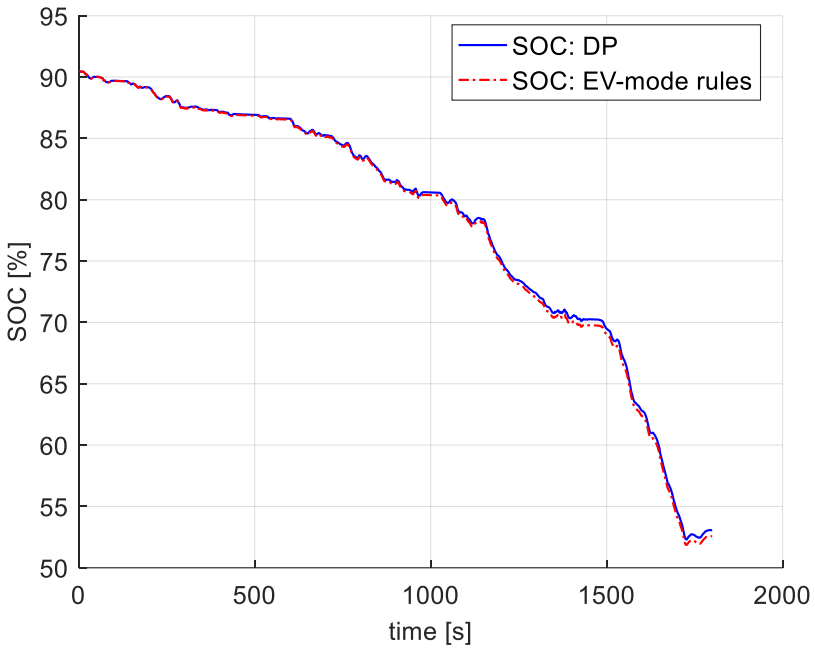

Figure 6-20. EV-mode: SOC.

The similar SOC profile (final SOC difference is lower than 0.5 %) is obtained due to the ability of the rule-based approach to recognize relevant speed and power trends in the driving cycle. In particular, it is worth underlining that the gear number selected before important braking events (EM power request lower than -20 kW) is similar in most cases. For example, Figure 6-21 shows that at 752 (6^{th} to 3^{rd}), 792 (5^{th} to 4^{th}) and 807 s (4^{th} to 3^{rd}) the same gearshifts are performed by both EMSs. The mechanical power request at the EM shaft of -38.17 kW (795 s), corresponds to the second lowest value seen for the WLTC.

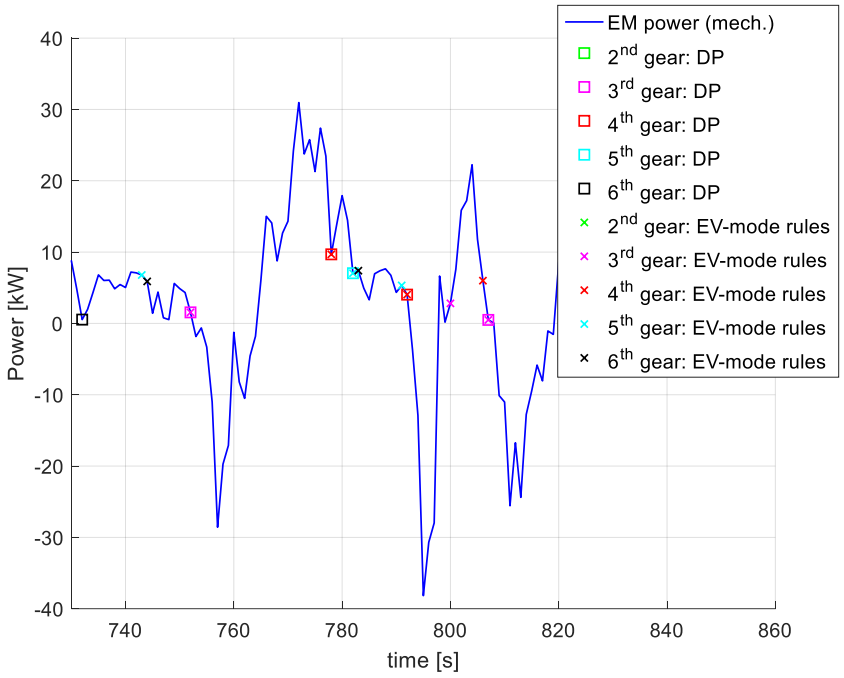

Figure 6-21. Gearshifts before braking events: 752, 792 and 807 s.

In addition, before the most important braking event of the driving schedule studied (mechanical power request at EM shaft equal to -43.77 kW), the 4th gear is selected by the rule-based approach. Instead, the 3rd gear is chosen in the DP results (see Figure 6-22). Note that since the 5th gear is engaged according to the rules extracted at 1120 s, when the established conditions for performing a downshift before decelerating the vehicle are verified, the 3rd gear is not an option (see section 5.4), therefore, the second most convenient gear (4th) is selected instead.

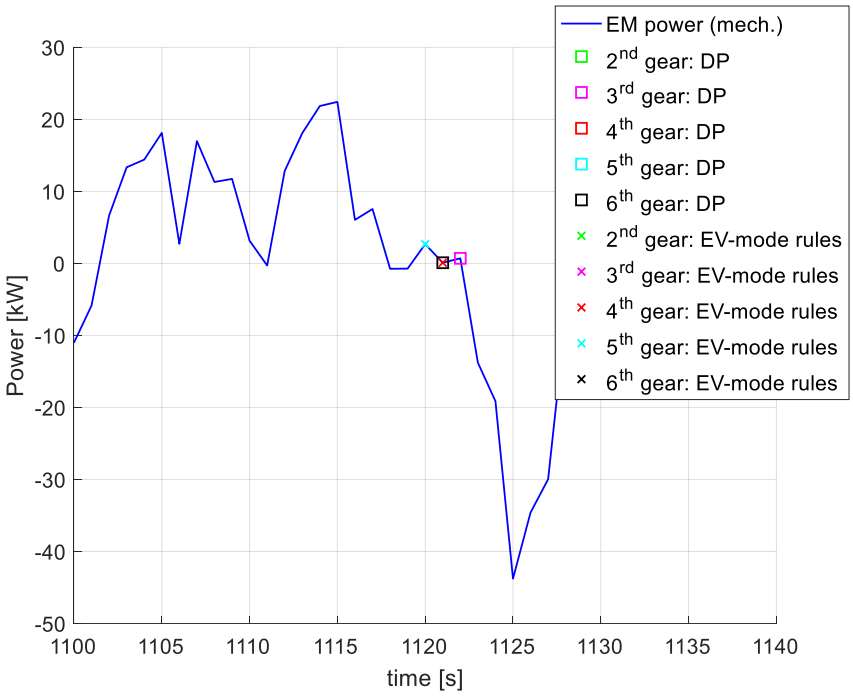

Figure 6-22. Gearshifts before braking events: 1125 s.

The latter two figures allow to appreciate the effectiveness of the rules designed to handle the gear selection before braking events.

6.1.5 Calibration of SOC tracking parameters

The main advantages of A-ECMS approaches are in their robustness and low computational burden when compared to other control techniques. However, its full potential can only be realized if the parameters of the adaptation law are properly tuned.

As stated before, the discrete adaptation scheme based on feedback from SOC discussed in section 4.6.3.1 is employed for the implementation of A-ECMS. Analyzing the adaptation law described in Eq. (4-59) shows that the main SOC tracking parameters are the sampling distance and the proportional gain.

In the following paragraphs, the effect of these parameters on the EMS performance is studied. Simulation results for cycles with very different characteristics are analyzed in order to tune the SOC tracking parameters. Such tuning is done aiming at achieving results close to the global optimal solution for most driving conditions.

On the other hand, in order to properly initialize the equivalence factor, a pre-computed offline map could be used in which the optimal values are stored for several different cycles based on the total traveled distance and the average speed. This approach has been adopted in previous studies [60] and finds its justification in the observations made about the co-state behavior in section 4.6.2.3.

6.1.5.1 Driving cycles

The WLTC, described in section 5.5.1, is seen to be composed of four speed phases with different characteristics: low (< 60 km/h), medium (< 80 km/h), high (< 110 km/h) and extra-high (> 110 km/h). This comes as a consequence of the cycle being designed to represent average driving conditions from all around the globe [130].

Two more cycles are studied in the following: US06 and FUDS.

The US06 driving cycle is representative of aggressive highway driving conditions in the USA [94]. The cycle is characterized by portions with rapid speed fluctuations and high acceleration [34]. The main driving cycle parameters are reported in Table 6-3.

Table 6-3. Driving cycle characteristics: US06.

Parameter	**Value**
Duration	596 s
Distance	12.8 km
Average speed	77.9 km/h
Maximum speed	129.2 km/h

In Figure 6-23 and Figure 6-24, the speed and acceleration profiles of the US06 cycle are presented.

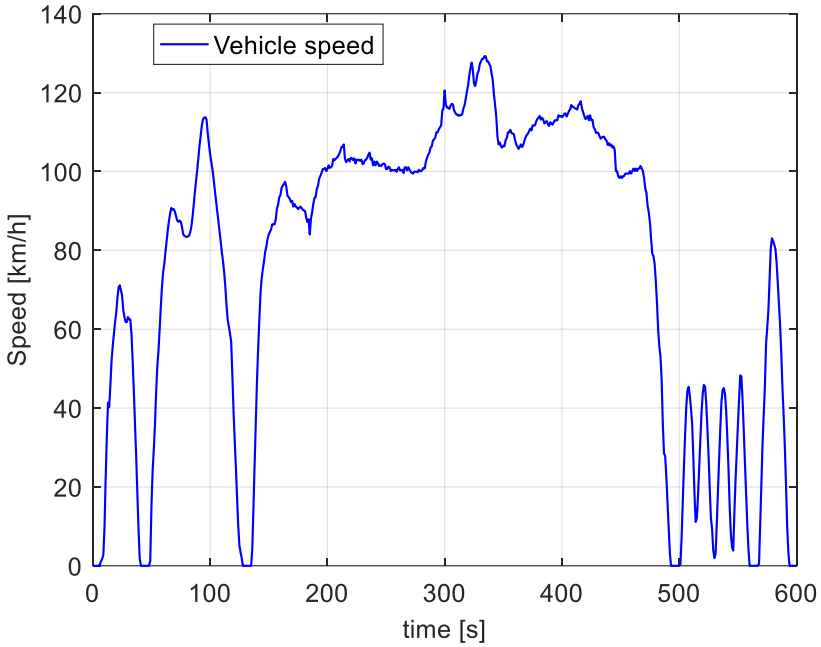

Figure 6-23. Speed profile: US06.

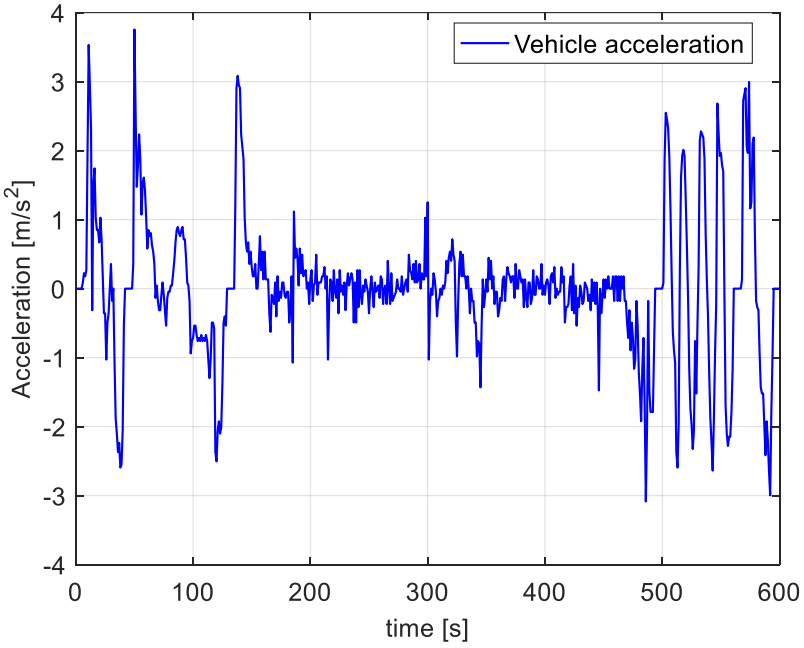

Figure 6-24. Acceleration profile: US06.

On the other hand, the FUDS is representative of an urban route with frequent stops [34]. The main driving cycle parameters are reported in Table 6-4.

Table 6-4. Driving cycle characteristics: FUDS.

Parameter	**Value**
Duration	1372 s
Distance	12.07 km
Average speed	31.5 km/h
Maximum speed	91.2 km/h

In Figure 6-25 and Figure 6-26, the speed and acceleration profiles of the FUDS cycle are presented.

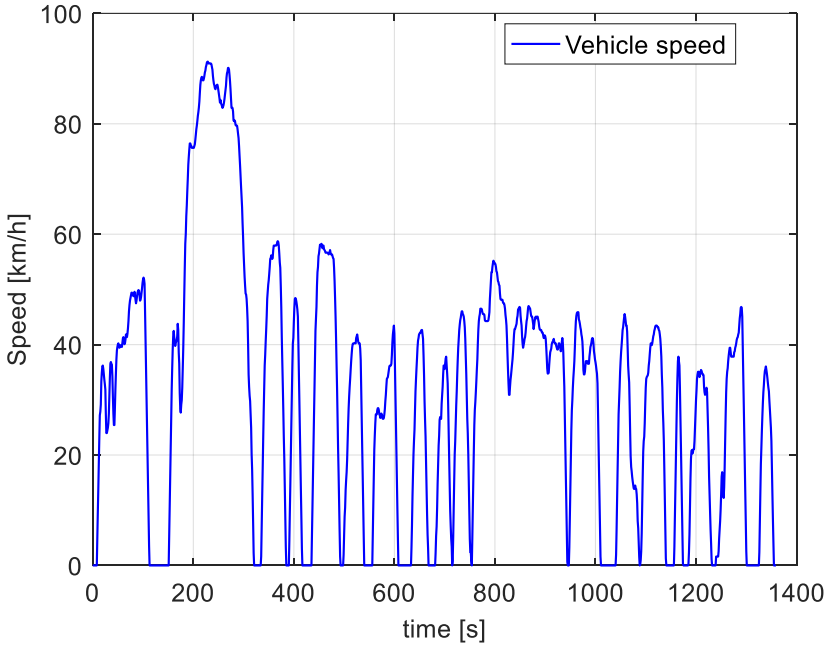

Figure 6-25. Speed profile: FUDS.

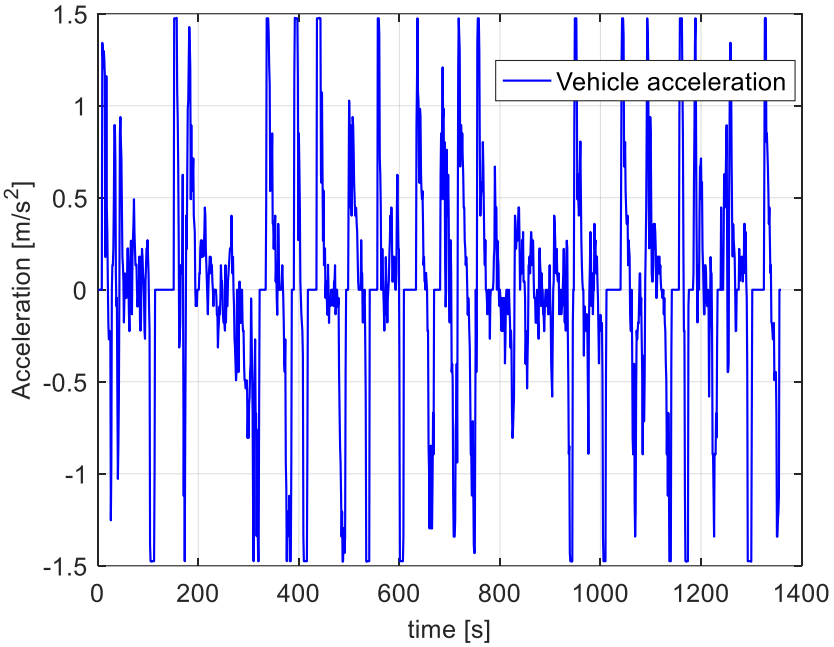

Figure 6-26. Acceleration profile: FUDS.

By analyzing these three cycles, the effectiveness of the algorithm can be assessed for different working conditions ranging from typical urban driving behavior to aggressive highway driving.

6.1.5.2 Calibration results

In order to study the effect of the SOC tracking parameters on the performance of the developed real-time EMS strategy, a series of simulations are performed testing different combinations of the sampling distance and the proportional gain used in Eq. (4-59).

For each set of SOC tracking parameters, the EMS is implemented for the following driving schedules:

- WLTC (1 repetition).
- FUDS (2 repetitions).
- US06 (2 repetitions).

The change in the number of repetitions allows to test for different driving profiles of a similar length in terms of distance.

In terms of boundary conditions, it was established:

$$SOC_{ref,N} = 0.75 \tag{6-8}$$

$$SOC_{max} = 0.93 \tag{6-9}$$

$$SOC_{min} = 0.74 \tag{6-10}$$

Differently from the charge-depleting simulation studied in section 5.5.3, a final target for the SOC is established. In this way, the cycle cannot be completed almost entirely in EV-mode and the interaction between the two energy sources present onboard can be studied.

Note that it is allowed to go 1 % below the final SOC target (control candidates yielding lower values will be penalized). This is to account for the fact that the EMS cannot guarantee to achieve the exact value required for the SOC at the end of the cycle. This feature is common for most ECMS-based approaches [1].

Consider for example a case in which two different control strategies yield the same fuel consumption but with a different final SOC. It is quite obvious that in terms of energy usage, the one with the highest SOC outperforms the other. This simple example is meant to illustrate that in order to make a fair comparison of the energy consumption for different strategies, it is necessary to account for the energy left in the battery. Hence, similarly to [60], [113], a total equivalent fuel mass is defined considering the fuel energy savings obtained by not providing the net amount of energy supplied by the battery through the thermal path, i.e.:

$$m_{f,eq,tot} = m_{f,tot} + \frac{E_{b,tot}}{\bar{\eta}_{ICE}\, LHV} \tag{6-11}$$

where,

$m_{f,tot}$ is the total amount of fuel consumed during a driving mission.

$E_{b,tot}$ is the total energy provided by the battery during a driving mission.

LHV is the fuel LHV.

$\bar{\eta}_{ICE}$ is the mean efficiency of the ICE seen during a driving mission.

In the rest of the chapter, the effectiveness of real-time implementable control strategies will be evaluated by using as a parameter the difference between the total equivalent fuel mass of the causal EMS and that of the optimal solution. This parameter is calculated as:

$$\Delta m_{f,eq,tot} = \frac{m_{f,eq,tot} - m^*_{f,eq,tot}}{m^*_{f,eq,tot}} \, 100 \tag{6-12}$$

where,

$m_{f,eq,tot}$ is the total equivalent fuel mass obtained with a causal strategy.

$m^*_{f,eq,tot}$ is the optimal total equivalent fuel mass.

Table 6-5 presents the value obtained for the quantity defined in Eq. (6-12) for each set of SOC tracking parameters considered. The values reported are computed for the WLTC.

Table 6-5. Effect of SOC tracking parameters: WLTC.

$\boldsymbol{K_p}$ [-]	1	3	5	8	10
$\boldsymbol{D_s}$ [km]	$\Delta m_{f,eq,tot}$ [%]	$\Delta m_{f,eq,tot}$ [%]	$\Delta m_{f,eq,tot}$ [%]	$\Delta m_{f,eq,tot}$ [%]	$\Delta m_{f,eq,tot}$ [%]
1	3.734	3.758	3.783	3.864	3.864
2	3.734	3.758	3.758	3.758	3.588
3	3.734	3.734	3.758	3.758	3.783
5	3.734	3.734	3,734	3.734	3.734

In Table 6-5, it can be appreciated that the maximum difference between the results obtained for different sets of parameters is lower than 1 %. The same happens for the other two driving schedules under analysis. This implies that the EMS developed in this chapter is robust with respect to the SOC tracking parameters. Therefore, the selection of the best values for the sampling distance and

the proportional gain of the equivalence factor adaptation law can be made offline and the same parameters can be used regardless of the driving cycle to be followed.

In order to select the mentioned parameters, in Table 6-6, the sum of the total equivalent fuel mass for the three driving schedules studied is reported for every pair of sampling distance and proportional gain under consideration.

Table 6-6. Effect of SOC tracking parameters: all cycles.

K_p [-]	1	3	5	8	10
D_s [km]	$\Delta m_{f,eq,tot}$ [%]	$\Delta m_{f,eq,tot}$ [%]	$\Delta m_{f,eq,tot}$ [%]	$\Delta m_{f,eq,tot}$ [%]	$\Delta m_{f,eq,tot}$ [%]
1	17.490	17.434	17.670	18.129	18.127
2	17.359	17.5140	17.477	17.708	17.538
3	17.359	17.359	17.383	17.514	17.794
5	17.359	17.359	17.359	17.339	17.495

Table 6-6 shows that the EMS is less sensible to the value of the proportional gain as the sampling distance increases.

Based on the data presented, the values selected are: 8 and 5 km.

6.1.6 Effect of restrictions on ICE state

With no restrictions in place for changes on the ICE state, this component will be used each time that the current value of the equivalence factor implies an instantaneous equivalent fuel consumption which is lower than that seen for the EV-mode (see section 6.1.2). Hence, as illustrated in Figure 6-27 and Figure 6-28, different TSFs are selected by the proposed technique with respect to those chosen in the DP results. Note that the ICE has a very intermittent on/off behavior. The driving schedule studied is still the WLTC and the final SOC target is 75%.

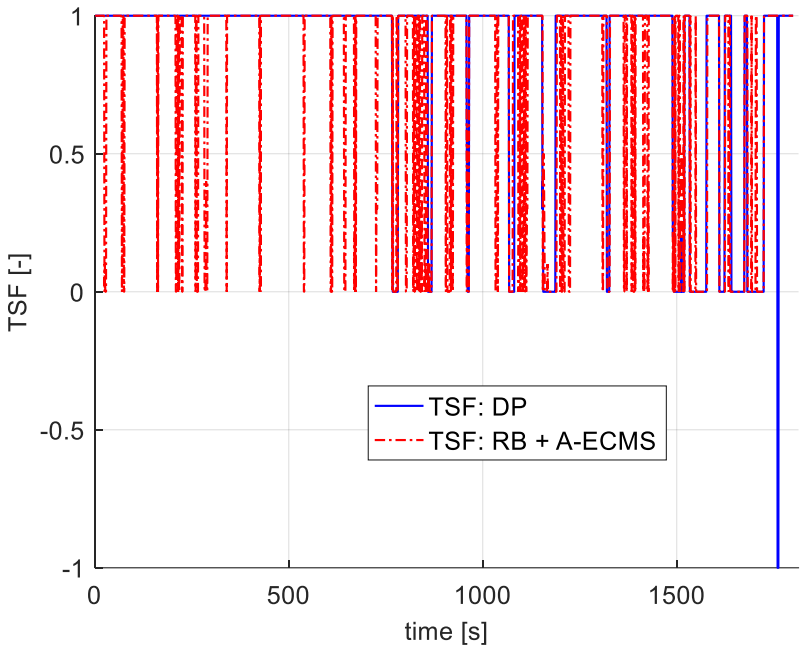

Figure 6-27. TSF: free ICE state.

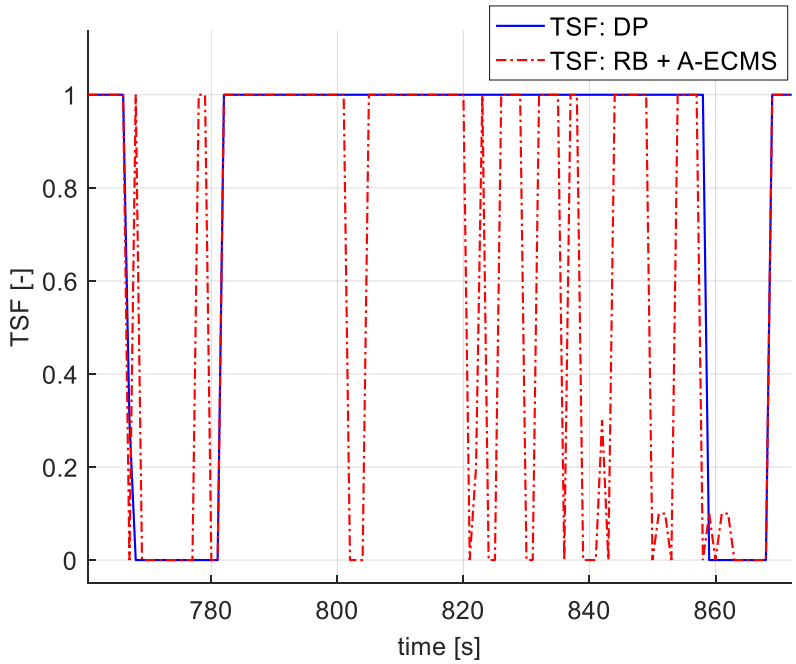

Figure 6-28. TSF: free ICE state (zoom).

Note that “RB + A-ECMS” refers to the EMS developed in this chapter which combines a rule-based gear selection in EV-mode with A-ECMS.

On the other hand, when the fuel penalties related to the ICE state discussed in section 6.1.3.2 are employed, the results improve significantly (see Figure 6-29).

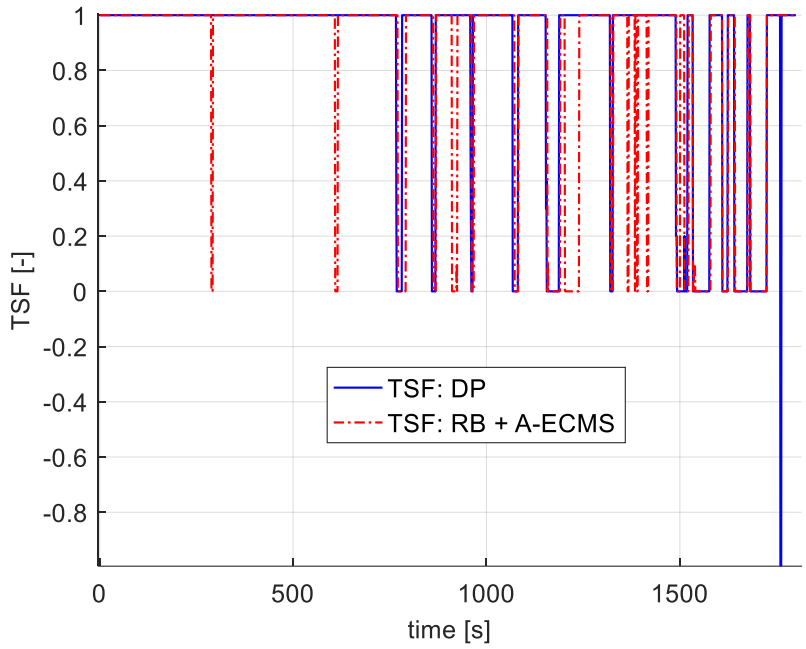

Figure 6-29. TSF: restrictions on ICE state.

In the former figures, the best values of the initial equivalence factor for both cases, with and without ICE state restrictions, were considered while implementing the EMS of interest. In order to isolate the effect of the penalties introduced on the solution, the proportional gain was set to 0. The driving schedule studied was the WLTC.

6.2 Benchmarking and comparison of real-time energy management strategies

In this section, the DP formulation presented in chapter 5, is used to benchmark the results of the developed EMS (referred to as RB + A-ECMS) and those of the A-ECMS. As mentioned before, besides realizing how close the results are from those

of the optimal solution, this also allows to compare the performance of the designed algorithm with that of a well-known real-time implementable control strategy.

For the A-ECMS implementation, the same powertrain model (see section 2.2), penalties (properly tuned) and equivalence factor adaptation scheme (see section 6.1.3) employed for the EMS described in the previous paragraphs are considered. The fundamental difference is that at each iteration the instantaneous equivalent fuel consumption defined in Eq. (6-2) is minimized by choosing both the TSF and the most appropriate gear. As for the other control strategies discussed, the main aspect that differentiates the A-ECMS implementation developed here from those published in previous works, is in the modeling of the energy consumption during gearshifts and ICE starts. A-ECMS was calibrated using the same procedure illustrated in section 6.1.5, the values selected for the SOC tracking parameters are: 3 and 5 km.

In the following, simulation results for the same driving cycles used to calibrate the real-time implementable EMSs are presented.

Figure 6-30 illustrates the performance of the RB + A-ECMS approach. The SOC, equivalence factor and fuel consumption are shown for 1 repetition of the WLTC. The SOC trajectory is very close to the optimal one through the entire cycle. Note that since the SOC stays close to its reference, the variations of the equivalence factor are not significant. It can also be appreciated that both the total fuel consumption and the final SOC are similar to those obtained with DP.

Figure 6-31 shows the EM operating points for both the DP solution and the RB + A-ECMS approach. It can be noticed that the EM continuous torque limit is breached more times in the online implementable approach than in the DP results.

On the other hand, by comparing the ICE operating points (see Figure 6-32), it can be stated that in both cases the ICE working conditions are selected to operate in the map region related to lower fuel consumption rates and higher efficiencies.

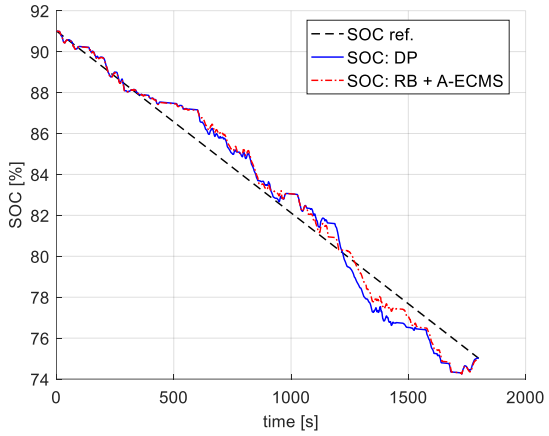

a) SOC

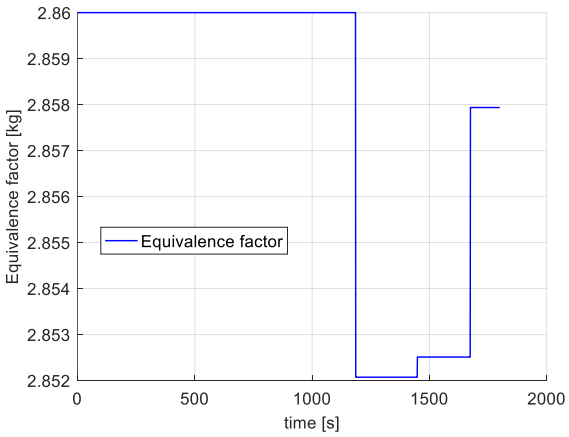

b) Equivalence factor

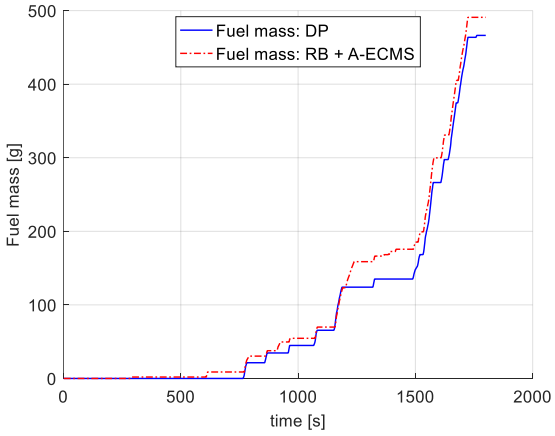

c) Fuel consumption

Figure 6-30. Benchmarking results for WLTC: RB + A-ECMS.

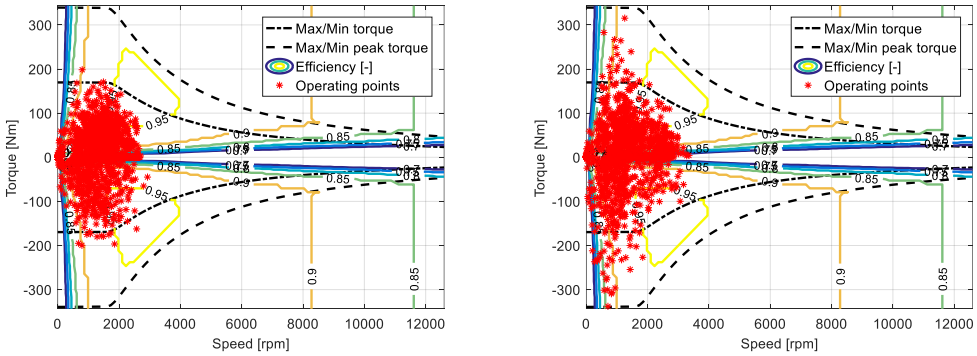

a) DP b) RB + A-ECMS

Figure 6-31.EM operating points for WLTC: DP vs. RB + A-ECMS.

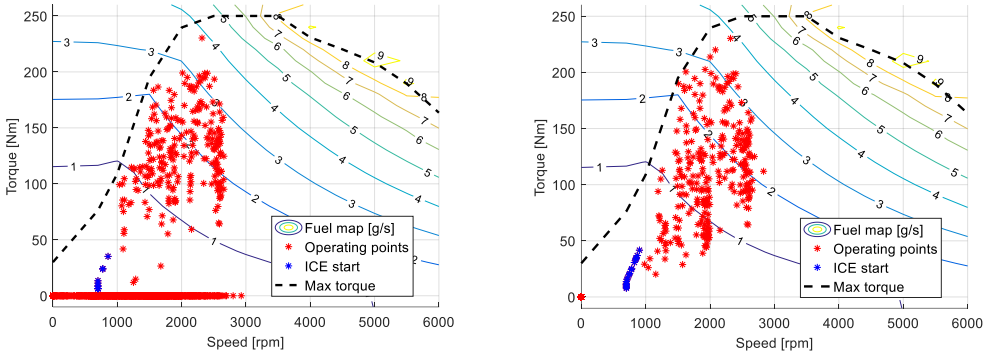

a) DP b) RB + A-ECMS

Figure 6-32. ICE operating points for WLTC: DP vs. RB + A-ECMS.

The results for two repetitions of the FUDS and the US06 driving cycles are presented in Figure 6-33 and Figure 6-34 respectively.

As for the WLTC, the SOC trajectory obtained for the FUDS is similar to that of the optimal solution. Nevertheless, the performance in terms of fuel consumption of the developed EMS is significantly better for the WLTC (see Table 6-7).

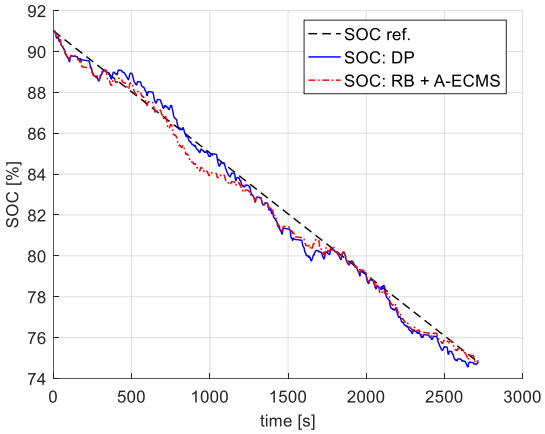

a) SOC

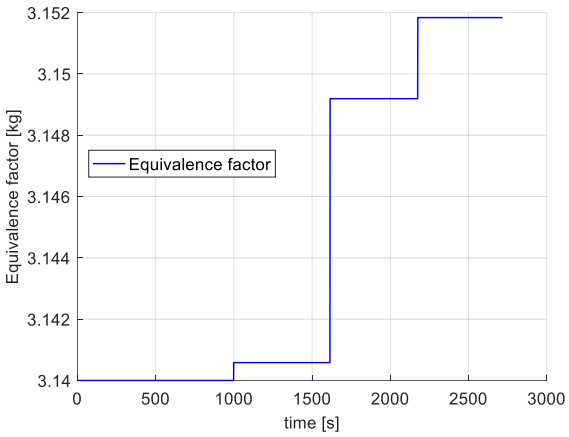

b) Equivalence factor

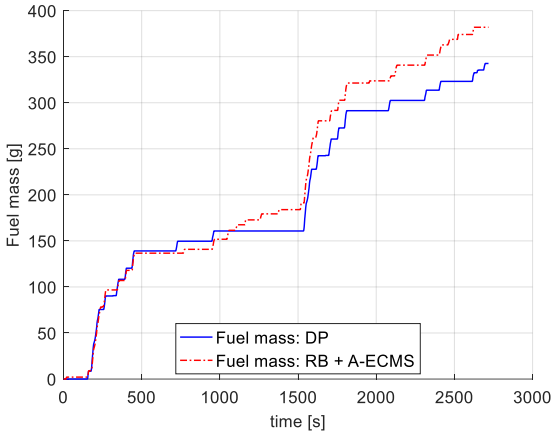

c) Fuel consumption

Figure 6-33. Benchmarking results for FUDS: RB + A-ECMS.

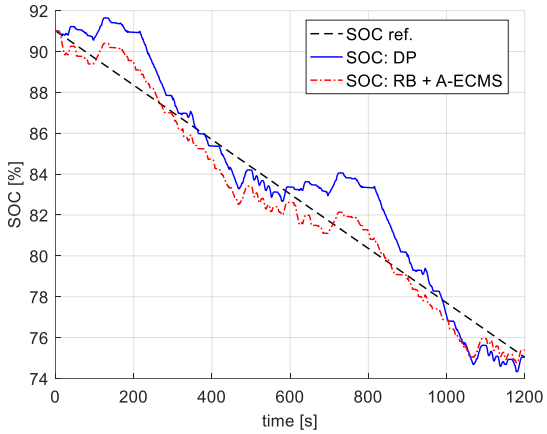

a) SOC

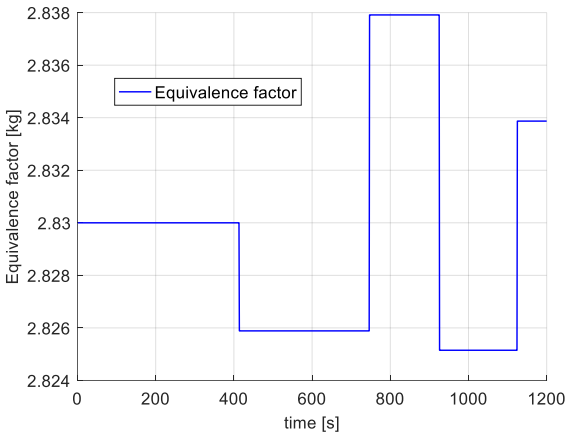

b) Equivalence factor

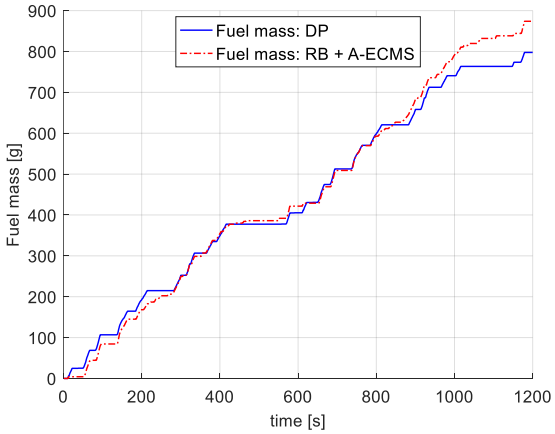

c) Fuel consumption

Figure 6-34. Benchmarking results for US06: RB + A-ECMS.

In Figure 6-34 it can be appreciated that the optimal SOC trajectory presents higher differences with respect to the given reference than those seen for the other two driving schedules. Instead, the SOC profile obtained with the RB + A-ECMS approach is kept closer to the mentioned reference thanks to the equivalence factor adaptation scheme in place. The effects of providing a suitable reference for the SOC are further discussed in section 6.3.2.

Besides the difference in the total equivalent fuel mass defined in Eq. (6-12), the percental difference in the total fuel consumption will be also used as a parameter for the benchmarking of real-time implementable EMSs. The latter is defined as:

$$\Delta m_{f,tot} = \frac{m_{f,tot} - m^*_{f,tot}}{m^*_{f,tot}} \, 100 \tag{6-13}$$

where,

$m_{f,tot}$ is the total fuel mass obtained with a causal strategy.

$m^*_{f,tot}$ is the optimal total fuel consumption.

Table 6-7 and Table 6-8 summarize the most relevant parameters for the benchmarking of the RB + A-ECMS and A-ECMS approaches for the driving cycles under consideration. It can be concluded that, in terms of the total equivalent fuel consumption, the RB + A-ECMS approach does not only yield results that are close to the optimal solution (within 8 %) but also outperforms those of the A-ECMS. The mentioned EMS also provides better results than the A-ECMS in terms of the actual fuel consumption.

Table 6-7. Benchmarking results: RB + A-ECMS.

Parameter	WLTC	FUDS	US06
$\Delta m_{f,eq,tot}$ [%]	3.739	7.565	6.035
$\Delta m_{f,tot}$ [%]	5.266	11.471	9.560
SOC_N [%]	74.937	74.857	75.388

Note that the final SOC and the parameters defined in Eq. (6-12) and Eq. (6-13) are retained as the most representative for the benchmark process.

Table 6-8. Benchmarking results: A-ECMS.

Parameter	WLTC	FUDS	US06
$\Delta m_{f,eq,tot}$ [%]	4.444	10.214	7.383
$\Delta m_{f,tot}$ [%]	5.720	15.889	12.589
SOC_N [%]	74.790	74.510	75.996

It can be seen in the former tables that the RB + ECMS approach is characterized by a higher final SOC at the end of the WLTC and the FUDS. From the analysis of the simulation results it was inferred that this could be related to a more efficient generation of electrical energy during braking events.

In particular, the FUDS, with a velocity profile characterized by frequent stops (see Figure 6-25), presents several opportunities for energy regeneration. Table 6-9 presents the gear selected by the studied EMSs for the braking events with the highest power available for regeneration at the EM shaft (highest, in absolute terms, mechanical power request to EM $P_{reg,k}$). It can be appreciated that, in general, the EV-mode gearshift rules designed for this type of situations, enable the RB + A-ECMS approach to operate in a similar gear (±1) with respect to that chosen by DP.

Instead, the instantaneous minimization approach used in the A-ECMS, tends to result in choosing higher gears. These considerations hold for the WLTC as well.

Table 6-9. Braking events: FUDS.

t [s]	104	409	601	1293	1463
P_{reg} [kW]	-25.79	-22.04	-22.67	-24.35	-25.79
gn: DP	3	3	3	3	3
gn: RB + A-ECMS	3	6	4	3	3
gn: A-ECMS	6	6	5	3	6

On the other hand, the mentioned tendency of choosing the higher gears seen for the A-ECMS is in agreement with the optimal solution for braking events performed at high speeds as seen at 345 and 446 s for the US06 driving cycle in Table 6-10. Differently, from the FUDS, in the US06 speed profile a lower number of vehicles stops are present but braking events are associated to higher power requests, so it is important to extract as much energy as possible from them. Note that the final SOC obtained with the A-ECMS is 0.6 % higher than for the RB + A-ECMS approach.

Table 6-10. Braking events: US06.

t [s]	119	345	446	486	588
P_{reg} [kW]	-49.78	-51.73	-51.29	-52.36	-47.95
gn: DP	4	6	6	3	3
gn: RB + A-ECMS	6	5	5	5	6
gn: A-ECMS	6	6	6	6	6

In order to analyze how powertrain operation resembles that of the optimal solution the TSFs obtained are also studied.

Figure 6-35 allows to compare the TSFs selected by the different EMSs for a portion of the FUDS. It can be seen that, in general, the optimal TSF trajectory is reproduced by the real-time implementable strategies even though the ICE appears to be employed in more occasions. This is in agreement with the higher number of ICE start events undertaken with respect to the DP results (see Table 6-11).

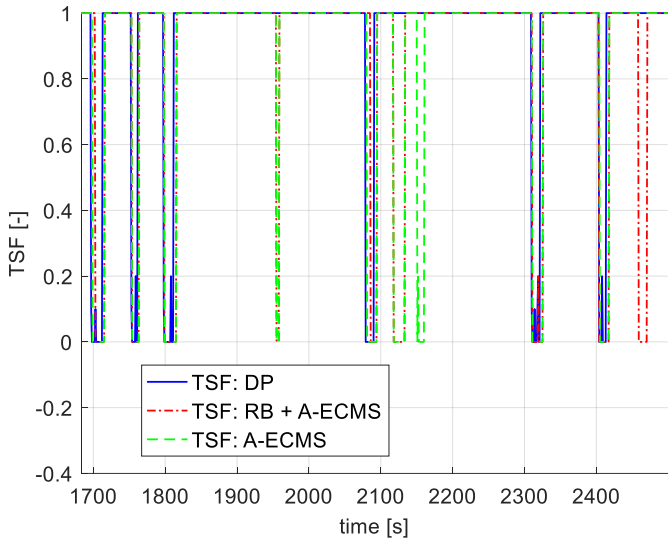

Figure 6-35. TSF: FUDS (zoom).

Figure 6-36 in analogous to Figure 6-35 but for the US06 driving schedule. At higher speeds, a more intermittent on/off behavior of the ICE is noted for the RB + A-ECMS and A-ECMS approaches, yielding a higher number of ICE start events with respect to the optimal solution (see Table 6-11).

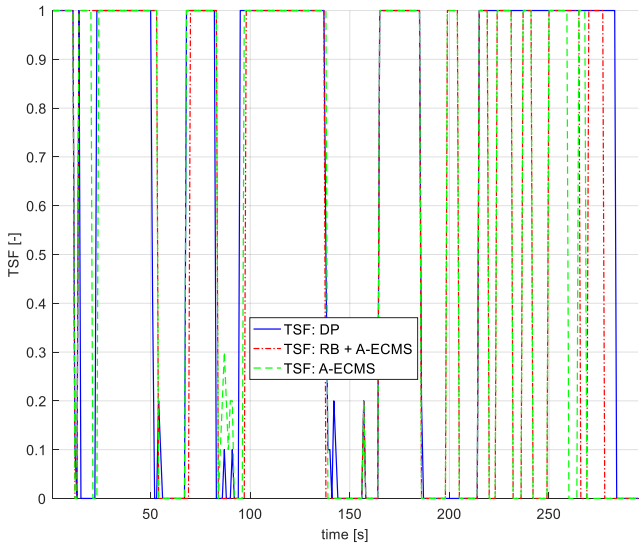

Figure 6-36. Fuel mass and TSF: US06 (zoom).

The total number of ICE starts for all cycles is presented in Table 6-11. In the real-time implementable EMSs developed here, a higher number of ICE starts events are generally undertaken when compared to the quantity seen in the DP results. As mentioned in section 6.1.1, the fuel cut-off functionality is not included in the A-ECMS based approaches which contributes to the higher number of ICE starts being performed.

Table 6-11. Total number of ICE starts.

	WLTC	**FUDS**	**US06**
DP	12	19	20
RB + A-ECMS	20	30	47
A-ECMS	17	33	55

Finally, the total number of gearshift maneuvers is reported in Table 6-12 for all the driving schedules and EMSs studied. Generally speaking, the RB + A-ECMS approach tends to result in more gearshifts than those performed in the optimal solution while the A-ECMS does the opposite.

Table 6-12. Total number of gearshifts.

	WLTC	**FUDS**	**US06**
DP	99	166	44
RB + A-ECMS	127	175	96
A-ECMS	78	156	54

6.3 Real-time energy management strategies validation

In this section, the RB + A-ECMS approach performance is assessed for a driving cycle which is different from those used during the calibration of the strategy. This is to demonstrate the causality of the mentioned control strategy.

6.3.1 Driving cycle

The driving cycle selected to validate the real-time implementable EMS developed through this chapter is the one used during the Emissions and Energy Consumption (EEC) event of the EcoCAR3 competition. Hence, it will be referred to as EC3-EEC in the following.

The cycle blends a series of EPA (Environmental Protection Agency) test cycles which makes it representative of real-world driving conditions that range from typical city driving to aggressive highway driving. The main driving cycle parameters are reported in Table 6-13.

Table 6-13. Driving cycle characteristics: EC3-EEC.

Parameter	**Value**
Duration	1290 s
Distance	22.72 km
Average speed	63.4 km/h
Maximum speed	113.4 km/h

In Figure 6-37 and Figure 6-38, the speed and acceleration profiles of the described driving cycle are presented.

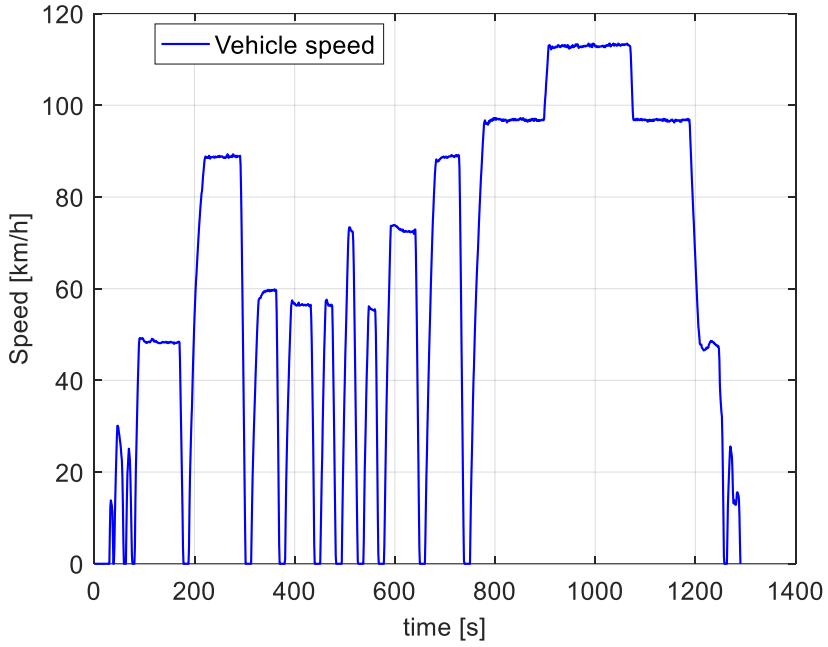

Figure 6-37. Speed profile: EC3-EEC.

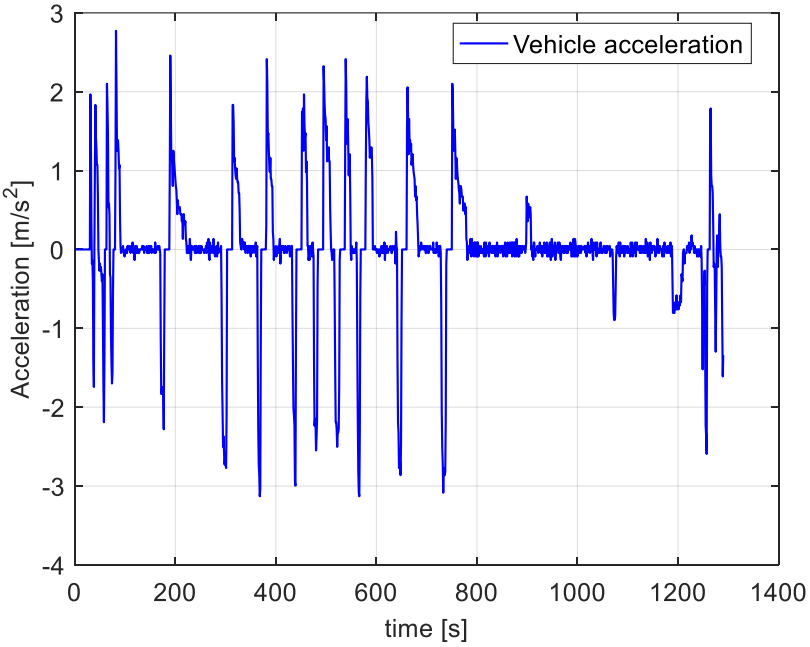

Figure 6-38. Acceleration profile: EC3-EEC.

6.3.2 Simulation results

In the following, simulation results comparing the results obtained with RB + A-ECMS, A-ECMS and DP are presented.

Figure 6-39 shows that the optimal SOC trajectory is consistently different than the given reference. Moreover, the RB + A-ECMS SOC is kept closer to the reference provided while with the A-ECMS the energy storage system operates at lower values.

On the other hand, Figure 6-40 shows that the optimal SOC trajectory would match better a reference given in the distance domain which is in contrast to what it is seen for the WLTC in section 6.1.3.3. This clearly illustrates a limitation of the equivalence factor adaptation schemes based on feedback from SOC: a technique to generate reference profiles for the SOC which are representative of the optimal solution regardless of the driving cycle is not available.

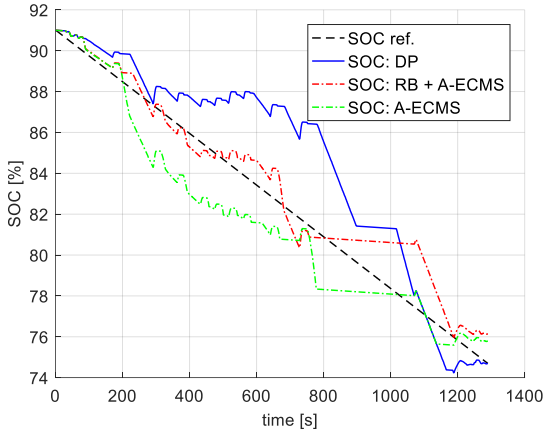

a) SOC

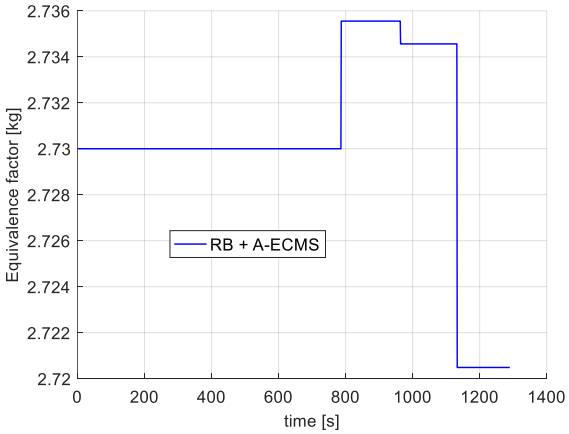

b) Equivalence factor: RB + A-ECMS

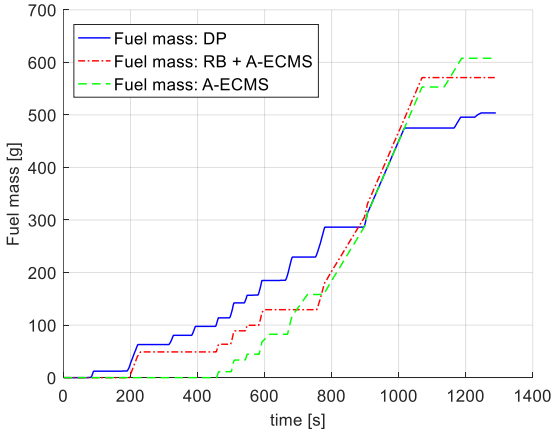

c) Fuel consumption

Figure 6-39. SOC and fuel consumption: EC3-EEC.

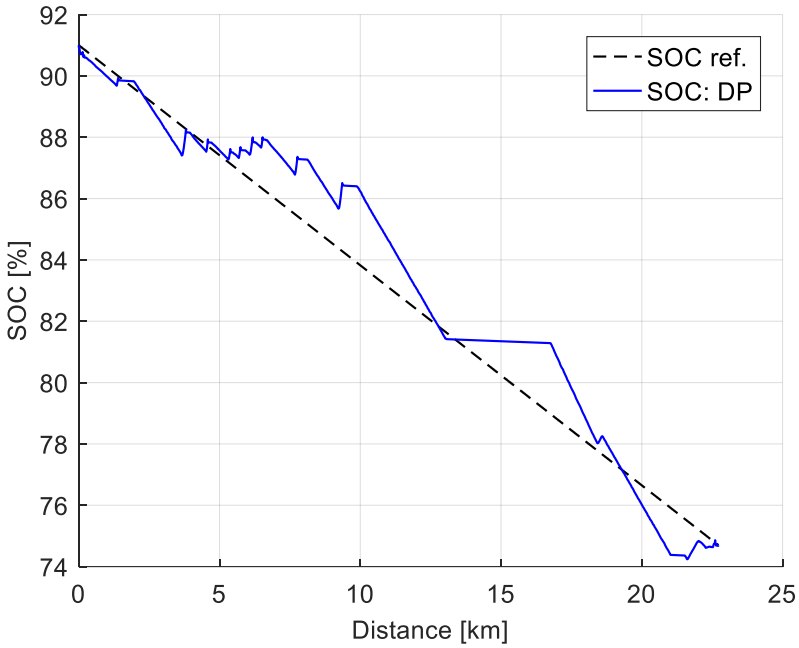

Figure 6-40. SOC: EC3-EEC (distance domain).

In Figure 6-41, the TSF is presented. Differently from the results seen in section 6.2, the real-time implementable EMSs tend to use less the ICE than the optimal solution. This is also expressed by the numbers of ICE start events undertaken (see Table 6-14).

Table 6-14. Total number of ICE starts: EC3-EEC.

DP	**RB + A-ECMS**	**A-ECMS**
13	6	7

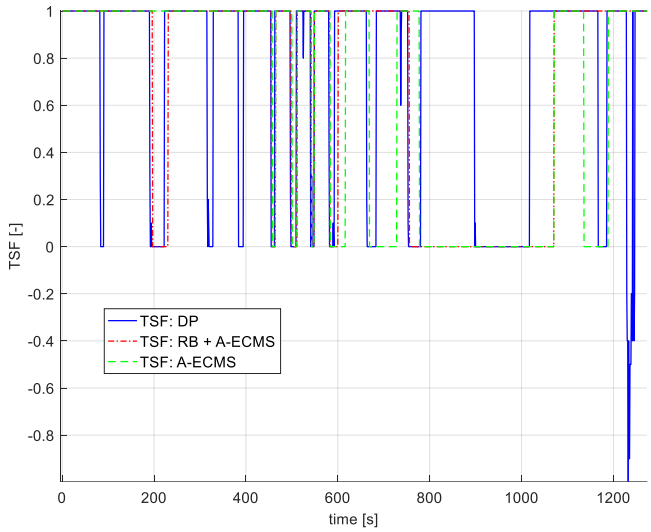

Figure 6-41. TSF: EC3-EEC.

The gearshift schedule is reproduced better by the RB + A-ECMS approach as it can be appreciated in Figure 6-42. The same trend regarding the total number of gearshifts is seen, i.e., the RB + A-ECMS technique tends to result in more gearshift than those performed in the DP solution while a lower quantity is undertaken when the A-ECMS is employed (see Table 6-15).

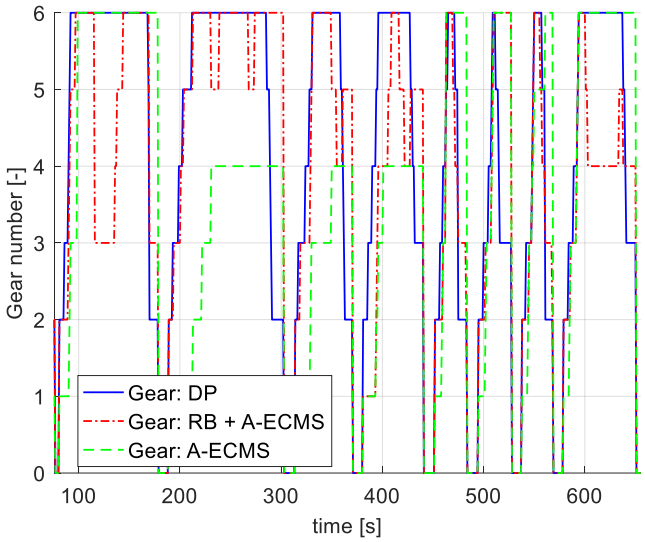

Figure 6-42. Gear number: EC3-EEC (zoom).

Table 6-15. Total number of gearshifts: EC3-EEC.

DP	RB + A-ECMS	A-ECMS
68	73	44

The EM operating points are presented in Figure 6-43. As for the WLTC results shown in section 6.2, the continuous torque limit is breached more times in the RB + A-ECMS results.

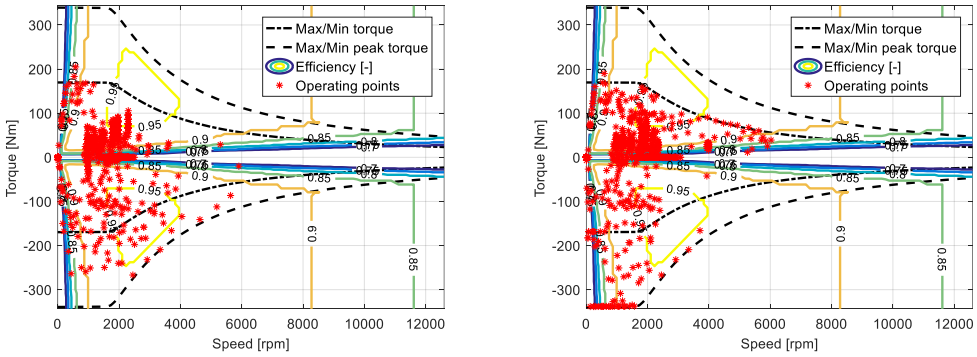

a) DP b) RB + A-ECMS

Figure 6-43.EM operating points: EC3-EEC.

In addition, the effects of the EM torque counter state introduced in the DP formulation can be appreciated in Figure 6-44. Note that when the counter reaches the maximum acceptable value, the mechanical brakes are employed to let the EM operate under its continuous torque limit. Hence, the counter proves itself to be useful in allowing to maximize energy regeneration during braking while respecting the physical limitations of the EM.

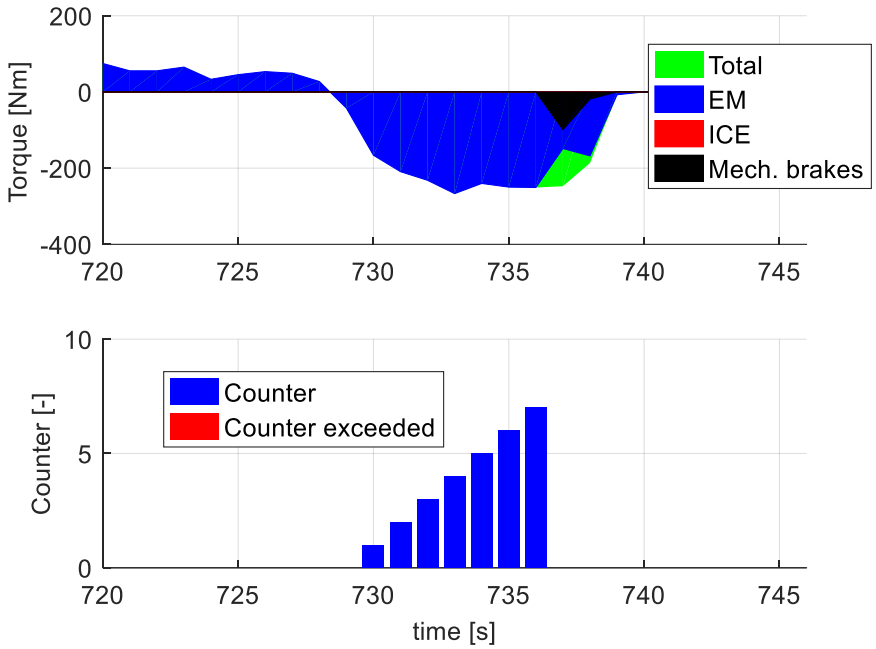

Figure 6-44. EM torque limits: EC3-EEC.

Finally, Table 6-16 presents the value of the parameters used to benchmark the causal strategies studied here. As in the previous section, the RB + A-ECMS control technique outperforms the A-ECMS in terms of both the equivalent and actual fuel consumption. Moreover, the RB + A-ECMS performance is very closed to that of the optimal solution (less than 3 % increase in equivalent fuel consumption).

Table 6-16. Benchmarking results: EC3-EEC.

Parameter	**RB + A-ECMS**	**A-ECMS**
$\Delta m_{f,eq,tot}$ [%]	2.642	7.948
$\Delta m_{f,tot}$ [%]	13.356	20.661
SOC_N [%]	76.145	75.789

An important remark to be made is that the equivalence factor is initialized here using the best possible values for each of the causal strategies. As explained in section 4.6.3, for real-time implementation, a pre-computed offline map could be

used to do this operation based on the total distance to be traveled and the average speed of the driving mission. However, given the extensive amount of simulations needed to compute such a map, this is left for future studies.

6.4 Summary

As discussed in chapter 4, PMP and DP are model-based techniques able to provide the optimal solution to the energy management problem in HEVs. However, the requirement of knowing the future driving conditions beforehand generates the need of searching for other EMSs that are real-time implementable. In this chapter, a causal EMS is designed in which:

- DP results are used to derive a set of rules aiming at reproducing the optimal gearshift schedule in EV-mode.
- A-ECMS is used to decide the powertrain operating mode (through the selection of the TSF) and the current gear if power from the ICE is needed.

In particular, a detailed description of the algorithm is given, including insights on the rule extraction and strategy calibration processes. Then, the DP formulation presented in chapter 5, is used to benchmark the results of the developed EMS and those of the A-ECMS.

After performing several simulations using DP, it was observed that, in general, when increasing the final SOC target:

- The deviations from the EV-mode gearshift schedule correspond to gearshifts performed when the intervention of the ICE is required.
- The most efficient operating region of the ICE map is covered first.

Hence, the idea behind the proposed approach is that if it can be understood how the optimal solution selects the gear in EV-mode, when the ICE is needed, gear selection is simply a matter of minimizing the equivalent fuel consumption as defined in the context of the ECMS. As for the DP formulation, one fundamental aspect that differentiates the real-time implementable EMSs developed here from those published in previous works, is the modeling of the energy consumption during gearshifts and ICE starts.

In the causal strategies studied, a discrete adaptation scheme based on feedback from SOC is employed. By analyzing the optimal solution, it was concluded that,

depending on the driving cycle characteristics and final SOC target, the linear SOC reference that is more in agreement with the DP results could be defined in either the time or the distance domain. This clearly illustrates a limitation of the mentioned adaptation schemes: a technique to generate reference profiles for the SOC which are representative of the optimal solution regardless of the driving schedule to be followed is not available.

Nevertheless, simulation results show that, in terms of the total equivalent fuel consumption, the RB + A-ECMS approach does not only yield results that are close to the optimal solution but also outperforms those of the A-ECMS. The mentioned EMS also provides better results than the A-ECMS in terms of the actual fuel consumption. In addition, both causal strategies proved to be robust with respect to the SOC tracking parameters. Hence, the same parameters can be used for different driving schedules.

When analyzing the behavior of the solutions found, it is observed that, in general, the implementation of the RB + A-ECMS approach tends to result in more gearshifts than those performed in the optimal solution while the A-ECMS does the opposite. Furthermore, thanks to the ability of the designed rule-based approach to recognize relevant speed and power trends in the driving cycle, the gear number selected before high power braking events is similar to the optimal one in most cases. Note that choosing the appropriate gear allows to maximize the energy regenerated with the EM.

On the other hand, with the real-time implementable EMSs, a higher number of ICE starts events are generally undertaken when compared to the quantity seen in the DP solution. The fuel cut-off functionality is not included in these approaches which contributes to the higher number of ICE starts. Moreover, with no restrictions in place for changes on the ICE state, a very intermittent use of this component is seen. Instead, when fuel penalties related to the ICE state are introduced, the results improve significantly.

Chapter 7

7. Conclusions

The increasing demand seen in the last few years for improved vehicle dynamic performance and reduced fuel consumption has raised the interest in the automotive industry to explore new forms of powertrain electrification. In the field of transmission systems, DCTs have been found to be good candidates to be integrated into HEV powertrain architectures since they are able to combine efficiency levels similar to those seen for MTs and almost seamless gearshift operation with a high software tunability. In this dissertation, among the many aspects that could be explored regarding the electrification of DCTs, attention is focused on developing control strategies for improving vehicle dynamic performance during gearshift maneuvers and the energy management of HEVs.

For the development of the mentioned control strategies, appropriate powertrain models are necessary. In chapter 2, the modeling work undertaken is addressed in detail.

In order to assess gearshift quality and its impact on drivability, a nonlinear dynamic model of a series-parallel PHEV is developed. Two variants of this powertrain are studied, the main difference between them is in the type of transmission employed: AMT or DCT. In both vehicles, an EM is connected to the driveshaft through a mechanical coupler enabling full or partial compensation of the torque gap during gearshifts. Thanks to the model features, the first torsional mode of the driveline is correctly estimated and an assessment of the vehicle drivability during gearshift maneuvers can be conducted.

On the other hand, a backward quasi-static model of a parallel PHEV is developed for energy management purposes. The model is designed to properly account for the energy needed to perform gearshift and ICE start operations. This allows to develop control strategies in which these maneuvers are undertaken when it is convenient in terms of the overall energy consumption with the extra benefit of having an EMS in which transient events are not frequently requested, thus improving also the vehicle drivability. It is worth mentioning that, to the best of the author's knowledge, the inclusion of a model that uses physical considerations to estimate the energy losses when changing gears in DCTs into a DP formulation or a causal EMS, like those developed in chapters 5 and 6 respectively, has not been undertaken in previous studies.

In chapter 3, the mentioned gearshift control strategies for the two variants of the series-parallel PHEV described in chapter 2 are developed. Such algorithms are very simple to implement and tune since they are based on the use of simple PI feedback controllers. Thus, transmission engineers without significant knowledge of advanced control theory will be able to use the developed tools.

The results obtained for both powertrains are promising in terms of vehicle dynamic performance. One fundamental implication of the previous remark is that the H-AMT studied has been proved capable of almost eliminating the torque gap during gearshifts while keeping the mechanical complexity of the system low with respect to its DCT counterpart. In the simulations undertaken, the main differences in the performance of both architectures are seen during upshift maneuvers where the energy requested from the EM is larger for the H-AMT. Hence, during this type of gearshifts, the H-DCT is shown to be more energy efficient. Instead, for the downshifts, in order to minimize clutch slip losses for the H-DCT, the EM works as a torque fill device, similar to what it does for the H-AMT, making the energy consumption indicators for both powertrains comparable.

In chapter 4, some of the most relevant EMSs for HEVs are reviewed, setting the theoretical basis for understanding the work presented in chapters 5 and 6.

DP is used in chapter 5 to find the global optimal solution to the energy management problem for the PHEV of interest. The general problem formulation is given including a description of how the modeling of the gearshift and ICE start losses is integrated into it.

In the DP charge-sustaining results, the optimal solution shows that keeping the SOC within a narrow range around the required final value is the best way to proceed. Another interesting observation to be made is that torque assist with the EM is used in just a few occasions. The vehicle operates mostly in ICE-only mode or EV-mode. Thus, parallel hybrid mode is mainly seen in the form of the ICE being used to recharge the battery. Instead, in the charge-depleting simulations, it is seen that the vehicle follows the WLTC almost entirely in EV-mode. Hence, these results can be used in the next chapter to extract a set of rules for the gear selection in EV-mode.

Furthermore, the effects of integrating into the DP formulation the loss models developed for gearshift and ICE start events are studied. It is noted that when both sources of losses are considered, there is no gear hunting behavior in the results nor chattering in the ICE state. In addition, the analysis made shows that, as expected, the number of gearshifts increases significantly when the losses associated with them are neglected. Another interesting conclusion is that neglecting the ICE start losses could lead to an unrealistic use of the ICE inertia to overcome the gearshift losses.

After performing several simulations using DP, it was observed that, in general, when increasing the final SOC target:

- The deviations from the EV-mode gearshift schedule correspond to gearshifts performed when the intervention of the ICE is required.
- The most efficient operating region of the ICE map is covered first.

Hence, the idea behind the real-time implementable EMS proposed in chapter 6 is that if it can be understood how the optimal solution selects the gear in EV-mode, when the ICE is needed, gear selection is simply a matter of minimizing the equivalent fuel consumption as defined in the context of the ECMS. In order to design such EMS:

- DP results are used to derive a set of rules aiming at reproducing the optimal gearshift schedule in EV-mode.
- A-ECMS is used to decide the powertrain operating mode (through the selection of the TSF) and the current gear if power from the ICE is needed.

Simulation results show that, in terms of the total equivalent fuel consumption, the RB + A-ECMS approach does not only yield results that are close to the optimal solution but also outperforms those of the A-ECMS. The mentioned EMS also provides better results than the A-ECMS in terms of the actual fuel consumption. In addition, both causal strategies proved to be robust with respect to the SOC tracking parameters. Hence, the same parameters can be used for different driving schedules.

When analyzing the behavior of the solutions found, it is observed that, thanks to the ability of the designed rule-based approach to recognize relevant speed and power trends in the driving cycle, the gear number selected before high power braking events is similar to the optimal one in most cases. Note that choosing the appropriate gear allows to maximize the energy regenerated with the EM. Moreover, it is seen that the introduction of the fuel penalties related to the ICE state allow to avoid having an intermittent use of this component.

In addition, a study of the optimal solution revealed that, depending on the driving cycle characteristics and final SOC target, the linear SOC profile which is more in agreement with the DP results could be expressed in either the time or the distance domain. A technique to generate reference profiles for the SOC which are representative of the optimal solution regardless of the driving schedule to be followed is not yet available.

The electrification of powertrains equipped with DCTs offers the possibility of improving both the vehicle dynamic performance and the energy consumption. The control algorithms presented in this dissertation are designed with the objective of fully realizing the potential of such systems. Further work should be focused on:

- Experimental validation of the developed models.
- Implementation of the proposed controllers in vehicle.
- Exploring the interaction of the proposed gearshift control algorithms with EMSs.
- Offline generation of the map needed to initialize the equivalence factor used by the causal EMSs.
- Adaptation of the DP formulation and the RB+A-ECMS approach to other HEV architectures.

References

[1] S. Onori, L. Serrao, and G. Rizzoni, *Hybrid Electric Vehicles: Energy Management Strategies*, 1st ed. Springer-Verlag London, 2016.

[2] M. Awadallah, P. Tawadros, P. Walker, and N. Zhang, "Dynamic modelling and simulation of a manual transmission based mild hybrid vehicle," *Mech. Mach. Theory*, vol. 112, pp. 218–239, 2017.

[3] E. Galvagno, M. Velardocchia, and A. Vigliani, "Dynamic and kinematic model of a dual clutch transmission," *Mech. Mach. Theory*, vol. 46, no. 6, pp. 794–805, 2011.

[4] E. Galvagno, G. R. Guercioni, and A. Vigliani, "Sensitivity Analysis of the Design Parameters of a Dual-Clutch Transmission Focused on NVH Performance," *SAE Tech. Pap. 2016-01-1127*, 2016.

[5] J. Kim *et al.*, "Simulation of the shift force for a manual transmission," *Proc. Inst. Mech. Eng. Part D J. Automob. Eng.*, vol. 217, no. 7, pp. 573–581, 2003.

[6] B. Gao, Y. Lei, A. Ge, H. Chen, and K. Sanada, "Observer-based clutch disengagement control during gear shift process of automated manual transmission," *Veh. Syst. Dyn.*, vol. 49, no. 5, pp. 685–701, 2011.

[7] G. R. Guercioni, A. Vigliani, E. Galvagno, and S. Midlam-Mohler, "Gearshift control for hybrid powertrains with AMTs," in *2017 International Conference of Electrical and Electronic Technologies for Automotive*, 2017, pp. 1–9.

[8] V. Ranogajec and J. Deur, "Bond graph analysis and optimal control of the hybrid dual clutch transmission shift process," *Proc. Inst. Mech. Eng. Part K J. Multi-body Dyn.*, vol. 231, no. 3, pp. 480–492, 2017.

[9] K. van Berkel, T. Hofman, A. Serrarens, and M. Steinbuch, "Fast and smooth clutch engagement control for dual-clutch transmissions," *Control Eng. Pract.*, vol. 22, pp. 57–68, 2014.

[10] M. Goetz, M. C. Levesley, and D. A. Crolla, "Dynamics and control of gearshifts on twin-clutch transmissions," *Proc. Inst. Mech. Eng. Part D J. Automob. Eng.*, vol. 219, no. 8, pp. 951–963, 2005.

[11] Y. Liu, D. Qin, H. Jiang, and Y. Zhang, “Shift control strategy and experimental validation for dry dual clutch transmissions,” *Mech. Mach. Theory*, vol. 75, pp. 41–53, 2014.

[12] M. Kulkarni, T. Shim, and Y. Zhang, “Shift dynamics and control of dual-clutch transmissions,” *Mech. Mach. Theory*, vol. 42, no. 2, pp. 168–182, 2007.

[13] J. Wu, P. D. Walker, J. Ruan, and N. Zhang, “Target torque estimation for gearshift in dual clutch transmission with uncertain parameters,” *Appl. Math. Model.*, vol. 51, pp. 1–20, 2017.

[14] G. Li and D. Görges, “Optimal control of the gear shifting process for shift smoothness in dual-clutch transmissions,” *Mech. Syst. Signal Process.*, vol. 103, pp. 23–38, 2018.

[15] F. Amisano, E. Galvagno, M. Velardocchia, and A. Vigliani, “Automated manual transmission with a torque gap filler Part 2: Control and experimental validation,” *Proc. Inst. Mech. Eng. Part D J. Automob. Eng.*, vol. 228, no. 14, pp. 1700–1717, 2014.

[16] L. Glielmo, L. Iannelli, V. Vacca, and F. Vasca, “Gearshift Control for Automated Manual Transmissions,” *IEEE/ASME Trans. Mechatronics*, vol. 11, no. 1, pp. 17–26, 2006.

[17] X.-Y. Song, Z.-X. Sun, X.-J. Yang, and G.-M. Zhu, “Modelling, control, and hardware-in-the-loop simulation of an automated manual transmission,” *Proc. Inst. Mech. Eng. Part D J. Automob. Eng.*, vol. 224, no. 2, pp. 143–160, 2010.

[18] V. Nezhadali and L. Eriksson, “Optimal control of engine controlled gearshift for a diesel-electric powertrain with backlash,” *IFAC-PapersOnLine*, vol. 49, no. 11, pp. 762–768, 2016.

[19] Z. Lei, D. Sun, Y. Liu, D. Qin, and Y. Zhang, “Analysis and coordinated control of mode transition and shifting for a full hybrid electric vehicle based on dual clutch transmissions,” *Mech. Mach. Theory*, vol. 114, pp. 125–140, 2017.

[20] A. M. Gavgani, A. Sorniotti, J. Doherty, and C. Cavallino, “Optimal gearshift control for a novel hybrid electric drivetrain,” *Mech. Mach. Theory*, vol. 105, pp. 352–368, 2016.

[21] A. Mehdizadeh Gavgani, T. Bingham, A. Sorniotti, J. Doherty, C. Cavallino, and M. Fracchia, “A Parallel Hybrid Electric Drivetrain Layout with Torque-

Fill Capability," *SAE Int. J. Passeng. Cars - Mech. Syst.*, vol. 8, no. 2, pp. 767–778, 2015.

[22] F. Garofalo, L. Glielmo, L. Iannelli, and F. Vasca, "Smooth engagement for automotive dry clutch," in *Proceedings of the 40th IEEE Conference on Decision and Control*, 2001, vol. 1, pp. 529–534.

[23] Z.-G. Zhao, H.-J. Chen, Y.-Y. Yang, and L. He, "Torque coordinating robust control of shifting process for dry dual clutch transmission equipped in a hybrid car," *Veh. Syst. Dyn. Int. J. Veh. Mech. Mobil.*, vol. 53, no. 9, pp. 1269–1295, 2015.

[24] J. Deur, J. Asgari, and D. Hrovat, "Modeling and Analysis of Automatic Transmission Engagement Dynamics-Nonlinear Case Including Validation," *J. Dyn. Syst. Meas. Control*, vol. 128, no. 2, pp. 251–262, 2005.

[25] B. Tepes, J. Kasac, and J. Deur, "Optimal control of automated transmission engagement process," in *2012 IEEE International Conference on Control Applications*, 2012, pp. 329–335.

[26] L. Guzzella and A. Sciarretta, *Vehicle Propulsion Systems: Introduction to Modeling and Optimization*, 3rd ed. Springer-Verlag Berlin Heidelberg, 2013.

[27] A. Sciarretta, M. Back, and L. Guzzella, "Optimal control of parallel hybrid electric vehicles," *IEEE Trans. Control Syst. Technol.*, vol. 12, no. 3, pp. 352–363, 2004.

[28] A. Chasse and A. Sciarretta, "Supervisory control of hybrid powertrains: An experimental benchmark of offline optimization and online energy management," *Control Eng. Pract.*, vol. 19, no. 11, pp. 1253–1265, 2011.

[29] C. Musardo, G. Rizzoni, Y. Guezennec, and B. Staccia, "A-ECMS : An Adaptive Algorithm for Hybrid Electric Vehicle Energy Management," *Eur. J. Control*, vol. 11, no. 4–5, pp. 509–524, 2005.

[30] S. Delprat, J. Lauber, T. M. Guerra, and J. Rimaux, "Control of a parallel hybrid powertrain: optimal control," *IEEE Trans. Veh. Technol.*, vol. 53, no. 3, pp. 872–881, 2004.

[31] C.-C. Lin, H. Peng, J. W. Grizzle, and J.-M. Kang, "Power management strategy for a parallel hybrid electric truck," *IEEE Trans. Control Syst. Technol.*, vol. 11, no. 6, pp. 839–849, 2003.

[32] L. Tang and G. Rizzoni, "Energy management strategy including battery life optimization for a HEV with a CVT," in *2016 IEEE Transportation*

Electrification Conference and Expo, Asia-Pacific (ITEC Asia-Pacific), 2016, pp. 549–554.

[33] L. Tang, G. Rizzoni, and S. Onori, "Energy Management Strategy for HEVs Including Battery Life Optimization," *IEEE Trans. Transp. Electrif.*, vol. 1, no. 3, pp. 211–222, 2015.

[34] L. Tang, "Optimal energy management strategy for hybrid electric vehicles with consideration of battery life," Ohio State University, 2017.

[35] V. D. Ngo, J. A. C. Navarrete, T. Hofman, M. Steinbuch, and A. Serrarens, "Optimal gear shift strategies for fuel economy and driveability," *Proc. Inst. Mech. Eng. Part D J. Automob. Eng.*, vol. 227, no. 10, pp. 1398–1413, 2013.

[36] K. M. Bovee, "Optimal Control of Electrified Powertrains with the Use of Drive Quality Criteria," Ohio State University, 2015.

[37] E. Ostertag, *Mono- and Multivariable Control and Estimation: Linear, Quadratic and LMI Methods*, 1st ed. Springer-Verlag Berlin Heidelberg, 2011.

[38] O. P. Sharma, S. Onori, and Y. Guezennec, "Analysis of Pontryagin's Minimum Principle-Based Energy Management Strategy for PHEV Applications," in *Volume 1: Adaptive Control; Advanced Vehicle Propulsion Systems; Aerospace Systems; Autonomous Systems; Battery Modeling; Biochemical Systems; Control Over Networks; Control Systems Design; Cooperativ*, 2012, pp. 145–150.

[39] D. E. Kirk, *Optimal Control Theory - An Introduction*. Dover Publications, 1998.

[40] F. R. Salmasi, "Control Strategies for Hybrid Electric Vehicles: Evolution, Classification, Comparison, and Future Trends," *IEEE Trans. Veh. Technol.*, vol. 56, no. 5, pp. 2393–2404, 2007.

[41] H. Waschl, I. Kolmanovsky, M. Steinbuch, and L. del Re, *Optimization and Optimal Control in Automotive Systems*, 1st ed., vol. 455. Springer International Publishing, 2014.

[42] N. Kim, S. Cha, and H. Peng, "Optimal Control of Hybrid Electric Vehicles Based on Pontryagin's Minimum Principle," *IEEE Trans. Control Syst. Technol.*, vol. 19, no. 5, pp. 1279–1287, 2011.

[43] N. Kim and A. Rousseau, "Sufficient conditions of optimal control based on Pontryagin's minimum principle for use in hybrid electric vehicles," *Proc. Inst. Mech. Eng. Part D J. Automob. Eng.*, vol. 226, no. 9, pp. 1160–1170,

2012.

[44] S. P. Boyd and L. Vendenberghe, *Convex Optimization*. New York, NY: Cambridge University Press, 2004.

[45] P. Elbert, T. Nüesch, A. Ritter, N. Murgovski, and L. Guzzella, "Engine On/Off Control for the Energy Management of a Serial Hybrid Electric Bus via Convex Optimization," *IEEE Trans. Veh. Technol.*, vol. 63, no. 8, pp. 3549–3559, 2014.

[46] N. Murgovski, L. Johannesson, J. Hellgren, B. Egardt, and J. Sjöberg, "Convex Optimization of Charging Infrastructure Design and Component Sizing of a Plug-in Series HEV Powertrain," *IFAC Proc. Vol.*, vol. 44, no. 1, pp. 13052–13057, 2011.

[47] G. Paganelli, "Conception et commande d'une chaîne de traction pour véhicule hybride parallèle thermique et électrique," Université de Valenciennes, 1999.

[48] R. E. Bellman and S. E. Dreyfus, *Applied Dynamic Programming*. Princeton University Press, 2015.

[49] R. E. Bellman and R. E. Kalaba, *Dynamic Programming and Modern Control Theory*, 1st ed. Academic Press, 1966.

[50] R. E. Bellman, *Dynamic Programming*, 1st ed. Princeton, NJ: Princeton University Press, 1957.

[51] D. Bertsekas, *Dynamic Programming and Optimal Control*. Belmont, MA: Athena Scientific, 1995.

[52] L. Pérez, G. Bossio, D. Moitre, and G. García, "Optimization of power management in an hybrid electric vehicle using dynamic programming," *Math. Comput. Simul.*, vol. 73, no. 1–4, pp. 244–254, 2006.

[53] L. Serrao, S. Onori, and G. Rizzoni, "A Comparative Analysis of Energy Management Strategies for Hybrid Electric Vehicles," *ASME J. Dyn. Syst. Meas. Control*, vol. 133, no. 3, p. 31012, 2011.

[54] D. Bianchi *et al.*, "Layered control strategies for hybrid electric vehicles based on optimal control," *Int. J. Electr. Hybrid Veh.*, vol. 3, no. 2, pp. 191–217, 2011.

[55] C.-C. Lin, Z. Filipi, L. Louca, H. Peng, D. Assanis, and J. Stein, "Modelling and control of a medium-duty hybrid electric truck," *Int. J. Heavy Veh. Syst.*, vol. 11, no. 3–4, pp. 349–371, 2004.

[56] D. Kum, H. Peng, and N. K. Bucknor, “Optimal Control of Plug-in HEVs for Fuel Economy Under Various Travel Distances,” *IFAC Proc. Vol.*, vol. 43, no. 7, pp. 258–263, 2010.

[57] D. Bianchi *et al.*, “A rule-based strategy for a series/parallel hybrid electric vehicle: an approach based on dynamic programming,” in *ASME 2010 Dynamic Systems and Control Conference*, 2010, pp. 507–514.

[58] L. Serrao, S. Onori, and G. Rizzoni, “ECMS as a realization of Pontryagin’s minimum principle for HEV control,” in *2009 American Control Conference*, 2009, pp. 3964–3969.

[59] B. Gu and G. Rizzoni, “An Adaptive Algorithm for Hybrid Electric Vehicle Energy Management Based on Driving Pattern Recognition,” in *ASME International Mechanical Engineering Congress and Exposition, Dynamic Systems and Control, Parts A and B*, 2006, pp. 249–258.

[60] S. Onori and L. Tribioli, “Adaptive Pontryagin’s Minimum Principle supervisory controller design for the plug-in hybrid GM Chevrolet Volt,” *Appl. Energy*, vol. 147, pp. 224–234, 2015.

[61] J. T. B. A. Kessels, M. W. T. Koot, P. P. J. van den Bosch, and D. B. Kok, “Online Energy Management for Hybrid Electric Vehicles,” *IEEE Trans. Veh. Technol.*, vol. 57, no. 6, pp. 3428–3440, 2008.

[62] D. F. Opila, X. Wang, R. McGee, R. B. Gillespie, J. A. Cook, and J. W. Grizzle, “An Energy Management Controller to Optimally Trade Off Fuel Economy and Drivability for Hybrid Vehicles,” *IEEE Trans. Control Syst. Technol.*, vol. 20, no. 6, pp. 1490–1505, 2012.

[63] M. Khodabakhshian, L. Feng, and J. Wikander, “Optimization of Gear Shifting and Torque Split for Improved Fuel Efficiency and Drivability of HEVs,” *SAE Tech. Pap. 2013-01-1461*, 2013.

[64] D. F. Opila, Xiaoyong Wang, R. McGee, J. A. Cook, and J. W. Grizzle, “Performance comparison of hybrid vehicle energy management controllers on real-world drive cycle data,” in *2009 American Control Conference*, 2009, pp. 4618–4625.

[65] D. F. Opila, X. Wang, R. McGee, and J. W. Grizzle, “Real-Time Implementation and Hardware Testing of a Hybrid Vehicle Energy Management Controller Based on Stochastic Dynamic Programming,” *J. Dyn. Syst. Meas. Control*, vol. 135, no. 2, pp. 21002-21002–11, 2012.

[66] V. Ngo, T. Hofman, M. Steinbuch, and A. Serrarens, “Effect of gear shift

and engine start losses on control strategies for hybrid electric vehicles," in *26th Electric Vehicle Symposium 2012*, 2012, vol. 5, pp. 125–136.

[67] E. Galvagno, D. Morina, A. Sorniotti, and M. Velardocchia, "Drivability analysis of through-the-road-parallel hybrid vehicles," *Meccanica*, vol. 48, no. 2, pp. 351–366, 2013.

[68] E. Pennestrì, V. Rossi, P. Salvini, and P. P. Valentini, "Review and comparison of dry friction force models," *Nonlinear Dyn.*, vol. 83, no. 4, pp. 1785–1801, 2016.

[69] T. Piatkowski, "Dahl and LuGre dynamic friction models - The analysis of selected properties," *Mech. Mach. Theory*, vol. 73, pp. 91–100, 2014.

[70] Hans B. Pacejka, *Tyre and Vehicle Dynamics*, 2nd ed. Butterworth-Heinemann, 2006.

[71] L. Serrao, "A comparative analysis of energy management strategies for hybrid electric vehicles," Ohio State University, 2009.

[72] A. Chasse, A. Sciarretta, and J. Chauvin, "Online optimal control of a parallel hybrid with costate adaptation rule," *IFAC Proc. Vol.*, vol. 43, no. 7, pp. 99–104, 2010.

[73] S. Onori, L. Serrao, and G. Rizzoni, "Adaptive Equivalent Consumption Minimization Strategy for Hybrid Electric Vehicles," in *ASME 2010 Dynamic Systems and Control Conference*, 2010, pp. 499–505.

[74] G. Rizzoni, L. Guzzella, and B. M. Baumann, "Unified modeling of hybrid electric vehicle drivetrains," *IEEE/ASME Trans. Mechatronics*, vol. 4, no. 3, pp. 246–257, 1999.

[75] L. Guzzella and A. Amstutz, "CAE tools for quasi-static modeling and optimization of hybrid powertrains," *IEEE Trans. Veh. Technol.*, vol. 48, no. 6, pp. 1762–1769, 1999.

[76] L. Guzzella, A. Amstutz, and F. Grob, "Optimal Operation Strategies for Hybrid Power-Trains," *IFAC Proc. Vol.*, vol. 31, no. 1, pp. 93–98, 1998.

[77] V. Ngo, T. Hofman, M. Steinbuch, and A. Serrarens, "Optimal Control of the Gearshift Command for Hybrid Electric Vehicles," *IEEE Trans. Veh. Technol.*, vol. 61, no. 8, pp. 3531–3543, 2012.

[78] M. Guiggiani, *The science of vehicle dynamics: handling, braking, and ride of road and race cars*, 1st ed. Springer Netherlands, 2014.

[79] C. D. Rahn and C.-Y. Wang, *Battery Systems Engineering*, 1st ed. John Wiley & Sons, 2013.

[80] G. L. Plett, "Sigma-point Kalman filtering for battery management systems of LiPB-based HEV battery packs: Part 2: Simultaneous state and parameter estimation," *J. Power Sources*, vol. 161, no. 2, pp. 1369–1384, 2006.

[81] L. Serrao, C. J. Hubert, and G. Rizzoni, "Dynamic Modeling of Heavy-Duty Hybrid Electric Vehicles," in *ASME International Mechanical Engineering Congress and Exposition, Volume 16: Transportation Systems*, 2007, pp. 121–128.

[82] P. Sendur, J. L. Stein, H. Peng, and L. S. Louca, "An Algorithm for the Selection of Physical System Model Order Based on Desired State Accuracy and Computational Efficiency," in *ASME International Mechanical Engineering Congress and Exposition, Dynamic Systems and Control*, 2003, vol. 1–2, pp. 891–902.

[83] Zongxuan Sun and K. Hebbale, "Challenges and opportunities in automotive transmission control," in *Proceedings of the 2005, American Control Conference, 2005.*, 2005, pp. 3284–3289.

[84] R. C. Baraszu and S. R. Cikanek, "Torque fill-in for an automated shift manual transmission in a parallel hybrid electric vehicle," in *Proceedings of the 2002 American Control Conference*, 2002, pp. 1431–1436.

[85] B. wook Jeon and S.-H. Kim, "Measurement and Modeling of Perceived Gear Shift Quality for Automatic Transmission Vehicles," *SAE Int. J. Passeng. Cars - Mech. Syst.*, vol. 7, no. 1, pp. 423–433, 2014.

[86] T. D'Anna, K. Govindswamy, F. Wolter, and P. Janssen, "Aspects of Shift Quality With Emphasis on Powertrain Integration and Vehicle Sensitivity," *SAE Tech. Pap. 2005-01-2303*, 2005.

[87] K. Koprubasi, "Modeling and Control of a Hybrid-Electric Vehicle for Drivability and Fuel Economy Improvements," The Ohio State University, 2008.

[88] J. M. W. Brownjohn and X. Zheng, "Discussion of human resonant frequency," in *International Conference on Experimental Mechanics*, 2001, vol. 4317, pp. 469–474.

[89] K. Koprubasi, G. Rizzoni, E. Galvagno, and M. Velardocchia, "Development and experimental validation of a low-frequency dynamic model for a Hybrid Electric Vehicle," *Int. J. Powertrains*, vol. 1, no. 3, pp.

304–333, 2012.

[90] F. U. Syed, M. L. Kuang, J. Czubay, and H. Ying, “Derivation and Experimental Validation of a Power-Split Hybrid Electric Vehicle Model,” *IEEE Trans. Veh. Technol.*, vol. 55, no. 6, pp. 1731–1747, 2006.

[91] *Proceedings of the FISITA 2012 World Automotive Congress : Volume 6: Vehicle Electronics.*, 1st ed. Springer-Verlag Berlin Heidelberg, 2013.

[92] Q. Huang and H. Wang, “Fundamental Study of Jerk: Evaluation of Shift Quality and Ride Comfort,” *SAE Tech. Pap. 2004-01-2065*, 2004.

[93] Suryanto, “Analysis and Improvement of the Drivability of a Four-Wheel-Drive Hybrid Electric Vehicle,” University of Surrey, 2013.

[94] W. Enang and C. Bannister, “Robust proportional ECMS control of a parallel hybrid electric vehicle,” *Proc. Inst. Mech. Eng. Part D J. Automob. Eng.*, vol. 231, no. 1, pp. 99–119, 2016.

[95] H. P. Geering, *Optimal Control with Engineering Applications*, 1st ed. Springer-Verlag Berlin Heidelberg, 2007.

[96] S. Uebel, N. Murgovski, C. Tempelhahn, and B. Bernard, “Optimal Energy Management and Velocity Control of Hybrid Electric Vehicles,” *IEEE Trans. Veh. Technol.*, vol. 67, pp. 327–337, 2017.

[97] D. Ambühl, O. Sundström, A. Sciarretta, and L. Guzzella, “Explicit optimal control policy and its practical application for hybrid electric powertrains,” *Control Eng. Pract.*, vol. 18, no. 12, pp. 1429–1439, 2010.

[98] D. Sinoquet, G. Rousseau, and Y. Milhau, “Design optimization and optimal control for hybrid vehicles,” *Optim Eng*, vol. 12, no. 1–2, pp. 199–213, 2011.

[99] E. Vinot, R. Trigui, Y. Cheng, C. Espanet, A. Bouscayrol, and V. Reinbold, “Improvement of an EVT-Based HEV Using Dynamic Programming,” *IEEE Trans. Veh. Technol.*, vol. 63, no. 1, pp. 40–50, 2014.

[100] T. Hofman, M. Steinbuch, R. van Druten, and A. Serrarens, “A Rule-based energy management strategies for hybrid vehicles,” *Int. J. Electr. Hybrid Veh.*, vol. 1, no. 1, pp. 71–94, 2007.

[101] R. Biasini, S. Onori, and G. Rizzoni, “A near-optimal rule-based energy management strategy for medium duty hybrid truck,” *Int. J. Powertrains*, vol. 2, no. 2–3, pp. 232–261, 2013.

[102] G. Rousseau, D. Sinoquet, and P. Rouchon, “Constrained Optimization of

Energy Management for a Mild-Hybrid Vehicle," *Oil Gas Sci. Technol.*, vol. 62, no. 4, pp. 623–634, 2007.

[103] F. L. Lewis, D. L. Vrabie, and V. L. Syrmos, *Optimal Control*. John Wiley & Sons, Inc, 2012.

[104] L. S. Pontryagin, V. G. Boltyanskii, R. V. Gamkrelidze, and E. F. Mishchenko, *The Mathematical Theory of Optimal Processes*. New York, NY: Interscience Publishers, 1962.

[105] A. Bryson and Y. Ho, *Applied Optimal Control: Optimization, Estimation, and Control (revised printing)*. New York, NY: Taylor & Francis Group, 1975.

[106] R. Biasini, S. Onori, and G. Rizzoni, "A rule-based energy management strategy for hybrid medium duty truck," *Int. J. Powertrains- Spec. issue Des. Model. Optim. Control Electr. Propuls. Syst.*, vol. 2, no. 2/3, pp. 232–261, 2013.

[107] A. Sciarretta and L. Guzzella, "Control of hybrid electric vehicles," *IEEE Control Syst.*, vol. 27, no. 2, pp. 60–70, 2007.

[108] N. Kim, A. Rousseau, and D. Lee, "A jump condition of PMP-based control for PHEVs," *J. Power Sources*, vol. 196, no. 23, pp. 10380–10386, 2011.

[109] L. Serrao, S. Onori, A. Sciarretta, Y. Guezennec, and G. Rizzoni, "Optimal energy management of hybrid electric vehicles including battery aging," in *American Control Conference (ACC), 2011*, 2011, pp. 2125–2130.

[110] N. Kim, S. Cha, and H. Peng, "Optimal equivalent fuel consumption for hybrid electric vehicles," *IEEE Trans. Control Syst. Technol.*, vol. 20, no. 3, pp. 817–825, 2012.

[111] Z. Yuan, L. Teng, S. Fengchun, and H. Peng, "Comparative Study of Dynamic Programming and Pontryagin's Minimum Principle on Energy Management for a Parallel Hybrid Electric Vehicle," *Energies*, vol. 6, no. 4, pp. 2305–2318, 2013.

[112] J. Jiang and C. Zhang, *Fundamentals and Applications of Lithium-Ion Batteries in Electric Drive Vehicles*. John Wiley & Sons, Inc, 2015.

[113] G. Paganelli, G. Ercole, A. Brahma, Y. Guezennec, and G. Rizzoni, "General supervisory control policy for the energy optimization of charge-sustaining hybrid electric vehicles," *JSAE Rev.*, vol. 22, no. 4, pp. 511–518, Oct. 2001.

[114] A. Sciarretta, L. Guzzella, and M. Back, "A Real-Time Optimal Control

Strategy for Parallel Hybrid Vehicles with On-Board Estimation of the Control Parameters," *IFAC Proc. Vol.*, vol. 37, no. 22, pp. 489–494, 2004.

[115] G. Paganelli, S. Delprat, T. M. Guerra, J. Rimaux, and J. J. Santin, "Equivalent consumption minimization strategy for parallel hybrid powertrains," in *Vehicular Technology Conference. IEEE 55th Vehicular Technology Conference. VTC Spring 2002 (Cat. No.02CH37367)*, 2002, vol. 4, pp. 2076–2081.

[116] G. Paganelli, G. Ercole, A. Brahma, Y. Guezennec, and G. Rizzoni, "A General Formulation for the Instantaneous Control of the Power Split in Charge-Sustaining Hybrid Electric Vehicles," in *Proceedings of 5th International Symposium on Advanced Vehicle Control*, 2000, pp. 73–80.

[117] G. Paganelli, T. M. Guerra, S. Delprat, J.-J. Santin, M. Delhom, and E. Combes, "Simulation and assessment of power control strategies for a parallel hybrid car," *Proc. Inst. Mech. Eng. Part D J. Automob. Eng.*, vol. 214, no. 7, pp. 705–717, 2000.

[118] L. Tribioli and S. Onori, "Analysis of energy management strategies in plug-in hybrid electric vehicles: Application to the GM Chevrolet Volt," in *American Control Conference (ACC), 2013*, 2013, pp. 17–19.

[119] O. P. Sharma, S. Onori, and Y. Guezennec, "Analysis of Pontryagins Minimum Principlebased energy management strategy for PHEV applications," in *5th annual dynamic systems and control conference and 11th motion and vibration conference*, 2012.

[120] D. Ambuhl and L. Guzzella, "Predictive Reference Signal Generator for Hybrid Electric Vehicles," *IEEE Trans. Veh. Technol.*, vol. 58, no. 9, pp. 4730–4740, 2009.

[121] L. Fu, U. Ozguner, P. Tulpule, and V. Marano, "Real-time energy management and sensitivity study for hybrid electric vehicles," in *Proceedings of the 2011 American Control Conference*, 2011, pp. 2113–2118.

[122] S. Jeon, S. Jo, Y. Park, and J. Lee, "Multi-Mode Driving Control of a Parallel Hybrid Electric Vehicle Using Driving Pattern Recognition," *J. Dyn. Syst. Meas. Control*, vol. 124, no. 1, pp. 141–149, 2000.

[123] P. Tulpule, V. Marano, and G. Rizzoni, "Energy management for plug-in hybrid electric vehicles using equivalent consumption minimisation strategy," *Int. J. Electr. Hybrid Veh.*, vol. 2, no. 4, pp. 329–350, 2010.

[124] P. Khayyer, J. Wollaeger, S. Onori, V. Marano, U. Ozguner, and G. Rizzoni, "Analysis of impact factors for plug-in hybrid electric vehicles energy management," in *2012 15th International IEEE Conference on Intelligent Transportation Systems*, 2012, pp. 1061–1066.

[125] F. Lacandia, L. Tribioli, S. Onori, and G. Rizzoni, "Adaptive Energy Management Strategy Calibration in PHEVs Based on a Sensitivity Study," *SAE Int. J. Altern. Powertrains*, vol. 2, no. 3, pp. 443–455, 2013.

[126] E. J. Schacht, B. Bezaire, B. Cooley, K. Bayar, and J. W. Kruckenberg, "Addressing Drivability in an Extended Range Electric Vehicle Running an Equivalent Consumption Minimization Strategy (ECMS)," *SAE Tech. Pap. 2011-01-0911*, 2011.

[127] O. Sundström and L. Guzzella, "A generic dynamic programming Matlab function," in *2009 IEEE International Conference on Control Applications*, 2009, pp. 1625–1630.

[128] O. Sundström, D. Ambühl, and L. Guzzella, "On implementation of dynamic programming for optimal control problems with final state constraints," *Oil Gas Sci. Technol.*, vol. 65, no. 1, pp. 91–102, 2010.

[129] O. Sundström and L. Guzzella, "DPM function." [Online]. Available: http://www.idsc.ethz.ch/research-guzzella-onder/downloads.html. [Accessed: 12-Feb-2018].

[130] M. Tutuianu *et al.*, "Development of the World-wide harmonized Light duty Test Cycle (WLTC) and a possible pathway for its introduction in the European legislation," *Transp. Res. Part D Transp. Environ.*, vol. 40, pp. 61–75, 2015.

[131] "Worldwide Harmonized Light Vehicles Test Cycle (WLTC)." [Online]. Available: https://www.dieselnet.com/standards/cycles/wltp.php. [Accessed: 23-Jan-2018].

[132] R. Joumard, M. André, R. Vidon, P. Tassel, and C. Pruvost, "Influence of driving cycles on unit emissions from passenger cars," *Atmos. Environ.*, vol. 34, no. 27, pp. 4621–4628, 2000.

[133] "From NEDC to WLTP: what will change?" [Online]. Available: http://wltpfacts.eu/from-nedc-to-wltp-change/. [Accessed: 23-Jan-2018].

[134] S. Hadj-Said, G. Colin, A. Ketfi-Cherif, and Y. Chamaillard, "Analytical Solution for Energy Management of Parallel Hybrid Electric Vehicles," *IFAC-PapersOnLine*, vol. 50, no. 1, pp. 13872–13877, 2017.

[135] P. Riedinger, C. Lung, and F. Kratz, “An Optimal Control Approach for Hybrid Systems,” *Eur. J. Control*, vol. 9, no. 5, pp. 449–458, 2003.

[136] B. Passenberg, M. Leibold, O. Stursberg, and M. Buss, “The minimum principle for time-varying hybrid systems with state switching and jumps,” in *IEEE Conference on Decision and Control and European Control Conference*, 2011, pp. 6723–6729.